STUDIES RELATED TO THE

BINDING OF DIOXYGEN TO METALS

A thesis presented in partial fulfilment of the requirements for the degree of Doctor of Philosophy in Chemistry at the University of Canterbury, Christchurch, New Zealand.

GEOFFREY BRIND JAMESON

August 1977

DEDICATION

To my parents and family.

ACKNOWLEDGEMENTS

I am most grateful for the advice and encouragement of my supervisors, Drs. Ward T. Robinson and Gordon A. Rodley. The collaboration with Professor James P. Collman and his group at Stanford University, California, U.S.A. is acknowledged with pleasure. The foundations of this thesis were laid by their synthetic efforts.

The receipt of results prior to publication from Professors James P. Collman, J. L. Hoard, William P. Schaefer and Christopher A. Reed, and Drs. R. G. Shulman and Alex Avdeef is also appreciated.

I would like to thank fellow students in X-ray crystallography for their advice and assistance.

Finally I am indebted to my family for their encouragement and support, and to the University Grants Committee for the award of a Postgraduate Scholarship and Shirtcliffe Fellowship.

CONTENTS

LIST OF FIGURES

LIST OF TABLES

ABSTRACT

Five crystal structures of which two involved Schiff-base derivatives and three involved "picket fence" porphyrin derivatives were determined.

1. α,α'-{2-(2'-pyridyl)ethyl}ethylenebis(salicylideniminato)-iron(II), Fe(salen-C_2H_4-py). Crystal and refinement data:- monoclinic, $P2_1/c$, a = 10.572(2), b = 11.465(2), c = 16.640(3) Å, β = 90.52(1)°; R = 0.056 for 1118 reflections having $I>3\sigma_I$; Z = 4. This high-spin complex has distorted trigonal-bipyramidal geometry with the following bond distances:- $r(Fe\text{-}N_{salen})_{average}$ 2.093(7) Å, $r(Fe\text{-}O_{salen})_{average}$ 1.959(6) Å, $r(Fe\text{-}N_{py})$ 2.147(8) Å. Its stereochemistry is generally similar to the cobalt analogue, which forms an isolable dioxygen adduct.

2. The dioxygen adduct of Co(salen-C_2H_4-py), [Co(salen-C_2H_4-py)(O_2)]·CH_3CN. Crystal and refinement data:- monoclinic, $P2_1/c$, a = 9.562(2), b = 19.490(4), c = 12.770(3) Å, β = 106.01(2)°; Z = 4; R = 0.128 for 915 reflections having $I>\sigma_I$. This low-spin (S=½) complex has approximately octahedral symmetry with bond distances:- $r(Co\text{-}N_{salen})_{average}$ 1.88(2) Å, $r(Co\text{-}O_{salen})_{average}$ 1.89(2) Å, $r(Co\text{-}N_{py})$ 2.03(2) Å and $r(Co\text{-}O_{O_2})$ 1.84(3)Å. Dioxygen is angularly coordinated

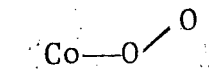

and the salen component is approximately planar. The results, and others, are interpreted in favour of a $Co^{III}\text{—}O_2^-$ species. This complex is a model for cobalt-substituted haemoglobin.

3. The dioxygen adduct of (1-methylimidazole)meso-tetra-(α,α,α,α-orthopivalamidephenylporphinatoiron(II), [Fe(TpivPP)-(1-Me-imid)(O_2)]·½(C_6H_6)·½($C_4N_2H_6$). Crystal and refinement data:- monoclinic C2/c, a = 18.690(3), b = 19.514(3), c = 18.638(3) Å, β = 91.00(1)°; Z = 4; R = 0.109 for 1784 reflections having $I>\sigma_I$. This essentially diamagnetic complex is approximately octahedral with bond distances:- r(Fe-N_{porph})av. 1.98(1) Å, r(Fe-N_{imid}) 2.07(2) Å and r(Fe-O_{O_2}) 1.75(2) Å. Dioxygen is angularly coordinated

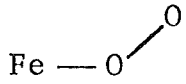

and there is an apparent trans effect in the axial connection. The validity of this complex as a model for the haem component of oxymyoglobin is assessed.

4. The dioxygen adduct of [Fe^{II}(TpivPP)(THT)]·$(THT)_2$, [Fe(TpivPP)(THT)(O_2)]·$(THT)_2$. Crystal and refinement data:- monoclinic $P2_1/c$, a = 16.951(3), b = 18.153(4), c = 25.470(4) Å, β = 107.14(8)°; Z = 4; R = 0.166 for 1521 reflections having $I>\sigma_I$. This complex is approximately octahedral, and the average r(Fe-N_{porph}) is 2.00 Å and r(Fe-S) is 2.49(2) Å. Dioxygen is angularly coordinated

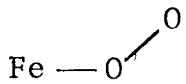

but definition is very poor. This complex is a possible model for the oxygenated intermediate in the catalytic cycle of cytochrome P450 camphor hydroxylase.

5. Catena-{μ-[(TpivPP)-N,N',N'',N''':O]-aquoiron(II)·THT, polymeric-[Fe(TpivPP)(OH_2)]·THT. Crystal and refinement data:- orthorhombic, $P2_12_12_1$, a = 15.448(4), b = 26.415(6), c = 14.960(4) Å; Z = 4; R = 0.116 for 2576 reflections having $I>\sigma_I$.

In this high-spin complex a pivalamide oxygen atom of one "picket" is coordinated to the iron atom of another Fe(TpivPP) unit at a separation of 2.22(1) Å, thereby creating an infinite chain. A water molecule is semicoordinated to the iron atom on the hindered side of the porphyrin at a separation of 2.90(2) Å. The iron atom is displaced 0.28 Å from the least-squares plane of the porphinato nitrogen atoms towards the coordinated pivalamide oxygen atom. The average $Fe-N_{porph}$ separation is 2.07(1) Å. The complex has stereochemical features in common with other high-spin metalloporphyrins.

ABBREVIATIONS

Ligands

dien	diethylenetriamine.
en	ethylenediamine.
diars	1,2-di(dimethylarsino)benzene.
HMPT	hexamethylphosphoramide.
L	general quadridentate, dianionic equatorial ligand system.
acacen	N,N'-ethylenebis(acetylacetoniminato).
bzacen	N,N'-ethylenebis(benzoylacetoniminato).
salen	N,N'-ethylenebis(salicylideniminato).
Ssalen	N,N'-ethylenebis(thiosalicylideniminato).
salen-C_2H_4-py	α,α'-{2-(2'-pyridyl)ethyl}ethylenebis-(salicylideniminato).
3-Fsalen	N,N'-ethylenebis(3-fluorosalicylideniminato).
3-MeOsalen	N,N'-ethylenebis(3-methoxysalicylideniminato).
saltmen	N,N'-(1,1,2,2-tetramethyl)ethylenebis-(salicylideniminato); the next two ligands are saltmen derivatives.
t-Bsalten	N,N'-(1,1,2,2-tetramethyl)ethylenebis-(3-t-butylsalicylideniminato).
3-Fsaltmen	N,N'-(1,1,2,2-tetramethyl)ethylenebis-(3-fluorosalicylideniminato).
salbn⊕	N,N'-butylenebis(salicylideniminato), Racemic form.
salprtr	3,3'-diimino-di-n-propylaminebis(salicylideniminato.

P	general porphinato species.
C_a	pyrrole carbon atom α to pyrrole nitrogen atom of porphinato skeleton.
C_b	pyrrole carbon atom β to pyrrole nitrogen atom of porphinato skeleton.
C_m	methine carbon atom linking pyrrole groups of porphinato skeleton.
Ct	radius of "hole" of porphinato skeleton; half the average separation between pyrrole nitrogen atom trans to each other.
TPP	meso-tetraphenylporphinato (also α,β,γ,δ-tetraphenylporphinato[191]).
p-CH_3TPP	meso-tetra(para-tolyl)porphinato.
TpivPP	meso-tetra(α,α,α,α-orthopivalamidephenyl)-porphinato.
polymeric—[Fe-(TpivPP)(OH_2)]·THT, or polymeric-Fe-(TpivPP)	catena-{μ-[meso-tetra(α,α,α,α-orthopival-amidephenyl)porphinato-N,N',N",N"':O]-aquo-iron(II)·THT}.
OEP	1,2,3,4,5,6,7,8-octaethylporphinato (Hoard's nomenclature[191]).
PP-IX^-	protoporphinato-IX-carboxylate anion.
Proto-IX-DME	protoporphinato-IX dimethyl ester.
Meso-IX-DME	mesoporphinato-IX dimethyl ester.
DMGH	bis(dimethylglyoximato).

Axial Bases

B	general axial base.
py	pyridine.
3-Me-py	3-methylpyridine.
4-NH_2-py	4-aminopyridine.
4-CN-py	4-cyanopyridine.
3,5-lut	3,5-dimethylpyridine (3,5-lutidine).
imid	imidazole.
1-Me-imid	1-methylimidazole.
2-Me-imid	2-methylimidazole.
1,2-Me_2-imid	1,2-dimethylimidazole.
1-Bz-imid	1-benzylimidazole.
pip	piperidine.
THT	tetrahydrothiophene.
SC_6H_4-p-NO_2) $SC_6H_4NO_2$)	para-nitrobenzenethiolate

Amino Acids

Gly	glycine.
His	histidine.
Tyr	tyrosine.
Val	valine.
Glu	glutamine.

Miscellaneous

X^-	general anion e.g. Cl^-, N_3^-, OH^-, SCN^-.
OMe	methoxide anion.
Hb	haemoglobin.
Mb	myoglobin.

Co-Hb	cobalt-substituted haemoglobin.
P450	cytochrome P450 camphor hydroxylase.
Ph	phenyl.
Et	ethyl.
Me	methyl.
$M\text{-}O_2$, $M\text{-}O_2\text{-}M$	general metal-dioxygen complex - nothing is implied about nature of metal-dioxygen linkage.

CHAPTER 1

INTRODUCTION

Organisms that respire aerobically invariably require at least some metal-containing proteins for the transport, storage and utilisation of molecular oxygen (dioxygen)[1,2].

Iron or copper ions or a macrocyclic porphyrin complex of the former element comprise the prosthetic group or non-protein component of the metalloprotein. The active site for dioxygen is presumed to be the metal centre since removal of the prosthetic group to give the apoprotein invariably destroys the activity of the protein towards dioxygen. Detailed knowledge of the structure and function of these proteins at the atomic level is frequently frustrated by various factors, most notably protein size which rarely drops below a molecular weight of 20,000. Thus acquisition of precise structural details for the coordination environment around the metal centre by high-resolution X-ray crystallographic techniques is not, at present, practicable. In addition it may be difficult to freeze out the stages of a catalytic cycle of which coordination of dioxygen is but one step.

Therefore, studies of simpler, protein-free, transition-metal complexes which are possible models for the metalloprotein's active site may help elucidate the structure of the active site and, perhaps also, aspects of the function of the protein itself. Such elucidation has been aided by major advances in the interpretation of results obtained by recently developed or improved techniques, such as resonance Raman spectroscopy[3], extended X-ray absorption fine struct-

ure (EXAFS)[4-7] and magnetic circular dichroism[8]. These have enabled a wide variety of spectral and magnetic features of the metal centre and its immediate coordination environment in the metalloprotein to be selectively probed and compared with data similarly obtained from purely inorganic model systems. In particular, advances in X-ray crystallographic techniques, consequent upon increasing computer sophistication, have greatly facilitated the precise stereochemical characterisation of compounds which model the metalloprotein's active site. Studies on metalloproteins and on their models are coupled in a synergistic manner.

This is the general background against which the studies embodied in this thesis are set. Attention is concentrated on the structures of several model compounds for the oxygen-binding component of one class of proteins, the haemoproteins, of which haemoglobin and myoglobin are both the best known and most widely studied examples. The single crystal X-ray diffraction structure analyses reported here are an essential part of a large collaborative effort, headed by Professor James P. Collman, which is probing the structure and function of oxygen-binding haemoproteins using an elegant model system. Other groups are also actively involved in this area. The relationships, both inorganic and biological, of the structural analyses reported herein to the studies (not necessarily just structural) of other workers are emphasised; to place the work of this thesis in perspective is felt to be of paramount importance.

The rest of this Chapter is devoted to outlining the structure of the thesis and, since some of the work is of

an inherited nature, the contributions of the author are delineated here so that continuity is preserved in the appropriate chapter.

1.1 General Review of Dioxygen, its Anions, and its Coordination to Metals in Inorganic and Biological Systems : Chapter 2.

In analysing the geometry and properties of dioxygen coordinated to metals, the free oxygen molecule O_2, its excited states, and its anions superoxide O_2^- and peroxide O_2^{2-} provide useful yardsticks against which various types of metal-dioxygen complexes may be classified and compared. These species are discussed in §2.1.

Dioxygen may coordinate to metals in two basic geometries – end-on M–O–O and side-on M(O–O). The metal-dioxygen complex may be mononuclear M-O_2 or dinuclear M–O_2–M. The O-O separation r(O-O) and the wavenumber of O-O stretching mode ν(O-O) of the anions superoxide and peroxide may be used to neatly divide metal-dioxygen complexes into two classes according to the apparent nature of the coordinated dioxygen ligand. Purely inorganic metal-dioxygen complexes are classified and reviewed in §2.2.

Finally, oxygen-binding proteins are examined briefly in §2.3. The inorganic model complexes reviewed and investigated here have facilitated clarification of probable geometries for the metal-dioxygen linkages in these various types of oxygen-binding proteins.

1.2 Structures Studied : Chapters 3 and 4

The compounds whose structures were determined by single-crystal X-ray diffraction techniques will be classified and discussed according to their quadridentate macrocyclic ligand system. The reason for dividing the compounds in this way, and not according to the presence or absence of the dioxygen ligand, is to facilitate comparison with their purely inorganic relatives so as to leave some of the biological implications common to complexes of both ligands to a subsequent chapter (Chapter 5). Implications of the structural results on bonding theories of metal-dioxygen complexes are also left to a later chapter (Chapter 6).

The two ligand systems employed were the Schiff base derivative α,α'-{2-(2'-pyridyl)ethyl}ethylene-bis(salicylidenimine) H_2salen-C_2H_4-py (Figure 1.1(a)) and the porphyrin derivative meso-tetra(α,α,α,α-orthopivalamidephenyl)-porphyrin H_2TpivPP (Figure 1.1(b)), commonly referred to as the "picket fence" porphyrin since the pivalamidephenyl groups or "pickets" are all oriented on one side of the porphyrin plane.

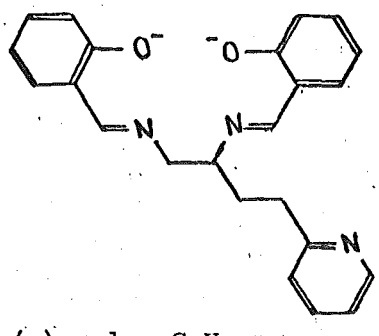

(a) salen-C_2H_4-py

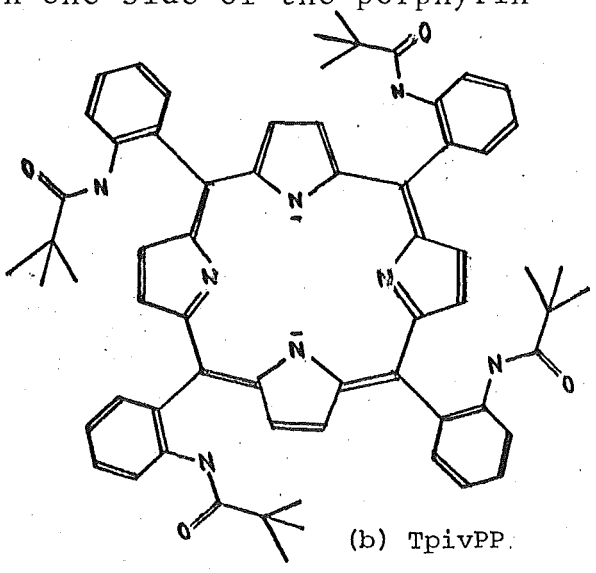

(b) TpivPP

Figure 1:1 Ligand systems used (deprotonated ligating form).

A general and lamentable feature of the compounds studied was their inherently poor crystallinity. Consequently the diffraction data obtained were generally limited in extent and quality, and the resultant structure analyses suffer an unfortunate lack of precision.

Appendix 1 outlines general methods of data collection, structure solution and also the computer programs used in these analyses. The contributions of the author to the collection of data and crystal structure solution are indicated.

1.2.1. Schiff-Base Complexes

The two crystal structures determined are described in Chapter 3. The first compound, five-coordinate Fe^{II} (salen-C_2H_4-py), used diffraction data of medium-good quality and extent collected by Dr. Ward T. Robinson from a crystal prepared at Stanford University, California, U.S.A. It was solved mainly to gain experience in the use of the University of Canterbury's suite of crystallographic programs. However, its dioxygen adduct is not readily isolated but its isostructural cobalt analogue does coordinate dioxygen to give a relatively stable adduct. The structural studies described in this thesis indicate that the stereochemistry of the non-isolated iron-dioxygen adduct should be generally similar to that observed for its cobalt-dioxygen analogue. Geometrical changes which accompany oxygenation are relevant to oxygen-binding haemoproteins.

The second complex, the cobalt-dioxygen adduct [Co(salen-C_2H_4-py)O_2)].CH_3CN alluded to in the preceding paragraph, was inherited in a state of partial solution.

The dioxygen and solvate moieties were poorly defined. A larger crystal was prepared here from the five-coordinate precursor Co(salen-C_2H_4-py) synthesised at Stanford University, and a larger data set collected. Final structure solution and refinement proceeded from the coordinates of the Co(salen-C_2H_4-py) fragment of the partial solution. This structure has already been mentioned in the literature[9,10,300].

1.2.2 "Picket Fence" Porphyrin Complexes

Three compounds were studied - two dioxygen complexes and one curious polymeric species. These are described in Chapter 4. The crystals were all prepared by Professor James P. Collman's research group at Stanford University. The bulky, flexible nature of the substituted porphyrin and other factors ensured that isolation of crystalline adducts was fraught with difficulties.

The original iron-dioxygen complex

$$[Fe(TpivPP)(1\text{-}Me\text{-}imid)(O_2)]\cdot\tfrac{1}{2}(C_6H_6)\cdot\tfrac{1}{2}(C_4N_2H_6)$$

was inherited in a state of partial solution from Drs Ward T. Robinson and G. A. Rodley[11,12]. Space group ambiguity, disorder of atoms of the "picket fence" and dioxygen components, and an ill-defined solvate species afflicted the structure of this highly significant model compound. The problems were characterised and refinement of structural parameters was eventually taken to a satisfactory conclusion. This compound is a model for the oxygen-binding haemoproteins of the haemoglobin type.

A second iron-dioxygen complex with a sulphur-axial ligand $[Fe(TpivPP)(THT)(O_2)]\cdot(THT)_2$ (THT = tetrahydrothiophene) was studied. The best data obtainable was appallingly limited in quality and extent. As a result, definition of many parts of the structure is poor and in the initial stages sensible refinement of structural parameters proved difficult. This compound is a possible model for one stage in the catalytic cycle of the dioxygen-utilising haemoprotein. cytochrome P450.

Repeated attempts, at Stanford University, to prepare better quality crystals of the above compound only led to a curious polymer,

catena-{μ-[TpivPP-N,N',N'',N''':O]-aquoiron(II)·THT}.

A data set of fair quality was obtained. Axial ligation of a $\rangle$=O species, semi-coordination of water and distinctive crystal packing of the monomeric Fe(TpivPP) units are novel features of the crystal structure. Biological implications can be extracted from this structure. Because of its novel features the diffraction data were used to the fullest extent to obtain structural parameters of the highest precision and accuracy possible. Lengthy and expensive computing was required to achieve this.

1.3 Implications of the Results on Theories of Protein Function and Dioxygen Bonding : Chapters 5 and 6.

In Chapter 5 the results of crystal structure determinations, particularly that of $[Fe(TpivPP)(1\text{-}Me\text{-}imid)(O_2)]$, are discussed with reference to models for the cooperative binding of dioxygen to haemoglobin. Cooperativity is the phenomenon whereby the binding of a molecule of substrate

(such as dioxygen) to a molecule with several binding sites (such as haemoglobin) increases the affinity of the protein for binding the next molecule of substrate - that is until all the binding sites are occupied.

The general features of various quantum-mechanical or pseudo-quantum-mechanical bonding schemes for oxygen-binding haemoproteins and their models are briefly reviewed in Chapter 6. Unfortunately, it would appear from the diversity of these schemes that most of these studies merely reinforce the prejudices of the proposer regarding the nature of the metal-dioxygen component. Structural features of both cobalt-and iron-dioxygen complexes that impinge on bonding theories are also discussed in an entirely qualitative manner in Chapter 6.

CHAPTER 2

GENERAL REVIEW : DIOXYGEN, ITS ANIONS AND ITS COORDINATION TO METALS

Dioxygen coordinates to a large number of metals in varying oxidation states. Two basic geometries for the metal-dioxygen linkage are observed – end-on bent M–O–O and side-on M(O–O) – and complexes may be mononuclear $M–O_2$ or dinuclear $M–O_2–M$ with respect to the metal atom. Despite this variety in form and geometry, a general feature accompanying the coordination of dioxygen to metals is the apparent oxidation of the metal ion and the concomitant reduction of the dioxygen ligand; to quote L. Vaska, "oxygenation = oxidation, even if it is reversible"[13]. In fact a remarkably sharp dividing line exists between complexes where dioxygen is formally reduced by one electron and those where it is formally reduced by two electrons. Results of structural, magnetic, spectroscopic (infrared to γ-ray Mossbauer) and oxidation-reduction studies have been used to support the formulation of dioxygen-metal complexes, $M–O_2$ or $M–O_2–M$, as essentially oxidised metal-coordinated superoxide or peroxide species

$$\left.\begin{array}{ll} M^{x+1}–O_2^-, & M^{x+1}–O_2^-–M^{x+1} \\ \text{or} \quad M^{x+2}–O_2^{2-} & M^{x+1}–O_2^{2-}–M^{x+1} \end{array}\right\} \quad x = 0,1,2.$$

Dissenting opinions which have from time to time existed[12,14-16], have in several cases been disproved or retracted[17-19]. That is, metal dioxygen complexes have features and properties more consistent with an oxidised metal-coordinated oxygen anion species than with an unoxidised metal-molecular oxygen species.

Controversy does still exist for some systems[19] and naive application of the formalism can lead to conceptual difficulties in others. Nonetheless, consideration of structural parameters such as r(O-O) and ν(O-O) for free molecular oxygen, its excited states and its anions superoxide O_2^- and peroxide O_2^{2-} is appropriate. The superoxide and peroxide anions are convenient yardsticks against which r(O-O) and ν(O-O) observed in dioxygen-metal complexes may be placed.

But several points must be stressed:-

1. "Free ion" values for superoxide and peroxide anions do not in most cases exist per se but can only be estimated by extrapolation.
2. ν(O-O) for coordinated dioxygen is not a pure O-O stretching mode but is perturbed through attachment to the metal and crystal packing or solvent effects.
3. Most importantly, r(O-O) and ν(O-O) do not alone provide evidence of a nett electron transfer from the metal onto dioxygen; they merely indicate an apparent reduction in the bond order of molecular oxygen upon coordination. It is regarded as significant, though, that the reduction in bond order coincides very closely with the reduction in bond order which accompanies a one-electron or two-electron reduction of molecular oxygen.

Hence conclusions about the superoxidic or peroxidic nature of the metal-dioxygen linkage based only on r(O-O) and/or ν(O-O) without any appreciation of other factors associated with the metal dioxygen linkage (such as magnetic properties) may be erroneous.

These caveats notwithstanding comparison of ν(O-O) for dioxygen and anions with ν(O-O) for coordinated dioxygen is illuminating in that ν(O-O), and also r(O-O), are still the most often discussed pointers to the nature of the metal-dioxygen linkage.

Table 2.1 lists values of r(O-O) and ν(O-O) for molecular oxygen and its ions, and for various types of metal-dioxygen complexes. Figure 2.1 shows the relationships between ν(O-O) and r(O-O) and bond order. One of the most notable features of metal-dioxygen complexes is that with very few exceptions there is little indication from r(O-O) and ν(O-O) values for a continuum of states for coordinated dioxygen. There is an unfortunate lack of both ν(O-O) and r(O-O) for the same dioxygen complex.

A large number of comprehensive reviews on aspects of metal dioxygen complexes exist[13,20-29]; consequently no attempt to provide an exhaustive literature survey is contemplated. However the field of metal-dioxygen chemistry is still developing rapidly and a number of interesting and significant new compounds have been reported since the most recent and excellent reviews of Vaska[13], and McLendon and Martell[29]. A review covering the different types of metal-dioxygen complexes (§2.2) is essential for subsequent classification of the oxygen-binding proteins (§2.3) since the nature of the metal-dioxygen linkage in protein systems has been largely deduced by analogy with well-characterised model systems. Because ν(O-O) and r(O-O) are the most widely determined parameters attention will be focussed on them.

Table 2.1 : Dioxygen, its anions and its complexes.

Species	$\nu(O—O)$ cm^{-1}	$r(O—O)$ Å
O_2^+	1860	1.12
$(^3\Sigma_g^-)O_2$	1556	1.2107
$(^1\Delta_g)O_2$	1484	1.2192
O_2^-	1090	1.34
O_2^{2-}	730	1.48
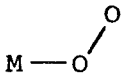	1120-1163	1.27(1)-1.302(3)
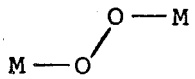 peroxo superoxo	800-808 1110-1122	1.339(6)-1.488(6) 1.243(13)-1.36(3)
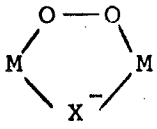 peroxo superoxo	790-830 1075-1110	1.46 1.320(5)
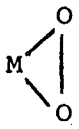	800-932	1.399(6)-1.52(1), Av. ≈ 1.45
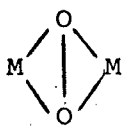	905	1.49(3)
Haemocyanin Cu_2O_2	742	
Haemerythrin Fe_2O_2	844	
Haemoglobin $Fe-O_2$ $Co-O_2$	1103-1107	

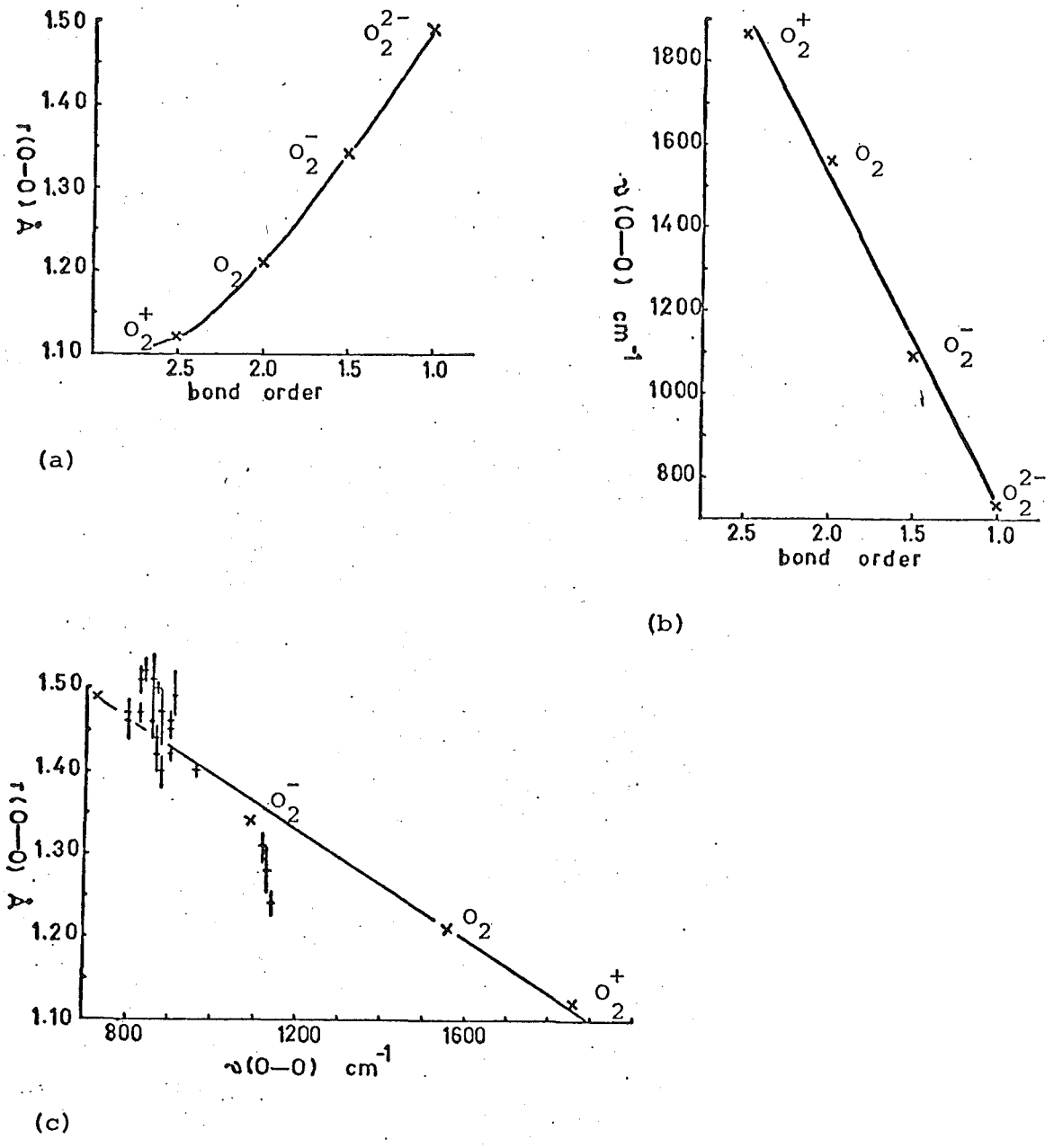

Figure 2.1 : Relationships between r(O-O), ν(O-O) and bond order for dioxygen, its ions and its complexes.

(a) Relationship between r(O-O) and bond order for dioxygen and its ions.

(b) Relationship between ν(O-O) and bond order for dioxygen and its ions.

(c) Relationship between r(O-O) and ν(O-O) for dioxygen(X) its ions(X) and its complexes. Error in r(O-O) for coordinated dioxygen is indicated.

This Chapter therefore, reviews important features of molecular oxygen and its anions superoxide and peroxide (§2.1) and metal-dioxygen complexes (§2.2). It is on this foundation that the metal-dioxygen component of oxygen binding proteins is considered (§2.3).

2.1 Molecular Oxygen and its Anions

Because confusion still exists in the literature over the most appropriate values to quote for the O-O separation, r(O-O), and the wavenumber of the O-O stretching mode, ν(O-O), for the anions superoxide and peroxide in an isolated "free ion" state, some detail will be provided with, as far as practicable, the original literature consulted rather than reviews. Figures 2.1(a) and 2.1(b) show the smooth relationship between ν(O-O), r(O-O) and bond order for molecular oxygen and its ions. Figure 2.2 is a qualitative molecular orbital energy level diagram for dioxygen.

2.1.1 Molecular Oxygen

From very high resolution spectroscopy r(O-O) for ground-state molecular oxygen has been determined as 1.2107 Å [30]. This value is the equilibrium separation r_o of the lowest vibrational state ν=0, which because of anharmonicity is different from the more frequently cited separation r_e (1.2074 Å) that applies to the non-existent vibrationless state. However, to within 0.01Å, r_o and r_e are equal. The observed ν(O-O) is 1556 cm^{-1}. Again the frequency ω_e of the vibrationless state is sometimes quoted (1580 cm^{-1}). Ground-state molecular oxygen is in a triplet $^3\Sigma_g^-$ electronic

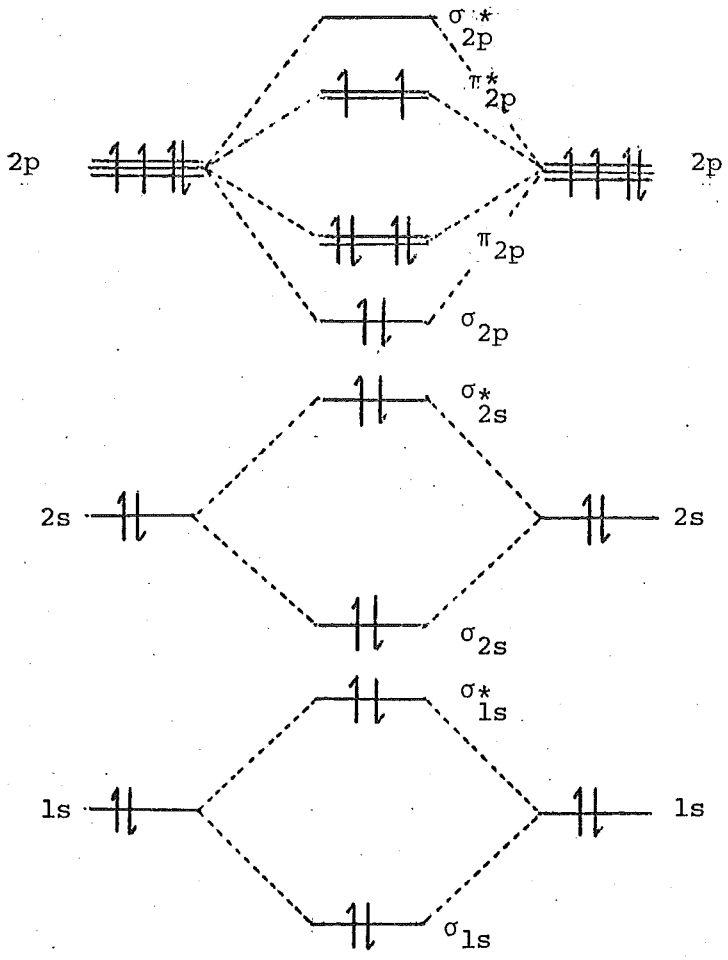

O_2 $(\pi^*_{2p})^1$ $(\pi^*_{2p})^1$

O_2^- $(\pi^*_{2p})^2$ $(\pi^*_{2p})^1$

O_2^{2-} $(\pi^*_{2p})^2$ $(\pi^*_{2p})^2$

Figure 2.2: Simple molecular orbital energy level diagram for molecular oxygen and its ions.

state. In simple molecular-orbital terminology (Figure 2.2) the electronic configuration is

$$(\sigma_{1s})^2(\sigma^*_{1s})^2(\sigma_{2s})^2(\sigma^*_{2s})^2 - (\sigma_{2p})^2(\pi_{2p})^4(\pi^*_{2p})^2$$

with two unpaired electrons occupying two π^* molecular orbitals; the nett bond order is 2. In valence-bond terminology molecular oxygen is sp-hybridised.

Molecular oxygen also has a number of excited states which have been suggested as relevant to the coordination of dioxygen to metals. There is a low-lying metastable $^1\Delta_g$ singlet state 7882 cm^{-1} (~94.5kJ/mole) above the $^3\Sigma_g^-$ ground state. ν(O-O) decreases to 1484 cm^{-1} and r_o(O-O) increases to 1.219 Å [31]. The π^* electrons are paired and occupy the same molecular orbital. In valence-bond terminology molecular oxygen is sp^2-hybridised; a lone pair of electrons occupy two sp^2 hybrids and the π orbital is empty.

A more excited state ($^3\Sigma_u^-$) has an r_e separation of ~1.60 Å [32], corresponding to an electronic configuration $(\pi_{2p})^3(\pi^*_{2p})^3$. This state was at one time thought to be relevant to r(O-O) of a particular dioxygen complex[16] (see also §2.23). Two other excited states of this configuration ($^3\Sigma_u^+$, $^1\Sigma_u^-$) have r_e separations of ~1.52 Å [32].

2.1.2 Superoxide

One-election reduction of molecular oxygen produces the superoxide anion radical $O_2^{\cdot -}$. This species has a formal bond order of 1.5 (Figure 2.2); r(O-O) has increased and ν(O-O) has decreased compared with molecular oxygen, (Figure 2.1). The most widely cited value for r(O-O) is

1.28(2) Å [33]: this value is almost certainly ∿0.06 Å too short. In the salt NaO_2 the O-O separation was determined as 1.33(6) Å [34] and 1.31(3) Å [35]; for KO_2 1.28(2) Å [33]. However, reinterpretation of the X-ray diffraction data for KO_2 has led to r(O-O) in the range 1.32 Å to 1.35 Å [36]. From vibrational features of free superoxide ion and molecular photodetachment spectrometry, r_e(O-O) was calculated to be 1.341(10) Å [37]. A value of 1.377 Å has been calculated empirically using Badger's Rule from vibrational features of free ion superoxide[38].

For the radical $HO_2^{\cdot}$ r_e(O-O) has been calculated quantum mechanically; different basis sets yield values between 1.31 Å and 1.39 Å [39]. Application of Pauling's empirical bond order relationship rule has given an O-O separation of 1.39 Å for $HO_2^{\cdot}$ [39].

The author is unaware of any recent precise and accurate X-ray crystallographically determined value of r(O-O) for superoxide salts. With an eye half-turned towards values for r(O-O) observed in certain classes of transition metal-dioxygen adducts, a separation of ∿1.34 Å appears reasonable and likely for free ion superoxide.

Crystal packing effects lend to difficulties in obtaining the free ion value for ν(O-O). Values of 1141 cm^{-1} (for RbO_2) and 1146 cm^{-1} (for KO_2) have been reported using laser Raman spectroscopy[40]. A somewhat lower value of 1097 cm^{-1} for LiO_2 has been obtained (G.A.Ozin, value quoted in reference [13]). Paradoxically, crystal packing effects have been used to estimate a free ion value for ν(O-O).

Raman-determined values of ν(O-O) for superoxide-doped alkali-metal halides vary systematically according to metal and halide due to crystal-packing effects. A free ion value of 1090 cm^{-1} was obtained[41]. A value of 1101 cm^{-1} has been determined for $HO_2^{\cdot}$ [42].

The value of 1090 cm^{-1} will be used as the free ion superoxide ion value of ν(O-O).

2.1.3 Peroxide

Reduction of the superoxide anion by one electron creates the peroxide anion. Bond order is now only 1 (Figure 2.2); an increase in r(O-O) and decrease in ν(O-O) are observed (Figure 2.1).

There is a similar uncertainty over the value of r(O-O) that is most appropriate for free ion peroxide as for superoxide. Analysis of high resolution gas phase infrared measurements for H_2O_2 has given a value for r(O-O) of 1.475(4) $\mathring{A}$ [43]. However assuming a different value (believed to be more accurate) for r(O-H) leads to a value for r(O-O) of 1.467 $\mathring{A}$ [44]. Single crystal neutron diffraction has given a separation of 1.453(7) $\mathring{A}$ [44]. More extensive hydrogen bonding in the solid state is probably responsible for the decreased O-O separation. Other less precisely determined values between 1.47 and 1.51 $\mathring{A}$ (average of eight $\sim$1.496 $\mathring{A}$) for peroxide salts of groups I and II metals have been reviewed [45,46]. The average O-O separation for crystalline metal peroxides is probably closer to the free ion value than is r(O-O) for H_2O_2 since the covalent bond between "$^{-}$O-O^{-}" and "$2H^{+}$" in hydrogen peroxide will disperse antibonding electron

density away from the peroxide moiety, thereby leading to a shorter r(O-O).

Thus, a value of 1.49 Å will be taken as the free peroxide ion separation. This value is also the one most generally cited in discussions of metal-dioxygen complexes.

In contrast to the superoxide anion, no attempt has been made to determine ν(O-O) for a free peroxide ion. For H_2O_2, ν(O-O) is 880 cm^{-1} which is a rather higher wavenumber than that observed for metal peroxide salts; this is consistent with trends in r(O-O) discussed above. Values supposedly for the peroxide ion, in the range 1093 cm^{-1} to 1054 cm^{-1} for various group Ia and IIa metal peroxides have been determined by laser Raman spectroscopy[40]. However, these have since been shown to be carbonate artefacts[47]. This latter investigation[47] revealed two values for ν(O-O) at 738 cm^{-1} and 793 cm^{-1} for Na_2O_2 corresponding to peroxide anions at two sites of different symmetry. Other values of 836 cm^{-1} for NH_4HO_2 [48], 802 cm^{-1} for Li_2O_2 (G. A. Ozin quoted in reference [13]) have been reported. From more recent and comprehensive studies[49], ν(O-O) has been observed in the range 790 cm^{-1} (for Li_2O_2) to 736 cm^{-1} (for Na_2O_2) for group IA metals (both extremes in moderate agreement with other independent observations); and 842 cm^{-1} (for BaO_2) to 944 cm^{-1} (for ZnO_2) for group II metals.

A free peroxide ion wavenumber of ~730 cm^{-1} appears likely in the absence of a value estimated similarly to that for the superoxide anion.

2.1.4 Summary

In conclusion the following values are to be taken as reference points in subsequent discussions of dioxygen complexes:-

for dioxygen	r(O-O) 1.21 Å,	(O-O)	1556 cm^{-1}
for superoxide ion	r(O-O) 1.34 Å	(O-O)	1090 cm^{-1}
for peroxide ion	r(O-O) 1.49 Å	(O-O)	730 cm^{-1}

2.2 Review of Metal-Dioxygen Complexes.

In this section historical aspects of the preparation and characterisation of metal-dioxygen complexes are firstly introduced in general terms (§2.2.1). Possible criteria for the classification of metal-dioxygen complexes are discussed in §2.2.2. Finally, the different types of complexes and their geometry are discussed more specifically in §2.2.3 and §2.2.4 with particular reference to r(O-O) and ν(O-O).

In §2.2.5 possible factors influencing the geometry and nature of the metal-dioxygen linkage and a number of less definitively characterised metal-dioxygen complexes are examined. Here and elsewhere terms such as "metal-dioxygen complex", "dioxygen complex", "coordinated dioxygen", etc., and abbreviations such as M–O_2, M–O_2–M, etc. are used without implying anything about the nature of the metal-dioxygen linkage - that is, nothing is implied about the strength of the M–O linkage, the nett amount of electron density transfer from the metal to ligand or vice versa, or about apparent

alteration in bond order of molecular oxygen as a consequence of coordination.

The results from well-characterised, comparatively simple, inorganic systems provide a foundation on which may be built an understanding of aspects of the function and structure of oxygen-binding proteins.

2.2.1 Historical Aspects.

Dioxygen-containing complexes of cobalt have been known for some time; the first report on salts of the cation $[(NH_3)_5(Co(O_2)Co(NH_3)_5]^{4+}$ appeared in 1852 [50]. The ubiquitous Werner also prepared and characterised numbers of related dioxygen-containing cobalt ammine complexes[51]. Two types were recognised. The first type were the "red diamagnetic" species which were early formulated as peroxo-bridged cobalt(III) species Co^{III}-O_2^{2-}-Co^{III}. Formulation of the second type, "the green paramagnetic" species, was debated for many years after Werner had suggested a Co^{III}-O_2^{2-}-Co^{IV} moiety. The rarity of the cobalt(IV) oxidation state led to suggestions dating from around 1938, of a superoxo-bridged species Co^{III}-O_2^--Co^{III} [52]. Support for this formulation has come from electron spin resonance studies which showed both cobalt atoms (^{59}Co, I=7/2) to be magnetically equivalent on the ESR time scale. The resonance band had a 15-line hyperfine structure[53]. Thus formulation of metal-dioxygen complexes as oxidised metal-reduced dioxygen (especially peroxide) species has a long history. This valence state approach did fall upon hard times[16] during the proliferation of complexes with π-donor and acceptor ligands and highly

covalent metal-ligand linkages which blurred distinctions between metal valence (or oxidation) states; but, more recently, at least for metal-dioxygen complexes, more precise and accurate crystal structure analyses have led to its resurrection[13]. A useful, although brief, review on these early studies may be found in reference[54].

Calvin and coworkers in the 1940's in the course of extensive studies on Schiff-base complexes prepared a number of cobalt-dioxygen complexes with a metal to dioxygen ratio of 2:1 [55]. Those dinuclear complexes have subsequently become relevant to those of oxygen-carrying proteins which have pairs of metal atoms in close proximity and bind dioxygen in an identical ratio (§2.3.1).

Mononuclear dioxygen complexes — that is, complexes with a metal to dioxygen ratio of 1:1-are of more recent vintage, although their (at least transient) existence is implicated in the formation of dinuclear adducts. Factors which lead to the isolation of mononuclear rather than dinuclear adducts will be considered in §2.2.5. Calvin also observed 1:1 uptake of dioxygen by cobalt-Schiff base complexes[56].

The first non-cobalt metal-dioxygen complex $IrCl(CO)(O_2)(PPh_3)_2$ was prepared by Vaska in 1963 [57]. A large number of related complexes are now known. Mononuclear adducts with more biologically appropriate ligand systems and metal centre were characterised in detail in 1969-1970 [58-66]. An immense array of studies on mononuclear cobalt-dioxygen systems and, more recently, iron-dioxygen systems has been published in the last seven years. These cobalt-and iron-dioxygen complexes are potential models for

the metalloproteins which bind oxygen in a 1:1 ratio. For many years there has been speculation over the geometry and nature of the metal-dioxygen linkage in oxygen-binding proteins, especially those which, through molecules such as myoglobin that contain only one iron atom, have long been known to bind oxygen in a 1:1 metal-to-dioxygen ratio to an iron porphyrin complex incorporated into the protein. Almost every possible geometry and formulation for this linkage has been proposed: proposals included coordination of an excited state of molecular oxygen such as $^1\Delta_g$ [12,14], linear coordination M–O–O [67], angular coordination M–O–O [68], covalent triangular coordination  [69], coordination of the superoxide ion[70], and triangular coordination of the peroxide ion[71]. This matter was partially resolved with the determination of the crystal structure of a 1:1 cobalt dioxygen complex Co(bzacen)(py)(O_2) which had a biologically-related ligand system[126], and more completely resolved with the determination of the structure of the iron porphyrin derivative, Fe(TpivPP)(1-Me-imid)(O_2) [11].

Precise determination of the stereochemistry of the metal dioxygen linkage not only for 1:1 but also for 2:1 metal-dioxygen species is comparatively recent, and the early literature, unfortunately, abounds in red herrings. The first structure determinations of 2:1 cobalt dioxygen complexes, namely the structures of the "green paramagnetic" complex $[(NH_3)_5Co(O_2)Co(NH_3)_5](NO_3)_5$ [54] and of the "red diamagnetic" complex $[(NH_3)_5(Co(O_2)Co(NH_3)_5](SCN)_4$ [72] have been proven inaccurate[73,74].

Moreover, the first mononuclear complex which was structurally characterised, $IrCl(CO)(O_2)(PPh_3)_2$ [75], has an O–O separation quite atypical for its type[76].

Dioxygen has been observed to coordinate to metals in a variety of geometries with a variety of supporting ligands. Of the possibilities listed in Figure 2.3 only the linear geometries (b) and (e) remain unobserved although there has been a false alarm[77] that was subsequently corrected[78]. Stereochemical considerations provide various sets of criteria by which dioxygen complexes may be classified; a number of such sets are discussed in the next subsection.

2.2.2 Classification of Metal-Dioxygen Complexes.

Metal-dioxygen complexes may be grouped in several ways. One possibility is to classify them according to the symmetry of the metal-dioxygen linkage, end-on (a)-(e) versus side-on (f) and (g); another, according to the number of metal-oxygen linkages, mononuclear $M–O_2$ versus dinuclear $M–O_2–M$ which also parallels the semi-historical introduction of the preceding section. However the most useful classification is according to the nature of the bound dioxygen ligand: is the coordinated dioxygen peroxide-like or peroxo, or is it superoxide-like or superoxo? A more careful definition of the terms peroxo and superoxo is given in a subsequent paragraph.

The dividing line between peroxo and superoxo species irrespective of geometry is remarkably clear-cut with regard to $\nu(O-O)$ and $r(O-O)$. The peroxo complexes have $\nu(O-O)$ in

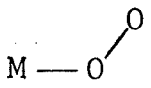

(a) mononuclear, end-on bent.

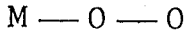

(b) mononuclear, linear.

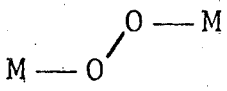

(c) dinuclear, end-on planar and non-planar.

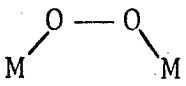

(d) dinuclear, end on planar and non-planar.

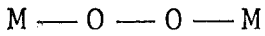

(e) dinuclear, linear

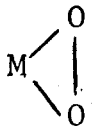

(f) side-on, triangular.

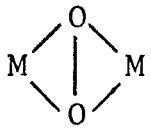

(g) dinuclear, side-on triangular.

Figure 2.3 : Possible modes of coordination of dioxygen.

the range 790 cm^{-1} to 932 cm^{-1} and r(O-O) with few exceptions in the range 1.42(1) Å to 1.51(1) Å with the distribution peaking and averaging at ∿1.46 Å [13] - hence, by comparison with the free peroxide ion (Table 2.1), the name peroxo. Complexes labelled superoxo have ν(O-O) in the narrower range 1075 cm^{-1} to 1140 cm^{-1} and r(O-O) in the range 1.24(1) Å to 1.320 (5) Å - hence, analogously, the name superoxo. Assignment of these infrared bands as essentially pure O-O stretching modes has been confirmed in several cases by isotopic substitution of $^{18}O_2$ for $^{16}O_2$; close agreement between the calculated and observed isotopic shifts in wavenumber indicate that modes involving dioxygen, ν(O-O) and also ν(M-O), are only weakly coupled with each other or with other modes[79,80,176]. Resonance Raman spectroscopy has also assisted identification of ν(O-O) in those complexes where it is infrared inactive.

Geometries (a), (c) and (d) are represented in the superoxo class; geometries (c), (d), (f) and (g) in the peroxo class. Especially noteworthy is the presence in the peroxo class of both the end-on geometry (c) and (d) and the side-on geometry (f) and (g). It is also noteworthy that the precise determination of the structures of end-on cobalt-dioxygen complexes has been the exclusive domain of Schaefer and coworkers. Figure 2.1(c) also highlights the division of dioxygen complexes into the two classes peroxo and superoxo, although there is an unfortunate lack of r(O-O) and ν(O-O) reported for the same complex.

Before dioxygen complexes are discussed in more detail in the next subsections a closer examination of the labels peroxo and superoxo is required. There is considerable covalent character in the metal-oxygen linkage; estimates for metal-dioxygen bond energies for certain types of complex are in the 360-400 kJ range[81]. But to formulate a metal-dioxygen complex as a purely covalent species $M^{\sigma/\pi}O_2$ or $M^{\sigma/\pi}O_2{}^{\sigma/\pi}M$ denies the nett transfer of electron density from metal to dioxygen which lines of evidence other than values for ν(O-O) and r(O-O) imply. Conversely, to formulate a metal-dioxygen complex as a purely ionic $M^{+1}{-}O_2^-$, $M^{+1}{-}O_2^{2-}{-}M^{+1}$ or $M^{+1}{-}O_2^-{-}M^{+1}$ species denies the covalent character that exists. However, the ionic formulation reflects better the distinction in r(O-O) and ν(O-O) between the two major types of coordinated dioxygen; it also reflects better the correspondence in these parameters for dioxygen complexes with those for the superoxide and peroxide anions. Therefore, the covalent character in the metal-dioxygen bond, which leads in systems formulated as $M^{x+1}{-}O_2^-$ to spin-pairing of the superoxide electron with an unpaired metal 3d electron (where applicable), is implicit in the formulation. The terms superoxo and peroxo have been respectively defined as "covalently bound dioxygen resembling superoxide O_2^-" and "covalently bound dioxygen resembling peroxide O_2^{2-}" [13]. Unfortunately some of the early literature uses the term peroxo to cover both superoxo and peroxo ligands. Thus in the titles of the literature cited, "(su)" will be prefixed to "peroxo" for clarification when necessary.

Furthermore, circumstantial evidence additional to r(O-O) and ν(O-O) is necessary to support the hypothesis that there is more than just a formal transfer of electron density in one or two electron quanta from the metal onto dioxygen. Further such evidence has come from a wide range of studies including ESR, uv-visible and X-ray photoelectron spectroscopy, and positive correlations of redox properties of unoxygenated species with the stabilities of their dioxygen adducts. A more detailed review on the formulation of 1:1 end-on bonded dioxygen complexes of cobalt and iron will be made in Chapters 3 and 4.

In the next two subsections metal-dioxygen complexes belonging to the peroxo and superoxo class will be reviewed as a prerequisite to understanding the nature of the oxygen-binding active site of metalloproteins.

2.2.3 Peroxo Complexes.

For complexes of this class, irrespective of their basic geometry, metal centre and supporting ligand system, r(O-O) is usually only marginally shorter than the "free ion" value (1.49 Å). Vaska's compilation[13] of r(O-O) distances for peroxo complexes is revised and updated and the distribution of r(O-O) plotted in Figure 2.4(a). Values for r(O-O) from structure analyses of low precision, doubtful accuracy or unspecified composition are denoted by thin lines and are excluded from calculations of the unweighted standard deviation and mean of the distribution of O-O separations.

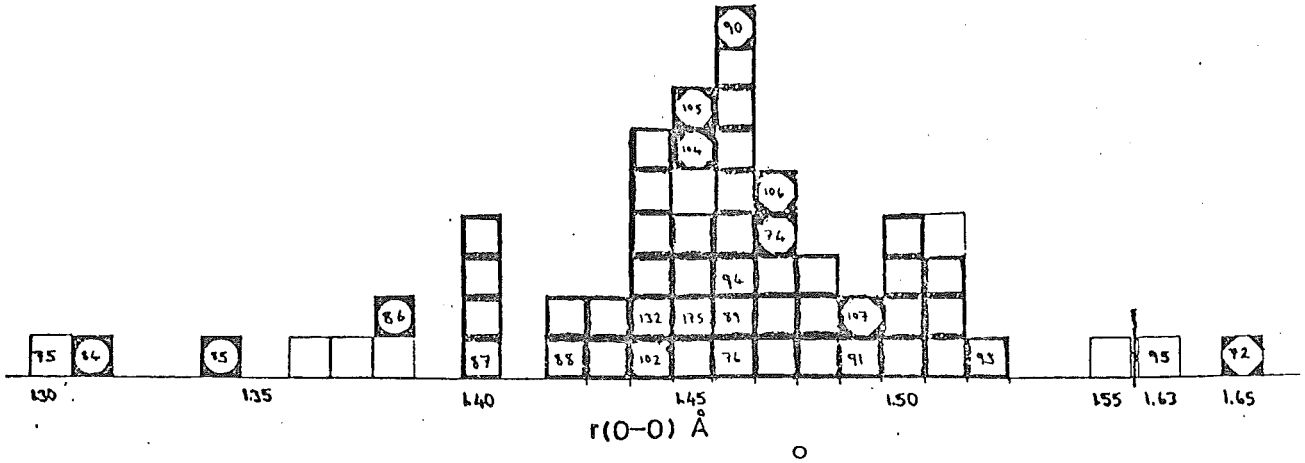

(a) Peroxo Complexes, Average r(O-O) = 1.45(4) Å.

M—O geometry

Average r(O-O) = 1.46(3) Å

M—O—M geometry

Average r(O-O) = 1.47(2) Å

M—O—M geometry (Schiff base complex)

Average r(O-O) = 1.34(4) Å

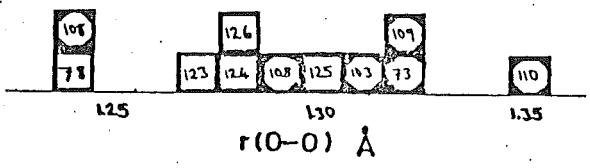

(b) Superoxo Complexes, Average r(O-O) = 1.29(3) Å.

M—O geometry

Average r(O-O) = 1.27(2) Å

M—O—M geometry

Average r(O-O) = 1.31(4) Å

Figure 2.4 : Distribution of r(O-O) for dioxygen complexes. For reference numbers, where not indicated, see Vaska's review[13].

For 49 peroxo complexes the average O-O separation is 1.45 Å with a standard deviation of 0.04 Å which is about twice the mean standard deviation for individual r(O-O) values. There is, however, an anomalous group of three complexes (see Figure 2.4) which have a much smaller r(O-O).

Values for ν(O-O) range from 790 cm^{-1} to 964 cm^{-1}; the distribution peaks and averages at $\sim$860 cm^{-1} which is in the region for ν(O-O) of simple peroxide salts (§2.1.3).

The different geometries exhibited by peroxo complexes will now be examined.

Type (f) M<O-O> geometry.

Dioxygen complexes with this geometry are generally referred to as side-on π-bonded adducts. Their average r(O-O) is 1.46(3) Å. The Dewar-Chatt ethylene model has provided the basis for much discussion on the bonding of dioxygen in these species[96,97]. In very general terms, electrons from a filled dioxygen π_p molecular orbital are σ-donated into some empty metal orbital; electrons in other metal orbitals may be π backdonated to the oxygen π_p^* orbitals.

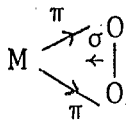

It may be noted that the bond order of the dioxygen ligand is decreased not only by σ donation to the metal from its $\pi(O_2)$ system but also by π backdonation from the metal to its $\pi^*(O_2)$ system.

The peroxide character of the coordinated dioxygen component as a function of the relative energies of suitably disposed metal orbitals and oxygen π_p^* molecular orbitals is illustrated in Figure 2.5.

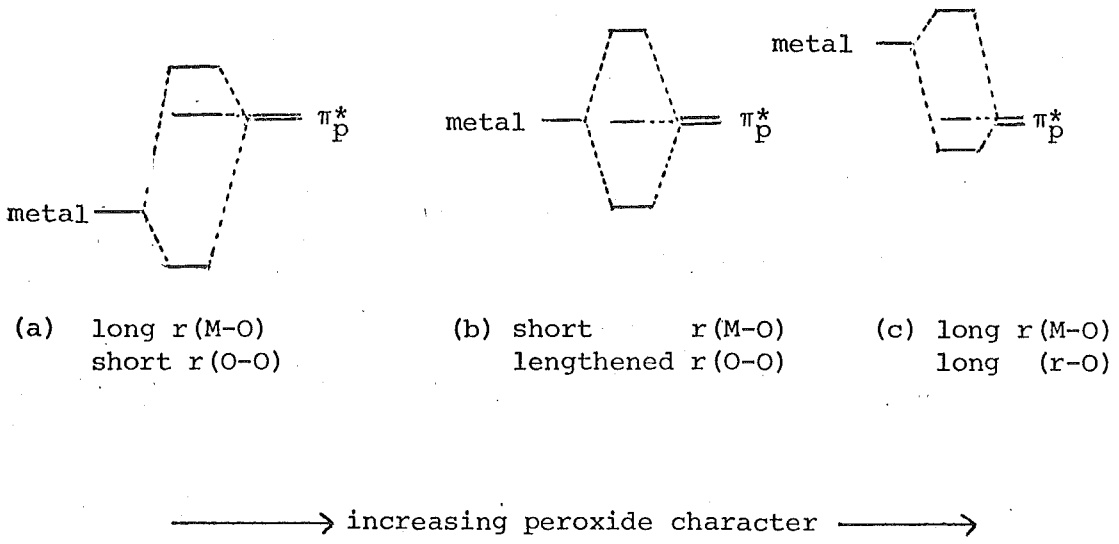

Figure 2.5: A metal-dioxygen π-bonding scheme.

At the most recent count[13] over 170 adducts with this geometry had been characterised with varying certainty. Complexes are known for transition metals from group IVb to group VIII(d^{10}) with the exception of hafnium, iron (notably) and group VIIb (manganese group) elements. There is an apparent dividing line in the nature of sideways coordinated peroxo complexes of the early and late transition metals:-

1. The early transition metals coordinate from one to four peroxo ligands; the late transition metals invariably coordinate just the one.

2. For the early transition metals the supporting ligand system comprises "hard", σ-donor species such as $\rightarrow P{=}O$, O^{2-}, $\diagup\!\!=\!\!N$ and H_2O, while for the late transition metals, "soft" π-acceptor species such as CO, CN^-, $P\lessdot$ and $As\lessdot$ are dominant.

3. High coordination numbers, between six and eight, are observed for the early transition metals; coordination numbers of four and six are observed for the late transition metals. The peroxo ligand is regarded as a bidentate chelate in both cases.

4. While no studies appear to have been made on the polarity of the metal-dioxygen component for the early transition-metal complexes, in view of the "hard" ligand systems associated with these complexes, a "harder", more polarised and more peroxide anion-like metal-dioxygen linkage appears reasonable by comparison with the late transition metal peroxo complexes. A less polar metal-dioxygen linkage may pertain to the latter peroxo complexes since very close relatives of a number of these complexes[75,76,171,173,175], will also coordinate ethylene[296]; and the metal-olefin bond is known to be covalent and non-polar, at least for $K[PtCl_3(C_2H_4)]\cdot H_2O$ [297,298]. Despite the apparent differences in polarity of the metal-dioxygen linkage for these two groups there are no significant differences in r(O-O) and ν(O-O) values.

Recently, a number of dioxygen adducts of metalloporphyrins with side-ways coordinated dioxygen have been characterised, including a group VIIb complex $Mn(TPP)(O_2)$[98,99]; a side-on geometry was inferred from spectroscopic and magnetic

data[98]. A titanium-dioxygen complex Ti(OEP)(O_2) has been structurally characterised; side-on coordination of dioxygen with an O-O separation of 1.458(9) Å was observed[89]. It is formally a titanium IV d^o species.

Another metalloporphyrin-dioxygen adduct Mo(p-CH_3TPP)(O_2)$_2$ has two dioxygen ligands trans to each other. It has one of the shortest-observed, precisely-determined O-O separations (1.399(6) Å) and also, satisfyingly, the highest ν(O-O) observed (964 cm^{-1})[87]. These parameters are readily rationalised by noting that as a molybdenum VI d^o peroxy species the electron-deficient molybdenum VI oxidation state will be assuaged by a larger-than-usual donation of electron density from the peroxide to the metal. That π bonding is very significant in these metalloporphyrin-peroxo complexes is demonstrated by the eclipsing configuration adopted by dioxygen so that the metal $d_{xz,yz}$ orbitals which are aligned along the M-N_{porph} bonds may accept $\pi^*_p(O_2)$ electron density from the peroxo group (Figure 2.6). These peroxo metalloporphyrins will be encountered again in Chapter 4.

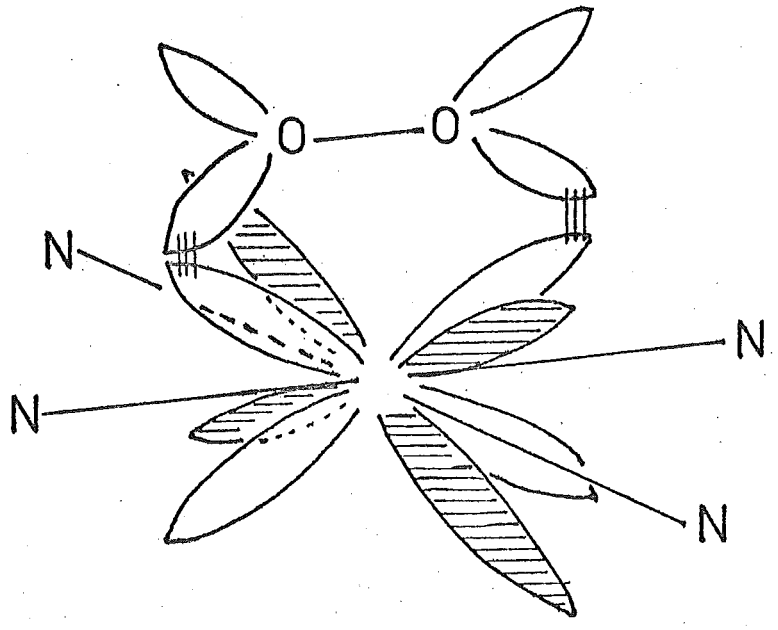

Figure 2.6: Possible π-bonding in M(porphinato)-(O_2) species.

At one time a rather elegant correlation which had considerable influence on discussions of the nature of the metal-dioxygen linkage[16] was thought to exist between r(O-O) and the reversibility (or lack of it) of dioxygen binding for iridium complexes[95,100]; this correlation gained considerable respectability[25,26,101]. $[Ir(O_2)(Ph_2PCH_2CH_2PPh_2)_2]^+$ had dioxygen bound irreversibly with r(O-O) 1.63(2) Å, whereas, at the other extreme, $IrCl(CO)(O_2)(PPh_3)_2$ had dioxygen bound reversibly with r(O-O) 1.30(3) Å. A dividing line between reversible and irreversible dioxygen binding appeared to exist at ~1.44Å. Formulation of these complexes as adducts of excited state dioxygen was proposed[16]; the excited state $^3\Sigma_u^-$ (r(O-O) ≃ 1.60 Å) was thought to be applicable to $[Ir(O_2)(Ph_2PCH_2CH_2PPh_2)_2]^+$. Anomalies soon appeared; for the very close relative of $IrCl(CO)(O_2)(PPh_3)_2$, $IrCl(CO)(O_2)(PPh_2Et)_2$, r(O-O) was found to be 1.46(1) Å[76]. Moreover, a recent redetermination of the crystal structure of $[Ir(O_2)(Ph_2PCH_2CH_2PPH_2)]^+$ found the long O-O separation to be a function of crystal decomposition; an improved value of 1.52(1) Å was obtained[92,93]. These workers also doubted the reliability of the 1.30(3) Å separation for $[IrCl(CO)(O_2)(PPh_3)_2]$.

A variation of this geometry is found in the dimeric species $[RhCl(O_2)(PPh_3)_2]_2$[102] (Figure 2.7) which also has features of a non-planar M–O(–O–M) species.

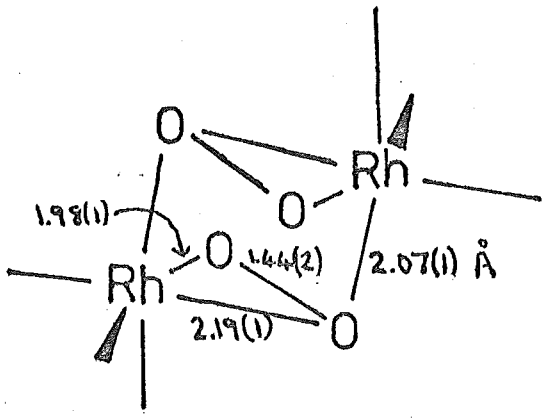

Figure 2.7: Structure of $[RhCl(O_2)(PPh_3)_2]_2$.

Type (g) 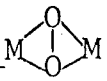

Complexes of this variation on the type (f)  geometry are rare; only the one example is known which has r(O-O) of 1.49(3) Å and ν(O-O) of 905 cm^{-1} [91]. The 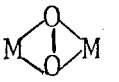 group is planar. An early report of a cobalt complex (albeit a superoxo species) $[(NH_3)_5Co(O_2)Co(NH_3)_5](NO_3)_5$ having this geometry[54] has been corrected;[73,103], the complex has typical type (c) geometry.

Type (c) 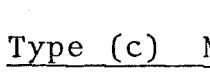 , Type (d) 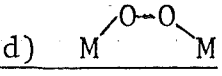

Table 2.2 contains r(O-O), $\angle$(M-O-O) and τ(M-O-O-M) for all structurally characterised compounds of this geometry. In contrast to the large number of metals and oxidation states associated with dioxygen complexes of type (f) geometry, type (c) or (d) geometries are known with certainty only for dioxygen adducts of cobalt(II) d^7 complexes, outside biological systems. These are the "red diamagnetic" compounds mentioned earlier (§2.2.1) and they are generally described as end-on σ-bonded structures. The complexes are invariably six-coordinate. The bonding of dioxygen may be approached from two directions using a hybrid of simple molecular orbital and valence bond

Table 2.2 : Stereochemistry of bent-bonded metal dioxygen complexes.

Complex	r(O—O) (Å)	∠(Co—O—O) (°)	r(M—O) (Å)	τ(Co—O—O—Co) (°)	Reference
(a) M—O—O Superoxo.					
Co(bzacen)(py)(O_2)	1.28(3)Å	125(2)	1.88(2)	-	[126]
$[Co(CN)_5(O_2)]^{3-}$	1.240(17)	153(2)	1.906(14)	-	[78]
Co(t-Bsalten)(1Bz-imid)(O_2)	1.273(10)	117.5(6)	1.873(7)	-	[123]
Co(saltmen)(1-Bz-imid)(O_2)	1.277(3)	120.0(2)	1.889(2)	-	[124]
Co(3-Fsaltmen)(1-Me-imid)(O_2)	1.302(3)	117.4(2)	1.881(2)	-	[125]
Co(salen-C_2H_4-py)(O_2)	-[a]	bent[a]	1.90(3)[b]	-	This work
Fe(TpivPP)(1-Me-imid)(O_2)	-[a]	bent[a]	1.75(2)	-	This work
(b) M—O—O, M—O—O—M Superoxo					
$K_5[(CN)_5Co(O_2)Co(CN)_5]\cdot H_2O$	1.243(13) 1.289(20)	121.2(7) 120.7(10)	1.944(9) 1.919(9)	166 180	[108]
$[(NH_3)_5Co(O_2)Co(NH_3)_5](SO_4)(HSO_4)_3$	1.312(~20)	118(2)	1.89(2)	175	[103]
$[(NH_3)_5Co(O_2)Co(NH_3)_5](NO_3)_5$	1.317(~15)	117.3(10)	1.895(8)	180	[73]
$[(NH_3)_4Co(O_2NH_2)Co(NH_3)_4](NO_3)_4$	1.320(5)	120.9(3)	1.867(4)	~180	[109]
$[(en)_2Co(O_2,NH_2)Co(en)_2](NO_3)_4\cdot H_2O$	1.353(11)	119.2(7)	1.880(8)	23.4	[110]
(c) M—O—O, M—O—O—M Peroxo					
[(DMF)(salen)Co(O_2)Co(O_2)(salen)(DMF)]	1.339(6)	120.3(2)	1.910(6)	110	[85]
$[(H_2O)(3\text{-Fsalen})Co(O_2)Co(3\text{-Fsalen})]_2\cdot 2CHCl_3\cdot pip$	1.31(3)	118	1.97(3)	122	[84]
$[(pip)(salen)Co(O_2)Co(salen)(pip)]\cdot 0.66(CH_3)_2CO\cdot 0.33pip$	1.383(7)[c]	120(1)	1.912(5)	122	[86]
$K_8[(CN)_5Co(O_2)Co(CN)_5](NO_3)_2\cdot 4H_2O$	1.447(4)	1183(3)	1.985(3)	180	[104]
$[(NH_3)_5Co(O_2)Co(NH_3)_5](SO_4)_2\cdot 4H_2O$	1.473(10)	1130(9)	1.882(7)	146	[106]
$[(NH_3)_5Co(O_2)Co(NH_3)_5](SCN)_4$	1.469(6)	110.8(4)	1.879(3)	180	[74]
[(en)(dien)Co(O_2)Co(en)(dien)](ClO_4)$_4$	1.488(6)	110.0(3)	1.896(4)	180	[107]
$[(en)_2Co(O_2,NH_2)Co(en)_2](SCN)_3\cdot H_2O$	1.46	-	-	non-planar	[90]
(salprtr)Co(O_2)Co(salprtr)	1.45(2)	118.5	1.93(1)	149	[105]

[a] Unreliable because of disorder.

[b] Corrected for riding motion; uncorrected, r(Co-O) = 1.84(3).

[c] Severe solvate problems; authors suggest true e.s.d's thrice those arising from the least-squares refinement.

considerations.

Firstly, using the $Co^{III}-O_2^{2-}-Co^{III}$ formalism, there is σ donation of a lone pair of electrons from an $\underline{sp^2}$-hybridised oxygen orbital to the empty metal $3d_{z^2}$ orbital. With the $\pi_p^*(O_2)$ and metal $d_{xz,yz}$ orbitals filled there can be little metal-oxygen π bonding, unless higher energy metal 4s and 4p, orbitals are considered. Moreover with little nett π bonding between oxygen atoms a non-planar Co-O-O-Co moiety is predicted to minimise electron repulsion. A Co-O-O angle close to 120^o is also predicted.

Secondly, a lone pair of electrons from an oxygen $\underline{sp^3}$-hybridised orbital may act as the σ-donor to the empty cobalt(III) d_{z^2} orbital. There can be no π-bonding component. Similarly, a non-eclipsing Co-O-O-Co configuration is predicted for minimum electron-pair repulsion, but a tighter Co-O-O angle nearer to the ideal tetrahedral value of 108^o may be expected. Hydrogen peroxide has torsion angles, τ(H-O-O-H), of 112^o (gas phase)[111] and 90^o (crystalline phase)[44]. As will be described later, this approach appears to give a better representation of the $Co-O_2-Co$ moiety.

Rigorous planarity of the Co-O-O-Co group is observed in about a third of the peroxo complexes (Table 2.2). Crystal packing effects and cation-cation repulsion of highly charged cobalt(III) centres appear to dominate purely electronic considerations of the dioxygen component; a planar conformation is therefore observed except where "neutralisation" of the positive cobalt centres is achieved with a delocalised ligand system such as a square-planar N,N'-ethylene Schiff-base or through an extensive hydrogen-bonding network involving the ligands[107].

Inspection of Table 2.2 and Figure 2.4(a) reveals a marked shortening in r(O-O) for N,N'-ethylene Schiff-base complexes compared to the ammine, amine and cyano complexes of this type; there also appears to be a slight lengthening in r(M-O) compared to the ammine and amine (but not cyano) complexes. In addition, the Co-O-O angles are more open for the Schiff-base dioxygen adducts than for the ammine and amine complexes. These observations are consistent with the dioxygen bridge having considerably less peroxide character for the Schiff-base type than for the ammine or amine type complex; a similar inference may be drawn, although less strongly, for the decacyano complex (r(O-O) = 1.447(4) Å, r(M-O) = 1.985(3) Å and ∠(Co-O-O) = 118.3(3)°) when it is compared to those ammine and amine complexes that are precisely determined. The rough correlation between r(O-O) and ∠(Co-O-O) has been noted by Schaefer[86]. With the tighter ∠(Co-O-O) associated with a longer r(O-O) - close to that for the free peroxide ion - the metal-dioxygen linkage for the amine and ammine species is best considered, using the second approach described above, as a coordinated sp^3-hybridised peroxide ion, while for the N,N'-ethylene Schiff-base species, description of the metal-dioxygen linkage as coordinated sp^2-hybridised dioxygen appears more appropriate. In the former (sp^3-hybridised) case the peroxide ligand has no π-bonding ability, in the latter (sp^2-hybridised) π-bonding ability exists. Following Schaefer's terminology these Schiff-base complexes are referred to as μ-dioxygen species[86].

No values for ν(O-O) have been reported for the μ-dioxygen Schiff-base species to test the correlation between r(O-O) and peroxide character of the coordinated dioxygen

ligand; ν(O-O) for the other μ-peroxo complexes are in the range 790 to 808 cm^{-1}, somewhat lower than for the triangular $M\langle^{O}_{O}$ species.

The differences in peroxide character have been attributed to the π-acceptor Schiff-base (and cyano) ligand system competing with the dioxygen for metal $d_{xz,yz}$ electron density[29]. It has been suggested that the tetranuclear complex $[(H_2O)$-(3-Fsalen)$Co(O_2)Co$(3-Fsalen-)$]_2$ is a bis-Co^{III}–O_2^-–Co^{II} species[84]. However, the low precision of the structure analysis renders tenuous any inferences made from differences in geometry about the two crystallographically independent cobalt atoms; moreover the other μ-dioxygen Schiff-base complexes have crystallographically imposed two-fold symmetry about the O-O linkage.

The N,N'-ethylene Schiff-base complexes, compared to the other μ-peroxo complexes, have torsion-angles τ(Co-O-O-Co) which are notably closer to that observed for hydrogen peroxide. This has been attributed to the minimisation of unfavourable contacts between the two μ-dioxygen-linked Schiff-base moieties of the square-planar Schiff-base rather than to just the Co–O$\langle^{O-Co}$ group[86]. Thus, these μ-dioxygen Schiff-base complexes form a small sub-group where the division between coordinated-peroxide and coordinated-superoxide formulations (under which almost all of the other metal-dioxygen may be classified) is blurred. Links between the various classes and types of dioxygen complexes are discussed further in §2.2.5.

One-electron oxidation of the decacyano,ammine and amine μ-peroxo complexes creates the μ-superoxo complexes. Such oxidation has not been reported for the μ-dioxygen Schiff-base species.

2.2.4 Superoxo Complexes.

Superoxo complexes are characterised by O-O separations less than 1.35 Å (average r(O-O) = 1.29(3) Å), and ν(O-O) is in the range 1075 cm^{-1} to 1163 cm^{-1} (Tables 2.1 and 2.2, Figure 2.4(b)); values for ν(O-O) and r(O-O) are known for only a few dioxygen adducts of this class (Figure 2.1(c)). The corresponding parameters for the free superoxide ion are 1.34 Å and 1090 cm^{-1}. Superoxo complexes are closely related to the peroxo complexes of types (c) M–O(O–M) and (d) M(O–O)M geometry with respect to the ligand system, metal centre and the end-on angular coordination of dioxygen. Dinuclear μ-superoxo complexes have long been known; mononuclear ones are of comparatively recent vintage, and it is only in the last four years that mononuclear iron-dioxygen complexes have been prepared and characterised without the agency of a protective protein envelope. Superoxo-cobalt complexes, in contrast to the peroxo analogues, are paramagnetic and the location of unpaired electron density may be probed using electron spin (paramagnetic) resonance spectroscopy, especially since the cobalt nucleus is paramagnetic (^{59}Co, I=7/2). Results obtained using ESR and uv-visible spectroscopy and other tehniques have also been used to support the superoxo-cobalt(III) formulations $Co^{III},Fe^{III}-O_2^-$ and $Co^{III}-O_2^--Co^{III}$. This other evidence will be examined in §3.1 and §4.1 for cobalt- and iron-dioxygen complexes, respectively.

Type (c) 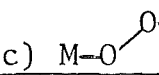 , Type (d) 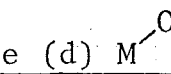

In contrast to the peroxo complexes of this geometry, the conformation for the Co-O-O-Co group is expected to be planar. Whereas in the peroxide ion the π_p and π_p^* orbitals are filled and there is no nett π bonding, in the superoxide ion there is still a nett half π bond so that a planar conformation is the most favoured. A bond angle $\angle$(Co-O-O) of 120^o is expected for sp^2-hybridised oxygen atoms.

Inspection of Table 2.2 shows that values of r(Co-O) for peroxo and superoxo complexes of this geometry are quite similar. Thus any π bonding between the half-filled $\pi_p^*(O_2^-)$ and the filled $3d_{xz,yz}(Co^{III})$ orbitals, which may occur for the superoxo-type complex but not for the peroxo-type, is minor.

Crystal packing effects may induce deviations from the ideal conformation. Indeed, in the crystal structure of the $[(CN)_5Co(O_2)Co(CN)_5]^{5-}$ anion, both rigorously planar and slightly non-planar conformations are observed[108]. This decacyano complex like its μ-peroxo analogue is somewhat anomalous; its two crystallographically independent anions have values for r(O-O) of 1.289(20) Å and 1.243(13) Å, and for r(Co-O) of 1.919(9) Å and 1.944(9) Å. The O-O separation is shorter and the Co-O separation longer than for other μ-superoxo complexes (Table 2.2). Moreover, in both the μ-superoxo and μ-peroxo decacyano complexes $r(Co-C_{ax})$ is shorter than $r(Co-C_{eq})$; in the analogous decammine and amine complexes $r(Co-N_{ax})$ is the same as or slightly longer than $r(Co-N_{eq})$.

The O-O stretching frequencies for the bridged trans-superoxo M-O^{O-M} species are in the range 1110 cm^{-1} to 1122 cm^{-1}, and for the bridged cis-superoxo M^{O-O}M species 1075 cm^{-1} to 1110 cm^{-1} [13]. This reduction is probably a kinematic effect.

At one time the "green paramagnetic" cobalt complexes (i.e. the superoxo type) were formulated as Co^{III}-O_2^{2-}-Co^{IV} species. However, ESR spectroscopy has shown this to be inappropriate[53].

Type (a) M-O^{O}

Preparation and structural characterisation of complexes of this type are quite recent. As will be shown in the next section these complexes are potential models for the haemoprotein class of oxygen-binding proteins. These complexes are synthetically closely related to the μ-peroxo M-O^{2-O-M} type. For example:-

$$[Co(CN)_5]^{3-} + O_2 \rightarrow [Co(CN)_5(O_2)]^{3-}$$

$$[Co(CN)_5O_2]^{3-} + [Co(CN)_5]^{3-} \rightarrow [Co(CN)_5(O_2)Co(CN)_5]^{6-}$$

The structure of the mononuclear $[Co(CN)_5O_2]^{3-}$ intermediate has been determined[78,79]. Curiously, $r(Co-C_{ax})$ is the same as $r(Co-C_{eq})$; this is in contrast to the dinuclear decacyano adducts.

A cobalt complex of this type (Co-O^{O}) has been structurally characterised and is described in Chapter 3. Several very precise structures of cobalt-dioxygen adducts of this type are now available[123-125]. The O-O separations range from 1.27(1) to 1.302(3) Å (Table 2.2); these are slightly shorter than the separations observed for most of the μ-superoxo complexes (1.31 to 1.35 Å, see also Figure 2.4(b). A shorter O-O bond length is consistent with the higher ν(O-O) wavenumber for the mono-

nuclear type; ν(O-O) is in the range 1120 - 1140 cm^{-1} (Table 2.1). This may, of course, be merely a kinematic effect. Except for $[Co(CN)_5(O_2)]^{3-}$, where the Co–O–O angle is 153(2)° [78], the Co–O–O angle is again close to 120° (as is found for the μ-superoxo species).

Two iron-dioxygen complexes have now been structurally characterised. Although various data support an Fe^{III}-O_2^- representation, analogous to that for cobalt-dioxygen systems, the apparent diamagnetism of these compounds[12,67] implies considerable covalency in a linkage formulated as $(d^5)Fe^{III}$-O_2^-. After a false alarm[14], ν(O-O) for iron-porphyrin-dioxygen complexes was determined to be in the range 1159 to 1163 cm^{-1}; for the corresponding cobalt complexes ν(O-O) was in the range 1150 to 1153 cm^{-1} [17]. The Fe-O separation, 1.75(2) Å for Fe(TpivPP)(1-Me-imid)(O_2), is apparently significantly shorter than the Co-O separation for cobalt-Schiff base-dioxygen complexes; the iron-axial ligand (Fe-N_{ax}) bond length is somewhat longer by comparison with Schiff base complexes.

A more detailed discussion on the structure of and bonding in mononuclear cobalt-and iron-dioxygen complexes may be found in Chapters 3 and 4 respectively, and Chapter 6.

2.2.5 Miscellaneous

Using the information gained from the potential model systems described in the previous subsections a clearer picture of the active site of oxygen-binding metalloproteins is possible. But before embarking on this course there are a number of threads from the previous subsections which may be woven together. There are four somewhat related matters to be considered:-

1. Does the oxidised metal-coordinated oxygen anion valence approach break down.

2. What other metal-dioxygen complexes not considered in §2.2.3 and §2.2.4 exist.

3. For a given metal centre what is the effect of changing its ligature on the metal-dioxygen linkage.

4. For a given ligature what factors influence the geometry of the dioxygen linkage as the metal centre is varied.

Does it Break Down

With the free peroxide ion having r(O-O) of 1.49 Å and ν(O-O) of $\sim$730 cm^{-1}, it would be difficult to rationalise, under the aegis of a coordinated-peroxide formulation, any dioxygen complex which had a value for r(O-O) significantly greater than 1.49 Å or a value for ν(O-O) substantially less than 730 cm^{-1}. It was this difficulty in accounting for the 1.63(2) Å O-O separation apparently observed for $[Ir(O_2)(Ph_2PCH_2CH_2PPh)_2]^+$ [95] that lead to the invocation of excited states of dioxygen [16] (see also §2.2.3). However, with the redetermination of this structure returning an oxygen-oxygen separation of 1.52(1) Å there now exist no structures where r(O-O) is significantly greater than 1.49 Å. Similarly the rarity of a cobalt(IV) or iron(IV) oxidation state means that cobalt- and iron-dioxygen complexes formulated as coordinated-superoxide species, $M^{III}-O_2^-$ or $M^{III}-O-O-M^{III}$, should not have an O-O separation significantly greater than the free superoxide ion value of 1.34 Å; nor should they have ν(O-O) substantially less than 1090 cm^{-1}. No exceptions to this have been observed. The only lower bound is that of free molecular oxygen (1.21 Å) which has also remained

inviolate.

The μ-dioxygen N,N'-ethylene Schiff-base complexes which, through their diamagnetism, betray their relationship to the μ-peroxo decammine complexes need not be considered grossly anomalous. Figure 2.5 illustrates a relationship between μ-dioxygen and μ-peroxide species as a function of the relative energies of metal and oxygen orbitals. Nonetheless they still remain as exceptions to the otherwise remarkably sharp division of dioxygen complexes into peroxo and superoxo classes on the basis of their O-O separations; they indicate that the nett electron transfer to dioxygen on its coordination to a metal is not always the near-integral number apparently observed in most other systems - namely, ∿1 electron for a superoxo species and ∿2 electrons for a σ-bonded peroxo species. For the π-bonded $M\begin{smallmatrix}O\\O\end{smallmatrix}$ species a division between a neutral covalent linkage and a polarised $M^{x+2}\text{-}O_2^{2-}$ appears to be observed; that is in the former there is little nett transfer of electron density onto dioxygen.

An apparent violation of the molecular oxygen upper bound for ν(O-O) was the solid-gas phase preparation of a dioxygen adduct of an iron porphyrin. The product had ν(O-O) values of 1663 and 1597 cm^{-1} [128] compared to the free molecular oxygen's wavenumber of 1556 cm^{-1}. However, other spectroscopic and magnetic evidence supported not an iron-dioxygen species but a donor-acceptor complex between dioxygen and the porphyrin species.

A number of complexes are known, for example $[RhCl(O_2)PPh_3)_2]_2$ (Figure 2.7)[102] where the distinction between a symmetrical triangular M<O>O species and an end-on bent M–O–M species is blurred. Involvement of the two orthogonally oriented $\pi^*_p(O_2)$ orbitals with the two rhodium atoms was postulated[102].

Between the peroxo and superoxo classes there is a correlation between r(O-O) and ν(O-O) (Tables 2.1, 2.2, 2.3, Figure 2.1(c)). But within a class (the peroxo class because it has more entries), there appears to be little or no correlation between r(O-O) and ν(O-O). Reasons for this could include crystal packing effects, non-purity of ν(O-O) and the low precision of many X-ray single crystal structure analyses of metal-dioxygen complexes.

Other Metal-Dioxygen Species

While iron-dioxygen complexes of M–O–M geometry in the solid state are unknown there has been a number of reports of such species existing in solution not just as transitory species on the way to the formation of a μ-oxo dinuclear complex. Recently oxygenation of cis-$[Fe^{II}(bt)_2(NCS)_2]$ (bt = 2,2'-bi-2-thiazoline) in non-aqueous media yielded a product "having properties consistent in which seven-coordinate iron(II) ions in the triplet S=1 ground state are bridged by singlet oxygen"[129]. Earlier it had been reported that iron(II) phthalocyaninetetrasulphonic acid reversibly coordinated dioxygen in a $2Fe:1O_2$ ratio in neutral aqueous solutions to give a proposed Fe-O-O-Fe species[130]. However it is as well to note that some iron(II)

Table 2.3 : r(O-O) and ν(O-O) for some dioxygen complexes.
Data plotted in Figure 2.1(c).

Compound	r(O-O) Å	ν(O-O) cm^{-1}	Reference
$Mo(p\text{-}CH_3TPP)(O_2)_2$	1.399(6)	964	[87]
$[Co(Ph_2PCH{=}CHPPh_2)(O_2)](BF_4)$	1.420(10)	909 (?)	[88,27]
$Cl_3OU(O_2)UOCl_3$	1.49(3)	905	[91]
$Ni(CNC(CH_3)_3)_2(O_2)$	1.45(1)	898	[175,176]
$Ti(OEP)(O_2)$	1.458(9)	898	[89]
$(CN)_2(PPhMe_2)_3Co(NC)Co(CN)_2(PPhMe_2)_2(O_2)$	1.441(11)	881	[132]
$CrO(py)(O_2)_2$	1.404(16)	875	[21]
$Mo(O_2)(HMPT)(py)$	1.441(15)	875,865	[179,180]
$K_3[Cr(O_2)_4]$	1.47(3)	875	[21]
$Mo(O_2)(HMPT)(H_2O)$	1.496(8)	875,865	[179,180]
$Cr(NH_3)_3(O_2)_2$	1.42(2)	865	[21]
$IrI(CO)(PPh_3)_2(O_2)$	1.51(3)	862	[171]
$[Rh(AsPhMe_2)_4(O_2)](ClO_4)$	1.46(2)	856	[94,172]
$[Ir(Ph_2PCH_2CH_2PPh_2)_2(O_2)](PF_6)$	1.52(1) (PF_6)	843(Cl)	[93,80]
$[O(O_2)_2Mo(OOH)_2MoO(O_2)_2][pyH]_2$	1.470(10)	832	[177,178]
$Pt(PPh_3)_2O_2\cdot CHCl_3$	1.505(16)	830	[173,174]
$[(NH_3)_5Co(O_2)Co(NH_3)_5](SO_4)_2$	1.473(10)	808	[106,168]
$[(en)_2Co(O_2,NH_2)Co(en)_2](SCN)_3$	1.46(SCN)	793 (NO_3)	[90,168]
$Co(bzacen)(py)(O_2)$	1.28(3)	1128	[126(b),170]
$[(NH_3)_5Co(O_2)Co(NH_3)_5](NO_3)_5$	1.312(~20)	1122	[73,169]
$[Co(CN)_5(O_2)][N(C_2H_5)_4]_3$	1.240(17)	1138	[78,338]

systems purported to coordinate dioxygen reversibly actually undergo complicated oxidation-ligand reduction reactions[131].

Recently a high-spin cobalt(II) dioxygen adduct, $[Co(pfp)(Hpfp)O_2]^-$ (pfp = perfluoropinacolato dianion), was reported. It was suggested that dioxygen was "attached to the metal by π-bonding"[133]. This high-spin species may represent an intermediate in the formation of an end-on bonded dioxygen complex. Definitive structural characterisation of this complex is awaited.

A paramagnetic iron-porphyrin dioxygen derivative has been reported[138], but its paramagnetism is due to incomplete oxygenation of the solid compound[137].

Influence of Other Ligands on the Geometry of Dioxygen Coordination

Cobalt is unique among transition metals in forming low-spin dioxygen complexes not only of the end-on angular type but also of the side-on triangular geometry. The dioxygen adduct of the cobalt(I) complex $[Co(Ph_2PCH=CHPPh_2)_2]^+$ has type (f) $M\langle^{O}_{O}$ geometry[88]. If the coordinated dioxygen molecule is regarded as a bidentate peroxo ligand (of unspecified hybridisation), then, in the dioxygen adduct, the cobalt centre not only possesses a formally desirable low-spin $Co^{III}d^6$ configuration but also the approximately octahedral coordination typical of other cobalt(III) complexes. "Soft" polarisable or π-acceptor ligands, such as phosphine, arsine, carbon monoxide and cyanide, feature as the supporting ligands. The role that this type of ligand plays in

encouraging triangular coordination of dioxygen is underlined in the reaction of dioxygen with the five-coordinate cobalt(II) complex $[Co^{II}(CN)_2(PPhMe_2)_3]$. The dioxygen adduct crystallised did not have end-on $Co-O^{O}$ or $Co-O^{O-Co}$ geometry, as might be expected by analogy with other five-coordinate cobalt(II) species such as $Co^{II}(NH_3)_5^{2+}$, but it had triangular $Co\langle^{O}_{O}$ geometry in a dinuclear formally cobalt(III) species[132].

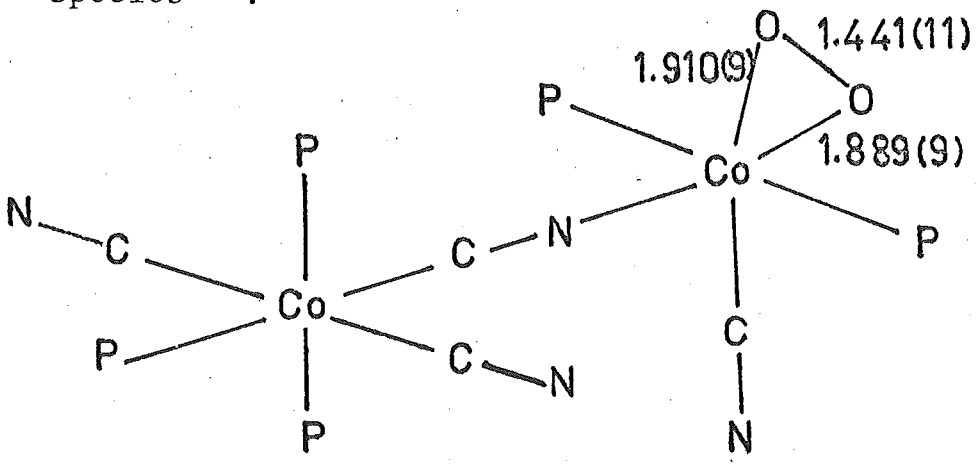

Figure 2.8: Stereochemistry of the dioxygen adduct of $Co^{II}(CN)_2(PPhMe_2)_3$

Replacement of the phosphine ligands of $Co^{II}(CN)_2(PPhMe_2)_3$ by weaker π-acceptor and "harder" cyano ligands perturbs the cobalt centre so that reaction of $Co^{II}(CN)_5^{3-}$ with dioxygen gives firstly a mononuclear superoxo $Co-O^{O}$ species which under suitable conditions reacts to give the more stable dinuclear μ-peroxo $Co-O^{O-Co}$ species. Schiff-base ammine and amine cobalt(II) complexes also give end-on dioxygen adducts.

Stabilisation of mononuclear end-on $M-O^{O}$ adducts over the dinuclear species may be enhanced by several factors. Firstly, and obviously, formation of a dinuclear adduct may be hindered or even prevented by steric factors; a cobalt-

cobalt separation of $\lesssim$4.7 Å must be attainable without unnaturally close ligand-ligand contacts if dioxygen is to bridge the two cobalt centres. Secondly, low temperatures enhance the stability of mononuclear adducts; or, more correctly, the reactivity of mononuclear adducts is decreased. Thirdly, aprotic solvents less polar than water discourage the aggregation of ionic species such as $[(CN)_5CoO_2]^{3-}$ into more highly charged ions. These factors are particularly important for iron porphyrin dioxygen adducts (Chapter 4), which in the absence of steric hindrance, or low temperatures and aprotic solvents are readily and irreversibly oxidised to a μ-oxo species:-

$$Fe^{III}-O^{2-}-Fe^{III}$$

A fourth factor which has more to do with the intrinsic nature of the ligand, rather than the environmental factors just mentioned, is that "hard" ligand systems, such as saturated amines, enhance formation of the dinuclear μ-peroxo species. The Schiff-base ligand which has π-acceptor/donor capability generally forms mononuclear cobalt dioxygen adducts. Dinuclear $M-O^{O-M}$ cobalt Schiff-base complexes are characterised by an unusually short r(O-O) (§2.2.3). More marked tendencies towards the formation of mononuclear dioxygen adducts are observed for cobalt porphyrins.

It is not easy to rationalise the observations that

1. "hard" strong σ-donor ligands such as saturated amine lead to μ-peroxo $M-O^{O-M}$ dioxygen adducts,
2. σ-donor ligands with π-acceptor/donor capabilities

lead to superoxo M–O–O dioxygen adducts, and

3. weak σ-donor, good π-acceptor ligands such as carbon monoxide and phosphines lead to side-on peroxo M(O–O) dioxygen adducts. The explanation that follows is not entirely satisfactory, but it is essentially an attempt to answer the question that is begged in the statement that "soft" ligands encourage coordination of dioxygen in a "soft"(?) manner."

By comparison with weak σ-donor good π-acceptor ligands, ligands which are strong σ donors but poor π acceptors will facilitate the transfer of electron density from the metal onto dioxygen. Equivalently expressed, a less polar metal-dioxygen linkage is to be expected if the supporting ligands are discouraging electron transfer from the metal onto dioxygen. While there is evidence for the formulation of side-on dioxygen-cobalt complexes as cobalt(III)-peroxo species

$$Co^{III}(O_2)^{2-}$$

(see below), there is also evidence, at least for platinum-metal complexes, which coordinate both dioxygen and ethylene, that the M(O–O) linkage is non-polar (§2.2.3). Evidence for a polar M–O–O–M linkage is adduced from the dioxygen-water hydrogen bonds invariably associated with the crystal structures of these species. In addition, sp^3-hybridised oxygen atoms are expected for a free peroxide ion from election-pair repulsion considerations; the peroxo complexes of the M–O–O–M type have M–O–O angles closer to the 108°

expected for sp^3-hybridised oxygen atoms than to the 120^o expected for sp^2-hybridised oxygen atoms (and observed for the superoxo complexes) (Table 2.2). Thus for these peroxo complexes, coordination of a "hard" σ-donor peroxide anion to give a $Co^{III}-O_2^{2-}-Co^{III}$ species is implied; a π-bonding component appears to be negligible.

Table 2.4 lists r(O-O) and ν(O-O) for the more precisely and, hopefully, more accurately determined cobalt-peroxo structures. The O-O separation appears to be marginally shorter and ν(O-O) somewhat higher for the side-on $M\langle^{O}_{O}$ type than for the end-on $M-O\langle^{O-M}$ type. Furthermore, for both types r(Co-O) is essentially identical; thus for the triangular species, but obviously not for the end-on species, this places the dioxygen π-electron density only ∿1.75 Å from the cobalt centre. Again, this may indicate greater covalency in the $Co\langle^{O}_{O}$ linkage than in the $Co-O\langle^{O-M}$ linkage. That for a side-on geometry r(O-O) is lengthened by both σ and π contributions complicates interpretation of differences in r(O-O) and ν(O-O) between the two types.

On the other hand, the electronic spectra of $[(diars)_2Co\langle^{O}_{O}]^+$ and the bonafide cobalt(III) complex $[(diars)_2Co(OH_2)_2]^{3+}$ are quite similar; a polarised species

$$Co^{III}\langle^{O}_{O}{}^{2-}$$

was inferred[82]. But, in the absence of spectra for a six-coordinate cobalt(I) complex, the possibility remains that the similarity is due to <u>intrinsic</u> geometrical factors rather than to a major electronic reorganisation of a

Table 2.4 : r(O-O) and ν(O-O) for selected cobalt dioxygen complexes.[a]

Compound	r(O-O) Å	ν(O-O) cm^{-1}	Reference
$[(NH_3)_5Co(O_2)Co(NH_3)_5](SO_4)_2 \cdot 4H_2O$	1.473(10)	808	[106,168]
$[(NH_3)_5Co(O_2)Co(NH_3)_5](SCN)_4$	1.469(6)	–[b]	[74]
$[(en)(dien)Co(O_2)(en)(dien)](ClO)_4$	1.488(6)	–[b]	[107]
$[(CN)_2(PPhMe_2)_3Co(NC)(Co(CN)_2(PPhMe_2)_2(O_2)]$	1.441(11)	881	[132,132]
$[(Co(Ph_2PCH=CHPPh_2)_2O_2]^+$	1.420(10)	905	[88,27]

[a] See Table 2.2 for more extensive compilations.

[b] Expected to be in the range 800-808 cm^{-1} [168].

cobalt(I) species consequent to the coordination of dioxygen. Moreover, the extent of electron transfer from cobalt onto dioxygen needed to change a cobalt(I) spectrum to a cobalt(III) type is unknown.

Thus, formation of a non-polar metal-dioxygen bond with $\sigma+\pi$ contributions is favoured by a side-on geometry. A polarised metal dioxygen linkage where the coordinated dioxygen has the hallmarks of an sp^3-hybridised peroxo species is favoured by end-on coordination; an sp^3-hybridised peroxide ion has no π-bonding capability and the peroxide ion can function only as a σ-donor ligand.

Metal and Other Influences on the Geometry of Dioxygen Coordination

Dioxygen adducts are known for porphyrin complexes of the following divalent transition metals, cobalt(II)$3d^7$ iron(II)$3d^6$, manganese(II)$3d^5$, chromium(II)$3d^4$, titanium-(II)$3d^2$, and molybdenum(II)$4d^4$.

The iron-dioxygen adducts[11] and cobalt-dioxygen adducts (by analogy with Schiff-base systems[63,123-126]) are observed to coordinate dioxygen in an end-on bent bond mode. A similar geometry has been deduced for the chromium-dioxygen adduct[134]. These complexes are best regarded as superoxo species. As such the metal has acquired a formal +III valence state and d^6 configuration for cobalt, d^5 for iron and d^3 for chromium - the valence states and configurations that are generally regarded as the most desirable for these elements. Moreover, the ease of one-electron oxidation[134(b)] for M^{II}(TPP)(2-Me-imid) species, $Cr^{II} > Fe^{II} > Co^{II}$, parallels

their affinity for dioxygen; the chromium complex binds dioxygen irreversibly[134] and dioxygen binds more readily to iron than to cobalt[137]. These complexes and other reasonably stable end-on superoxo-type complexes are six-coordinate and have a strong σ-donor ligand such as pyridine or imidazole trans to dioxygen (excepting $[Co(CN)_5O_2]^{3-}$). Five-coordinate $\overset{\backslash\backslash}{\underset{//}{Co}}\text{-}O\diagup O$ species are known through ESR spectroscopy but their stability is low[62(a),121], and, interestingly, a $Co(TPP)(CO)(O_2)$ complex with a similar low stability has also been detected - the carbon monoxide molecule presumably functioning entirely as a σ donor[121].

On the other hand, by coordinating dioxygen in a side-on peroxo mode, $Mn^{II}(TPP)$ formally achieves a desirable $d^3(Mn^{IV})$ configuration[98,99]. A molybdenum porphyrin (molybdenum is a member of the chromium group) by coordinating <u>two</u> molecules of dioxygen achieves a formal $d^o(Mo^{VI})$ valence state[87]. Similarly the dioxygen adduct of a titanium(II) porphyrin acquires a formal $d^o(Ti^{IV})$ state[89].

A similar trend for the metal centre to coordinate dioxygen in a manner that allows it to achieve a more usual or stable oxidation state is also observed for dioxygen adducts of d^{10} metal complexes. The few dioxygen adducts known are approximately square-planar if the triangularly coordinated dioxygen ligand is regarded as bidentate peroxo ligand[173,175]. Thus, the metal centre acquires a d^8 configuration; square-planar coordination is typical of d^8 species.

Conclusion

Naive crystal-field considerations predict that for octahedral 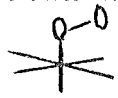 , quasi-octahedral 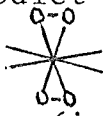 , or quasi-square pyramidal  geometries (in this case treating dioxygen regardless of its coordination mode as a single ligand) the following d-orbital splitting occurs

——— $d_{x^2-y^2}$)
) degenerate for pure octahedral symmetry
——— d_{z^2})

——— d_{xy})
) degenerate for pure octahedral symmetry
═══ $d_{xz,yz}$)

Thus, spin-paired-d^6, or d^3 configurations are favoured. For a square-planar geometry the d_{z^2} orbital is stabilised with respect to $d_{x^2-y^2}$. Thus a d^8 configuration is favoured. The coordination of dioxygen to metals appears such that the dioxygen ligand is formally reduced by one or two electrons (with concomitant and equivalent oxidation of the metal) so that the metal centre requires one of these stable configurations.

For a given metal, side-on  coordination of dioxygen is encouraged by "soft" π-acceptor ligands; end-on coordination 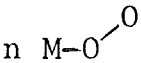 or 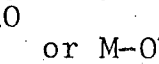 is encouraged, particularly the bridging geometry, by hard σ-donor ligands.

The valence state approach sketched by Vaska[13], with its oxidised metal-reduced molecular oxygen formalism, if not always accurately representing the electronic states of the metal and dioxygen ligand, certainly categorises all dioxygen complexes in an illuminating fashion.

The success of this approach is one factor which promotes confidence in deductions made from limited data about the mode of dioxygen coordination in biological systems.

2.3 Oxygen-Binding Proteins. Use of Model Compounds.

It is well-known that dioxygen binds to the metal atom of oxygen-binding metalloproteins. Thus simple model systems will assist in understanding the stereochemistry of the oxygen-binding site and the geometry of dioxygen coordination in such metalloproteins. In this section, characterisation of the binding site that has been achieved by the low-resolution X-ray crystal structure analyses of examples of these proteins and by comparison of $\nu(O\text{-}O)$ for dioxygenated metalloproteins with $\nu(O\text{-}O)$ for complexes of known stereo-chemistry is described. At a more sophisticated level, model complexes with a metal centre and ligature that approximate the active site of the protein may be constructed. The primary problem of such model studies is to incorporate aspects of protein function into the ligand system.

Two classes of oxygen-binding proteins are recognised. Firstly, there are the oxygen transport and storage proteins whose sole role is to bind dioxygen reversibly

$$\text{protein-M} + O_2 \rightleftharpoons \text{protein-M-}O_2.$$

It is interesting to note that aerobically respiring organisms have elaborate defence mechanisms to counter the presumably deleterious effects of the superoxide anion radical[139]. For example, in oxyhaemoglobin the coordinated dioxygen is susceptible to nucleophilic displacement by anions (X^-) to give the superoxide ion and met-Fe^{III}-haemoglobin which is inactive to dioxygen[140-142].

$$HbO_2 + X^- \rightleftharpoons \text{met-HbX} + O_2^-$$

The dismutation of the superoxide anion to hydrogen peroxide is catalysed by the copper-containing enzyme superoxide dismutase[139], and the dismutation of hydrogen peroxide to water by another copper-containing enzyme catalase[1]. Another enzyme met-haemoglobin reductase[1] exists to return met-haemoglobin to oxygen-active Fe^{II}-haemoglobin. The enzymes coexist with haemoglobin in the erythrocytes or red blood cells.

Secondly, there are metalloproteins which bind dioxygen for subsequent activation and utilisation as part of some catalytic cycle. In both classes an iron or copper atom is present at the active site.

To the uninitiated the naming of the oxygen-transport and -storage proteins is confusing. Haemoglobin, haemocyanin and haemerythrin are oxygen transport proteins; the prefix "haem" is derived from the Greek word "haima" for blood. However haemerythrin and haemocyanin are non-haem proteins; in particular haemerythrin is a non-haem iron-containing protein. Non-haem refers to the absence of an iron-porphyrin or haem as the prosthetic group. Hence, for example, haemoglobin which contains an iron-porphyrin complex as the prosthetic group is an haemoprotein; haemocyanin and haemerythrin are not. Oxygen-carrying proteins are generally composed of subunits each of which bind one molecule of dioxygen. Monomeric molecules similar to isolated subunits may be found in cell tissue where they store oxygen. Such species as often prefixed "myo" as in myoglobin and myohaemerythrin from the Greek root "muos" for muscle. Finally, haemoglobin which is composed of four myoglobin-like subunits is usually and loosely referred to as a tetrameric molecule.

2.3.1 Oxygen Transport/Storage Proteins

These proteins which are responsible for the transport of molecular oxygen to respiring cells or for the storage of dioxygen in regions of high oxygen demand such as muscle tissue may be divided into two subclasses - the haemocyanins and haemerythrins, and the haemoglobins which are, respectively, dinuclear and mononuclear with respect to the metal-to-dioxygen binding ratio.

Haemocyanin, Haemerythrin

This first subclass contains those proteins where the prosthetic group comprises only the metal ion. Various amino acid residues provide the supporting ligands for the active site. Haemocyanin is a copper-containing oxygen-carrying molecule found in certain molluscs and arthropods. In its oxygenated state it has a blue colour characteristic of copper(II). The active site is believed to be a dinuclear copper complex.

In probing the structure of its active site, resonance Raman spectroscopy has proved to be a valuable technique. The intensities of vibrations associated with a metal-ligand moiety can be selectively and greatly enhanced with respect to other vibrations by using some frequency within a metal-ligand electronic absorption band as the Raman excitation frequency. Using this technique, with the exciting frequency in the 570 nm band, ν(O-O) was found to be 742 cm^{-1}. A typical non-planar μ-peroxo $Cu^{II}-O_2^{2-}-Cu^{II}$ species was inferred[143] and confirmed in very recent resonance Raman studies on oxyhaemocyanin which, using the $^{18}O-^{16}O$ isotope, showed the oxygen atoms

to be equivalent[302]. The value of ν(O-O) is the lowest observed for any peroxo-complex.

Haemerythrins are a non-haem, iron-containing oxygen carrier found in a number of invertebrate phylla[144]. Again oxygen binds to the metal in a 2:1 ratio. The ν(O-O) frequency was observed at 844 cm^{-1} [145]. This observation together with a close similarity of the optical spectra for met-Fe^{III}-haemerythrin and oxy-haemerythrin support a peroxo-Fe^{III}-O_2^{2-}-Fe^{III} formulation[145]. Furthermore, the crystal structure of an octameric haemerythrin at 2.8 Å resolution reveals that the coordination geometry about pairs of iron atoms is trigonal antiprismatic; the antiprisms have one face in common (Figure 2.9 (a))[146].

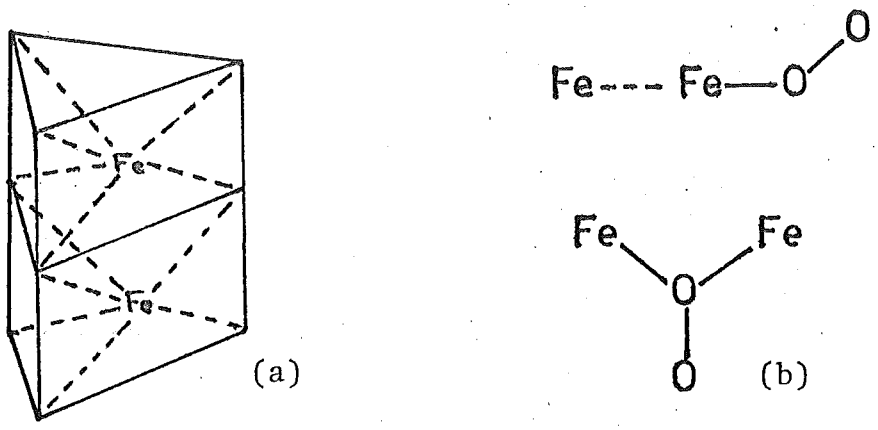

Figure 2.9: Coordination geometry of the iron centres in haemerythrin.

However, in a contemporaneous study on myohaemerythrin (a monomeric haemerythrin) at 5.5 Å resolution a different coordination geometry was proposed[147]. Recently, it was reported (result quoted in reference [302]) that for pairs of iron atoms in haemerythrin the Fe-Fe separation was less than 3.0 Å. Moreover resonance Raman spectroscopy using the

$^{18}O-^{16}O$ isotope showed the oxygen atoms in oxyhaemerythrin to be inequivalent[303] (c.f. oxyhaemocyanin). Thus unsymmetrical peroxo species were inferred (Figure 2.9(b)). The bridging peroxo geometry is not unrelated to the cobalt(III)-hydroperoxy complex[262]:-

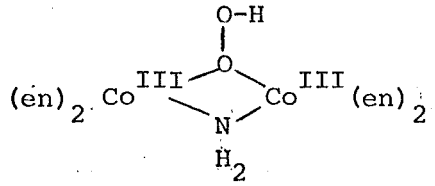

The weak correlation between ν(O-O) and r(O-O) (Figure 2.1(c) and Table 2.3) renders presumptuous any prediction of a longer O-O separation for oxyhaemocyanin compared to oxyhaemerythrin that is made on the basis of their different values for ν(O-O).

Haemoglobin

The second subclass are oxygen transport and storage haemoproteins often referred to as the haemoglobins after the best known example. This subclass is more pertinent to this thesis.

The prosthetic group is an iron porphyrin, in most cases protoporphyrin-IX, commonly called the protohaem or haem group when it is coordinated to iron (Figure 2.10).

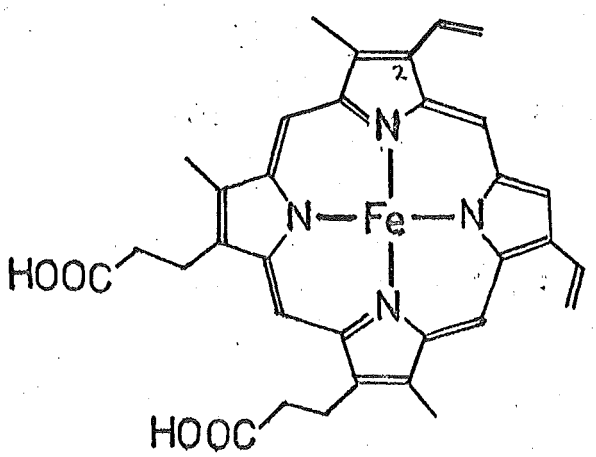

Figure 2.10: Protohaem (Iron protoporphyrin-IX).

The haem group is attached to the protein chain by axial ligation of the imidazole group of an histidine residue. This is commonly called the proximal histidine as opposed to the distal histidine which hovers above the dioxygen binding site on the other side of the haem. The haem group is oriented in the binding pocket by a host of van der Waals interactions. X-ray crystal structure analyses of various haemoproteins have shown that the haem group largely resides in a cleft in the protein and does not lie on the protein surface (for example refs.[148-151,167]). One molecule of oxygen may bind to each iron atom. As well as providing a fifth ligand, the protein has other essential functions such as protecting the haem centre from oxidation and consequent inactivation towards dioxygen, and modulating the absolute and relative affinity of the metal centre for dioxygen and competitor ligands such as carbon monoxide.

The iron atom of the prosthetic group may be replaced by cobalt to give cobalt-substituted haemoglobins, popularly known as coboglobins. These species also bind dioxygen reversibly[161,162]. Thus, cobalt-dioxygen complexes are relevant as models for oxygen-binding haemoproteins.

The simplest of the haemoglobins are the monomeric myoglobins (1Fe:1molecule:$1O_2$) which are primarily used to store oxygen in muscle tissue. Alteration of certain amino acids permits the formation of oligomers from myoglobin-like subunits. The best known of these is the tetrameric haemoglobin molecule. The association of myoglobin-like subunits into haemoglobin confers special physiologically desirable properties on the tetramer. Haemoglobin is able to bind

dioxygen cooperatively. That is, in its unliganded (unoxygenated) state haemoglobin has a lowered affinity for dioxygen compared to a protein-free iron-porphyrin-imidazole species[135]. Oxygen affinity increases as the degree of dioxygen ligation increases so that fully liganded oxyhaemoglobin has a dissociation constant for the first molecule of oxygen only slightly greater than that for myoglobin[152].

Models for the cooperative binding of dioxygen which explain the macroscopic thermodynamic data have been proposed[153,154]. Perutz's stereochemical model provides the most detailed molecular description of cooperativity[155-159]. In Chapter 5 implications of the structures of several model compounds for the prosthetic group (Chapters 3 and 4) on Perutz's model are discussed. Cobalt-substituted haemoglobins, mentioned earlier, also bind dioxygen in a cooperative manner[161,351].

The haemoglobins occur in all vertebrates as well as in some non-vertebrates but they are sometimes disguised under other names for non-mammalian phylla. Erythrocruorins which may have up to 400 protohaem groups per molecule are found in invertebrates such as annelid worms and insects[1]. Monomeric myoglobin-like monomers do exist[151]. A small number of species (e.g. annelid worms such as Spirographis) utilise chlorocruorohaem instead of protohaem (iron protoporphyrin-IX) as their prosthetic group[1]. Chlorocruorohaem is only a minor variant of protoporphyrin-IX (protohaem); a $-CH=CH_2$ group at position 2 is replaced not, as might be expected from its name, by chlorine but by a formyl group, -CHO. The prefix "chloro" derives from the Greek root chloros for green. Accordingly, in contrast to the reddish-purple

colour of other haemoglobins, including erythrocruorins, chlorocruorin (as it is called) has a green colour[1]. Apparently-minor changes in porphyrin substituents significantly perturb the electronic structure of the porphinato iron complex.

An ubiquitous feature of all haemoglobins is axial ligation of an histidine residue, except in mutants whose owners usually fare poorly because dioxygen binding is non-cooperative. Haemoglobins are not confined to the animal kingdon; they are also found in the root nodules of legumes[167, 293]. The geometry of the iron-dioxygen linkage has long been a source of speculation.

Pauling originally proposed a linear Fe-O-O covalent structure[67], and later a bent Fe-O(=O) model[68]. Griffith proposed a π-bonded triangular Fe(O)(O) model[69] and Weiss an iron(III)-superoxide Fe(III)-O_2^- model[70]. The final possibility was proposed by Gray and Mingos - a side-on $Fe^{IV}-O_2^{2-}$ species[71,301]. Resolution of the geometry of the iron-dioxygen linkage has only recently been achieved; the description of the electronic nature of the linkage is still a matter of controversy. The crystal structure of an iron-porphyrin dioxygen complex Fe(TpivPP)(1-Me-imid)(O_2) (reference [11] and Chapter 4) revealed end-on bent-bond geometry. Caughey and coworkers contemporaneously measured ν(O-O) and found the wavenumber (1107 cm^{-1} for oxyhaemoglobin[163] and 1103 cm^{-1} for oxymyoglobin[164]) to be typical of a superoxo species. Using Caughey's difference infrared technique ($^{18}O_2$ minus $^{16}O_2$) Collman and coworkers subsequently found ν(O-O) to be 1159 cm^{-1} for the model iron-dioxygen complex[17].

The previously reported values[14] were artefactual. Values have also been obtained for the cobalt analogues — 1105 cm^{-1} for cobaltdeuteroporphyrin-IX-substituted haemoglobin[165] and 1150 cm^{-1} for Co(TpivPP)(1-Me-imid)(O_2)[17]. See Table 2.1 for comparison with other metal-dioxygen complexes. Conceptual difficulties that may exist for an Fe^{III}-O_2^- representation of an essentially diamagnetic complex are discussed later.

Substituent effects and axial ligation endow haemoproteins with roles other than oxygen cartage or storage.

2.3.2 Oxygen-Utilising Proteins or Enzymes

A vast number of iron-and copper-containing proteins which coordinate and activate dioxygen for subsequent use in catalytic hydroxylation are known. There are two kinds, which are classified according to how molecular oxygen is incorporated into the substrate[1]:-

$$DH_2 + {}^{18}O_2 \xrightarrow{\text{oxygenase}} D({}^{18}OH)_2$$

and

$$DH_2 + {}^{18}O_2 + X\,H_2 \xrightarrow{\text{hydroxylase}} DH^{18}OH + X + H_2{}^{18}O$$

Knowledge and understanding of their structure and function at the molecular level is in many cases limited because the proteins are bound to cell membranes. However, cytochrome P450 hydroxylases are better characterised than most. Various stages in the catalytic cycle of the soluble cytochrome P450 camphor hydroxylase ($P450_{cam}$) have been identified[2]. Cytochromes P450 have a protohaem prosthetic group. However, highly distinctive electronic and magnetic

circular dichroism spectra of certain stages of the catalytic cycle indicate an axial ligation which is quite different from that observed for the oxygen-carrying haemoproteins. In the absence of X-ray crystal structure analyses for these proteins, model compounds have been extensively used to probe the nature of axial ligation. The catalytic cycle deduced for cytochrome $P450_{cam}$ and the inorganic models for its intermediates will be described in Chapter 4 when the structure of a possible model compound for the oxygenated intermediate is described.

CHAPTER 3

SCHIFF-BASE COMPLEXES

A Schiff base comprises the conjugated system:-

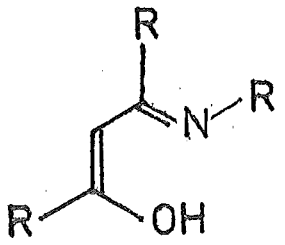

In its deprotonated anionic form it has been extensively studied as a bidentate chelate to transition metals, especially cobalt. A number of comprehensive reviews have been published[181,182,183,185]. The two parent Schiff bases, from which are derived most of the others used as chelating agents, are the quadridentate bridged species, N,N'-ethylenebis(acetylacetonimine (H_2acacen) and N,N'-ethylenebis(salicylidenimine) (H_2salen) shown in Figure 3.1 in their deprotonated dianionic chelating forms.

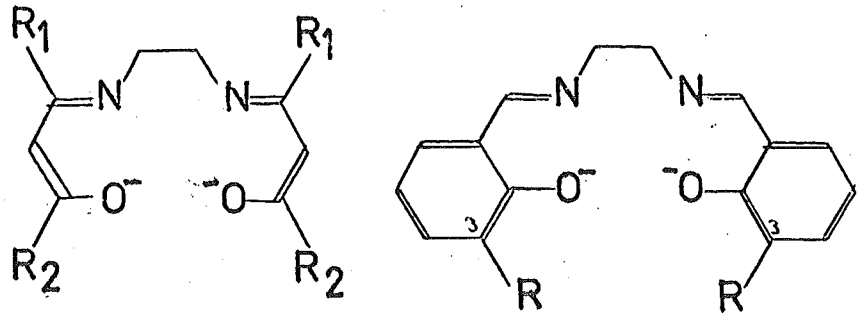

(a) $R_1 = R_2 = CH_3$ acacen , (b) R = H salen

$R_1 = CH_3$, $R_2 = C_6H_5$ bzacen = OCH_3 3-MeOsalen

Figure 3.1: Commonly used Schiff bases.

The equivalent names bis(acetylacetone)ethylenediimine (for H_2acacen) and bis(salicylaldehyde)ethylenediimine (for H_2salen) are sometimes used[183].

There are several notable features pertaining to the structure analyses of "salen" complexes regardless of the relative orientation which the two salicylideniminato residues adopt as a result of coordination to some metal. Firstly, each salicylideniminato residue remains approximately planar. Secondly, statistically insignificant differences are generally observed between bond distances and angles of the two residues which are formally chemically equivalent. Metal-ligand (Schiff base) separations are rather dependent on the metal, its spin state and the presence of other ligands.

The ability of cobalt(II) Schiff-base complexes to bind dioxygen has been known for some time[55,56,184]. The ability of the cobalt(III) species to coordinate carbanions is also well known[183]. Mononuclear dioxygen adducts of cobalt(II) complexes featuring aromatic quadridentate ligand systems such as Schiff bases are models for the oxygen-binding haem component of at least cobalt-substituted haemoglobin and myoglobin if not also of haemoglobin and myoglobin themselves. Carbanion complexes are models for the vitamin B_{12} (cobalamin) group of complexes (Figure 4.4) which, in their metabolically active form, feature a $Co^{III}-C^-$ σ bond[1,186,187]. These complexes are not unrelated to cobalt-dioxygen species which may be formulated as $Co^{III}-O_2^-$.

In this Chapter the structures of two Schiff-base complexes of the "salen" type are reported. The first complex α,α'-{2-(2'-pyridyl)ethyl}ethylenebis(salicylideniminato)iron(II), Fe(salen-C_2H_4-py), features a 2-ethylpyridyl appendage to the ethylene bridge of the parent Schiff base. Coordination of the pyridyl group is accompanied by considerable distortion of the quadridentate Schiff base. The geometry of this complex will be compared in some detail with its cobalt analogue [Co(salen-C_2H_4-py)]. C_2H_5OH whose structure has been reported briefly[9,10,188], but not discussed in any depth. For this and other reasons the structures of other five-coordinate cobalt(II) Schiff-base complexes will be alluded to.

The cobalt complex, unlike its iron analogue, forms an isolable mononuclear dioxygen adduct. On oxygenation the two salicylideniminato residues adopt the more familiar approximately coplanar conformation. This dioxygen adduct is compared with other mononuclear cobalt-dioxygen species. The stereochemical changes occurring on oxygenation will also be discussed in this Chapter, but some biological implications on models for cooperative binding of dioxygen in haemoglobin and cobalt-substituted haemoglobin will be left to a later chapter (Chapter 5). Evidence for and against the formulation of cobalt-dioxygen complexes as cobalt(III)-coordinated superoxide species ($Co^{III}-O_2^-$) will be assessed in §3.2.

3.1 The Crystal and Molecular Structure of α,α'-{2-(2'-pyridyl)ethyl}ethylenebis(salicylidenimato)iron(II), Fe(salen-C_2H_4-py).

In this subsection the crystal and molecular structure of the above-named compound is described and compared with its cobalt analogue and other related complexes. Because of their distinctive stereochemistry, the coordination geometry will be examined in some detail with reference to square-pyramidal and trigonal-bipyramidal species in §3.1.4.

3.1.1 Introduction

The structures of five-coordinate iron(II) and cobalt(II) complexes are of interest with regard to changes in geometry that occur on formation of a dioxygen adduct. These changes are of significance in attempting to understand the mechanism by which haemoglobin and cobalt-substituted haemoglobin achieve cooperative binding of dioxygen and of other small molecules such as carbon monoxide, nitric oxide and ethyl-isocyanide. Five-coordinate complexes of iron(II) and cobalt(II) have been reviewed although their spectral and magnetic properties were the main concern of that review[189].

Crystal structures of five-coordinate iron(II) and cobalt(II) complexes with a dianionic quadridentate ligand capable of assuming an essentially square-planar geometry (such as a porphyrin or Schiff base) and with an aromatic nitrogen heterocycle (such as imidazole or pyridine) are comparatively rare. In their crystal structures the tetraphenylporphinato complexes Fe(TPP)(2-Me-imid)[190], Co(OEP)(1-Me-imid)[192], Co(TPP)(1-Me-imid)[193], Co(TPP)-(1,2-Me_2-imid)[194], and Co(TPP)(3,5-lut)[195] are all square-

pyramidal; the iron complex is high-spin (S=2), the cobalt complexes are low-spin(S=½). The low-spin complex Co(salen)(py)[196] and the high-spin (S=3/2) complex Co(3-MeO-salen)(OH_2)[197] which feature a more flexible Schiff-base ligand system also exhibit square-pyramidal geometry in the crystalline state. On the other hand Co(3-Fsaltmen)(1-Bz-imid) has a distorted trigonal-bipyramidal geometry[198]; similarly for Co(salen-C_2H_4-py)[9,188] which is high-spin[199]. The complex Co(salbn⊕)(py),curiously, crystallises with two independent molecules in the asymmetric unit such that one molecule has square-pyramidal geometry and the other is considerably distorted towards trigonal-bipyramidal geometry[200]. The four-coordinate parent,Co(salen),has a tendency to crystallise as a low-spin oxygen-inactive dimer $[Co(salen)]_2$ of square-pyramidal structure[201,202]:-

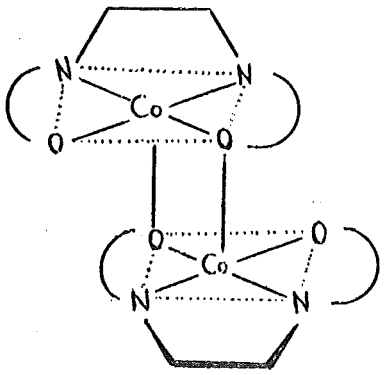

The sulphur-analague $[Co(Ssalen)]_2$ is a similarly constructed dimer[203].

Thus,while a number of five-coordinate cobalt(II) Schiff-base and porphyrin complexes with aromatic nitrogen axial ligation are structurally characterised,only the one

such iron(II) species has been reported. Structures of metal complexes with a pentadentate ligand system are rare irrespective of the metal. Five-coordinate iron(II) and cobalt(II) complexes with a quadridentate ligand system but with the fifth ligand being nitric oxide (NO) or carbon monoxide (CO) are known[204,205,206] but are not germane to this chapter.

Thus the structure of the iron(II) complex of the pentadentate ligand, α,α'-{2-(2'-pyridyl)ethyl}ethylenebis-salicylidenimine), is of interest.

3.1.2 Collection and Reduction of Intensity Data

The preparation, preliminary crystallographic characterisation and collection of data for Fe(salen-C_2H_4-py) were performed by Dr. Ward T. Robinson at Stanford University. Symmetry and systematic absences uniquely consistent with the monoclinic space group $P2_1/c$ (No.14)[207] were established by precession photography using Cu Kα X-radiation. A bright red plate-like crystal of maximum dimension 0.18 mm and 0.06 mm thick was chosen for data collection upon a Syntex $P2_1$ four-circle automatic diffractometer using graphite monochromatised Cu Kα (λ= 1.5418 Å) radiation. Cell dimensions -

$$a = 10.572(2),$$
$$b = 11.465(2),$$
$$c = 16.640(3)\ \text{Å}$$
$$\beta = 90.52(1)^{\circ}$$

and crystal orientation at 20°C were obtained by least-squares refinement of the setting angles of 10 accurately centred

reflections. For the empirical formula $FeC_{23}H_{21}N_3O_2$ (formula weight 427.3), the calculated and observed (obtained by flotation) densities for four formula units per unit cell (Z=4) were 1.41 and 1.40(1), respectively. Data were collected by the conventional $\theta/2\theta$ scan technique but the variable scan width, scan time and background time used were based on a preliminary scan through each reflection. Excluding systematic absences 2106 unique reflections were collected to a Bragg angle $2\theta_{max}$ of 50.0^{o} (i.e. to $\sin\theta/\lambda$ = 0.50). The 1118 reflections having $I>3\sigma_I$ were used in the determination and refinement of the structure. The coefficient for linear absorption, μ, was 63.1 cm^{-1}; and transmission coefficients ranged from $\sim$0.55 to $\sim$0.70. Although the absorption correction is therefore significant, it was not possible to correct the data for absorption effects.

Details on relevant crystallographic theory, definition of symbols, data reduction and computing aspects are provided in Appendix 1.

3.1.3 Solution and Refinement of the Structure.

Two possible positions for the iron atom were deduced from the Patterson synthesis. Least-squares refinements failed to discriminate between the two possibilities; both refinements led to a discouraging agreement factor, R ≃ 0.56. Direct methods were tried using symbolic addition procedures. Phases were obtained for 428 out of the 464 E-values having $E \geq 1.30$. Due to a program bug the E-map calculated had E-values all assigned identical magnitude. Perhaps surprisingly the E-map was still interpretable, although it

had to be contoured onto glass plates since the solution was not obvious from inspection of peak lists and interpeak distances and angles. One peak stood out above all others and its coordinates were consistent with those for one of the possible solutions of the Patterson synthesis for the unique iron atom position. Possible coordinates for the two salicylideniminato residues were extracted and the orientation of the pyridyl group estimated. The trial model comprised an iron and two nitrogen atoms with individual isotropic temperature factors, and three rigid groups each with a single isotropic temperature factor for the salicylideniminato residues (excepting the imine nitrogen atoms) and the pyridyl ring. The following dimensions were assumed for the rigid groups:- $r(C\text{-}C) = 1.39$ Å, $r(N\text{-}C) = 1.39$ Å, $r(C\text{-}O) = 1.32$ Å, $r(C\text{-}C_{C=N}) = 1.48$ Å, and $\angle(XYZ) = 120^{\circ}$. Four cycles of least-squares refinement of positional and thermal parameters together with an overall scale factor led to the following discrepancy indices:-

$$R = 0.26 , \quad R_w = 0.34 .$$

That the pyridyl group had been misplaced was obvious from the refinement. However, in the subsequent difference Fourier synthesis the pyridyl ring and the remaining carbon atoms were located in chemically reasonable positions. The pyridyl ring (a rigid group as before) and the carbon atoms (with individual isotropic temperature factors) were added to the model and their positional and thermal parameters were refined while the rest of the model was held constant.

Two cycles of least-squares refinement led to

$$R = 0.12 , \quad R_w = 0.14 .$$

Group constraints were now released. The idealised positions of hydrogen atoms attached to phenyl and pyridyl rings were derived, assuming r(C-H) = 1.08 Å, and the contributions of hydrogen atoms to the structure factors calculated assuming temperature factors $B_H = 6.0$ Å^2. All non-hydrogen atoms were refined for two cycles so that

$$R = 0.071, \quad R_w = 0.081.$$

In the subsequent difference Fourier synthesis most of the remaining hydrogen atoms on the tetrahedrally bonded carbon atoms were located. The positions of all hydrogen atoms were determined for an idealised tetrahedral or trigonal geometry, as appropriate, but with r(C-H) corrected to 1.0 Å. Isotropic temperature factors for hydrogen atoms were derived from those for the attached carbon atom by the following formula;-

$$B_H = B_C + 1.0 \text{ Å}^2.$$

Positional and thermal parameters of hydrogen atoms were recalculated after every cycle. The iron atom was allowed an anisotropic model for its thermal motion.

After three cycles of refinement with 122 variable parameters and using 1118 reflections having $I > 3\sigma_I$ convergence was achieved with

$$R = 0.056, \quad Rw = 0.062 .$$

The final scale factor to place the observed and calculated structure factors on the same scale was 1.0059(39). In the final cycle of refinement the ratios of the change in a parameter to its estimated standard deviation were all less

than 0.02. Further refinement with non-hydrogen atoms assigned anisotropic thermal parameters was not considered justified in terms of the available data and the non-correction for absorption. The final error in an observation of unit weight calculated for data used in refinement was 1.522 and was independent of $|F_o|$ and $\sin\theta/\lambda$; indicating that the weighting scheme (p=0.05) was satisfactory. For all data (with negative intensities set to zero) the error was 1.566 and the agreement factors were R = 0.155, R_w = 0.090. There was no evidence for secondary extinction among strong low angle reflections. There were no serious discrepancies among the unobserved data between $|F_c|$ and $|F_o|$ with respect to σ_I. Moreover for only 38 reflections out of 2401 were the calculated intensities outside the range

$$I-3\sigma_I < I_c < I + 3\sigma_I.$$

The final model is therefore considered to be accurate; although precision is moderate due to lack of high angle data.

Table A1 in the Appendix contains $|F_o|$ and $|F_c|$ for all data. Final atomic parameters are contained in Table 3.1.

Table 3.1 : Final atomic parameters for Fe(salen-C_2H_4-py).

Atom	X	Y	Z	B	Atom	X	Y	Z	B
Fe	07733(14)	24212(14)	65621(8)	-[b]	C(23)	5421(10)	2733(10)	8289(6)	5.2(2)
O(1)	-0168(6)	3419(5)	5812(3)	4.0(1)	C(24)	5282(10)	3760(10)	7878(6)	5.4(3)
O(2)	2269(5)	3342(5)	6856(3)	4.0(1)	C(25)	4204(9)	3967(9)	7406(6)	4.6(2)
N(1)	-0972(7)	1770(7)	6926(4)	3.85(17)	C(26)	3240(9)	3129(9)	7339(6)	4.0(2)
N(2)	1320(7)	1258(7)	7477(4)	4.19(18)	H(1A)	-157	030	753	-[d]
N(3)	1611(7)	1260(7)	5706(4)	4.19(18)	H(1B)	-104	133	813	-
C(1)	-0903(10)	0909(10)	7606(6)	5.5(3)	H(2)	054	-000	816	-
C(2)	0388(9)	0337(9)	7617(6)	4.7(2)	H(3A)	-011	-127	716	-
C(3)	0524(10)	-0659(10)	7007(6)	5.7(3)	H(3B)	140	-098	708	-
C(4)	0339(9)	-0426(9)	6119(6)	5.2(3)	H(4A)	-038	013	606	-
C(5)	1457(9)	0079(9)	5687(6)	4.5(2)	H(4B)	012	-118	585	-
C(6)	2299(10)	-0602(9)	5264(6)	5.2(3)	H(6)	222	-147	528	-
C(7)	3234(11)	-0114(11)	4826(7)	6.6(3)	H(7)	382	-062	451	-
C(8)	3372(11)	1091(11)	4823(7)	7.0(3)	H(8)	405	148	451	-
C(9)	2525(11)	1727(10)	5277(6)	6.1(3)	H(9)	261	260	528	-
C(10)	-2099(9)	2076(8)	6691(6)	4.2(2)	H(10)	-284	170	696	-
C(11)	-2326(8)	2926(8)	6068(5)	3.5(2)	H(12)	-430	269	615	-
C(12)	-3622(9)	3102(9)	5853(6)	4.6(2)	H(13)	-484	393	508	-
C(13)	-3927(10)	3833(10)	5235(6)	5.6(3)	H(14)	-328	498	439	-
C(14)	-3020(10)	4435(9)	4828(6)	5.3(2)	H(15)	-109	475	471	-
C(15)	-1740(9)	4308(8)	5012(6)	4.3(2)	H(20)	253	058	824	-
C(16)	-1377(9)	3522(8)	5655(5)	3.6(2)	H(22)	457	119	859	-
C(20)	2378(10)	1244(9)	7865(6)	4.5(2)	H(23)	621	258	860	-
C(21)	3359(9)	2096(8)	7809(6)	3.8(2)	H(24)	596	436	791	-
C(22)	4478(10)	1929(9)	8270(6)	5.1(3)	H(25)	412	473	711	-

[a] Fractional coordinates are generated by placing 0. prior to the first digit.

[b] Anisotropic thermal parameters for Fe: β_{11} = 0.00933(16), β_{22} = 0.00588(13), β_{33} = 0.00343(6), β_{12} = 0.00009(17), β_{13} =-0.00027(7), β_{23} = 0.00045(10) where the form of the anisotropic thermal ellipsoid is $\exp[\beta_{11}h^2 + \beta_{22}k^2 + \beta_{33}l^2 + 2\beta_{12}hk + 2\beta_{13}hl + 2\beta_{23}kl)]$. RMS components of thermal displacement along the principal ellipsoidal axes are 0.193(3), 0.220(2) and 0.233(2) Å.

[c] Hydrogen atom positions were not refined.

Hydrogen atom H(1A) bonded to carbon atom C(1), etc.

[d] Temperature factor derived from attached carbon atom $B_H = B_C + 1.0$.

3.1.4 Description and Discussion of the Structure

General Description of Structure and Packing

The crystal structure consists of well-separated molecules of Fe(salen-C_2H_4-py). The pentadentate "salen-C_2H_4-py" ligand coordinates so that the iron centre has a distorted trigonal-bipyramidal geometry. Figure 3.2 is a perspective view of one molecule; the atom labelling system used for this and other Schiff-base complexes described in this chapter is defined therein. Bond distances and angles for Fe(salen-C_2H_4-py) together with those of its cobalt analogue, for comparative purposes, may be found in Tables 3.2 and 3.3 respectively. The cobalt analogue crystallises with two crystallographically independent molecules in the asymmetric unit, and it is also noted that a salicylideniminato oxygen atom is hydrogen bonded to an ethanol solvate molecule - the orientation and O(1)... (H)-OC_2H_5 separation (2.82(2) Å) are strikingly similar for both Co(salen-C_2H_4-py)·C_2H_5OH species[9,188].

Figure 3.3 shows the packing of molecules of Fe(salen-C_2H_4-py) with respect to its unit cell. The only non-hydrogen intermolecular contacts less than 3.50 Å are:- O(2)... C(1) 3.40 Å, O(1)... C(2) 3.43 Å, C(6)... C(11) 3.47 Å and N(1)... C(3) 3.47 Å. The Fe... C(3) intermolecular separation is rather close at 3.53 Å. Non-hydrogen intermolecular contacts less than 3.75 Å are summarised in Table 3.4.

Both Fe(salen-C_2H_4-py) and its cobalt analogue are high spin; the iron complex has a magnetic moment of 5.14 BM (S=2)[208], the cobalt complex ∿4.25 BM (S=3/2)[199].

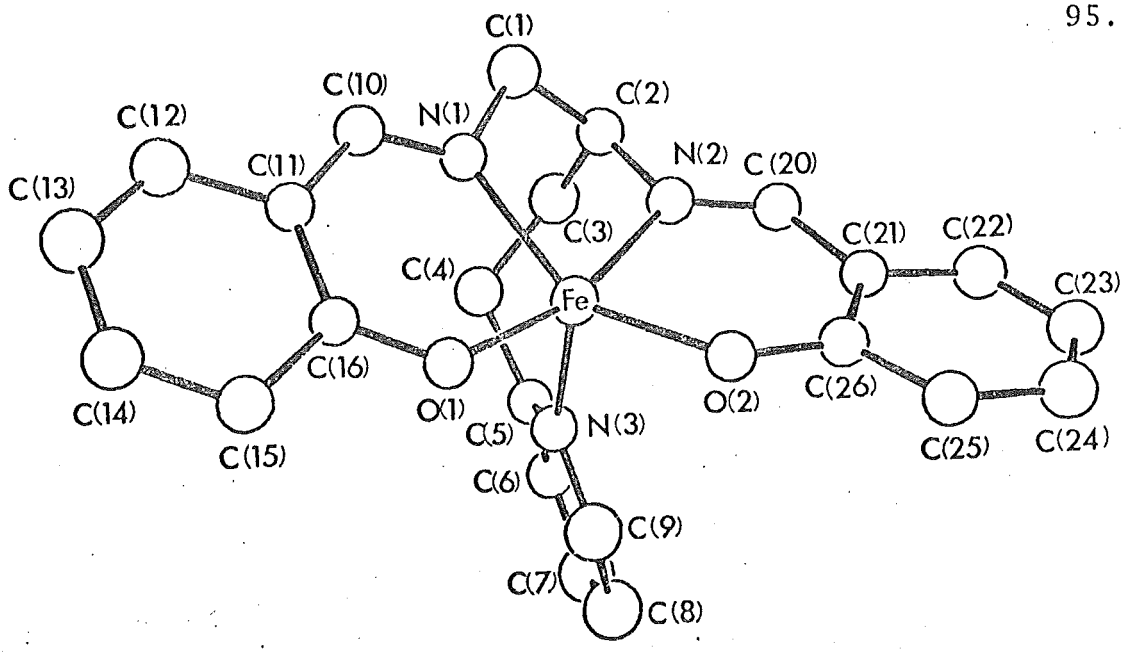

Figure 3.2 : Perspective diagram of Fe(salen-C_2H_4-py).

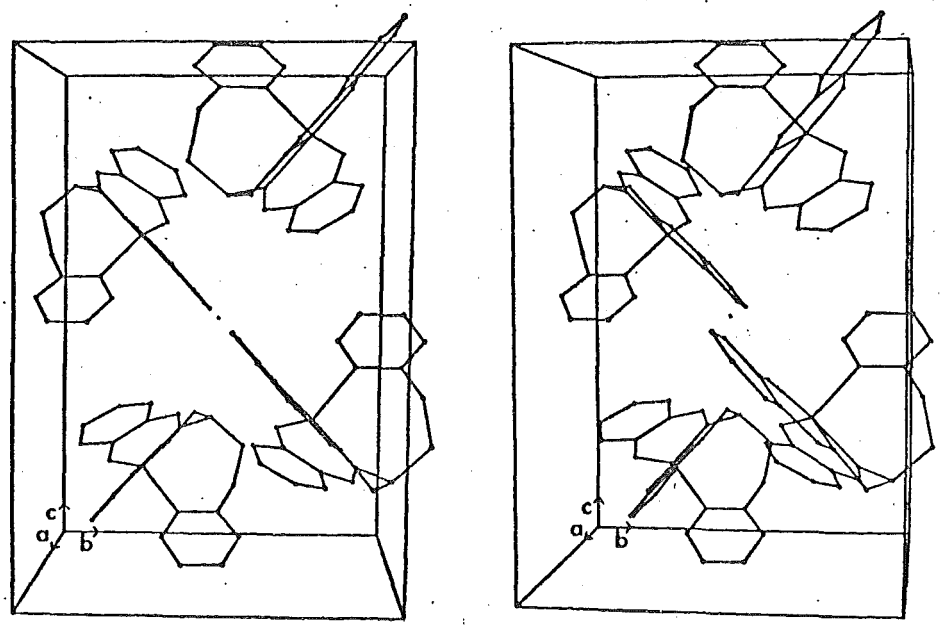

Figure 3.3 : Stereoscopic diagram of the packing of Fe(salen-C_2H_4-py) with respect to the unit cell.

Table 3.2 : Bond distances for Fe(salen-C_2H_4-py) and Co(salen-C_2H_4-py).

Atoms	Fe(salen-C_2H_4-py)		Co(salen-C_2H_4-py)(A)		Co(salen-C_2H_4-py)(B)		Average over class of "chem. equiv." bonds
	Distance(Å)	Average[a](Å)	Distance	Average[a]	Distance	Average[a]	
M-O(1)	1.958(6)	*	1.933(13)	*	1.939(13)	*	
M-O(2)	1.960(6)	1.959(6)	1.926(10)	1.930(13)	1.909(10)	1.924(13)	
M-N(1)	2.085(7)	*	1.945(14)	*	2.004(16)	*	
M-N(2)	2.101(8)	2.093(8)	1.929(17)	1.937(17)	1.992(16)	1.998(16)	
M-N(3)	2.147(8)	-	2.142(13)	-	2.147(14)	-	
N(1)-C(1)	1.503(11)	*	1.49(3)		1.48(3)	*	1.483(13)
N(2)-C(2)	1.464(11)	1.484(11)	1.48(2)	1.48(3)	1.48(2)	1.48(3)	
N(1)-C(10)	1.299(10)	*	1.28(2)	*	1.25(3)	*	1.276(16)
N(2)-C(20)	1.286(10)	1.293(10)	1.27(2)	1.28(2)	1.27(2)	1.26(3)	
O(1)-C(16)	1.307(9)	*	1.33(2)	*	1.31(2)	*	1.309(12)
O(2)-C(26)	1.320(10)	1.314(10)	1.30(2)	1.31(2)	1.30(2)	1.30(2)	
C(1)-C(2)	1.514(12)	*	1.50(3)	*	1.50(3)	*	
C(2)-C(3)	1.536(13)	*	1.57(3)	*	1.58(2)	*	
C(3)-C(4)	1.513(13)	*	1.50(3)	*	1.52(3)	*	
C(4)-C(5)	1.504(12)	1.517(14)	1.48(3)	1.51(4)	1.51(3)	1.53(4)	
C(10)-C(11)	1.441(11)	*	1.44(3)	*	1.43(3)	*	1.445(16)
C(20)-C(21)	1.429(11)	1.435(11)	1.46(2)	1.45(3)	1.47(3)	1.45(3)	
N(3)-C(5)	1.364(11)	*	1.42(2)	*	1.35(2)	*	
N(3)-C(9)	1.320(11)	1.342(11)	1.32(3)	1.37(3)	1.34(3)	1.34(3)	
C(5)-C(6)	1.382(12)	*	1.43(3)	*	1.38(3)	*	
C(6)-C(7)	1.354(13)	*	1.38(3)	*	1.36(3)	*	
C(7)-C(8)	1.389(14)	*	1.37(3)	*	1.33(3)	*	
C(8)-C(9)	1.384(14)	1.377(16)	1.41(3)	1.40(3)	1.39(3)	1.37(3)	
C(11)-C(12)	1.428(11)	*	1.41(3)	*	1.43(3)	*	1.419(16)
C(12)-C(13)	1.362(12)	*	1.36(3)	*	1.41(3)	*	1.370(21)
C(13)-C(14)	1.367(13)	*	1.37(3)	*	1.37(3)	*	1.375(11)
C(14)-C(15)	1.393(12)	*	1.34(3)	*	1.37(3)	*	1.373(22)
C(15)-C(16)	1.448(11)	*	1.43(3)	*	1.42(3)	*	1.424(14)
C(16)-C(11)	1.400(11)	*	1.41(3)	*	1.41(3)	*	1.429(18)
C(21)-C(22)	1.417(12)	*	1.41(3)	*	1.39(3)	*	
C(22)-C(23)	1.359(12)	*	1.35(3)	*	1.38(3)	*	
C(23)-C(24)	1.368(13)	*	1.37(3)	*	1.40(3)	*	
C(24)-C(25)	1.398(12)	*	1.38(3)	*	1.36(3)	*	
C(25)-C(26)	1.405(12)	*	1.42(2)	*	1.42(3)	*	
C(26)-C(21)	1.424(12)	1.397(29)	1.43(3)	1.39(3)	1.45(3)	1.40(3)	

[a] The e.s.d. about a mean is calculated from the dispersal of values about their mean for the case where there are three or more values in a class; otherwise the e.s.d. of an individual value is quoted.

Table 3.3 : Bond angles for Fe(salen-C_2H_4-py) and Co(salen-C_2H_4-py).

Atoms	Fe(salen-C_2H_4-py)		Co(salen-C_2H_4-py)(A)		Co(salen-C_2H_4-py(B)	
	Angle (°)	Average[a](°)	Angle	Average[a]	Angle	Average[a]
O(1)-M-N(1)	87.0(3)	*	91.8(6)	*	90.5(6)	*
O(2)-M-N(2)	86.8(3)	86.9(3)	92.5(6)	92.1(6)	90.2(6)	90.4(6)
N(1)-M-N(2)	78.5(3)	-	83.8(7)		82.9(7)	
O(1)-M-O(2)	104.4(3)	-	89.6(5)		94.0(5)	
N(1)-M-O(2)	146.6(3)	-	155.5(6)		149.2(6)	
N(2)-M-O(1)	165.4(3)	-	173.5(6)		172.8(7)	
N(1)-M-N(3)	110.0(3)	-	108.6(6)		110.3(6)	
N(2)-M-N(3)	88.6(3)	-	88.9(6)		88.3(6)	
O(1)-M-N(3)	98.6(3)	-	97.0(5)		96.8(6)	
O(2)-M-N(3)	99.4(3)	-	95.5(6)		99.4(6)	
M-N(1)-C(1)	114.6(6)	*	111.8(13)	*	112.5(14)	*
M-N(2)-C(2)	113.0(6)	113.8(6)	114.3(13)	113.2(13)	112.4(13)	112.4(13)
M-N(1)-C(10)	128.9(7)	*	128.6(14)	*	127.4(16)	*
M-N(2)-C(20)	127.2(7)	128.1(7)	129.0(15)	128.8(15)	130.3(16)	128.8(15)
M-O(1)-C(16)	132.1(6)	*	127.7(14)	*	130.0(14)	*
M-O(2)-C(26)	132.3(6)	132.2(6)	126.6(13)	127.1(14)	129.0(13)	129.5(14)
O(1)-C(16)-C(11)	124.2(9)	*	123.6(20)	*	121.1(19)	*
O(2)-C(26)-C(21)	123.6(9)	123.9(9)	125.5(19)	124.6(20)	124.0(19)	122.6(19)
N(1)-C(10)-C(11)	123.0(9)	*	123.5(19)	*	123.4(21)	*
N(2)-C(20)-C(21)	125.9(10)	124.5(10)	123.3(19)	123.4(19)	121.5(20)	122.5(20)
C(10)-C(11)-C(16)	124.6(8)	*	124.3(21)	*	126.8(20)	*
C(20)-C(21)-C(26)	122.9(9)	123.8(9)	122.0(18)	123.2(21)	123.0(19)	124.9(20)
O(1)-C(16)-C(15)	117.1(8)	*	118.1(20)	*	119.9(20)	*
O(2)-C(26)-C(25)	118.8(9)	118.0(9)	117.3(19)	117.7(20)	121.0(20)	120.4(20)
C(10)-N(1)-C(1)	116.2(8)	*	119.0(17)	*	119.8(18)	*
C(20)-N(2)-C(2)	119.6(8)	117.9(8)	116.3(18)	117.7(18)	117.3(18)	118.6(18)
N(1)-C(1)-C(2)	109.3(8)	*	112.5(18)	*	111.8(18)	*
N(2)-C(2)-C(1)	107.1(8)	*	104.7(17)	*	107.6(17)	*
N(2)-C(2)-C(3)	111.4(8)	*	113.4(17)	*	109.1(17)	*
C(1)-C(2)-C(3)	113.8(8)	*	109.1(18)	*	110.6(18)	*
C(2)-C(3)-C(4)	120.1(9)	*	119.8(18)	*	121.3(18)	*
C(3)-C(4)-C(5)	116.1(9)	113.0(47)	116.8(20)	112.7(54)	115.4(17)	112.6(50)
M-N(3)-C(5)	125.5(7)	-	126.1(15)	-	127.1(15)	-
M-N(3)-C(9)	114.6(7)	-	116.2(15)	-	115.0(15)	-
C(5)-N(3)-C(9)	118.6(9)	*	117.5(19)	*	117.8(19)	*
N(3)-C(5)-C(6)	119.7(10)	*	119.8(21)	*	121.8(20)	*
C(5)-C(6)-C(7)	121.2(10)	*	117.4(23)	*	118.9(21)	*
C(6)-C(7)-C(8)	119.3(11)	*	123.8(23)	*	120.3(23)	*
C(7)-C(8)-C(9)	117.0(11)	*	115.7(21)	*	119.2(22)	*
C(8)-C(9)-N(3)	124.1(11)	120.0(4)	125.4(21)	119.9(39)	121.9(21)	120.0(17)
C(4)-C(5)-N(3)	117.8(9)	-	118.3(21)	-	117.5(20)	-
C(4)-C(5)-C(6)	122.6(10)	-	121.9(22)	-	120.4(20)	-
C(10)-C(11)-C(12)	115.5(9)	*	117.0(22)	*	114.6(22)	*
C(20)-C(21)-C(22)	118.3(9)	116.9(9)	119.7(18)	118.4(22)	115.7(21)	115.1(21)
C(11)-C(12)-C(13)	119.8(10)	*	122.4(22)	*	122.4(22)	*
C(12)-C(13)-C(14)	121.5(10)	*	117.1(22)	*	115.8(22)	*
C(13)-C(14)-C(15)	121.6(10)	*	125.3(22)	*	124.8(22)	*
C(14)-C(15)-C(16)	118.5(9)	*	118.4(21)	*	119.4(21)	*
C(15)-C(16)-C(11)	118.7(8)	*	118.3(21)	*	119.1(20)	*
C(16)-C(11)-C(12)	119.9(9)	*	118.7(21)	*	118.2(21)	*
C(21)-C(22)-C(23)	121.9(10)	*	124.6(19)	*	121.3(22)	*
C(22)-C(23)-C(24)	119.8(10)	*	116.2(21)	*	118.1(21)	*
C(23)-C(24)-C(25)	120.7(10)	*	124.0(22)	*	122.1(21)	*
C(24)-C(25)-C(26)	121.0(10)	*	120.0(20)	*	122.3(20)	*
C(25)-C(26)-C(21)	117.6(9)	*	117.0(19)	*	114.9(20)	*
C(26)-C(21)-C(22)	118.7(9)	120.0(14)	118.0(19)	120.0(32)	121.2(20)	120.0(29)
C(S2)-C(S1)-O(S1)			111.2(23)		117.1(23)	

[a] See footnote (a) of Table 3.2.

Table 3.4 : Non-hydrogen intermolecular contacts for Fe(salen-C_2H_4-py) less than 3.75 Å.

Atoms	Distance
Fe ...C(3)	3.53
O(1)... C(2)	3.43
O(1)... C(15)	3.58
O(2)... C(1)	3.40
O(2)... C(3)	3.70
O(2)... C(2)	3.73
N(1)... C(3)	3.47
C(4)... C(5)	3.56
C(6)... C(11)	3.47
C(6)... C(10)	3.67
C(6)... C(12)	3.70
C(7)... C(10)	3.58
C(7)... C(12)	3.63
C(7)... C(11)	3.67
C(8)... C(23)	3.62
C(8)... C(22)	3.64
C(12)... C(25)	3.61
C(12)... C(24)	3.65
C(13)... C(13)	3.59

Stereochemistry About the Metal Centre

The coordination geometry about the iron and also the cobalt centre may be described as a trigonal-bipyramidally distorted square pyramid or, more simply, a distorted trigonal bipyramid. The O(1)-Fe-N(2) group is the quasi-trigonal axis; the bond angle is 165.4(2)° (173.5(6)° and 172.8(7)°). Here and elsewhere a parameter for Fe(salen-C_2H_4-py), is followed, where appropriate, by the corresponding parameters for Co(salen-C_2H_4-py) molecule A and molecule B, respectively, in parentheses. Figure 3.4 shows some of the differences among the three molecules.

While the cobalt and iron complexes share a basically similar geometry there are significant differences in metal-ligand bond lengths. The metal-pyridyl nitrogen separations r(M-N_{py}) for the cobalt species are insignificantly different from those observed for Fe(salen-C_2H_4-py) (2.147(8) Å). Compared with the two independent molecules A and B of Co(salen-C_2H_4-py), the Fe-O_{salen} separations, 1.958(6) and 1.960(6) Å, are marginally longer but the Fe-N_{salen} separations, 2.085(7) and 2.101(8) Å, are longer by more than 0.14 Å (for molecule A) and by more than 0.08 Å (for molecule B). The differences in Co-N_{salen} separations for molecules A and B are significant at a confidence level greater than three e.s.d.s for the difference. These differences had been considered to be insignificant[188]. Associated with the longer r(Fe-N_{salen}) is a more obtuse O(1)-Fe-O(2) bond angle of 104.4(3)° (89.6(5)° and 94.0(5)°). While other bond angles in the salen component generally show somewhat smaller but still significant differences, the bond angles about the metal

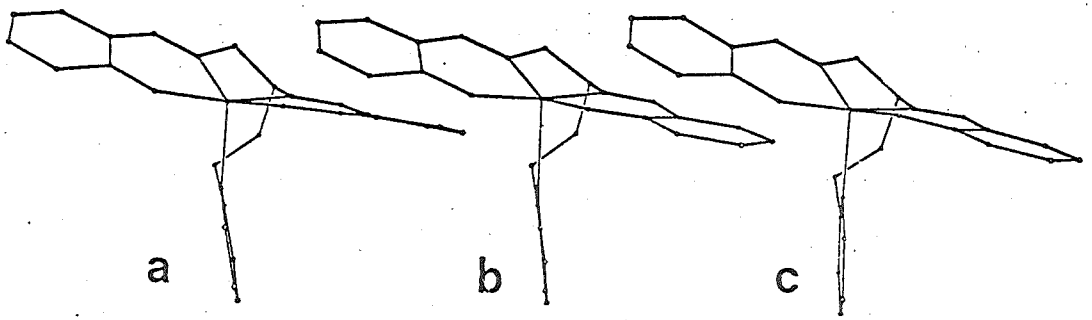

Figure 3.4 : Perspective diagram of (a) Fe(salen-C_2H_4-py), (b) Co(salen-C_2H_4-py) A and (c) Co(salen-C_2H_4-py) B. Identical vectors are used to define the orientation of the molecules.

involving the salen ligand and the pyridyl nitrogen atoms are reasonably similar for the iron and cobalt complexes.

The bond lengths about the iron atom are generally similar to those for the molecule of Co(salbn®)(py) that has distorted trigonal-bipyramidal geometry[200].

The geometry of the metal-ligand system may be quantified in a number of ways—firstly by looking at the N(1)-O(1)-O(2)-N(2) torsional angle and the twisting of the two salicylideniminato residues, and secondly by applying the Zemann test[209] to summarise deviations from ideal square-pyramidal or trigonal-bipyramidal geometries. Correlations between basic geometry, metal-ligand bond lengths and spin state are also discussed.

1. In contrast to the non-covalently linked pyridyl species Co(salen)(py) which, as a consequence of a crystallographically imposed mirror plane, has a torsional angle τ(N(1)-O(1)-O(2)-N(2)) of 0^{o} (that is, the N(1),O(1),O(2),-N(2) group is planar) and square-pyramidal geometry[196], the iron and cobalt complexes of "salen-C_2H_4-py" have a markedly non-planar N(1),O(1),O(2),N(2) group. The mean absolute displacement of atoms from their least-squares plane is 0.213 Å (0.157 Å and 0.217 Å) and the torsional angle τ(N(1)-O(1)-O(2)-N(2)) is $16.3(3)^{o}$ ($12.5(5)^{o}$ and $17.2(5)^{o}$).

The chelate rings are approximately planar (Chel-1 = M, O(1),C(16),C(11),C(10),N(1), similarly for Chel-2). In both the iron and cobalt structures Chel-1 displays smaller departures from planarity than Chel-2; the mean absolute displacements are 0.015 Å (0.023 and 0.026 Å) and 0.050 Å (0.049 and 0.057 Å), respectively. They are approximately

Table 3.5 : Selected unweighted least-squares planes for Fe(salen-C_2H_4-py) and Co(salen-C_2H_4-py).

Plane	Equation of Plane[b] Ax + By + Cz - D = 0 (Coeff x 10^4)				Atoms in Plane / Deviations of Atoms from Plane (Å x 10^3)[a]								Displacement of Other Atoms from Plane (Å x 10^3)[a]	
I[c]					N(1)	O(1)	N(2)	O(2)					M	
	3130	-6212	-7184	-96629	-231(7)	197(6)	230(7)	-195(6)					319(1)	
	-4275	-8867	-1758	-19452	160(15)	-153(12)	-161(17)	153(12)					-250(3)	
	-8188	5528	-1550	-83253	222(18)	-208(15)	-225(18)	211(13)					293(3)	
Py					N(3)	C(5)	C(6)	C(7)	C(8)	C(9)			M	C(4)
	-6042	0653	-7941	-84080	-014(7)	021(10)	-014(10)	000(12)	007(12)	000(11)			-516(1)	130(10)
	5797	-4155	-7009	5502	026(16)	-039(22)	028(28)	-004(24)	-010(22)	-001(22)			293(3)	-105(21)
	3467	6119	-7109	-66637	001(16)	006(20)	-010(21)	009(24)	-002(23)	-002(21)			120(3)	-108(25)
Ph-1					C(11)	C(12)	C(13)	C(14)	C(15)	C(16)				
	0674	-7541	-6532	-92993	002(9)	-009(10)	010(11)	-004(10)	-003(10)	003(9)				
	-2180	-9697	-1106	-17587	010(21)	-005(18)	-002(22)	004(22)	002(21)	-008(21)				
	-6512	7554	-0729	-89112	-026(23)	031(23)	-018(23)	000(25)	004(22)	009(22)				
Ph-2					C(21)	C(22)	C(23)	C(24)	C(25)	C(26)				
	4514	-4304	-7817	-96222	-020(9)	-006(10)	023(10)	-013(10)	-013(10)	029(9)				
	-5052	-8228	-2603	-21047	-021(19)	006(20)	006(22)	-004(21)	-012(21)	023(20)				
	-8395	4788	-2568	-83583	017(22)	-016(26)	007(23)	-002(24)	004(23)	-011(22)				
Sal-1					N(1)	C(10)	C(11)	C(12)	C(13)	C(14)	C(15)	C(16)	O(1)	M
	0625	-7361	-6740	-93925	061(7)	-008(9)	-041(9)	-034(10)	022(11)	031(10)	016(10)	-018(9)	-028(6)	035(2)
	-2186	-9679	-1244	-17910	-061(15)	037(18)	028(21)	006(18)	-009(22)	-015(22)	-013(21)	-003(21)	031(12)	-029(3)
	-6526	7538	-0768	-89255	-051(17)	046(22)	-025(23)	033(23)	-021(23)	-008(25)	-005(22)	004(22)	027(14)	-026(3)
Sal-2					N(2)	C(20)	C(21)	C(22)	C(23)	C(24)	C(25)	C(26)	O(2)	M
	4404	-4676	-7664	-95997	-046(7)	-043(10)	029(9)	048(10)	033(10)	-056(10)	-065(10)	023(9)	076(6)	250(1)
	-5008	-8275	-2538	-20812	-000(17)	020(21)	-035(19)	-005(20)	006(22)	006(21)	-004(21)	019(20)	-007(12)	-200(3)
	-5434	4714	-2578	-83580	-056(18)	-047(21)	027(22)	-015(26)	-003(23)	-014(24)	000(23)	-004(22)	016(13)	-291(3)
Chel-1					M	N(1)	C(10)	C(11)	C(16)	O(1)				
	0478	-7193	-6930	-95223	-007(2)	022(7)	-016(9)	-010(9)	023(9)	-012(6)				
	-2061	-9682	-1419	-17955	005(3)	-036(15)	036(18)	001(21)	-032(21)	025(12)				
	-6483	7563	-0875	-89995	-005(3)	-031(17)	053(22)	-033(23)	-009(22)	025(14)				
Chel-2					M	N(2)	C(20)	C(21)	C(26)	O(2)				
	4773	-5060	-7185	-89838	077(1)	-073(7)	003(10)	071(9)	-023(9)	-055(6)				
	-5390	-8109	-2278	-22746	-075(3)	058(17)	016(21)	-072(10)	018(20)	056(12)				
	-8872	4069	-2176	-80850	-082(3)	039(18)	031(22)	-056(22)	-032(22)	100(14)				

[a] Displacements of atoms are from a fixed plane and hence the accompanying e.s.d's are derived only from the e.d.s.'s in the positional coordinates of the atoms.

[b] The coefficients of the least-squares plane are for an orthogonalised Angstrom coordinate system.

[c] The first line of numbers for each plane pertains to Fe(salen-C_2H_4-py); the succeeding two lines to Co(salen-C_2H_4-py) molecules A and B, respectively.

Table 3.6 : Selected dihedral angles (in °) between least-squares planes for Fe(salen-C_2H_4-py) and Co(salen-C_2H_4-py).

	Ph-1	Ph-2	Py	Sal-1	Sal-2	Chel-1	Chel-2
I[a]	16.5	14.0	70.1	16.1	11.8	16.3	11.5
	13.5	7.5	75.9	13.2	7.0	13.7	8.3
	15.8	7.3	80.5	15.7	7.7	15.8	9.9
Ph-1	-	30.1	64.6	1.6	28.0	3.2	28.0
	-	20.5	69.3	0.8	20.0	1.9	21.7
	-	22.0	73.2	0.3	22.5	0.9	25.7
Ph-2		-	71.3	29.3	2.4	29.2	5.8
		-	76.6	20.1	0.5	20.3	2.8
		-	79.4	21.8	0.5	21.7	5.4
Py			-	63.3	71.8	61.7	75.6
			-	68.7	76.6	67.5	79.4
			-	73.2	79.7	72.5	84.5
Sal-1				-	27.3	1.7	27.6
				-	19.6	1.2	21.4
				-	22.3	0.7	25.5
Sal-2					-	27.3	4.1
					-	19.9	2.8
						22.2	5.0
Chel-1						-	27.8
						-	21.8
						-	25.6

[a] See footnote (c) Table 3.5.

coplanar with their host phenyl groups which are defined:- Ph-1= C(11), C(12), C(13), C(14), C(15), C(16), and Ph-2, similarly . The dihedral angles are 3.2° (1.9° and 0.9°) between planes Chel-1 and Ph-1, and 5.8° (2.8° and 5.4°) between planes Chel-2 and Ph-2. The dihedral angle between the two chelate rings is 27.8° (21.8° and 25.6°) and between the two phenyl-groups 30.1° (20.5° and 22.0°). Table 3.5 lists the equations of a number of least-squares planes together with the atoms comprising the plane and their deviations therefrom; Table 3.6 gives the dihedral angles between the planes.

2. The Zemann test[209] may be used to summarise in a semi-quantitative manner whether a pentagonally-coordinated species approximates more closely to square-pyramidal or to trigonal-bipyramidal geometry. The residual Δ is defined:-

$$\Delta = \sum_{i=1}^{10} |\angle(XMX_{obs})_i - \angle(XMX_{theor})_i| / \sum_{i=1}^{10} \angle(XMX_{theor})_i$$

where $\angle(XMX_{obs})$ is the observed angle and $\angle(XMC_{theor})$ is the angle calculated for idealised square-pyramidal or trigonal-bipyramidal geometry (Figure 3.5). In the square-pyramidal case the displacement of the metal atom from the least-squares plane, comprising atoms N(1), O(1), N(2) and O(2), and the average metal to Schiff-base ligand (as the quasi-square plane) separation must be calculated as a prerequisite to the derivation of certain bond angles for the idealised square-pyramidal geometry.

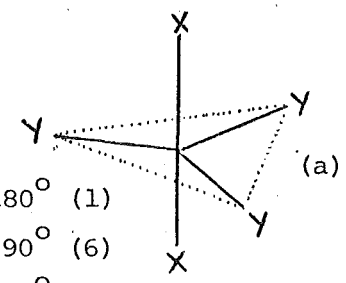

$\angle(XMX) = 180^{o}$ (1)

$\angle(XMY) = 90^{o}$ (6)

$\angle(YMY) = 120^{o}$ (3)

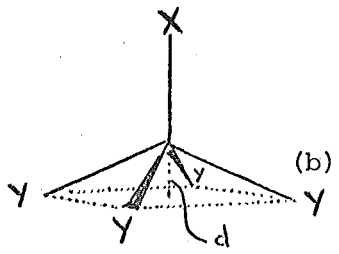

$$\angle(XMY) = 90^{o} + \sin^{-1}\frac{d}{r(M-Y)} \quad (4)$$

$$\angle(YMY) = \cos^{-1}\frac{d^{2}}{r(M-Y)^{2}} \quad (4)$$

$$\angle(YMY) = 2\cos^{-1}\frac{d}{r(M-Y)} \quad (2)$$

Figure 3.5: Idealised geometries; (a) trigonal-bipyramidal and (b) square-pyramidal. Number of each type in parentheses.

The residuals for Fe(salen-C_2H_4-py) and a number of other five-coordinate Schiff base-cobalt structures are tabulated in Table 3.7. The residual for a perfect trigonal bipyramid viewed as distorted perfect square pyramid (and vice versa) are also tabulated. The higher residuals for both a square-pyramidal and trigonal-bipyramidal description of Fe(salen-C_2H_4-py) than the corresponding residuals for Co(salen-C_2H_4-py) indicate greater distortion for Fe(salen-C_2H_4-py) not only from a trigonal-bipyramidal geometry but also from a square-pyramidal geometry. Co(salen-C_2H_4-py) A is closer to square-pyramidal geometry than molecule B. Furthermore, the metal-Schiff base ligand bond lengths of A are marginally shorter than those of B. This may be attributed to the greater cobalt-Schiff base π bonding with consequent shortening of metal-ligand separations that is possible for the structure which more closely approximates to square-pyramidal geometry; π bonding will be maximal for square planar or octahedral geometries. More pronounced differences in general geometry and bond lengths are observed for the two crystallographically independent molecules of

Table 3.7 : Zemann test for square-pyramidal and trigonal-bi-pyramidal conformations for selected Schiff-base complexes.

Compound		d[a]	r(M-Y)[a]	Residual Δ Sq.py.	Trig.bipy[b]	Trig.bipy[b]	Reference
AB_5 sq.py.		0.0	2.0	0	0.111 (360°)	0.111 (360°)	-
		0.5	2.0	0	0.124 (360°)	0.124 (360°)	-
AB_5 trig.bipy.		-	2.0	0.126	0 (360°)	0 (360°)	-
Co(salen)(py)		0.20	1.90	0.022	0.124 (360°)	0.124 (360°)	[196]
Co(3-MeO-salen)(OH_2)		0.43	2.00	0.029	0.125 (358.6°)	0.121 (358.6°)	[197]
Co(salbn⊕)(py)	A[c]	0.206	1.887	0.027	0.113 (360°)	0.135 (360°)	[200]
	B	0.399	2.019	0.080	0.082 (352.5°)	0.195 (357.4°)	
Co(3-Fsaltmen)(1-Bz-imid)		0.411	2.031	0.098	0.068 (358.3)	0.198 (356.2)	[198]
Co(salen-C_2H_4-py)	A	0.250	1.933	0.048	0.090 (359.4°)[d]	0.155 (359.6)[e]	[9,188]
	B	0.293	1.961	0.058	0.081 (357.9°)[d]	0.167 (358.9)[e]	
Fe(salen-C_2H_4-py)		0.319	2.026	0.065	0.105 (352.6)[d]	0.170 (356.0)[e]	This work.

a The average metal-ligand (Schiff base) separation, r(M-Y); displacement of metal from N_2O_2 plane, d. Distances in Å.

b The number in brackets is the sum of the angles of the quasi-trigonal plane; if planar the sum should be 360°.

c Some of the residuals of reference [200] appear to be incorrect.

d Pseudo-trigonal axis O(1)-Co-N(2).

e Pseudo-trigonal axis N(1)-Co-O(2).

Co(salbn⊕)(py)[200]; the metal-ligand separations, except for r(Co-N_{py}), are considerably shorter (particularly r(Co-N_{salen})) in the square-pyramidal molecule than in the trigonal-bipyramidally distorted square-pyramidal molecule. The similarity of bond lengths for the square-pyramidal molecule, Co(salbn⊕)-(py)A, with those for the low spin complexes Co(salen)(py) and $[Co(salen)]_2$ indicates that Co(salbn⊕)(py)A may be low spin; comparison of the bond lengths of the trigonally distorted molecule, Co(salbn⊕)(py)B, with the high spin Co(3-MeO-salen)-$(OH)_2$ and Fe(salen-C_2H_4-py) indicates that Co(salbn⊕)(py)B may be high spin. Unfortunately, Calligaris and coworkers omitted the magnetic moment of solid Co(salbn⊕)(py) in their tabulation[197] of the magnetic moments of other related complexes. The pairs of molecules of Co(salbn⊕)(py) and Co-(salen-C_2H_4-py) well illustrate the effects of crystal packing on molecular stereochemistry.

For Fe,Co(salen-C_2H_4-py) the coordination of the pyridyl group, which is linked by an ethyl group to the ethylene bridge of the Schiff base, is largely responsible for the deviations of the quadridentate bis(salicylideniminato) or "salen" fragment from the essentially square-planar conformation commonly adopted by four-coordinate species such as Co(salen)[210], Co(bzacen)[211], and Co(t-Bsalten)[123], and from the square-pyramidal geometry adopted by Co(salen)(py)[196] and Co(3-MeO salen)(OH_2)[197]. It is appropriate to note that the complex Co(salen-C_3H_6-py) which has a three-carbon link is low spin and probably square-pyramidal[199].

The Salicylideniminato Residues

Over a wide range of metals, oxidation states, and coordination geometry, the two salicylideniminato residues maintain nearly invariant stereochemistry. The weighted averages and standard deviations for bond lengths of sixteen "salen" complexes have been calculated[183] assuming chemical equivalence for the two residues. These are shown in Figure 3.6 together with the corresponding parameters for Fe(salen-C_2H_4-py) and for Co(saltmen)(1-Bz-imid)(O_2) the structure of which is the most precisely determined "salen" derivative presently available[124]. In the case of Fe(salen-C_2H_4-py) the difference (δ) between chemically equivalent bond lengths (r(x-y) and r(x'-y')) of the two residues is always less than 2.7 (and generally well within one) estimated standard deviations of the difference ($\sigma_\delta = (\sigma^2_{r(x'-y')} + \sigma^2_{r(x-y)})^{\frac{1}{2}}$). The internal consistency is reassuring. Although the differences in bond lengths around the phenyl ring are mostly of marginal significance they do follow very closely similar trends observed in other "salen" complexes. Moreover, that the scatter of the six phenyl bond lengths about their mean value (average r(C-C) = 1.397 Å, σ = 0.029 Å) is more than twice the e.s.d. of an individual bond length is also indicative of large perturbations in electron density around the phenyl ring induced by $-C=N^{R}$ and $-O^-$ substituents. For Co(salen-C_2H_4-py) the larger e.s.d.s. associated with individual bond lengths mask any possible significance in the deviations which do, nevertheless, follow a similar pattern to its iron analogue. The consistency of the pattern of bond lengths for Co,Fe(salen-C_2H_4-py) is reflected in the

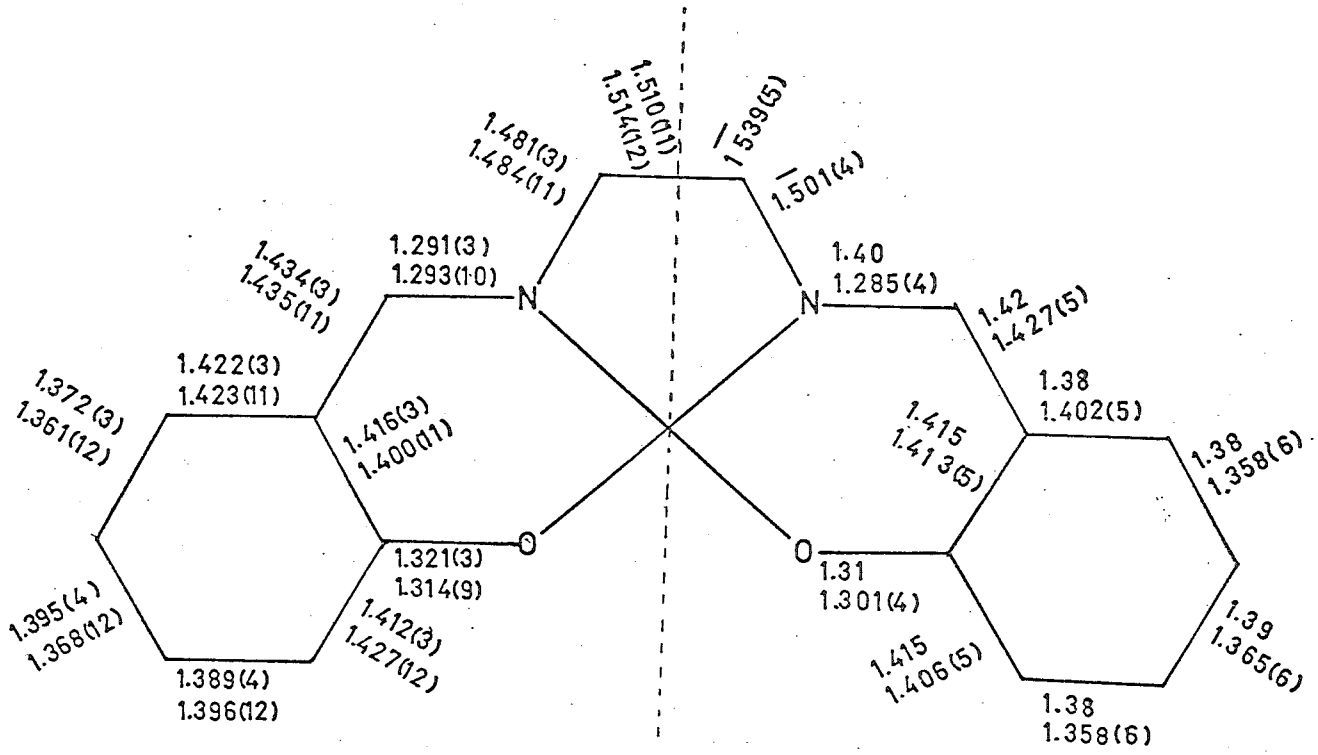

Top left hand values : from compilation of reference [183].

Top right hand values : average of two chemically equivalent separations for Co(saltmen)(1-Bz-imid)-(O_2)[124].

Bottom left hand values : average of two chemically equivalent separations for Fe(salen-C_2H_4-py).

Bottom right hand values : theoretically derived separations[212] for a salicylideniminato residue.

Figure 3.6 : Bond lengths in the salen system, in Å.

e.s.d. of the average of the six crystallographically independent bonds lengths comprising each chemical class (two measurements from Fe(salen-C_2H_4-py) plus four from the two independent molecules of Co(salen-C_2H_4-py); in all cases this e.s.d. is less than 2/3 the e.s.d. of an individual value for Co(salen-C_2H_4-py) - the less precisely determined structure - and this e.s.d. in some cases approaches that for Fe(salen-C_2H_4-py) (see Table 3.2). The observed pattern of three consecutive shorter outer bonds and three consecutive longer inner bonds has been reproduced in Hückel molecular orbital calculations for an uncoordinated salicylaldimate residue; the agreement between the calculated and observed separations is remarkably good[212].

Although bond lengths in the phenyl rings differ significantly from an unsubstituted benzene ring C-C separation of 1.392 Å, the bond angles for Fe(salen-C_2H_4-py) (Table 3.3) do not; neither do those for Co(salen-C_2H_4-py).

Deviations of the phenyl groups from planarity are not considered to be significant; the greatest deviation being 0.010(11) for Ph-1 and 0.029(9) for Ph-2. The salicylideniminato residues (Sal-1 = O(1), C(16), C(15), C(14), C(13), C(12), C(11), C(10), N(1), similarly for Sal-2) maintain approximate planarity; the mean absolute displacements of atoms from the planes are 0.029 Å (0.023 and 0.024 Å) for Sal-1 and 0.047 Å (0.011 and 0.020 Å) for Sal-2, although deviations of atoms from the planes are statistically significant. For Fe(salen-C_2H_4-py) it is noteworthy that the phenyl ring, Ph-2(C(21),...,C(26)), the salicylideniminato

residue, Sal-2, and also the chelate ring, Chel-2, all display greater deviations from planarity than the other fragment.

The Ethylene-ethyl Moiety

Structural manifestations of the coordination of the Schiff base-linked pyridyl group are not limited merely to the immediate coordination environment around the iron or cobalt centre but are also found in the ethyl linkage.

The N N'-ethylene bridge adopts the non-eclipsing or gauche conformation observed in most other Schiff-base structures, although this may be disguised as a cis-conformation with irresolvable disorder between two gauche conformations, as occurs for Co(salen)(py)[196]. The N(1)-C(1)-C(2)-N(2) torsional angle is $43(1)^{o}$ ($36(2)^{o}$ and $37(2)^{o}$). The bond angles $\angle$(C(10)-N(1)-C(1)) and $\angle$(C(20)-N(2)-C(2)) around N(1) and N(2) are not significantly different from an expected value of 120^{o} for an sp^{2}-hybridised nitrogen atom; neither are the angles $\angle$(N(1)-C(1)-C(2)) and $\angle$(N(2)-C(2)-C(1)) different from the expected tetrahedral values (109^{o}). However, other bond angles in the ethyl link show highly significant departures from tetrahedral symmetry, particularly values for $\angle$(C(2)-C(3)-C(4)) and $\angle$(C(3)-C(4)-C(5)) which are $\sim 120^{o}$ and $\sim 116^{o}$ respectively, for the iron and cobalt complexes. It is also noted, although in this case the significance is marginal, that, for the three molecules, the C(2)-C(3) bond is slightly longer than the other C-C single bonds. Any correction for the moderate thermal motion of these atoms would only lengthen this bond. Although the pyridyl ring maintains planarity, carbon atom C4 is pushed, by the ethyl linkage,

from the pyridyl plane by 0.130(10) Å (0.105(21) and 0.108(25) Å). Figure 3.4 best illustrates this. In addition, ligation of the pyridyl group is not symmetrical. Firstly, the ring is rotated about its normal — ∠(Fe-N(3)-C(5)) = 125.5(7)° (126.1(15)° and 127.1(15)°) and ∠(Fe-N(3)-C(9)) = 114.6(7) (116.2(15) and 115.0(15)°). Secondly, the ring is tilted with respect to the Fe-N(3) vector so that the iron atom is displaced from the pyridyl plane by 0.516(1) Å (0.293(3), and 0.120(3) Å). Figure 3.4 also shows this.

The pyridyl group is oriented with respect to the "salen" component such that the torsional angle τ(N(1)-Fe-N(3)-C(5)) is 31.4(8)° (29(2)° and 27(2)°), and τ(N(2)-Fe-N(3)-C(5)) is 45.9(8)° (54(1)°and 55(2)°).

A selection of torsional angles for this fragment of the molecule is presented in the next section (Table 3.17) in the discussion of stereochemical changes accompanying oxygenation.

Concluding Remarks

The structure of Fe(salen-C_2H_4-py) is generally similar to those for the two crystallographically independent molecules of Co(salen-C_2H_4-py). Significant differences in stereochemistry exist between the three structures although the differences between the two cobalt molecules are much smaller. In common with a number of other high-spin cobalt complexes, but not in common with any low-spin cobalt Schiff-base complex, the high-spin Fe(salen-C_2H_4-py) molecule has a considerably distorted trigonal-bipyramidal coordination geometry.

3.2 The Crystal and Molecular Structure of the Dioxygen Adduct of α,α'-{2-(2'-pyridyl)ethyl}ethylenebis-(salicylideniminato)cobalt(II), [Co(salen-C_2H_4-py-(O_2)].CH_3CN.

In this section the structure of [Co(salen-C_2H_4-py)(O_2)].CH_3CN is described and discussed. Although there are now a number of very precisely determined dioxygen adducts of cobalt-Schiff base complexes, this complex has several interesting features, some of them related to the axial ligand being appended to the Schiff base rather than coordinating as a free ligand. The stereochemical changes accompanying oxygenation of Co(salen-C_2H_4-py) are quite dramatic.

Cobalt-dioxygen adducts are generally represented as cobalt(III)-coordinated superoxide, $Co^{III}-O_2^-$ species. In §3.2.1 evidence for and against this formulation will be examined. In §3.2.4 some structural evidence (in addition to the O-O separation and Co-O$\diagup^{O}$ angle) will be presented in support of a $Co^{III}-O_2^-$ formulation.

3.2.1. Introduction and General Review

That the 1:1 dioxygen complexes of cobalt(II) Schiff-base, porphyrin and corrin ligand systems are best categorised as cobalt(III)-coordinated superoxide species rather than cobalt(II)-neutral dioxygen species has been widely accepted since the first detailed characterisations of the complexes in 1969-70 [58-66]. The infrared and structural studies on the O-O bond (ν(O-O) ~1130 cm^{-1}, r(O-O) ~1.29 Å and $\angle$(Co-O-O) ~120°), which were reviewed in Chapter 2, if not indicating actual superoxide character, certainly indicated that on

coordination dioxygen loses characteristics of the free molecule and acquires characteristics similar to the free superoxide anion. Comparison of the parameters for these superoxo complexes with those for peroxo complexes makes the assumption that coordinated dioxygen has actual superoxide character more plausible even if it is not strictly justified. Because of their paramagnetism ($S=\frac{1}{2}$), the location of the odd electron of superoxo-cobalt complexes has been intensively probed using ESR spectroscopy. There has been little doubt that the unpaired electron resides almost exclusively on the dioxygen ligand. But to conclude that the transfer of unpaired electron density from cobalt on to dioxygen equates with a nett transfer of electron density to give a [diamagnetic d^6 cobalt(III)] - [paramagnetic ($S=\frac{1}{2}$) superoxide] species is again unjustified. This assumption, commonly made, has only recently been challenged[15] and tested[19].

Furthermore, inferences drawn from spectroscopic data about the nature of the coordinated dioxygen molecule must be made with recognition of two possibilities. Firstly, that differences between a five-coordinate cobalt(II) species and its six-coordinate dioxygen adduct and, also, similarities between such an adduct and a genuine six-coordinate cobalt(III) complex, may, in both cases, be attributable to intrinsic geometrical factors rather than to a major electronic reorganisation specifically associated with coordination of dioxygen.

Because of their lower susceptibility to irreversible oxidation of the kind that plagues iron-dioxygen systems (§4.1), these 1:1 cobalt-dioxygen complexes with angularly

coordinated dioxygen have been studied as models for the oxygen-binding cobalt-substituted haemoglobins and as possible models for native haemoglobin in the absence — only recently rectified — of iron-dioxygen models.

It is with the qualifications of earlier paragraphs in mind that various lines of evidence for and against a $Co^{III}-O_2^-$ formulation will be presented.

ESR Results

Literature on ESR studies of 1:1 cobalt-dioxygen complexes is voluminous. A representative collection of hyperfine parameters from such studies on the free superoxide and peroxy radicals, and on five- and six-coordinate cobalt(II) complexes, including dioxygen adducts, are presented in Table 3.8. Despite the variation in quadridentate ligand system L and axial base B, there is considerable uniformity in ESR parameters (including g values) among cobalt-dioxygen complexes. ESR spectra of 1:1 cobalt-dioxygen adducts have a characteristic 8-line cobalt (I=7/2) hyperfine structure.

Coordination of dioxygen to Co(acacen)(py) is accompanied by a large decrease in the $A_{\parallel}^{Co}$ hyperfine coupling constant from ∿98G to ∿20G and loss of ^{14}N superhyperfine structure[62(a)]. This has been interpreted as evidence for a much decreased interaction of the unpaired electron with the cobalt nucleus. It was assumed, correctly as it happened, that the unpaired electron had taken up residence on the dioxygen ligand; the extent of such transfer of unpaired electron density, which was assumed to correspond to a nett

Table 3.8 : ^{59}Co, ^{17}O, ^{14}N hyperfine parameters (in Gauss) for superoxide ion, peroxy radicals and cobalt dioxygen complexes[a,b,c].

Compound	$-A_{\parallel}^{Co}$	$-A_{\perp}^{Co}$	$-a_{iso}^{Co}$	$\lvert A_{\parallel}^{N}\rvert$	$\lvert A_{\perp}^{O}\rvert$[d,e]	$\lvert a_{iso}^{O}\rvert$[d,e]	Reference
$^{17}O_2^-$ in KCl[d,e]					+69.3,-0,16.2	(27.5)	[112]
t-Bu-O-^{17}O·						-,23.5	[114]
R-^{17}O-^{17}O[f]					60,88	14.0, 21.8	[115,116]
Co(p-OCH$_3$TPP)(py)	-84.4	+11	(20.6)	15.6			[63]
Co(TPP)(O_2)[g]	-12.5	+29.5	(15.5)	–[h]			[121]
Co(p-OCH$_3$TPP)(py)$_2$	-63	+55	(15.8)	11.2			[63]
Co(p-OCH$_3$TPP)(py)(O_2)	+17.1	+11.8	(13.6)	–[h]			[63]
Co-MbO_2, Co-HbO_2[i]	+16	(+) 9	(11.3)	–[h]	65,93	(22,31)	[213,229]
Co(bzacen)(py)($^{17}O_2$)	–[j]	–[j]	(+)12.8	–[h]	60,88	21.6[k]	[117,118]
Co/NH_3/$^{17}O_2$/Y-zeolite	(+)17.8	(+)12.5	(14.3)	–[h]	60,80	(20,27)	[119]
μ-(O_2,NH_2)[Co(NH_3)$_4$]$_2^{4+}$			(+)12.4	–[h]		22.5	[120]

a. Resonance condition $H_i = h\nu/(g_i\beta_j)$ leads to conversion factor for hfcc from cm^{-1} to Gauss.

b. Signs of Co hfcc derived in ref [19]; those signs parenthetically enclosed obtained by analogy with the signs of closely related complexes.

c. Unless directly observed $a_{iso} = \frac{1}{3}(A_x+A_y+A_z) = \frac{1}{3}(A_{\parallel}+2A_{\perp})$; values so calculated in parentheses.

d. When oxygen atoms non-equivalent, terminal oxygen hfcc quoted second; assignment by analogy with t-Bu-O-^{17}O.

e. Except for $^{17}O_2^-$ in KCl when A_x, A_y, A_z resolved, only $A_{\perp}$ component observed for Co-O_2 species; for O_2^- in $K_2S_2O_8/h\nu$[113] A_x=75.7, A_y=0, A_z=-14, $\lvert a_{iso}\rvert$ = 20.5G.

f. R=tetralin for $A_{\perp}$, R=t-Bu for a_{iso}

g. Assuming $\lvert a_{iso}^{Co}\rvert$ similar to that for Co(acacen)(O_2) (13.3G) [62(a)] yields relative signs $A_{\parallel}^{Co}$ and $A_{\perp}^{Co}$ and thence a_{iso}^{Co} for Co(TPP)(O_2). Slight rhombic distortion in $A_{\perp}^{Co}$ resolved; $A_{\perp} = \frac{1}{2}(A_x+A_y)$.

h. Not observed

i. ^{59}Co hfcc for Co-MbO_2 [229], ^{17}O hfcc for Co-HbO_2 [213].

j. Not reported but for Co(bzacen)(py)(O_2) $\lvert A_{\perp}^{Co}\rvert$=19.69, $\lvert A_{\parallel}^{Co}\rvert$ =10.7G, $\lvert a_{iso}^{Co}\rvert$=13.7G

k. Oxygen atoms magnetically equivalent on ESR timescale in liquid solution.

transfer of electron density, was calculated to be ∿80 - ∿90%[62(a)].

The first assumption of residency was verified by $^{17}O(I=5/2)$ studies which, through the magnitude of the A^O hyperfine splitting, showed the unpaired electron density on the dioxygen ligand to be very similar to that for peroxy radicals[117-119,213]. Although subject to verification it is reasonable to assume, by analogy with peroxy radicals[114], that the unpaired electron was apportioned to the terminal and coordinated oxygen atoms in the ratio 0.6: 0.4 (see also Table 3.8). Oxygen-17 isotope studies on cobalt-substituted haemoglobin have shown that the ^{17}O hyperfine splitting is confined to the perpendicular anisotropic component $A_{\perp}^{O}$ [213].

However the second assumption concerning the nett electron transfer apparently leads to inconsistencies, which were noted by Tovrog, Kitko and Drago[19]. Analysis of the hyperfine anisotropy for six-coordinate cobalt-dioxygen complexes led to the conclusion that the unpaired electron was residing in a molecular orbital with approximately 10% metal-3d character[62(a)]. But when the hyperfine parameters of six-coordinate complexes of the type $Co(L)(B)_2$ were compared with those of its dioxygen derivative (ostensibly a comparison that is no less rigorous than the Hoffman-Diemente-Basolo analysis[62(a)]) the metal-3d character of the unpaired electron was calculated to be approximately 50% [19,63].

Table 3.8 lists a selection of parameters pertinent to the above remarks. It may be noted that whereas it is only the

$A_{\perp}^{Co}$ hyperfine splitting (but not $A_{\parallel}^{Co}$) which is markedly less for the comparison of complexes of the types Co(L)(B)(O_2) and Co(L)(B)[62(a)], for comparison of complexes of the types Co(L)(B)(O_2) and Co(L)$(B)_2$ both $A_{\perp}^{Co}$ and $A_{\parallel}^{Co}$ are less for the dioxygen complex[63].

In addition to noting apparent inconsistencies in earlier interpretations on the location of the unpaired electron, Tovrog, Kitko and Drago have proposed a different mechanism for the reduced ^{59}Co(I=7/2) hyperfine coupling and the very large ^{17}O(I=5/2) hyperfine coupling. They initially reported that the ESR parameters for the dioxygen, carbon monoxide and isocyanide adducts of a five-coordinate cobalt(II)-Schiff base derivative were identical[15]. The report of a carbon monoxide adduct occasioned some surprise; that adduct was soon shown to be an artefact due to the presence of dioxygen in the carbon monoxide[18]. However, the conventional interpretation of the cobalt hyperfine parameters was questioned. More recently, in a detailed analysis of the ESR parameters for series of dioxygen complexes of cobalt Schiff-base, porphinato and glyoximato derivatives, they deduced that, while unpaired electron density resides entirely on dioxygen, the nett electron transfer varies from 0.1 to 0.8 electrons - a much wider range than previously calculated[19]. They postulated that the appearance of cobalt hyperfine coupling arises not through π backbonding from $\pi^*(O_2)$ to metal $3d_{xz,yz}$ orbitals but through a spin polarisation mechanism.

Table 3.9 : Calculated nett electron transfer for some cobalt-dioxygen complexes[a].

Compound	Nett Transfer $Co^{II} \rightarrow O_2$ (electrons)	
Co(acacen)(OH_2)(O_2)	0.1	
Co(acacen)(py)(O_2)	0.4	
Co(salDAPE)(O_2)	0.2	
Co(p-OCH_3TPP)(py)(O_2)	0.6	
Co(DMGH)$_2$(py)(O_2)	0.7	
Co(acacen)(py)(O_2)	0.3	(Calculated quantum mechanically.)[b]

[a] Reference [19]

[b] Reference [214]

The former rationale[62(a)] for the appearance of cobalt hyperfine splitting is more widely accepted. The latter hypothesis[19] has gained credence but not proof through the recent appearance of molecular orbital calculations for Co(acacen)-$(NH_3)(O_2)$[214], which predicted relatively small spin densities in metal $d_{xz,yz}$ orbitals and an electron transfer from cobalt to dioxygen of an amount similar to that derived by Tovrog, Kitko and Drago for Co(acacen)(py)(O_2)[19]. This and other molecular orbital studies on cobalt-dioxygen systems will be described in Chapter 6.

Table 3.9 lists a number of dioxygen adducts and the calculated nett transfer of electron density from cobalt onto dioxygen. Thus while a $Co^{III}-O_2^-$ formulation is still appropriate for many complexes it would appear to be inadequate for some. Complexes with weak axial ligands, such as H_2O or $R{\diagdown}O{\diagup}R$, are characterised by a transfer of electron density less than 0.5; strong σ donors appear to enhance electron transfer. However the quadridentate equatorial ligand system appears to play a major role as well; witness the differences in nett electron transfer between the Schiff-base and glyoximato complexes with identical axial bases. It must be noted that the Tovrog-Kitko-Drago analysis is not without assumptions which deserve close scrutiny.

The detection, by ESR spectroscopy, of complexes of the type Co(TPP)(CO), Co(TPP)(O_2), Co(TPP)(CO)(O_2) Co(TPP)(B)(O_2) but <u>not</u> Co(TPP)(B)(CO)[121] also indicates that for a six-coordinate carbonyl adduct to form some transfer of electron density (specifically $3d_z2$) must occur; that is a $Co^{III}-O_2^-$ formulation pertains. For the five-coordinate carbonyl adduct the $3d_z2$

electron can be concentrated trans to carbon monoxide as a "phantom" ligand.

End-on bent bond geometry for the metal-dioxygen moiety was deduced from ESR parameters and infrared data (specifically the observation of a prominent infrared active O-O stretching mode ruled out linear coordination)[62(a)]. This prediction was confirmed by the crystal structure of Co(bzacen)(py)(O_2)[126]. Subsequent ^{17}O isotope studies[118,119,213], which showed the two oxygen atoms to be magnetically inequivalent, unequivocally precluded the triangular mode of coordination which had been tentatively proposed on the basis of ESR measurements for cobo-globins[215] and a Co(gly)$_2$(imid)(O_2) species[216].

X-ray Photoelectron Spectroscopy

The results of X-ray photoelectron studies (also known as ESCA—electron spectroscopy for chemical analysis) on cobalt-Schiff base complexes have also been used to infer a $Co^{III}-O_2^-$ formulation[217,218]. Co $2p_{3/2}$ binding energies increased by 0.9-1.9 eV when cobalt(II) complexes were oxygenated[218] — a result consistent with an oxidative addition of dioxygen.

The range of binding energies has been noted[19] as evidence for marked differences in the amount of electron transfer, Co→O_2. Furthermore, the binding energies of the dioxygen adducts were similar to six-coordinate cobalt(III) species. In the absence of binding energies for "bona fide" six-coordinate cobalt(II) species these results must remain somewhat ambivalent. The dioxygen $1s_{\frac{1}{2}}$ peak was separated from other peaks and compared with a μ-peroxo type complex[218]; the higher binding energy of the former suggested greater negative charge on the latter.

Linear Free Energy Correlations and Solvent Effects

Positive correlations for a range of ligands and axial bases, have been observed[219,221] between the stability constants of dioxygen adducts formed thus

$$Co(L)(B) + O_2 \rightleftharpoons Co(L)(B)(O_2) \qquad R3.1$$

and the ease of oxidation as measured by cyclic voltametry for the reaction

$$Co^{III}(L)(B)_2 + e \rightleftharpoons Co^{II}(L)(B)_2 \qquad R3.2(a)$$

or

$$Co^{III}(L) + e \rightleftharpoons Co^{II}(L) \qquad R3.2(b)$$

Furthermore, Hammett plots of substituent constants for para-substituted tetraphenylporphyrins versus, firstly, $E_{\frac{1}{2}}$ values for the one-electron oxidation of Co^{II}(p-X-TPP) and, secondly, versus equilibrium constants for the formation of a dioxygen adduct of Co^{II}(p-X-TPP)(py) in toluene at 20°C are linear with slopes (ρ) of the same sign.[221]. The correlation is such that electron-donating substituents favour oxidation and oxygenation (that is ρ is negative under the sign convention used). That the oxidation reaction is more sensitive to substituent effects than the oxygenation reaction indicates an incomplete removal of a cobalt electron for the latter reaction. It may be noted that the derivation of ρ for the oxygenation equilibrium at 20° was obtained by extrapolation of results obtained at lower temperatures where ρ was considerably more negative; accordingly, at sufficiently high temperatures ρ will become positive (e.g. in butyronitrile solvent, $\rho^{20^\circ} = +0.04$). It may also be noted that whereas electron-donating substituents encourage oxidation

or oxygenation (ρ negative) such substituents discourage coordination of an axial base

$$Co^{II}(L) + B \rightleftharpoons Co^{II}(L)(B) \qquad R3.3$$

Correlations between the basicities of para-substituted pyridines and the oxygen affinities of associated five-coordinate cobalt(II) Schiff-base[61] or porphyrin[222] complexes have been established. Stronger bases such as 4-NH_2-py (pK_a=9.30) enhance the formation of the dioxygen adduct compared with weaker bases such as 4-CN-py (pK_a=1.86); their presumed-greater donor power facilitates transfer of electron density onto dioxygen. The correlation has been disputed[223] and vigorously defended[224]. Moreover it was found[222] that the oxygenation reaction R3.1 was more sensitive to ligand basicity than the ligand addition reaction R3.3. It is also observed that imidazole-based dioxygen complexes were more stable despite the lower basicity of imidazoles compared to some substituted pyridines[222]; piperidine-based dioxygen adducts were less stable than would be expected from their basicities[222]. The different steric requirements of pyridine (6-membered ring), imidazole (5-membered ring) and piperidine (sp^3-hybridised nitrogen leading to tilted coordination Co–N(H)< [234,235]) may be responsible for the differences.

Porphinato cobalt(II) derivatives display a much lower affinity for dioxygen than the sulphur-containing thiosalicylideniminato cobalt(II) derivatives, and both of these types display a lower affinity for dioxygen than Schiff-base ligands[219]. Porphyrins are more highly regarded than Schiff bases for their ability to delocalise electron density that could otherwise be available for transfer onto dioxygen[222(a)]. It is this factor

which had led to the use of Schiff-base ligand systems as models for the porphyrin ligand of biological systems.

For the not unrelated μ-peroxo complexes, a linear relationship has been observed between the stability constant of the dioxygen adduct and the sum of the pK_a's (i.e. the total "basicity" or "donicity") of the supporting ligands[220].

It is also observed that polar solvents enhance the stability of the dioxygen adduct[225]; this is consistent with the greater stabilisation afforded a polar $Co^{III}-O_2^-$ species by more polar aprotic solvents.

These correlations provide cogent evidence for transfer of electron density from cobalt onto dioxygen, although the nett amount of such transfer has not been determined.

Other Thermodynamic Considerations

Identical cobalt-dioxygen adducts of vitamin B_{12} (as evidenced by ESR parameters) have been produced by reaction of vitamin B_{12r} (Co^{II}) with dioxygen and vitamin B_{12a} (aquocobalamin Co^{III}) with superoxide anions[83].

The equilibrium constant for the reaction

$$Co(TPP)(py)(O_2) \rightleftharpoons Co^{III}(TPP)(py) + O_2^-$$

has been estimated to be in the range 10^{-12}-10^{-17} M^{-1} [221]; in contrast the equilibrium constant for the reaction

$$Co(TPP)(py)(O_2) \rightleftharpoons Co^{II}(TPP)(py) + O_2$$

is $\sim 10^{-0.6}$ M^{-1} at 20°C. [221]. That the transfer of charge is incomplete was inferred[221].

Electronic Spectra

A detailed analysis of the spectra of the not unrelated μ-dioxygen complexes $[(NH_3)_5Co(O_2)Co(NH_3)_5]^{5+}$ and $[(CN)_5Co(O_2)Co(CN)_5]^{5-}$ "conclusively establishes the presence of low-spin d^6Co^{III} centres in the ground states of the decaammino and decacyanide. The $\pi^*(O_2^-)$ level is split into a filled in-plane component involved in strong σ bonding with Co^{III} and a weakly π-bonding, half-filled, out-of-plane component"[122].

Concluding Remarks

Taken together the various independent lines of evidence strongly support a cobalt(III)-coordinated superoxide formulation for many cobalt-dioxygen complexes. Not only does the unpaired electron essentially reside on the dioxygen ligand but in most complexes, there is also a substantial nett transfer of electron density from cobalt onto dioxygen so that the cobalt centre acquires features of a cobalt(III) oxidation state.

Recently a new interpretation of ESR parameters indicated that the nett transfer of electron density may range from ∿0.1 to 0.8 electrons. Corroborative evidence, or otherwise, in the form of quantitative stereochemical and infrared data on those complexes where the nett electron transfer is at one or other of the extremes, is at present not available.

Further evidence in support of a Co^{III}-O_2^- formulation at least for dioxygen adducts of cobalt(II)-Schiff base-amine derivatives is presented in the next section.

3.2.2 Collection and Reduction of Intensity Data.

Dark orange-red crystals of the compound shown by this analysis to be $[Co(salen\text{-}C_2H_4\text{-}py)(O_2)]\cdot CH_3CN$ were prepared by a modification of the high pressure oxygenation method of reference [10]. It was found that by cooling and deoxygenating the acetonitrile solvent prior to addition to $Co(salen\text{-}C_2H_4\text{-}py)$ larger crystals could be obtained. The dioxygen pressure used was $\sim$200lb in^{-2}. The structure was initially solved using data from a smaller crystal to the one used in the final analysis. All crystals were obtained as extremely thin approximately rectangular plates. Symmetry and systematic absences uniquely consistent with the monoclinic space group $P2_1/c$ (No.14) [207] were established by precession photography using Cu K_α X-radiation.

The crystal selected for data collection had dimensions 0.42 x 0.35 x 0.01 mm^3 with the smallest dimension parallel to the crystal b-axis. It was randomly aligned with respect to the diffractometer ϕ-circle axis. Crystal mosaicities ranged from 0.12° to 0.20° and peak profiles were symmetrical. Crystal orientation and unit cell dimensions,

a = 9.563(2), b = 19.490(4), c = 12.770(3) Å, β = 106.04(2)°,

were obtained at 24°C using the standard methods (Appendix 1). For Z=4 and empirical formula $CoC_{23}N_3O_4H_{21}\cdot CH_3CN$ the calculated and measured (by flotation) densities were 1.46 and 1.44(1) g cm^{-3}. Elemental analysis — found (calculated): % C=60.2 (59.7), % H = 5.1(4.8), % N = 11.7(11.1) — and infrared spectroscopy–$Co(salen\text{-}C_2H_4\text{-}py(O_2)\cdot CH_3CN$ (neat CH_3CN): ν(C=N) = 2260 cm^{-1} (2270), δ(C-C) = 917 cm^{-1} (916 cm^{-1}) — identified the solvate species as acetronitrile. Coordination of dioxygen is established by ν(O-O) at 1135 cm^{-1}. The linear absorption coefficient calculated using the above formula, and for Mo K_α radiation, was

8.24 cm^{-1} and since transmission coefficients varied between 0.98 and 0.75 an absorption correction was subsequently applied to the intensity data. Excluding systematic absences, 1573 unique reflections for which $2\theta \leq 36^{o}$ (i.e. $\sin\theta/\lambda = 0.43$) were collected using a symmetric scan range of 1.20^{o} in 2θ. The scan comprised 60 steps each of one second duration. Background counts of 15 seconds were recorded at each end of the scan. Three standard reflections well separated in reciprocal space and monitored every 50 reflections showed a nett 10% decrease over the period of data collection although decomposition was not isotropic. There was also a long term power fluctuation. Data were appropriately scaled and corrected for Lorentz and polarisation effects. Prior to embarking on limited anisotropic refinement the absorption correction was applied to the intensity data.

Details on crystallographic theory, techniques used and computing aspects may be found in Appendix 1.

3.2.3 Solution and Refinement of the Structure

From the three-dimensional Patterson synthesis possible coordinates were obtained for the cobalt atom in a general position. Least-squares refinement of an overall scale factor, with the positional parameters and isotropic thermal parameter ($B = 4.0$ $\AA^2$) held constant for cobalt, led to values for R and R_W of 0.43 and 0.53 respectively. Successive cycles of least-squares refinement and difference Fourier syntheses eventually established coordinates for the remaining non-hydrogen atoms of the Co(salen-C_2H_4-py)(O_2) species. The two phenyl and one pyridyl rings were initially refined as rigid groups each group

having a single isotropic temperature factor; the positional and isotropic thermal parameters of other atoms were not so constrained. This model refined, using 665 reflections having $I>2\sigma_I$, so that

$$R = 0.172, \quad R_W = 0.20$$

Characterisation of the solvate species was uncertain and it was at this stage that the author was introduced to this structure analysis. After many attempts a larger crystal was prepared, a more intense data set was collected, and a careful investigation of this and other problems with the structure initiated.

An ill-defined region of electron density not associated with the cobalt complex was interpreted with the assistance of infrared and microanalytical evidence described in the previous subsection as an acetonitrile solvate molecule. It was included in the model which was then refined so that

$$R = 0.115 \text{ and } R_W = 0.102.$$

The absorption correction was applied and further refinement of the model led to values for R and R_W of 0.114 and 0.101, respectively. Residual electron density around some atoms, especially those in the ethylene-ethyl linkage, which density was revealed in a difference Fourier synthesis, indicated inadequacies in the isotropic models used to describe the thermal motions of these atoms. Closer investigations of the "trouble spots" were made:-

1. As a result of the abnormally large thermal motion of the dioxygen ligand, the dioxygen binding site was examined with various Fourier syntheses. An F(obs) Fourier synthesis derived from a model without dioxygen could not resolve the two atom positions; only an elongated football of electron density

angled to the equatorial square-plane defined by the Schiff-base donor atoms was observable. A difference Fourier synthesis derived from a model lacking the terminal oxygen atom also indicated only the one general orientation of the dioxygen ligand.

Nonetheless, the abnormal thermal parameters of the dioxygen ligand are attributable to irresolvable disorder, this is discussed further in the next section. In view of the limited data available it was considered unprofitable to attempt to quantify this disorder since the overall description of the structure would not be improved.

2. Difference and F(obs) Fourier syntheses derived from models lacking one or more of the four carbon atoms of the ethylene-ethyl linkages failed to indicate disorder. The abnormal interatomic separations which occurred during all least-squares refinements of this group using not only the second data set but also the original data set were also reproduced in all Fourier syntheses. The possibility that the carbon atom of the ethyl bridge that is β to the pyridyl ring was alternately bonded to one or other of the two ethylene carbon atoms was examined. Such disorder could have rationalised quite nicely the shape and orientation of the anisotropic thermal ellipsoids and the interatomic separations ultimately obtained for the ethylene-ethyl linkages. Despite evidence from Fourier syntheses that such disorder did not exist, models incorporating disorder were tested and, not surprisingly, failed to refine sensibly. Moreover the atoms, if moved to more chemically reasonable positions drifted back to their former "abnormal" positions. The infelicities of this component must be attributed to the limited and weak data obtained and to the crystal

decomposition that occurred. The exotic high pressure preparation of the crystals may be another factor.

For the final cycles of refinement, group constraints were removed and anisotropic models for the thermal motion of appropriate atoms applied. Hydrogen atom positions for hydrogen atoms attached to phenyl and pyridyl groups were calculated ($r(C\text{-}H) = 1.0$ Å) prior to each cycle of refinement and included in F_c as a fixed contributions. This model, specified by 187 variable parameters, was refined using 915 reflections having $I>\sigma_I$, and at convergence the discrepancy factors were

$$R = 0.128,\ R_w = 0.089.$$

The standard error in an observation of unit weight was 1.45 and was independent of $\sin\theta/\lambda$ and $|F_o|$. The p-factor for the optimal weighting scheme was 0.07. The final scale factor to place calculated and observed structure factors on the same scale was 0.3382(21). There was no evidence for secondary extinction among strong low angle reflections. For the 665 reflections having $I>2\sigma_I$ the discrepancy factors were

$$R = 0.088,\ R_w = 0.076.$$

In the final cycle, the ratios of the change in a parameter to its estimated standard deviation were less than 0.2 and 0.4 for all positional and thermal parameters, respectively, except for the solvate molecule where the ratios were less than 1.0.

A significant decrease in the estimated standard deviations of almost all parameters accompanied the relaxation of constraints. During the final cycles of refinement the thermal ellipsoid parameters for the ethylene carbon atom C(1) became non-positive definite and those for the β ethyl carbon atom alarmingly eccentric.

The anomalously short and long interatomic separations of earlier models persisted.

The acetonitrile solvate molecule also behaved poorly in both early and final cycles of refinement. Its final geometry is somewhat different from that expected for free acetonitrile. Indeed the correct orientation of the molecule is uncertain since the middle atom was inclined to drift during least-squares refinements.

The final difference Fourier synthesis calculated using all data, including reflections having $I<\sigma_I$, was flat and had no peaks greater than $0.76\bar{e}/\mathring{A}^3$ - this is less than half the height of the last located carbon atom despite the higher noise level of this synthesis because the less precisely measured data were also utilised. Residual electron density was mostly concentrated around atom C(1) which had physically meaningless ellipsoid parameters.

Among the "unobserved" reflections there were no systematic discrepancies between $|F_o|$ and $|F_c|$. Moreover for all data the intensities of only 14 reflections out of 1573 are calculated to lie outside the range

$$I-3\sigma_I < I_c < I + 3\sigma_I \quad .$$

That several of those reflections were low angle reflects the inadequacies in the description of the solvate and parts of ethylene-ethyl moieties. Table A2 in the Appendix lists the calculated and observed structure factors for all data. The discrepancy factors for all data were R = 0.24, R_w = 0.093; the standard error in an observation of unit weight was 1.168.

Table 3.10 : Final atomic parameters for $[Co(salen\text{-}C_2H_4\text{-}py)(O_2)]\cdot CH_3CN$.

(a) Non hydrogen atoms

Atom	X	Y	Z	B or β_{11}	β_{22}	β_{33}	β_{12}	β_{13}	β_{23}
Co	2231(4)	1745(2)	-1579(3)	0114(6)	0032(2)	0064(3)	-0004(3)	0008(3)	0001(3)
O(1)	4203(18)	2020(8)	-1039(13)	4.9(5)					
O(2)	2406(18)	1333(8)	-0217(13)	4.5(4)					
N(1)	2038(23)	2174(10)	-2920(17)	4.2(5)					
N(2)	0242(24)	1517(11)	-2127(19)	5.2(6)					
N(3)	2929(24)	0868(11)	-2129(19)	4.6(5)					
O(3)	166(4)	2527(14)	-100(2)	042(6)	0032(10)	016(3)	005(3)	-002(3)	-0004(20)
O(4)	130(5)	3017(13)	-132(3)	071(11)	0023(14)	026(5)	005(3)	008(5)	-001(2)
C(10)	304(3)	2456(13)	-327(2)	4.8(6)					
C(20)	-055(3)	1262(14)	-160(2)	4.5(7)					
C(1)	045(3)	2197(18)	-368(2)	002(4)	0098(20)	012(4)	-004(2)	-006(3)	012(2)
C(2)	-035(3)	1713(22)	-332(2)	007(5)	010(2)	007(3)	000(3)	003(3)	006(2)
C(3)	-009(5)	0978(20)	-412(3)	035(9)	0050(18)	18(5)	006(4)	-013(6)	-009(2)
C(4)	131(4)	0847(20)	-404(3)	024(8)	0066(20)	012(4)	007(3)	-009(5)	-005(2)
C(11)	457(3)	2530(12)	-265(2)	2.9(6)					
C(12)	550(3)	2825(14)	-321(2)	5.6(8)					
C(13)	694(3)	2892(13)	-259(2)	4.8(7)					
C(14)	748(3)	2702(14)	-152(2)	6.3(7)					
C(15)	650(3)	2386(14)	-106(2)	4.9(7)					
C(16)	499(3)	2299(14)	-155(2)	4.2(7)					
C(21)	-018(3)	1109(14)	-049(2)	5.2(7)					
C(22)	-122(3)	0837(15)	-001(2)	6.1(8)					
C(23)	-084(3)	0670(14)	108(3)	6.2(8)					
C(24)	055(3)	0705(15)	175(2)	5.5(7)					
C(25)	158(3)	0932(13)	127(2)	5.0(7)					
C(26)	130(3)	1101(14)	016(2)	4.7(7)					
C(5)	241(3)	0521(15)	-308(2)	4.3(7)					
C(6)	303(3)	-0108(17)	-321(2)	6.7(8)					
C(7)	420(3)	-0389(15)	-249(3)	7.1(8)					
C(8)	478(3)	-0018(15)	-152(2)	4.7(7)					
C(9)	407(3)	0570(15)	-136(2)	3.8(7)					
N(S)	-529(5)	1199(20)	-497(4)	047(11)	0052(19)	045(8)	001(4)	031(8)	001(3)
C(S1)	-405(8)	071(3)	-435(4)	054(19)	003(3)	022(7)	-009(5)	018(9)	-003(3)
C(S2)	-329(5)	016(5)	-396(4)	018(8)	046(10)	017(6)	-001(7)	-001(5)	023(7)

(b) Hydrogen atoms[c]

Atom	X	Y	Z	B	Atom	X	Y	Z	B
H(10)	276	264	-405	5.5	H(23)	-163	054	140	6.9
H(20)	-162	112	-203	5.0	H(24)	079	054	252	6.4
H(12)	514	294	-400	6.4	H(25)	259	102	174	5.6
H(13)	760	313	-294	5.6	H(6)	261	-034	-394	7.5
H(14)	853	278	-113	7.3	H(7)	457	-084	-261	8.1
H(15)	691	221	-029	5.8	H(8)	570	-016	-097	6.1
H(22)	-224	075	-047	7.1	H(9)	440	081	-064	5.1

[a] Fractional coordinates and anisotropic thermal parameters may be generated by placing 0. in fron of first digit.

[b] The form of anisotropic ellipsoid is $\exp[\beta_{11}h^2 + \beta_{22}k^2 + \beta_{33}l^2 + 2\beta_{12}hk + 2\beta_{13}hl + 2\beta_{23}hl)]$.

[c] Hydrogen atom H(10) is bonded to carbon atom C(10), etc.

Table 3.11 : RMS components of thermal displacement (in Å) along principal ellipsoid axes for $[Co(salen\text{-}C_2H_4\text{-}py)(O_2)]\cdot CH_3CN$.

Atom	RMS1	RMS2	RMS3
Co	0.204(6)	0.239(7)	0.256(8)
O(3)	0.22(5)	0.32(3)	0.49(3)
O(4)	0.18(7)	0.45(4)	0.57(4)
C(1)	-[a]	-	-
C(2)	0.12(9)	0.18(6)	0.47(5)
C(3)	0.05(22)	0.28(7)	0.61(5)
C(4)	0.19(8)	0.24(6)	0.52(5)
N(S)	0.31(6)	0.33(5)	0.61(5)
C(S1)	0.16(10)	0.35(6)	0.53(8)
C(S2)	0.19(9)	0.30(6)	0.99(11)

[a] Non-positive definite ellipsoid parameters but probable shape similar to atom C(2).

Final atomic parameters for all atoms are contained in Table 3.10. Derived root-mean-square components of thermal displacement along the principal ellipsoidal axes are contained in Table 3.11.

3.2.4 Description and Discussion of the Structure

General Features and Crystal Packing

The crystal structure consists of neutral monomeric molecules of the complex, (dioxygen) α,α'-{2-(2'-pyridyl)ethyl}-ethylenebis(salicylideniminato)cobalt, and an ill-defined solvate molecule, acetonitrile. Figure 3.7 illustrates the complex and defines the atom labelling system. Figure 3.8 shows the packing of the molecules with respect to the unit cell.

The complex comprises an approximately planar quadridentate Schiff-base species, N,N'-ethylenebis(salicylideniminato), with the coordinated pyridyl group attached to the ethylene bridge by an ethyl group. Approximately octahedral coordination about the cobalt centre is completed by the dioxygen ligand which is coordinated in the end-on bent bond mode that is now well-established for complexes of this type[123-126]. Bond lengths and angles are listed in Tables 3.12 and 3.13 respectively. The O-O separation is 1.06(3) Å and the Co-O-O angle is 134(4)° but these parameters are not considered to be the actual bond length or angle (see below).

Chemically equivalent bond lengths (and angles) for the two salicylideniminato residues display statistically insignificant differences. Moreover, the pattern of three long and three short phenyl bond lengths observed in other structures (Table 3.2 Figure 3.6) is observed despite the low precision of

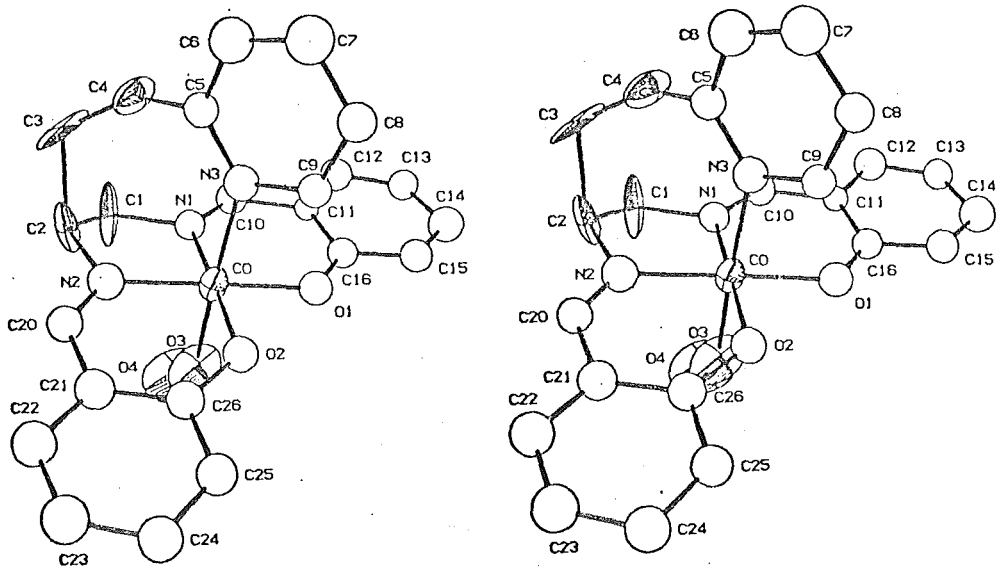

Figure 3.7 : Stereoscopic diagram of Co(salen-C_2H_4-py)(O_2). The thermal ellipsoids are drawn at the 30% probability level.

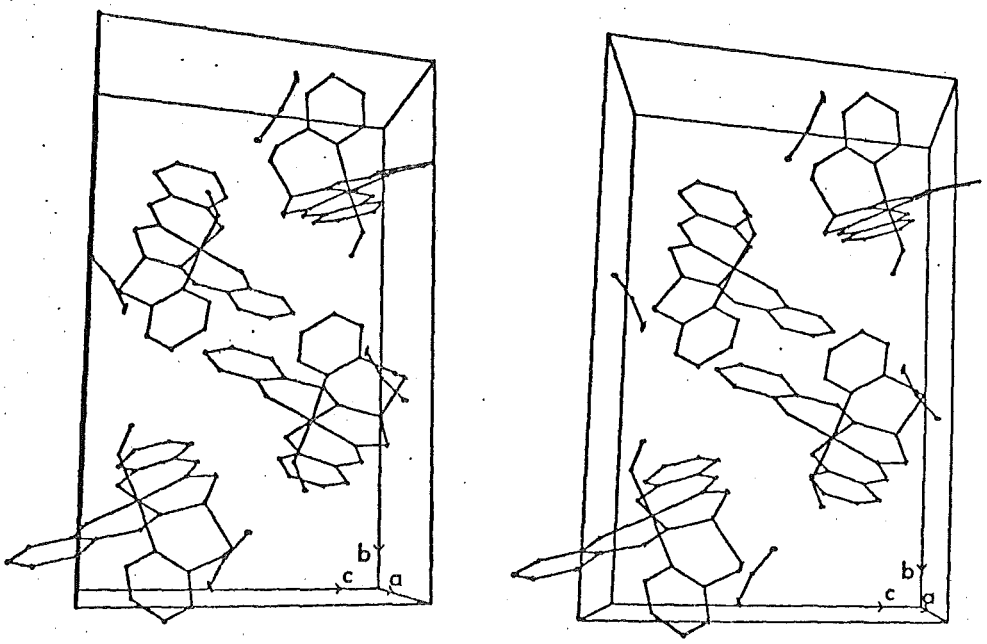

Figure 3.8 : Stereoscopic diagram of the packing of Co(salen-C_2H_4-py) and CH_3CN with respect to the unit cell.

this analysis which generally renders insignificant the differences between the short and long bonds of this structure.

Intermolecular separations, not involving hydrogen atoms, less than 3.40 Å include O(2)...C(10) 3.36(3), C(10)...O(3) 3.37(4), C(20)...C(14) 3.40(4) and N(S)...C(S2) 3.11(9) Å. The first two separations are somewhat shorter than van der Waals contact separations (~3.4 Å). The last separation involves atoms with very high thermal motion; some disorder is likely to relieve this close contact. Intermolecular contacts less than 3.75 Å are contained in Table 3.14.

The Co-O_2 Moiety

With free molecular oxygen having a bond length of ~1.21 Å (see §2.1.1) the O-O separation obtained must, therefore, be considered an unrealistically short bond length. The Co-O(3) separation 1.84(3) Å, is shorter, but not significantly so, than the separations observed for other salen derivatives and Co(bzacen)-(py)(O_2) (Table 2.2). If atom O(4) is assumed to ride on atom O(3) the corrected O-O separation is 1.13(4) Å, and if atom O(3) is assumed to ride on the cobalt atom the value for r(Co-O(3)) becomes 1.90(3) Å. Since the thermal motion of the cobalt atom is not extravagant the latter correction is valid. However, to apply the riding model to the O-O separation is inappropriate since both atoms exhibit high thermal motion. If these atoms are assumed to move independently the value for r(O-O) is increased to 1.45(2) Å. Disorder of the dioxygen ligand may be inferred from the eccentricity and orientation of the thermal ellipsoids (Table 3.11, Figure 3.7), and from the near eclipsing configuration that the dioxygen ligand adopts with respect to

Table 3.12 : Bond distances (in Å) for [Co(salen-C_2H_4-py)-(O_2)]·CH_3CN.

Atoms	Distances	Atoms	Distances
Co-O(1)	1.898(16)	Co-O(2)	1.882(16)
Co-N(1)	1.868(21)	Co-N(2)	1.889(22)
Co-O(3)[a]	1.84(3)	Co-N(3)	2.029(22)
N(1)-C(1)	1.56(3)	N(2)-C(2)	1.52(3)
N(1)-C(10)	1.29(3)	N(2)-C(20)	1.25(3)
O(1)-C(16)	1.25(3)	O(2)-C(26)	1.35(3)
O(3)-O(4)	1.06(3)	N(3)-C(5)	1.36(3)
C(1)-C(2)	1.37(3)	N(3)-C(9)	1.38(3)
C(2)-C(3)	1.82(4)	C(5)-C(6)	1.39(3)
C(3)-C(4)	1.34(4)	C(6)-C(7)	1.36(3)
C(4)-C(5)	1.52(4)	C(7)-C(8)	1.41(3)
		C(8)-C(9)	1.38(3)
C(10)-C(11)	1.47(3)	C(20)-C(21)	1.40(3)
C(11)-C(12)	1.41(3)	C(21)-C(22)	1.42(3)
C(12)-C(13)	1.39(3)	C(22)-C(23)	1.37(3)
C(13)-C(14)	1.37(3)	C(23)-C(24)	1.37(3)
C(14)-C(15)	1.38(3)	C(24)-C(25)	1.38(3)
C(15)-C(16)	1.42(3)	C(25)-C(26)	1.41(3)
C(11)-C(16)	1.42(3)	C(21)-C(26)	1.42(3)
N(S)-C(S1)	1.56(6)	C(S1)-C(S2)	1.32(8)

[a] 1.90(3) Å when corrected for riding motion.

Table 3.13 : Bond angles (in °) for $[Co(salen\text{-}C_2H_4\text{-}py)(O_2)]\cdot CH_3CN$.

Atoms	Angles	Atoms	Angles
N(1)-Co-O(2)	178.5(9)	N(2)-Co-O(1)	177.2(9)
N(1)-Co-O(1)	92.5(9)	N(2)-Co-O(2)	93.7(9)
O(1)-Co-O(2)	87.6(7)	N(1)-Co-N(2)	86.1(10)
N(1)-Co-O(3)	91.7(11)	N(2)-Co-O(3)	87.8(12)
O(1)-Co-O(3)	89.8(12)	O(2)-Co-O(3)	86.9(11)
N(1)-Co-N(3)	91.1(9)	N(2)-Co-N(3)	93.9(9)
O(1)-Co-N(3)	88.6(8)	O(2)-Co-N(3)	90.4(8)
Co-O(3)-O(4)	134(4)		
Co-N(1)-C(1)	114.3(15)	Co-N(2)-C(2)	111.8(17)
Co-N(1)-C(10)	128.2(20)	Co-N(2)-C(20)	127(2)
Co-O(1)-C(16)	127.8(18)	Co-O(2)-C(26)	126.2(16)
C(1)-N(1)-C(10)	118(2)	C(2)-N(2)-C(20)	122(2)
N(1)-C(1)-C(2)	108.2(20)	N(2)-C(2)-C(1)	115(3)
N(1)-C(10)-C(11)	125(3)	N(2)-C(20)-C(21)	127(3)
O(1)-C(16)-C(15)	120(3)	O(2)-C(26)-C(25)	119(3)
O(1)-C(16)-C(11)	127(3)	O(2)-C(26)-C(21)	122(3)
C(10)-C(11)-C(12)	116(3)	C(20)-C(21)-C(22)	121(3)
C(10)-C(11)-C(16)	118(3)	C(20)-C(21)-C(26)	122(3)
C(12)-C(11)-C(16)	126(3)	C(22)-C(21)-C(26)	117(3)
C(11)-C(12)-C(13)	114(3)	C(21)-C(22)-C(23)	120(3)
C(12)-C(13)-C(14)	126(3)	C(22)-C(23)-C(24)	124(3)
C(13)-C(14)-C(15)	115(3)	C(23)-C(24)-C(25)	115(3)
C(14)-C(15)-C(16)	126(3)	C(24)-C(25)-C(26)	124(3)
C(15)-C(16)-C(11)	112(3)	C(25)-C(26)-C(21)	118(3)
C(1)-C(2)-C(3)	100(3)	Co-N(3)-C(5)	131(2)
N(2)-C(2)-C(3)	107(3)	Co-N(3)-C(9)	112.2(19)
C(2)-C(3)-C(4)	113(3)	C(5)-N(3)-C(9)	117(2)
C(3)-C(4)-C(5)	127(4)	N(3)-C(5)-C(6)	119(3)
C(4)-C(5)-C(6)	119(3)	N(3)-C(9)-C(8)	125(2)
C(4)-C(5)-N(3)	121(3)	C(5)-C(6)-C(7)	125(3)
N(S)-C(S1)-C(S2)	163(5)	C(6)-C(7)-C(8)	116(3)

Table 3.14 : Non-hydrogen intermolecular contacts (<3.75 Å) for $[Co(salen\text{-}C_2H_4\text{-}py)(O_2)]\cdot CH_3CN$.

Atoms	Distances	Atoms	Distances
O(1)... C(12)	3.69(3)	N(S)... C(S2)	3.11(9)
O(1)... N(S)	3.71(4)	N(S)... C(16)	3.61(5)
O(2)... C(10)	3.36(3)	N(S)... C(15)	3.71(5)
O(2)... C(12)	3.72(3)	C(S2)... C(S1)	3.31(7)
N(2)... C(14)	3.75(3)	C(S2)... C(7)	3.59(6)
C(10)... O(3)	3.37(4)	C(S2)... C(S2)	3.65(10)
C(10)... C(25)	3.42(3)	C(S2)... C(24)	3.68(6)
C(10)... C(26)	3.58(4)	C(S2)... C(6)	3.69(7)
C(20)... C(14)	3.40(4)	C(S1)... C(S1)	3.47(8)
C(1)... O(3)	3.52(4)	C(S1)... C(6)	3.70(5)
C(1)... O(4)	3.71(5)	C(12)... C(7)	3.59(4)
C(3)... C(S2)	3.51(8)	C(13)... C(7)	3.53(4)
C(4)... O(4)	3.66(6)	C(15)... C(22)	3.75(4)
O(4)... C(24)	3.44(4)	C(21)... C(23)	3.73(4)
O(4)... N(S)	3.58(6)	C(8)... C(9)	3.69(3)
O(4)... C(14)	3.64(5)		

the Co-N(1) bond; τ(N(1)-Co-O(3)-O(4)) is 3.8° and r(N(1)-O(4)) is only 2.86(4) Å. Quantitatively, the RMS components of thermal displacement, parallel to the O(1)-N(2) vector, for atoms O(3) and O(4) are 0.42(3) and 0.55(4) Å, respectively; these may be compared with the RMS components along the principal ellipsoid axes 0.22(3), 0.32(3), 0.49(3) Å for atom O(3) and 0.18(7), 0.45(4) and 0.57(4) for atom O(4). Disorder of atom O(3) involving a displacement of ~0.4 Å from its mean refined position along the O(1)-N(2) vector would lengthen r(Co-O(3)) to 1.88 Å and r(O-O) to 1.13 Å. Such canting of the bonded oxygen away from the normal to equatorial plane formed by ligand atoms N(1), O(1), N(2), O(2) has been observed[124]. Further similar disorder of atom O(4) along the vector N(2)-O(1) would lengthen r(O-O) to ~1.3 Å and sharpen ∠(Co-O-O).

Notwithstanding the disorder of the terminal oxygen atom, the report[300] of a bisecting conformation for the Co-O$^{O}_{\diagup}$ group is incorrect. The data do not justify any attempt to futher quantify this probable disorder. Disorder of a similar nature has been inferred for cobalt-nitrosyl compounds where distinctive thermal motion coupled with abnormal bond distances and angles (compared to related compounds) has been observed[226-228].

The Ethylene-Ethyl Bridge

The geometry of the ethylene-ethyl linkage is not well defined. When the parameters describing the non-positive definite thermal ellipsoid of atom C(1) are adjusted by, at most, one estimated standard deviation, the physically meaningful thermal ellipsoid thereby created has a similar aspect to that for C(2) (as depicted in Figure 3.7). Disorder between two

gauche conformations has been observed in several related complexes[126(b),230] where there is similar pronounced thermal motion perpendicular to the equatorial plane. However, the attached ethyl group at atom C(2) would appear to render this sort of disorder unlikely, and furthermore, no evidence could be found for alternative attachment of the ethyl group to atom C(1). Model building does indicate that despite the ethyl pyridyl group, which is attached to atom C(2), atom C(1) still possesses considerable conformational freedom which is transmitted to atom C(3) leaving atom C(2) relatively fixed. But while this may rationalise the exotically shaped thermal ellipsoids for atoms C(1) and C(3) it explains neither the abnormally long C(2)-C(3) (1.82(4) Å) nor the abnormally short C(3)-C(4) (1.34(4) Å) separations. Possible factors influencing these are mentioned in §3.2.3. It is noted however that the C(2)-C(3) separation in the five-coordinate precursor is apparently slightly lengthened (Table 3.2).

The possibility that this bond is severely stretched cannot be excluded; the conditions under which the dioxygen adduct is obtained are not conventional. As the two salicylideniminato fragments display no inconsistencies between bond lengths and angles that are chemically equivalent, it is considered unlikely that the refinement has converged to a false minimum.

Geometrical changes which occur in the ethylene-ethyl linkage as a result of oxygenation will be examined below.

Conformational Aspects of the Complex

Least-squares planes of selected groups of atoms, and deviations of those atoms therefrom (Table 3.15), and angles between planes (Table 3.16) are tabulated.

In contrast to its five-coordinate precursor, the dioxygen adduct Co(salen-C_2H_4-py)(O_2) not only has a square planar arrangement of the Schiff base donor atoms but the two salicylideniminato fragments are approximately coplanar : the maximum displacement of atoms N(1), O(1), N(2), O(2) from their least-squares plane is only 0.008(22) Å; the dihedral angle between the two phenyl groups is 5.7° and between the two chelate rings 5.6°. The salicylideniminato residues adopt a "step" conformation. The two such residues Sal-1 and Sal-2 which are both approximately planar (Table 3.15) are inclined 6.0° and 11.4°, respectively, to the equatorial ligand plane, and 5.5° with respect to each other. Such buckling, which has also been observed in other complexes[183] including the dioxygen adduct of Co(t-Bsalten)(1-Bz-imid)[123], ameliorates strain in the equatorial chelate rings and probably in the N(1), C(1), C(2), N(2), C(3), C(4) chain as well. The "umbrella" conformation has also been observed in related species[183].

The angle between the plane of the pyridyl group and the equatorial ligand plane is 89.4°. The cobalt atom is displaced 0.032(4) Å from the equatorial ligand plane towards the pyridyl ligand. An edge-on representation of the molecule is shown in Figure 3.9. The pyridyl plane approximately bisects the N(1)-Co-N(2) bond and the dihedral angle made with the Co-O(3)-O(4) plane is 41.1°; whereas in all other

Table 3.15 : Selected least-squares planes (unweighted) for Co(salen-C_2H_4py)(O_2).

Name of Plane	Equation of Plane[b] Ax + By + Cz - D = 0 (Coeff x 10^4).				Atoms in Plane / Deviations of Atoms from Plane (Å x 10^3)[a]									Displacement of Other Atoms from Plane (Å x 10^3)[a]		
I	3841	-8534	-3524	-12176	N(1)	O(1)	N(2)	O(2)						Co	C(1)	C(2)
					008(20)	-008(17)	-008(22)	008(16)						032(4)	-186(33)	124(39)
Py	7655	4974	-4082	46181	N(3)	C(5)	C(6)	C(7)	C(8)	C(9)				Co	C(4)	
					010(23)	026(29)	-029(33)	-002(33)	037(27)	-042(27)				-075(4)	273(39)	
Ph-1	3004	-9027	-3082	-18468	C(11)	C(12)	C(13)	C(14)	C(15)	C(16)						
					-008(24)	011(28)	004(25)	-024(29)	028(27)	-012(27)						
Ph-2	2322	-9409	-2467	-18332	C(21)	C(22)	C(23)	C(24)	C(25)	C(26)						
					-051(28)	029(29)	003(29)	-012(29)	-012(26)	043(27)						
Sal-1	3020	-9017	-3094	-18289	N(1)	C(10)	C(11)	C(12)	C(13)	C(14)	C(15)	C(16)	O(1)	Co		
					016(20)	-018(26)	-008(24)	013(28)	008(25)	-022(29)	027(27)	-014(27)	-002(17)	175(4)		
Sal-2	2328	-9386	-2545	-18344	N(2)	C(20)	C(21)	C(22)	C(23)	C(24)	C(25)	C(26)	O(2)	Co		
					-048(22)	035(27)	-040(28)	033(29)	-004(29)	-024(29)	-018(26)	048(27)	018(15)	-238(4)		
Chel-1	3439	-8798	-3282	-14871	Co	O(1)	C(16)	C(11)	C(10)	N(1)						
					057(4)	-050(17)	001(27)	042(24)	-009(26)	-040(20)						
Chel-2	2788	-9138	-2954	-17022	Co	O(2)	C(26)	C(21)	C(20)	N(2)						
					-083(4)	070(16)	015(27)	-094(28)	046(27)	045(22)						

[a] Displacements of atoms are from a fixed plane and hence the accompanying e.s.ds are derived only from the e.s.d.'s in the positional coordinates of the atoms.

[b] The coefficients of the least-squares plane are for an orthogonalised Ångstrom coordinate system.

Table 3.16 : Selected dihedral angles (in °) between least-squares planes.

	Ph-1	Ph-2	Py	Sal-1	Sal-2	Chel-1	Chel-2
I	6.1	11.8	89.2	6.0	11.4	3.1	7.7
Ph-1	-	5.7	95.4	0.1	5.4	3.0	1.6
Ph-2		-	100.9	5.8	0.6	8.7	4.2
Py			-	95.2	100.7	92.3	96.9
Sal-1				-	5.5	2.9	1.7
Sal-2					-	8.4	3.8
Chel-1							4.6

dioxygen complexes characterised[123-126,231] the pyridyl plane approximately bisects the N(1)-Co-O(1) bond angle and the dioxygen ligand bisects this or the N(1)-Co-N(2) bond angle.

Allowance for disorder in the terminal oxygen atom position (see above) still does not give a bisecting orientation for the Co-O$^{O}_{\diagup}$ group of Co(salen-C_2H_4-py)(O_2).

Bisecting orientations for the axial ligands are the most favourable on steric grounds. For Co(salen-C_2H_4-py)-(O_2) the pyridyl orientation is largely constrained by the ethylene-ethyl linkage to bisect the N(1)-Co-N(2) bond angle. This is not achieved without some distortion. Compared to Co(salen-C_2H_4-py) (whose corresponding parameters are parenthetically placed after that for the dioxygen adduct) atom C(4) is displaced 0.27(4) Å (0.11(2) and 0.11(3) Å) from the pyridyl plane; the cobalt atom is displaced 0.075(4) Å (0.293(3) and 0.120(3) Å) from the same plane; and the Co-N(3)-C(5) and Co-N(3)-C(9) angles are, respectively 131(2)° (115(1)° and 115(1)°) and 112(2)° (127(1) and 126(1)°). This orientation of the pyridyl group serves to minimise intramolecular contacts between the pyridyl's ethyl substituent and the Schiff-base donor atoms. The rotation of the pyridyl plane about its normal does, however, lead to tight C(9)-O(1) and C(9)-O(2) contacts of 2.85(3) Å.

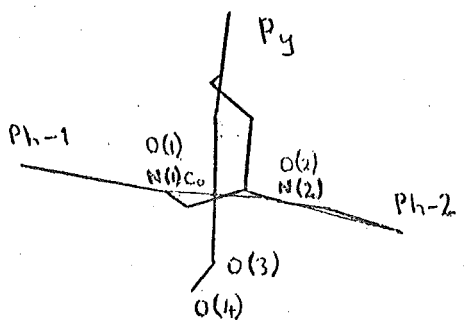

Figure 3.9: Edge-on view of Co(salen-C_2H_4-py) showing disposition of salicylideniminato residues and pyridyl ring.

Stereochemical Trends in Four-,Five-and Six-Coordinate Schiff Base Complexes.

Marked stereochemical changes in the cobalt-Schiff base moiety accompany the coordination of dioxygen; the average Co-N bond length decreases from 1.94(1) and 2.00(1) Å for two independent molecules of Co(salen-C_2H_4-py) to 1.88(2) Å in the dioxygen adduct, the average Co-O separation likewise decreases from 1.93(1) and 1.92(1) Å to 1.89(2) Å and the Co-N(3) separation decreases from 2.14(1) and 2.15(1) Å to 2.03(2) Å. The stereochemical changes can be considered to be initiated by a movement of atom N(1) into the O(1), O(2), N(2) plane with the dihedral angle between the planes Co,O(1), N(1) and Co, O(2), N(2), changing from 25.2° and 30.6° to 2.9° in the six-coordinate dioxygen adduct.* This twists the two salicylideniminato planes Sal-1 and Sal-2 into near-coplanarity. Changes in the torsional angles of the N(1), C(1), C(2), N(2), C(3), C(4), C(5) backbone culminate in the adoption of a more nearly bisecting orientation of the pyridyl ligand - τ(N(1)-Co-N(3)-C(5)) increases from an average value of 25(2)° to 46(2)° and τ(N(2)-Co-N(3)-C(5)) decreases from 156(1)° to 139(3)°. Table 3.17 lists selected torsional angles for the five-coordinate complexes Fe,Co(salen-C_2H_4-py) and for Co(salen-C_2H_4-py)(O_2). Bond angles between the cobalt and the Schiff-base ligand atoms display only small departures from square-planar symmetry. (Table 3.13). In the following discussions consideration of the structure of Co(acacen)(py)(O_2)[231], which is of very low precision, is excluded. While dioxygen adducts of

* Figures 3.4 and 3.9 illustrate the changes.

Table 3.17 : Selected torsional angles (in °) for Co(salen-C_2H_4-py)(O_2), Fe(salen-C_2H_4py) and Co(salen-C_2H_4-py).

Atoms	Fe[a]	Co(A)	Co(B)	Average Co(A) and Co(B)	Co-O_2
	Angle	Angle	Angle	Angle	Angle
N(1)-O(1)-O(2)-N(2)	16.3(3)	12.6(5)	17.2(5)	14.9	0.7(7)
O(1)-N(1)-N(2)-O(2)	19.0(3)	13.2(5)	18.3(6)	15.8	0.7(7)
N(2)-M-N(3)-C(5)	45.9(8)	54.2(14)	55.1(15)	54.7	40.4(23)
N(2)-M-N(3)-C(9)	120.5(7)	121.5(13)	120.9(13)	121.2	135.2(25)
N(1)-M-N(3)-C(5)	31.4(8)	28.9(15)	26.7(16)	27.8	45.8(23)
N(1)-M-N(3)-C(9)	162.3(8)	155.4(14)	157.3(14)	156.4	138.7(25)
C(10)-N(1)-C(1)-C(2)	160.6(11)	167.3(22)	166.2(24)	166.8	162(3)
C(20)-N(2)-C(2)-C(1)	141.0(12)	149.7(21)	143.2(22)	146.5	157(4)
C(20)-N(2)-C(2)-C(3)	93.9(12)	91.5(23)	96.8(22)	94.2	92(3)
N(1)-C(1)-C(2)-N(2)	42.8(10)	35.6(19)	36.5(20)	36.1	24(3)
N(1)-C(1)-C(2)-C(3)	80.8(11)	86.0(21)	82.5(21)	84.3	90(3)
N(2)-C(2)-C(3)-C(4)	61.5(13)	61.2(25)	64.5(23)	62.9	68(4)
C(1)-C(2)-C(3)-C(4)	59.7(13)	55.0(24)	53.6(24)	54.6	53(4)
C(2)-C(3)-C(4)-C(5)	81.6(14)	80.8(27)	83.3(25)	82.1	75(5)
C(3)-C(4)-C(5)-C(6)	96.3(14)	101.5(29)	109.5(25)	105.5	117(5)
N(1)-M-O(3)-O(4)	-	-	-	-	3(4)

[a] M = Co, Fe = M(salen-C_2H_4-py)

cobalt Schiff bases, including Co(salen-C_2H_4-py)(O_2), share very similar dimensions in the Schiff base core and the Co-O(3) bond length[123-126], there are some peculiarities in the cobalt-axial base bond lengths. The Co-N_{imid} bond length for Co(t-Bsalten)(1-Bz-imid)(O_2), 1.974(8) Å [123], is apparently significantly shorter than those for Co(saltmen)-(1-Bz-imid)(O_2), 2.011(2) Å [124], and Co(3-Fsaltmen)(1-Me-imid)-(O_2), 2.004(2) Å [125]. Short of invoking crystal packing effects, the reasons for this variation, if real, are not apparent. Moreover the Co-N_{py} bond lengths for Co(salen-C_2H_4-py)(O_2) and Co(bzacen)(py)(O_2) are 2.03(2) and 1.99(1) Å [126(b)], respectively, and it is surprising that the Co-N(3) separations appear to be independent of the axial base. A Co-N_{imid} separation no longer than that for Co-N_{py} could be expected on the following interrelated electronic and steric grounds. That imidazoles generally give more stable dioxygen adducts[222], at least for a porphyrin ligand system, has been attributed to their greater ability to donate electron density to the metal. The tighter C-N-C angle of 105° compared with 120° for pyridine would lead to smaller interaction of an imidazole ligand with the Schiff-base plane and hence allow closer approach of the ligand to the metal centre. But for Co(bzacen)(py)O_2), r(Co-N(3)) is marginally shorter than that for Co(saltmen)(1-Bz-imid)(O_2).

The four-coordinate parent compounds such as Co(salen)[210], Co(bzacen)[211] and Co(t-Bsalten)[123] are all square planar although the last complex has a small tetrahedral distortion possibly attributable to the bulky

t-butyl groups (values for τ(N(1)-O(1)-O(2)-N(2)) are 2.2^{o}, 0.7^{o}, 10.9^{o}, respectively). The metal-Schiff base bonds are shorter than those for the five-coordinate adducts. It has been noted[210] that stronger, shorter bonds are likely simply because there are only four ligands. The shorter bond lengths observed for the four-coordinate parent compound compared to those for the six-coordinate derivatives may, in part, be attributed to this. However, the substantially longer bonds of the five-coordinate complexes compared to the low-spin four-coordinate species may be attributable, in the low spin five-coordinate case, to diminished metal-ligand πbonding (see also §3.1.4) and, in the high spin case, to the larger cobalt ion radius as well. Similar considerations apply in rationalising the longer bond lengths observed for the five-coordinate species compared to those for its six-coordinate dioxygen adduct. Table 3.18 lists quantitative data for a representative selection of compounds.

Factors Influencing Co-L_{ax} Separations

Although no crystal structures of the type Co(Schiff-base)$(L_{ax})_2^{n+}$ (n=0,1; L_{ax} = imidazole or pyridyl species) have been determined it is not unreasonable to use parameters from related porphinato complexes but with cognisance of the tighter Schiff-base equatorial core, since r(CoL_{eq}) are approximately 0.1 Å shorter for Schiff-base ligands compared with the less flexible porphyrin ligand.

If one L_{ax} ligand in a Co(Schiff base)$(L_{ax})_2$ complex is replaced by dioxygen, a contraction of the other Co-L_{ax} bond by more than 0.3 Å can confidently be expected by

Table 3.18 : Equatorial bond lengths for selected cobalt Schiff-base derivatives[a].

Complex	4-coord.	5-coord[b] +base	6-coord $+O_2$	Reference
Co(salen)	1.847(5)	1.90(1)	-	[210,196]
(added base py)	1.852(5)	1.90(1)	-	
Co(salen-py)	-	1.94(1), 2.00(1)	1.88(2)	[188], This work.
	-	1.93(1), 1.92(1)	1.89(2)	
Co(t-Balten)	1.856(3)	-	1.896(8)	[123]
(added base 1-Bz-imid)	1.853(2)	-	1.895(6)	
Co(3-Fsaltmen)	-	2.090(9)	1.901(3)	[198,124]
(added base, B[c])	-	1.973(8)	1.893(3)	

a. Average Co-N separation quoted above average Co-O separation in Å.

b. Except for Co(salen)(py) which is low spin other five-coordinate species high spin.

c. For five-coordinate, B=1-Bz-imid; for six-coordinate, B=1-Me-imid.

analogy with related porphyrin species. In Co(OEP)-(3-Me-py)$_2$ Co-L_{ax} is 2.386(2) Å [232] and a similar, possibly even longer, separation can be expected for the corresponding Schiff-base species. The long Co-L_{ax} separation has been attributed to the presence of an electron in the cobalt $3d_{z^2}$ orbital which is aligned along the Co-L_{ax} bonds [191]. For the Schiff-base cobalt-dioxygen complexes structurally characterised, Co-L_{ax} is between 1.974(8) and 2.03(2) Å.

Now the Co-L_{ax} separation for cobalt-dioxygen complexes is not dissimilar to that observed for some cobalt(III) complexes in which there is no $3d_{z^2}$ electron. For example, in Co(TPP)(3,5-Me_2-py)(NO_2) the Co-L_{ax} separation is 2.036(4) Å [233]. The cobalt(III)-methoxy complex Co(salen)-(py)(OMe) has a similar value for the Co-L_{ax} separation of 2.03(1) Å [240] and, furthermore, the Co-OMe separation of 1.89(1) Å is very similar to the Co-O_2 separation[240]. It is as well to note, however, that carbanion complexes of cobalt(III)-Schiff bases display marked trans effects; for Co(acacen)(py)(Me), r(Co-N_{py}) is 2.16 (1) Å [230]. In addition, for some axially symmetric cobalt-porphyrin complexes, a similarly large decrease in Co-L_{ax} also accompanies the removal of the cobalt $3d_{z^2}$ electron. For Co(TPP)$(pip)_2$ r(Co-L_{ax}) is 2.436(2) Å [234] and for Co(TPP)-$(pip)_2^+$ r(Co-L_{ax}) is 2.060(2) Å [235]. Moreover with the less sterically demanding imidazole ligand r(Co-L_{ax}) is 1.93(2) Å for Co(TPP)$(imid)_2^+$ [236].

On the other hand for related porphinatoiron systems quite small changes are induced by the oxidation of Fe^{II} to Fe^{III}; in this case oxidation does not involve the loss of a $3d_{z^2}$ electron. For Fe(TPP)(1-Me-imid)$_2$ r(Fe-L_{ax}) is 2.016(5) Å [237] which may be compared with 1.996(5) and 1.988(5) Å for Fe^{III}(PP-IX$^-$)(1-Me-imid)$_2$ [238], and 1.957(4) and 1.991(5) Å for Fe(TPP)(imid)$_2^+$ [239]. Because the orientation of the porphyrin plane is not in the optimum bisecting position the Fe-L_{ax} bonds are somewhat stretched. However, the second and longer r(Fe-L_{ax}) quoted for the two iron(III) complexes is associated with the imidazole plane in a similar orientation to that for the iron(II) complex. Thus a reduction of only about 0.025 to 0.028 Å has occurred; the shortening may be attributed to the greater charge concentrated on iron(III) compared with iron(II).

Therefore, noting firstly the long Co-L_{ax} separation of "bona fide" cobalt(II) complexes compared to the separation for cobalt-dioxygen complexes, secondly the similarity of r(Co-L_{ax}) for such dioxygen complexes and "bonafide" cobalt(III) species, and thirdly the, perhaps fortuitously, similar cobalt(III)-methoxide and cobalt-dioxygen separations, it seems reasonable to conclude on structural evidence alone that a cobalt(III)-coordinated superoxide formulation is applicable to those dioxygen complexes structurally characterised. Furthermore there can be no π component in the Co-OMe bond; the similarity of r(Co-O_{OMe}) with r(Co-O_{O_2}) may indicate little π-bonding

component in the cobalt-dioxygen linkage. Such a representation is in general accord with other independent data reviewed in §3.2.1.

Comparison of cobalt-dioxygen complexes with the iron-dioxygen complex Fe(TpivPP)(1-Me-imid)(O_2) will be made in §4.2.4.

3.3 Concluding Remarks

Coordination of dioxygen to cobalt(II) complexes is accompanied by large stereochemical changes not only in general geometry but also in metal-ligand separations. In general 1:1 cobalt-dioxygen complexes of Schiff-base and porphyrin ligand systems are adequately represented by a cobalt(III)-coordinated superoxide formulation. The stereochemical evidence for a $Co^{III}-O_2^-$ for Co(salen-C_2H_4-py)-(O_2) complements other independent spectroscopic evidence for this and closely related systems. For some other cobalt-dioxygen complexes such a formulation may not be appropriate[19].

CHAPTER 4

PORPHYRIN COMPLEXES

Porphyrin and its substituted derivatives are highly versatile ligands. On deprotonation to the dianionic chelating form (Figure 4.1)

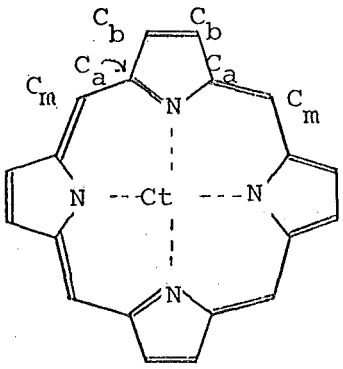

Figure 4.1: A general atom-labelling scheme for porphyrins. The central site is labelled Ct.

they coordinate to most metals with a wide range of supporting ligands occupying one or both of the two axial positions. Porphinato complexes are known for nearly 50 elements[241], the only notable exceptions being the lathanide and actinide series. In contrast to complexes of the more flexible Schiff-base ligand, most metalloporphyrins possess quasi-four fold axial symmetry; that is, they are either square planar, square pyramidal or octahedral with the porphyrin ligand as the equatorial component. Some heavy metals prefer a more exotic mode of coordination – for example the μ-(porphyrin)-$[Re(CO)_3]_2$ species[242] (Figure 4.2).

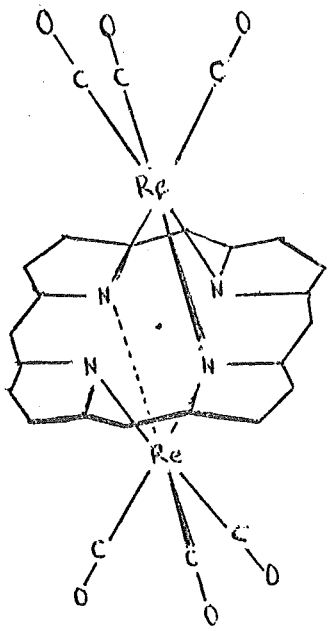

Figure 4.2: Structure of (TPP)$[Re(CO)_3]$.

An exceptionally thorough analysis of the stereochemistry of and stereochemical trends for metalloporphyrins of more orthodox structure has been made[191]. Many of the structure analyses are very precise.

The porphinato ring, being a macrocycle with a highly delocalised π-bonding network, has a strong tendency to remain planar. Thus, if metal ions of different radii are to be accommodated in the plane of the porphinato ring or, more particularly, in the plane of the porphinato nitrogen atoms, then expansion or contraction of the "central hole" (i.e. an increase or decrease in $r(Ct...N_{porph})$) is necessary. Hoard has suggested[243] that, at a radius $r(Ct\text{-}N_{porph})$ of $\sim$2.01 Å, bond angle strain in the porphinato skeleton is minimised. Fleischer has suggested 2.04 Å[244]. The radius varies between 2.098(2) Å for the structure of $[Sn(TPP)Cl_2]$, which has crystallographically imposed planarity of the Sn(TPP) component[245], and 1.958(2) Å for the structure of Ni(OEP) which, although planarity is not crystallographically imposed, nevertheless shows only small departures from a planar C_{4h} symmetry[246]. This contraction is achieved through

a tightening of the angle $\angle(C_a-N_{porph}-C_a)$ by $\sim 5.3^o$, opening of $\angle(N-C_a-C_b)$ by $\sim 3.4^o$ and contractions of $r(C_a-C_m)$ by ~ 0.036 Å and $r(C_b-C_b)$ by ~ 0.034 Å (see Figure 4.1 for definition of the labelling scheme). Contraction of the central hole below the bound of 1.958(2) Å may be achieved by marked ruffling of the porphinato skeleton and reduction to quasi-D_{2d} symmetry[247]. For example, Ni(OEP) also exists in a strongly ruffled D_{2d} geometry. The dihedral angle between the mean porphinato plane and an individual pyrrole ring is 14.2^o and $r(Ct...N_{porph})$ or equivalently $r(Ni-N_{porph})$ is 1.929(3) Å [248]. The reduction in delocalised π bonding for the porphinato macrocycle, caused by the adoption of a non-planar geometry, is counterbalanced by stronger $M-N_{porph}$ σ bonds.

In most five-coordinate porphinato complexes, even when the metal atom is substantially out of the plane of the four porphinato nitrogen atoms, planarity of the porphinato species is largely maintained; in other words, there is little "doming" of the porphinato ligand.

These, therefore, are some general features of metalloporphyrins. The porphinato skeleton maintains nearly invariant stereochemistry and only in crystal structures of very high precision do the small deformations in bond angles and distances (wrought by contraction or expansion of the central hole from its "ideal" radius of ~ 2.01 Å) become apparent. No matter how severe the ruffling of the porphinato skeleton is, the atoms within individual pyrrole rings maintain planarity.

The porphyrins found in biological systems have asymmetrical substitution on the carbon atoms of type C_b (Figure 4.1). The parent porphyrin of biological systems, haem, is shown in Figure 4.3. The metal coordinated is invariably iron. Other porphyrin-derived species are the chlorophylls (Figure 4.4(a)) and the corrins, of which vitamin B_{12} is the most popularly known example (Figure 4.4(b)). Axial ligation and porphyrin substituents divide the haemoproteins into their two main classes, the haemoglobins and the cytochromes.

Except for mutants whose owners usually fare poorly physiologically, the axial ligand in haemoglobins is an imidazole group of an histidine amino acid residue. Dioxygen (and other small molecules) coordinate trans to this "proximal" histidine. Coordination of dioxygen is reversible and the haemoglobins transport and store dioxygen for respirative processes. The porphyrin, in almost all cases, is protoporphyrin-IX which is shown in Figure 4.3 (see also §2.3). In §4.2 a model for myoglobin, a monomeric haemoglobin, is described. The stereochemistry of this model porphinatoiron-dioxygen adduct will be described and its validity as a model assessed.

The cytochromes are a more diverse group[249]. The members of one subclass, which includes the well-characterised cytochromes c, function as electron transport species. The redox potentials of these cytochromes are modulated by different peripheral substituents on the porphyrin and axial ligation to the iron centre. The electron transport chain terminates cytochrome oxidase, a rather complex copper-contain-

(a) Protohaem

$R_1=R_2=$ $-CH=CH_2$, $R_3=$ CH_3

haemoglobin

cytochrome P450

catalase

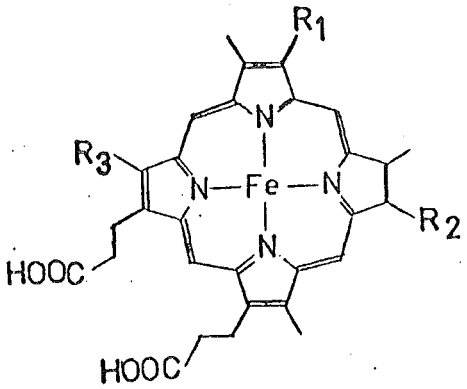

(b) Haem c

$R_1=R_2=$ $-\underset{\underset{\text{S-protein}}{|}}{CH}-CH_3$, $R_3=$ CH_3

cytochrome c

(c) Haem a

$R_1=$ $-\underset{\underset{OH}{|}}{CH}-CH_2-(\underset{\underset{CH_3}{|}}{CH}-(CH_2)_3)_2-\underset{\underset{CH_3}{|}}{CH}$, $R_2=$ $-CH=CH_2$, $R_3=$ $-CHO$

cytochrome a

Figure 4.3 : Haem and its derivatives.

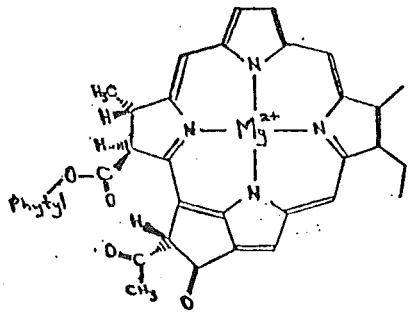

(a) Chlorophyll a

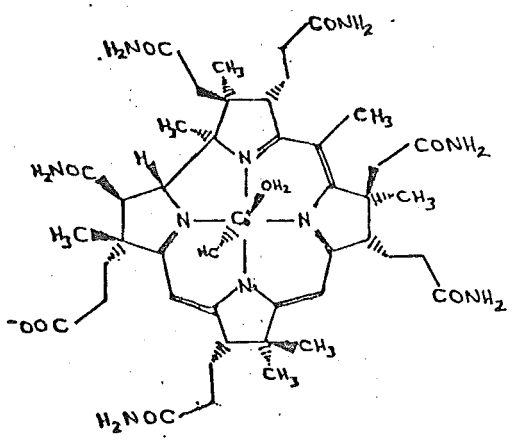

(b) Cobyric acid (the simplest naturally occurring corrinoid).

Figure 4.4 : Porphyrin-related biologically occurring macrocycles.

ing haemoprotein, which coordinates and reduces dioxygen. Another subclass coordinates dioxygen but also catalyses directly its incorporation into some substrate (see also §2.3). The best-characterised example is the bacterial camphor hydroxylase, cytochrome $P450_{cam}$, which has a protohaem prosthetic group identical to the haemoglobins. However, the quite different spectral properties of cytochrome P450, particularly the reduced enzyme-(ironII)-carbonyl adduct, appear to preclude axial ligation similar to the haemoglobin class of oxygen-binding haemoproteins. A dioxygen adduct of a porphinatoiron(II) derivative with mercaptan S< axial ligation is described in §4.3; this complex is a possible model for the dioxygenated cytochrome P450 enzyme. In §4.1 dioxygen adducts of porphinatoiron(II) derivatives are reviewed, and the protein role is analysed.

4.1 Dioxygen Adducts of Porphinatoiron(II) Derivatives.

Speculation over the geometry of the iron-dioxygen linkage in oxygen-binding haemoproteins of the haemoglobin type has only recently been settled, firstly and indirectly, by analogy with the structures of mononuclear dioxygen adducts of cobalt(II) complexes (Chapter 3) and, secondly and more directly, by the structure analysis of a mononuclear adduct of an iron(II)-porphyrin-imidazole derivative (reference [11] and §4.2).

A knowledge of the fates that may befall porphinatoiron(II) species removed from their protein matrix has clarified the role of the protein and has led ultimately to the isolation of stable crystalline iron-dioxygen model complexes.

Although the general geometry of the metal-dioxygen moiety is now established, the validity or otherwise of an $Fe^{III}-O_2^-$ formulation, analogous to that which appears to adequately represent spectroscopic and structural features of many cobalt-dioxygen complexes of comparable ligature, remains unresolved.

The reactions of iron-dioxygen species and the role of the protein, and the results of a number of studies which indicate something about the nature of the iron-dioxygen linkage will be examined in some detail.

4.1.1 Irreversible Oxidation and the Evolution of Model Iron-Dioxygen Systems.

At this stage it is appropriate to distinguish between the terms "oxidation" and "autoxidation". Oxidation will apply to the process

$$Fe^{II}\,L \xrightarrow{[O]} Fe^{III}L$$

which, in the ensured absence of other oxidants, is mediated by molecular oxygen. Autoxidation , a term commonly and sometimes imprecisely used in studies on the formation of met-Fe^{III}-haemoglobin (metHb), will be applied specifically to the process

$$LFe\text{-}O_2 \longrightarrow LFe^{III}.$$

Autoxidation of Oxyhaemoglobins

The reluctance of oxyhaemoglobins to autoxidise or otherwise be oxidised under physiological conditions is remarkable when compared with the extremely facile oxidation undergone by free iron(II)-porphyrin or-Schiff base complexes. Disturbance of the normal routine of reversible oxygen uptake and release by haemoglobins is rare; only about 3% of the haemoglobin in a normal red blood cell is oxidised daily[250]. Oxyhaemoglobin autoxidation proceeds mainly by proton-assisted displacement of a superoxide anion radical by a nucleophile Y^-:-

$$(B)(P)Fe\text{-}O_2 + Y^- \xrightarrow{H^+} (P)(B)Fe^{III}Y^- + O_2^- \qquad R4.1$$

and not by a simple dissociative pathway[140-142]:-

$$(B)(P)Fe\text{-}O_2 \longrightarrow (B)(P)Fe^{III} + O_2^- \qquad R4.2$$

Indeed, the concentration of the gentle nucleophile Cl^- in erythrocytes may well account for the daily production of met-Hb[142].

Oxidation of Simple Iron(II)-porphyrins and the Role of the Protein.

Reversible binding of dioxygen to iron(II)-porphyrin-axial base species, Fe(P)(B), freed from a protein matrix, has been reported (see below). But Collman et al[12] and Gagne[251] have noted that in a number of ill-characterised systems the reversible binding of dioxygen was an illusion due to axial base redox reactions.

It is more usual for haems freed from their protein environment, and for other iron(II) species, to undergo

rapid "irreversible" oxidation in the presence of dioxygen to well-characterised μ-oxo species[252-254]

$$4Fe(P)(B)_2 + O_2 \rightarrow 2(P)Fe\text{-}O\text{-}Fe(P) + 8B \qquad R4.3$$

Elucidation of the mechanism for irreversible oxidation led to a better appreciation of the role of the protein and of the factors which enhance the reversible binding of dioxygen over irreversible oxidation. Studies have been made on the oxidation of iron(II) species by dioxygen[255-258]. For the oxidation of the haemochrome $Fe(P)(py)_2$ the following mechanism was proposed by Caughey[257] and supported by Collman and Gagne[12,251] in a critical assessment of the literature.

$$Fe^{II}(P)(py)_2 \rightleftharpoons Fe^{II}(P)(py) + py \qquad R4.4$$

$$Fe^{II}(P)(py) + O_2 \xrightarrow[\text{determining}]{\text{rate}} (py)(P)Fe\text{-}O_2 \qquad R4.5$$

$$(py)(P)Fe\,O_2 + Fe^{II}(P)(py) \longrightarrow (py)(P)Fe\text{-}O_2\text{-}Fe(P)(py) \qquad R4.6$$

$$(py)(P)Fe\text{-}O_2\text{-}Fe(P)(py) \longleftrightarrow 2\,(py)(P)Fe^{IV}{=}O \qquad R4.7$$

$$(py)(P)Fe^{IV}{=}O + Fe^{II}(P)(py) \longrightarrow Fe^{III}\text{-}O^{2-}\text{-}Fe^{III} + 2py \qquad R4.8$$

Therefore, in encouraging the reversible binding of dioxygen to the haemoglobins the following roles for the protein surrounding the dioxygen binding site are implied.

1. The protein prevents bimolecular contact of two iron centres as in reaction R4.6. In haemoglobin this is achieved by embedding the haem prosthetic group in the protein. In some model studies reversible binding of dioxygen has been observed by immobilising a porphinatoiron(II) species in a synthetic polymer[259].

2. The protein supplies an imidazole ligand to the iron centre and also maintains five-coordination in the absence of dioxygen or its competitors. In the presence of excess pyridine, the diamagnetic haemochromes, $Fe(P)(py)_2$, are stable towards oxidation by molecular oxygen[258]. Oxygenation and oxidation proceed from the five-coordinate product of reaction R4.4.

3. The protein provides an aprotic environment for the coordinated dioxygen ligand. Hydrogen ions are known to promote the autoxidation of oxyhaemoglobin in the presence of nucleophiles (see above and reaction R4.1.)[141,142]. Moreover, in the abnormal haemoglobin, $Hb^{M\ Boston}$ (α58(E7) His→Tyr), the distal tyrosine (taking the place of histidine) coordinates to the iron(III) centre of each α chain via its phenolate anion[327]; the analogous β-chain mutant $Hb^{M\ Saskatoon}$ (β63(E7) His→Tyr) is similarly oxidised[328]. Other acidic groups protruding into the binding pocket, such as occurs in $Hb^{M\ Milwaukee-I}$ (β67(E11)Val→Glu),[329], may lead to valency hybrids also.

It is appropriate at this point to elaborate further on the nature of the binding pocket since it has been suggested[259], and widely accepted, that the protein provides a non-polar hydrophobic environment.

Although the binding pocket is largely lined with non-polar residues, compared with the hydrophilic residues on the outside of the protein[148-151], it is too simplistic

to regard the binding pocket as non-polar and hydrophobic. Firstly, in most haemoglobins there exists a polar imidazole group poised above the dioxygen binding site. Model studies have subsequently shown that for both cobalt-dioxygen[225] and iron-dioxygen systems[266, 267], coordination of dioxygen is enhanced in polar solvents.

Secondly, while access of water to the binding site may be inhibited it is certainly not prohibited. In the α chains of adult deoxyhaemoglobin a water molecule is to be found hydrogen-bonded to the imidazole group of the distal histidine, and approximately 3.6 Å from the iron[150]. In addition met-HbX ($X=N_3^-, SCN^-, F^-$) species undergo quite rapid exchange of anionic ligands[152,260,261]. This implies easy access of anions to the binding sites. A less polar species, such as water, should therefore be able to approach a binding site presumed to be non-polar and hydrophobic with equal or greater ease. Nor should the presence of water near the coordinated dioxygen of HbO_2 be regarded as disastrous. Although the autoxidation of HbO_2 in the presence of nucleophiles is proton-assisted, in the presence of weak nucleophiles such as chloride ion, and at neutral pH, the reaction is very slow. Conversely, the oxidation of protein-free, sterically unencumbered $Fe^{II}(P)(B)$ complexes in water is very rapid. Thus the effect of protic solvents such as water is manifested upon an $Fe\text{-}O_2\text{-}Fe$ species rather than the $Fe\text{-}O_2$ species.

Thus the protein's major role is to prevent bimolecular contact of iron centres. Under physiological conditions (neutral-to-basic pH and very weak nucleophiles) the copresence,

in the binding pocket, of coordinated dioxygen and a protic species, such as water, does not appear to be inimical to the stability of HbO_2.

The role of the distal histidine has been much discussed. Pauling proposed[68(b)] that the coordinated dioxygen ligand was hydrogen bonded to the distal histidine which existed as an imidazolium species. However, the distal imidazole appears to be unimportant to the stability of HbO_2 since some insect haemoglobins have a non-polar distal residue in place of histidine[151]. The distal residues do however, appear to be of critical importance in enhancing the relative stability of HbO_2 over that of HbCO[13,17].

Protein-free Iron-dioxygen Systems

Appreciation of the protein's function has led to well-characterised dioxygen adducts of iron porphyrins in solution and in the crystalline state.

As with cobalt(II) systems low temperatures enhance the kinetic stability of the mononuclear dioxygen adduct. At low temperatures ($\sim$-50°C) reversible binding of dioxygen has been observed for porphinatoiron(II)-amine derivatives with an unshielded oxygen binding site[263-268]. That reversible oxygenation of sterically unhindered porphyrin derivatives was also found to occur at low temperatures in a protic solvent (butanol)[264], and for axial bases other than imidazole-type ligands,[264] finally dispelled notions on the indispensability of the protein and of an imidazole-type base for reversible oxygen binding to haems. An axial base of some

sort still appears essential. At room temperature the sterically unhindered dioxygen adducts all irreversibly autoxidised very rapidly.

A second approach, using steric encumbrance to inhibit the bimolecular contact of FeO_2 and Fe^{II} species, has led to the observation of reversible oxygenation in solution at ambient temperatures and to the isolation of crystalline dioxygen adducts. An early non-porphyrin, N_4-macrocyle iron(II) derivative with built-in steric hindrance was found to oxygenate reversibly (1 O_2:1 Fe) at -78°C [269]. In the absence of the phenyl shields, irreversible oxidation occurred at that temperature.

An elegant porphyrin derivative with a considerably more protected oxygen-binding site (Figure 4.5) has been synthesised and found capable of reversibly binding dioxygen at 25°C [270].

Collman and coworkers utilised the atropisomerism of ortho-substituted meso-tetraphenyl porphyrins (Figure 4.6(a)-(d)) to prepare a porphyrin derivative, meso-tetra(α,α,α,α-orthopivalamide phenyl) porphyrin H_2TpivPP, popularly known as the "picket fence" porphyrin, which had hindered and unhindered binding sites (Figure 4.6(e))[12,271]. Although formation of diamagnetic six-coordinate species, such as Fe(TpivPP)(1-Me-imid)$_2$, could still occur, dioxygen adducts were quite stable in solvents as diverse as benzene and non-acidic aqueous N,N'-dimethylformamide, provided an excess of base was present to inhibit coordination of dioxygen on the unhindered site with consequent irreversible oxidation[271].

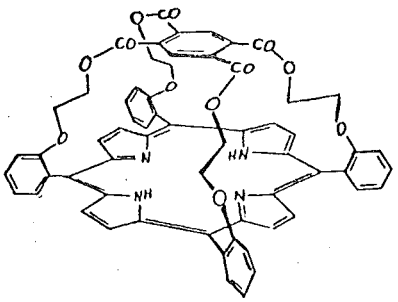

Figure 4.5 : Diagram of the "capped" porphyrin.

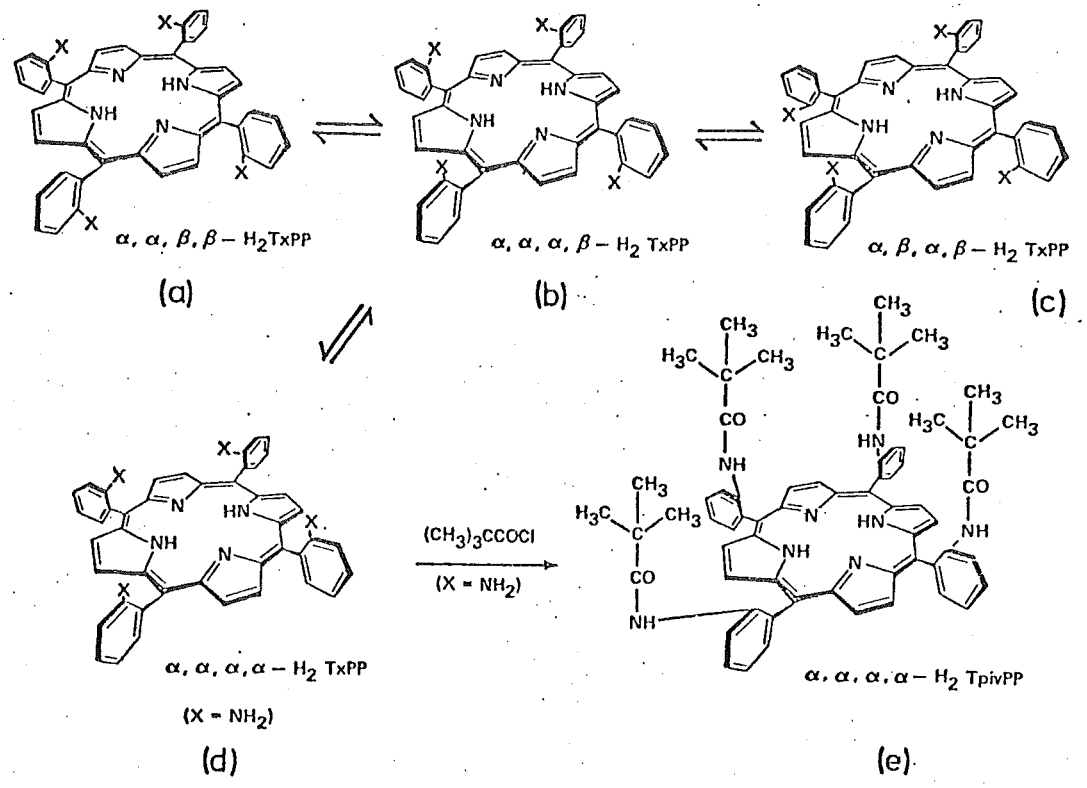

Figure 4.6 : Atropisomerism of ortho-substituted meso-tetraphenyl-porphyrins, (a) - (d); and the "picket fence" porphyrin, (e).

With regard to the importance of an aprotic environment it is relevant to note that dioxygen adducts of derivatives with "pickets" containing protons more acidic than the amide proton of a pivalamide group were found to autoxidise [12]. Characterisation of the iron(III) product of this autoxidation reaction has not been made.

In contrast to other cobalt(II) porphyrin complexes which only bind dioxygen at low temperature, Co(TpivPP)-(1-Me-imid) will reversibly bind dioxygen in solution (and also in the solid state) at ambient temperatures[272]. A crystalline dioxygen adduct of Fe^{II}(TpivPP)(1-Me-imid) was obtained and a preliminary report of the structure analysis has been made[11,12]. The complete structure analysis is the subject of §4.2.

4.1.2 The Nature of the Metal-Dioxygen Linkage

In this subsection the results of a number of physical studies on iron-dioxygen systems which relate to the natures of the coordinated dioxygen ligand and the iron atom are presented. The paradox between the long-assumed rigorous diamagnetism of oxyhaemoglobin and the evidence from other studies that a polarised $Fe^{III}-O_2^-$ formulation appeared to be valid has been the cause of much speculation over the bonding in oxyhaemoglobin.

Various bonding theories will be inspected in more detail in Chapter 6. A number of possibilities were introduced earlier(§2.3.1). What will be covered in this subsection are physical studies whose results indicate something about the extent of electron transfer from iron onto

dioxygen. The two extremes consistent with maintenance of rigorous diamagnetism are a d^4(S=0) iron(IV)–peroxide (S=0) species, $Fe^{IV}–O_2^{2-}$ [71,301], and a d^6(S=0) iron(II)-singlet oxygen (S=0) species, $Fe^{II}–O_2$, with dioxygen featuring mainly as a $\sigma(sp^2)$ donor[12]. Both extremes are excluded by the data presented below.

Very recently, precise measurements on the magnetic susceptibility of oxyhaemoglobin have shown, that oxyhaemoglobin is not rigorously diamagnetic.

Magnetic Properties

Since Pauling and Coryell's original measurements on the magnetic susceptibility of oxyhaemoglobin and carbonmonoxyhaemoglobin,[67] the diamagnetic nature of these two species has remained largely unquestioned.

While most cobalt-dioxygen complexes are adequately represented as polarised $Co^{III}–O_2^-$ species, a similar formulation for diamagnetic iron-dioxygen complexes (and also for the low-spin (S=1) Cr(TPP)(py)(O_2) complex[134]) poses conceptual problems. For the cobalt-dioxygen species strong metal-dioxygen π bonding need not be invoked to rationalise the magnetic and spectral properties of a diamagnetic d^6 cobalt(III)–coordinated superoxide (S=½) system. On the other hand for a rigorously diamagnetic iron-dioxygen complex, such as has been widely accepted for HbO_2, strong π bonding between oxygen $(\pi^*)1$ and iron $(3d_{xz,yz})^3$ orbitals must be invoked to rationalise a polarised low-spin d^5 iron(III)–coordinated superoxide (S=½) species — a contradiction is apparent.

Cerdonio and coworkers[330] have recently shown that oxyhaemoglobin is not diamagnetic above temperatures greater than $50^{o}K$. There is a triplet (S=1) state only 146 cm^{-1} above the singlet (S=0) groundstate. The two spin states are in thermal equilibrium:-

$$\underset{\text{Singlet } S=0}{HbO_2} \rightleftharpoons \underset{\text{Triplet } S=1}{HbO_2} \qquad |2J| = 146\ cm^{-1}$$

This result appears to support a $d^5(S=\frac{1}{2})$ iron(III)—coordinated superoxide ($S=\frac{1}{2}$) system with the π-bonding contribution that leads to spin-pairing being rather weak. Equivalently expressed, Weiss' $Fe^{III}—O_2^-$ representation with the electron spins "antiferromagnetically coupled"[70] is supported. Another formulation is possible — a partially spin-paired $d^6(S=1)$ iron(II)—dioxygen (S=1) species. The ESR spectrum of triplet-state oxyhaemoglobin would be of interest to examine the location of the unpaired electrons.

This spin equilibrium is not unique. Hydroxymethaemoglobin is in thermal equilibrium between high- and low-spin forms[69,152]:-

$$\underset{\text{low-spin } S=\frac{1}{2}}{\text{met-HbOH}} \rightleftharpoons \underset{\text{high-spin } S=5/2}{\text{met-HbOH}}$$

On the other hand, the diamagnetism of carbonmonoxyhaemoglobin was confirmed. A lower bound for the separation between the singlet groundstate and triplet excited state was estimated to be at least 800 cm^{-1} [330]. This rigorous diamagnetism of HbCO strongly refutes an $Fe^{III}—CO^-$ formulation.

Electronic Spectra

Weiss[70] and later Wittenberg et al[273] compared the optical spectra of HbO_2 and HbCO with that of alkaline methaemoglobin, metHbOH, and concluded that the configuration of all three species was low-spin ($S=\frac{1}{2}$) d^5 iron(III). The configuration of ligated dioxygen was deduced[273] to be superoxide-like by specious analogy with cobalt-dioxygen complexes. The electronic spectra of HbCO and HbO_2 are quite similar. Table 4.1 lists spectral properties in the uv-visible region for a number of haemoglobin derivatives and for a six-coordinate essentially diamagnetic haemochrome. The data therefore support an Fe^{III}-CO^- representation just as closely as an Fe^{III}-O_2^- one; the former formulation is now generally regarded as grotesque, since, for example, HbCO is even less susceptible to nucleophilic attack than HbO_2 [141]. Unfortunately, no studies have yet been published on the effects of solvent polarity on the binding of carbon monoxide; such studies could settle claims that the Fe-CO group is non-polar.

However a more extensive spectral study, subsequent to those of Weiss[70] and Wittenberg et al[273], has shown that HbO_2, but not HbCO, has a low energy absorption at $\sim$950 nm[381]. This band has been rationalised in terms of an $Fe^{II}(S=1)$–$O_2(S=1)$ formulation[348], although an $Fe^{III}(S=\frac{1}{2})$–$O_2^-(S=\frac{1}{2})$ formulation appears to be equally valid.

Table 4.1 : Electronic features of various protohaem derivatives[a].

	Visible α	β	Soret γ	UV δ	
Met-MbOH	582(9.1)	542(9.5)	414(97.2)	358(33.5)	281(32.1)
MbO_2	581(14.6)	543(13.6)	418(128)	348(26.2)	280(36.6)
MbCO	579(12.2)	542(14)	423(187)	345(26.9)	275(37.5)
Fe(Proto-IX)$(py)_2$	558(30.9)	525(16.3)	418(130)	-	-

a

Data from reference [152].

λ_{max} in nm; extinction coefficient in mM (in parentheses).

Infrared

The O-O stretching mode has been identified at 1107 cm^{-1} for HbO_2 [163] and 1103 cm^{-1} for MbO_2 [164], and near 1160 cm^{-1} for dioxygen iron "picket fence" porphyrin derivatives[17]. These values are in the same range as ν(O-O) for cobalt-dioxygen adducts of the superoxo class (Table 2.1). These infrared values of ν(O-O) do not per se indicate a coordinated superoxide species; they only indicate a bond order similar to that for the superoxide anion. Caughey proposed a covalent linkage, $Fe{=}O^{=O}$, for the iron-dioxygen moiety. He also proposed a similar covalent linkage for cobalt-substituted haemoglobins because of their similar values for ν(O-O)[165]. With regard to the extra electron possessed by cobalt-dioxygen species and the other evidence assessed in §3.2.1, such a formulation seems untenable.

Thus infrared data for ν(O-O) indicate nothing about the polarity of the metal dioxygen bond; they do indicate a similar bond order to superoxide and are not inconsistent with magnetic susceptibility data.

Resonance Raman Spectroscopy

Analysis of the resonance Raman scattering of iron porphyrins had shown a number of porphyrin bands to be sensitive to the oxidation and spin states of the iron centre[3,274-276]. An $Fe^{III}{-}O_2^-$ representation for dioxygen was inferred from the similarity of the frequencies for the oxidation state markers of HbO_2 and HbCO with low-spin

metHb derivatives such as metHbCN; a similar representation for HbCO appeared to be inescapable. Evidence for such a polarised iron-carbonyl bond is scarce (see paragraph above on electronic spectra for supporting evidence, see subsequent paragraphs for contrary evidence).

A recent paper[277] with data from a wider range of high-spin, low-spin, iron(II), iron(III) complexes indicated that some oxidation state markers were unreliable. Diamagnetic iron complexes could be separated into two classes depending on whether the sixth ligand L is primarily a σ donor of a lone pair of electrons (for example, L=imidazole, pyridine) or on whether L is involved in substantial Fe-L π bonding (for example, L=CO,NO,O_2). The similar Raman scattering of the latter class and "bonafide" iron(III) species is resolved with the realisation that those bands are sensitive to the extent of electron transfer from the iron onto the porphyrin. That this is apparently identical for species such as FeO_2 and $Fe^{III}-CN^-$ implies nothing about electron transfer onto dioxygen[277].

The dangers of arguing by analogy without a fundamental understanding of factors responsible for the effects being compared may be noted.

Thus contrary to early proposals, resonance Raman spectroscopy, although able to distinguish between σ-donor and σ-donor plus π-acceptor sixth ligands, has not been shown to indicate the nett extent of electron transfer onto dioxygen.

X-Ray Fluorescence Spectroscopy

The iron Kβ fluorescence spectrum of MbO_2 has indicated a spin equilibrium process:-

$$\text{diamagnetic } Fe^{II}\text{-}O_2 \rightleftharpoons Fe^{III}\text{-}O_2^- \text{ (intermediate spin S=1).}$$

Under these conditions of high radiation flux MbCO remains a diamagnetic Fe^{II}–CO species[278]. Thus a paramagnetic state appears to be reasonably accessible for an iron-dioxygen species but not for an iron-carbonyl species.

Results and conclusions from X-ray fluorescence studies parallel those for magnetic susceptibility.

Mossbauer Spectroscopy

Mossbauer spectra are sensitive to the electron density around the iron nucleus.

The Mossbauer spectrum of HbO_2 exhibits a negative electric field gradient and a large and temperature dependent, nuclear quadrupole splitting ΔE_q[279]. Oxygenated cytochrome P450 has a similar large ΔE_q value but ΔE_q is only weakly temperature dependent[280]. No paramagnetic effects were observable when the Mossbauer spectra of HbO_2 and oxygenated P450 were examined in high magnetic fields at 4.5°K [280]; this result is not inconsistent with the magnetic susceptibility measurements of Cerdonio et al[330]. A proposal that the temperature dependence of ΔE_q for HbO_2 (and its inorganic model Fe(TpivPP)(1-Me-imid)(O_2)) is attributable to different conformational states adopted by dioxygen has been advanced[281].

Both HbCO and the carbon monoxide-reduced cytochrome

P450 adduct have quadrupole splitting constants similar to low spin iron(II) derivatives despite dissimilar Soret spectra for these two carbonyl adducts. An Fe^{II}-CO representation was inferred[280].

For HbO_2, on the other hand, the large ΔE_q values, not dissimilar to those for iron(III) complexes, and the negative sign of the electric field gradient were found compatible with partial loss of a metal t_{2g} electron and with 3d electron delocalisation through covalent bonding of dioxygen[279,280]. That is, there is some nett electron transfer onto dioxygen.

However, recent theoretical calculations have shown that the Mossbauer parameters of HbO_2 and oxygenated cytochrome P450 may be accounted for by both an $Fe^{II}-O_2$ and an $Fe^{III}-O_2^-$ formulation[282].

Electrochemical Data

The ease of oxidation of M^{II}(TPP)(2-Me-imid)(M=Co, Fe,Cr) species (Co<Fe<Cr) has been correlated with the affinity of M^{II}(TPP)(py) species for dioxygen (Co<Fe<<Cr)[134]. This would indicate some transfer of electron density from iron onto dioxygen.

Solvent Effects

That the binding of dioxygen to iron[266,267] and to cobalt complexes[225] is apparently enhanced by polar solvents is indicative of some polarity in the iron-dioxygen linkage. Parallel studies with carbon monoxide do not appear to have been published; if the iron-carbonyl linkage is indeed

non-polar and covalent, solvent effects should be less pronounced. It should be noted that the conclusions of these studies remain unaffected by the neglect to correct for the variation in solubility of dioxygen in different solvent systems.

Concluding Remarks

The various lines of evidence, summarised in Table 4.2, tend to suggest a polarised iron-dioxygen species. The $M^{III}-O_2^-$ formulation that adequately represents magnetic and spectral properties of many cobalt-dioxygen systems appears to be reasonable for oxyhaemoglobin and possibly for other iron-dioxygen complexes as well. But the evidence remains equivocal since some studies on carbon monoxide systems and their dioxygen analogues are nearly parallel while other studies indicate a fundamental dissimilarity between the two systems.

Some evidence for greater covalency in the Fe-O bond than in the Co-O bond arises from analysis of the crystal structure of Fe(TpivPP)(1-Me-imid)(O_2). This structure is described in the next section.

Table 4.2 : Summary of evidence for and against $Fe^{III}-O_2^-$ formulation for HbO_2.

Type of Study	Comments
Magnetic susceptibility	HbO_2 : S=1⟷S=0; HbCO S=0 , Supports $Fe^{III}-O_2^-$ or $Fe^{II}(S=1)-O_2(S=1)$ and $Fe^{II}-CO$.
X-ray fluorescence	As above.
Electronic spectra	Spectra HbO_2, HbCO, met-HbOH not identical, Uv-vis region has been used to support $Fe^{III}-O_2^-$ and $Fe^{III}-CO^-$, but near-IR region indicates differences between HbO_2 and HbCO.
Mossbauer	O_2 different type of ligand to CO ⇒ $Fe^{III}-O_2^-$ (?), $Fe^{II}-CO$.
Infrared	Bond order coord. O_2 similar to O_2^-.
Resonance Raman	O_2 similar type of ligand to CO $Fe^{III}-O_2^-$, $Fe^{III}-CO^-$ now disputed.
Electrochemical	Ease of oxid: : Cr>Fe>Co Supports $Fe^{III}-O_2^-$ by analogy with $Co^{III}-O_2^-$.
Solvent	Polar solvents enhance O_2 binding Supports $Fe^{III}-O_2^-$.

4.2 The Crystal and Molecular Structure of the Dioxygen Adduct of (1-methylimidazole) meso-tetra(α,α,α,α,-orthopivalamidephenyl) porphinatoiron(II), [Fe(TpivPP)(1-Me-imid)(O_2)].½(C_6H_6).½($C_4N_2H_6$).

In this section the crystal and molecular structure of the title compound will be described. Aspects of the structure will be discussed and the validity of this compound as a model for the oxygen-binding component of myoglobin will be examined. Because of the non-routine nature of this structure analysis, considerable detail on the evolution of the final model for the structure will be given.

4.2.1. Introduction

There has been considerable interest in the geometry of the iron-dioxygen linkage in oxyhaemoglobin long before the structures of iron-dioxygen complexes or related species were determined. Pauling and Coryell on determining that HbO_2 and HbCO were diamagnetic proposed a linear Fe-O-O linkage for both species[67]. Pauling subsequently amended his proposal to an angular end-on $Fe{-}O\diagup^{O}$ geometry[68]. Griffith proposed a side-on π-bonded $Fe\langle^{O}_{O}$ structure[69]. Gray[71] and Mingos[301] have also postulated a triangular structure. Dioxygen adducts with the Griffith geometry are known for a wide range of metals and ligand systems[13] (see also §2.2.3). The Pauling geometry has been observed for the dioxygen adducts of cobalt(II) complexes[13]. Dinuclear complexes of the diamagnetic $Co^{III}{-}O\diagup^{2-}O{-}Co^{III}$ and paramagnetic $Co^{III}{-}O\diagup^{-}O{-}Co^{III}$ type were the first to be

characterised by X-ray single-crystal structure analysis; their mononuclear parents were characterised later. The stereochemistry of mononuclear and dinuclear cobalt-dioxygen complexes is now precisely established largely through the efforts of Schaefer and coworkers[103-109,123-125] (see also Table 2.2).

While these mononuclear cobalt-dioxygen adducts are valid models for cobalt-substituted haemoglobins, their applicability to native haemoglobins may be questioned since they possess an additional electron. The reviews of §3.2 and §4.1 indicate that differences do exist in the nature of the metal-dioxygen linkage, although both native and cobalt-substituted haemoglobin coordinate dioxygen reversibly and cooperatively. The oxygen affinities of cobalt porphyrin derivatives are less than those of cobalt(II) Schiff-base derivatives[61] and iron(II) porphyrin derivatives[135-137]. The differences between cobalt and iron are highlighted by the non-existence of cobalt-carbonyl complexes analogous to cobalt-dioxygen complexes that have an amine axial ligand[121], and by the greater stability of iron-carbonyl adducts compared to their dioxygen analogues[17,152]. Thus to conclude that the Pauling geometry pertains to iron-dioxygen complexes by analogy with the structures of cobalt analogues is specious.

However, nitrosyl adducts of cobalt(II) complexes are formally isoelectronic with dioxygen adducts of iron(II) complexes. A strongly bent $Co-N\overset{O}{\diagup}$ group is exhibited by these complexes[206,226-228]. Thus an angular geometry for the iron-dioxygen linkage may be expected. In addition, contemporaneously with the preliminary structure determination of Fe(TpivPP)(1-Me-imid)(O_2), a model for the oxygen-

binding haem component of haemoglobins, the results of infrared studies by Caughey and coworkers on HbO_2 and MbO_2 were published. A bent bond was predicted[163,164].

An end-on bent bond geometry for iron-dioxygen complexes has now been unequivocally established.

Utilising the atropisomerism of meso-tetra(ortho-substituted phenyl) porphyrins (Figure 4.6) to create a protected binding site for dioxygen the irreversible oxidation of porphinatoiron(II) species (§4.1.1, reactions R4.4-R4.8) that occurs rapidly at ambient temperatures through bimolecular contact of $Fe\text{-}O_2$ and Fe(II) species can be avoided, and crystalline iron-dioxygen complexes isolated. The preliminary structure of this compound has been communicated[11].

4.2.2 Preliminary Studies and Data Collection

Dark red crystals of the compound shown by this structure analysis to be $[Fe(TpivPP)(1\text{-}Me\text{-}imid)(O_2)]$. $\frac{1}{2}C_6H_6 \cdot \frac{1}{2}C_4N_2H_6$ were recrystallised from benzene and examined by precession photography using Cu Kα X-radiation. Symmetry and systematic absences consistent with the monoclinic space groups C2/c(No.15) or Cc (No.9) were observed[207]. All crystals exhibited some degree of twinning and/or poor mosaicity. The 10-faced crystal eventually selected was irregularly shaped with maximum and minimum dimensions of 0.40 and 0.22 mm and volume 0.0145 mm^3. On the diffractometer it was aligned with the ϕ-circle and c axes approximately coincident.

Crystal mosaicity (peak width at half-peak height), as determined by open-counter ω-scans at a take-off angle of 3^{o}, ranged from 0.12^{o} to 0.19^{o} for strong, low angle reflections. For some reflections a minor maximum of intensity, at worst less than 9% of the total integrated intensity, was observed in such scans. Peak profiles for a number of reflections are shown in Figure 4.7. The 040 peak is quite symmetrical. Furthermore, the relative integrated intensities of the principal peaks for the 204 and $40\bar{2}$ reflections are in reverse order to those of the minor peaks; one minor maximum occurs on the low ω-angle side of its major maximum (204) and the other occurs on the high ω-angle side ($40\bar{2}$). This may indicate twinning of the type hkl and $l\bar{k}h$. Note, this is not a case of intimate twinning (cell constants preclude this) but rather the major crystal has a minor crystallite differing in orientation by $\sim 90^{o}$ about their parallel b-axes. Such twinning would not be surprising in view of the near tetragonality of the unit cell dimensions (see below) and the four-fold symmetry which may be possessed by meso-tetraphenylporphyrins.

Crystal orientation and unit cell dimensions at 24^{o}C were obtained by least-squares refinement of the setting angles of 12 reflections accurately determined using a diffracted beam collimator with a 5 mm aperture set 230 mm from the crystal. Dimensions thereby obtained were $a = 18.690(3)$, $b = 19.514(3)$, $c = 18.638(3)$ Å, $\beta = 91.00(1)^{o}$. The linear absorption coefficient calculated for four formula units in the cell, and Mo Kα radiation, was 2.93 cm^{-1}, and, since the maximum likely error due to neglect of X-ray

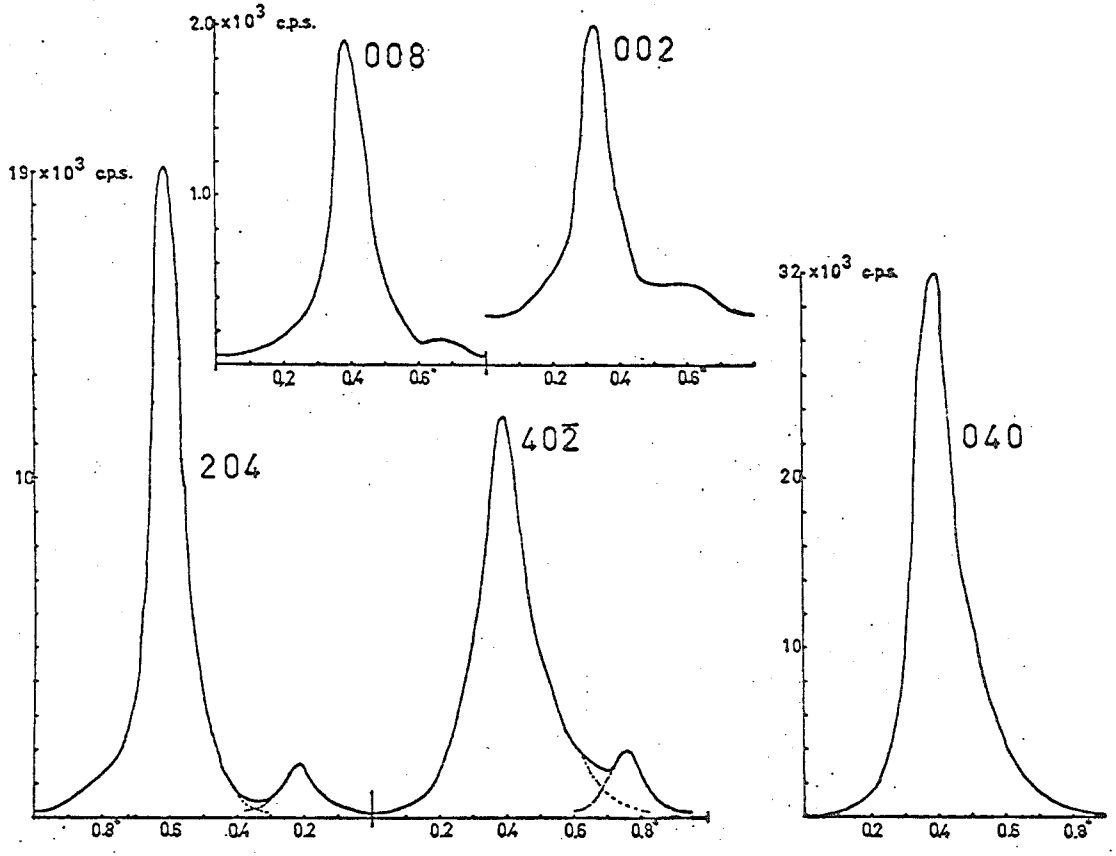

Figure 4.7 : Crystal mosaicity for Fe(TpivPP)(1-Me-imid)(O_2).

absorption was less than 3%, absorption corrections were not applied. The preservation of the very limited number of crystals for other analyses precluded the sacrifice of a crystal for density measurements.

Excluding systematic absences,3155 unique reflections in the range $0^{o}<2\theta<40^{o}$ were collected by the θ-2θ scan technique. A symmetric scan range of 1.20^{o} in 2θ centred on the calculated peak position comprised 60 steps each of four seconds duration. Stationary counter, stationary crystal background counts at each end of the scan were recorded for 12 seconds. Reflections with peak count rates greater than 8,000 per second were re-recorded with a copper foil attenuator placed in the path of the diffracted beam to bring the count rate within the linear response range of the scintillation counter. Three standard reflections monitored every 100 reflections showed no systematic variation in intensity. The data were scaled and corrected for Lorentz and polarisation effects. Due to a computer mishap half the 0kl data were collected later under changed experimental conditions (orientation, incident beam intensity). Accordingly in refinement of the structure two scale factors were applied.

4.2.3 Solution and Refinement of the Structure

Analysis of the three-dimensional Patterson synthesis established coordinates for the iron atom on special positions 2e in space group C2/c. Successful least-squares refinements of the structure were carried out in this space group which imposes two-fold rotational symmetry on the molecular species. That the porphinato plane was parallel to the a-c crystal plane was inferred from the plane of the strongest reflection(040) and the location of the iron atom on the two-fold axis parallel to the crystal b-axis for space group C2/c. This was confirmed in a plot of the u,0,w plane of this Patterson synthesis (Figure 4.8); the plot possessed approximate 4mm symmetry and since the c-glide plane is parallel to the a-c plane the orientation of the meso-tetraphenylporphinato skeleton was unambiguously established.

Phenyl and pyrrole rings were initially refined as rigid groups each with a single isotropic temperature factor. The initial model assumed the two crystallographically independent pivalamide nitrogen atoms were ortho substituents on two phenyl rings which were oriented to give the α,α-atropisomer. Application of the two-fold symmetry operation generates the α,α,α,α-atropisomer for the whole molecule. It was also assumed that nitrogen (from 1-methylimidazole) and oxygen (from dioxygen) atoms occupied the unhindered and hindered axial coordination sites, respectively. This partial model was refined so that $R = 0.28$ and $R_w = 0.36$ for those 1105 reflections having $I > 3\sigma_I$. At this stage the weighting scheme p-factor was assigned a value of 0.08.

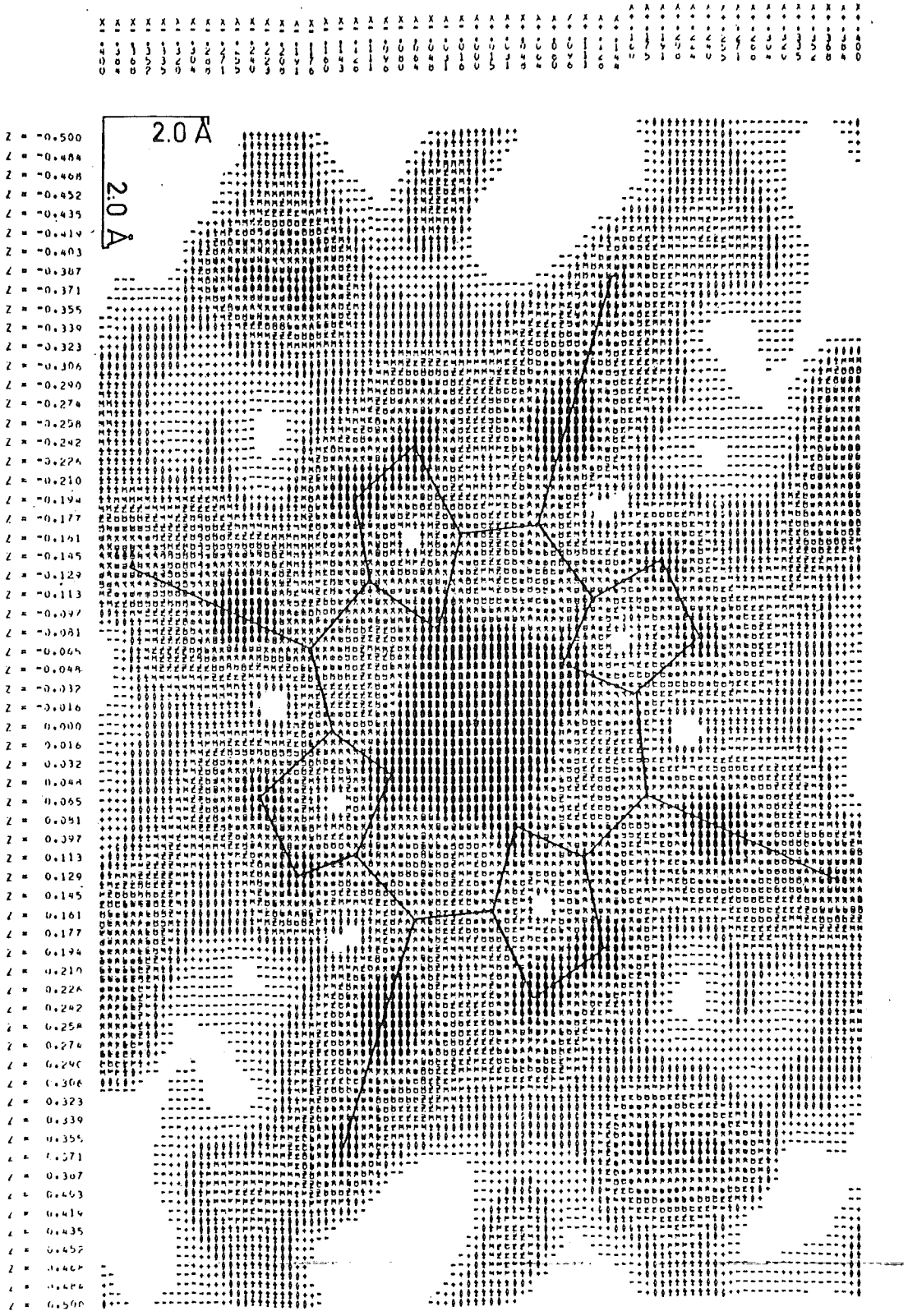

Figure 4.8 : Plot of the u,O,w plane of the Patterson synthesis for the solvate of Fe(TpivPP)(1-Me-imid) (O_2).

From two weighted F(obs) Fourier syntheses, positions for the remaining atoms of the 1-methylimidazole ligand and the pivalamide "pickets" (except for the terminal methyl groups) were obtained. Two-fold rotational disorder is imposed on the 1-methylimidazole ligand; in particular this leads to a hybrid carbon-nitrogen position (½C + ½N scattering factor) and half-occupancy of the methyl group position. Least-squares refinement of improved models based on the above syntheses led to R = 0.20 and R_w = 0.28.

To confirm the disorder in the pivalamide methyl carbon atoms, which was indicated in Fourier syntheses, further F(obs) Fourier syntheses were calculated parallel to the presumed mean planes of the two groups of such atoms. Notwithstanding the spurious features and distortions induced by transforming the hkl indices into a new axial system based on the mean planes, it is evident that for each "picket" these methyl carbon atoms are disordered into two sets (Figure 4.9). High thermal motion is also evident. Six half-carbon atoms, with individual isotropic temperature factors, for each "picket" were included in the model which, on refinement, led to R = 0.16 and R_w = 0.22. One half-carbon atom was unfortunately misplaced due to a punching error and failed to refine sensibly. Its position was corrected prior to subsequent refinements.

At this stage a difference Fourier synthesis revealed four-fold disorder in the terminal oxygen atom of the dioxygen ligand; that is there were two crystallographically independent positions. Figure 4.10 depicts this disorder. One section of a difference Fourier syntheses calculated parallel to the

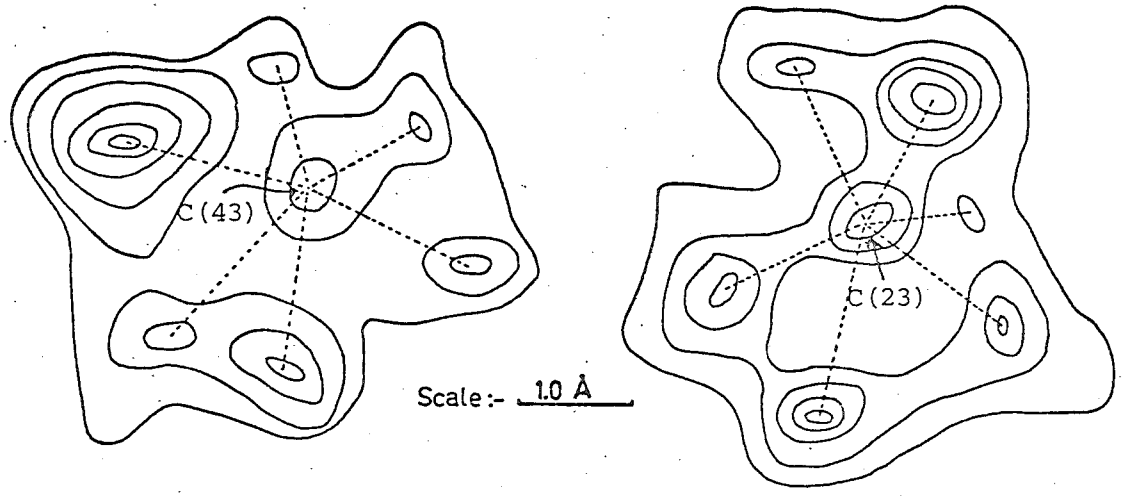

Figure 4.9 : Sections of Fourier syntheses showing the disorder of the pivalamide methyl carbon atoms for Fe(TpivPP)(1-Me-imid)(O_2).

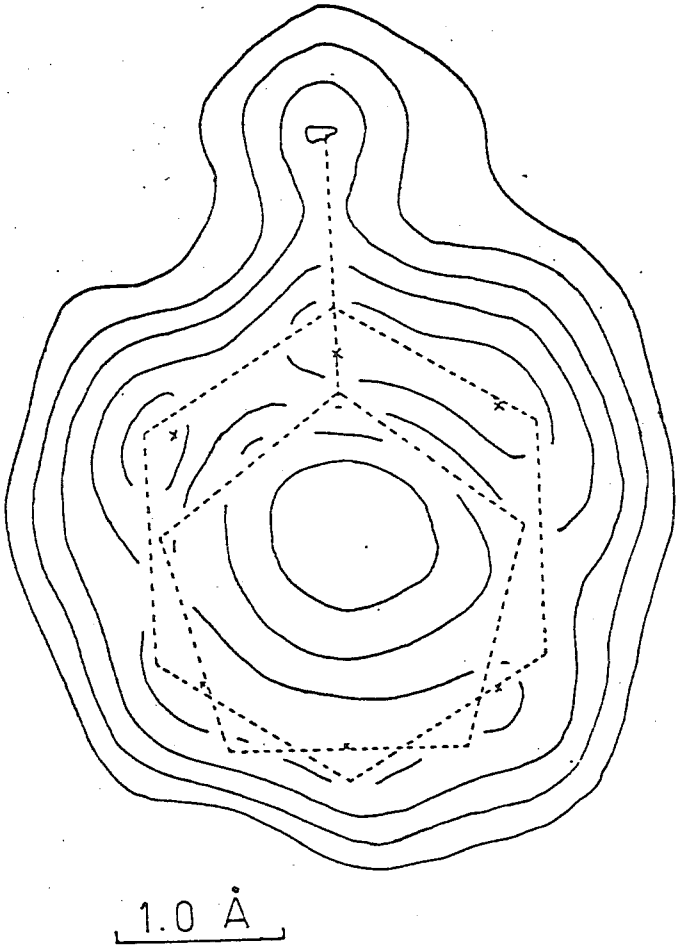

Figure 4.11 : Section of a Fourier synthesis in the plane of the solvate species for Fe(TpivPP)(1-Me-imid)-(O_2). The final interpretation of the electron density is indicated.

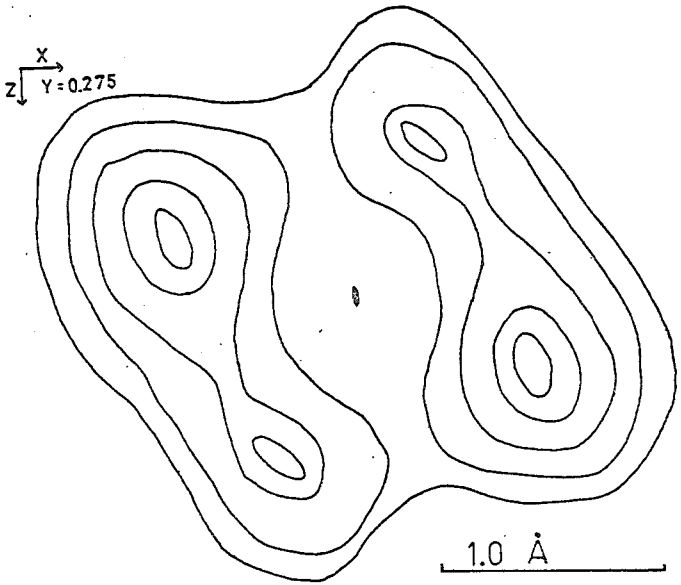

Figure 4.10 : Section of a Fourier synthesis showing the disorder of terminal oxygen atom for Fe(TpivPP)(1-Me-imid)(O_2).

plane of the solvate species is shown in Figure 4.11. The terminal oxygen atom (distributed equally between the two crystallographically independent positions), as well as the solvate species, tentatively presumed to be a benzene molecule, were added to the model. Two cycles of least-squares refinement led to

$$R = 0.106 \text{ and } R_w = 0.130.$$

Atoms of the pivalamide "pickets" and the solvate species exhibited high thermal motion. Moreover, analysis of the locations of residual electron density, calculated in a difference Fourier synthesis, indicated the necessity for anisotropic models to describe the thermal motions of these atoms. In addition, atoms in phenyl groups were allowed individual temperature factors, rigid group constraints on the pyrrole rings were relaxed and anisotropic thermal parameters were applied to the iron, porphinato nitrogen and imidazole ligand atoms.

This model was refined in two blocks, but the benzene solvate molecule refined poorly. Re-examination of Fourier syntheses indicated that it could perhaps be more appropriately described as a mixture of 1-methylimidazole and benzene molecules. The contributions of the rest of the model to the structure factors were held constant and various mixed-solvate models were tested. Because of the near-superposition of atoms of 1-methylimidazole and benzene molecules, refinement of a single-atom model would have been inappropriate. Consequently, for the final cycles of refinement, the geometry, relative proportions and disposition of the two species were held constant in a rigid group.

This model is also illustrated in Figure 4.11. In view of the large number of parameters needed to adequately describe the structure it was necessary to use more data. Consequently, in the final cycles of full-matrix least-squares refinement using 1784 reflections having $I>\sigma_I$, the 60 non-hydrogen atoms were described by 312 variable parameters. The weak data, $I\leq 3\sigma_I$, which had consistently returned poor agreement between $|F_c|$ and $|F_o|$ in earlier structure factor calculations were not utilised.

The final model refined from $R = 0.117$ and $R_w = 0.125$ to

$$R = 0.109 \text{ and } R_w = 0.116$$

at convergence. The standard error in an observation of unit weight was 1.324. For the portion of data having $I>3\sigma_I$

$$R = 0.076 \text{ and } R_w = 0.096.$$

In the final cycle the ratios of the change in a parameter to its estimated standard deviation were less than 0.10 and 0.20 for all positional and thermal parameters, respectively, except for those describing the pivalamide methyl carbon atoms where the respective ratios were 0.50 and 0.60. The final difference Fourier synthesis was flat; some peaks did occur in chemically reasonable positions for pyrrole hydrogen atoms, others occurred near the solvate species and pivalamide methyl carbon atoms.

Physically meaningful thermal ellipsoids were obtained for all atoms refined with anisotropic thermal parameters. While there is gross eccentricity in the thermal motion of the pivalamide methyl groups, the earlier Fourier syntheses did not indicate complete rotational disorder. It is

generally true that refining structural models with limited data causes anisotropic thermal ellipsoid eccentricity to be accentuated. Deficiencies inevitably inherent in this or any other description of the solvate species are also acknowledged.

Since the averaged values of the minimised function appeared to be generally independent of $|F_o|$ and $\sin\theta/\lambda$ the weighting scheme was judged satisfactory, although low angle reflections ($\sin\theta/\lambda<0.23$ Å^{-1}) returned a higher value of the function than the remainder of the data. Although the p-factor for the optimal weighting scheme is high (0.11), this is attributable not to instrumental instabilities but to (i) the preponderance of weak (and hence less precisely measured) data used in refinements, (ii) the twinned nature of the crystal used for data collection, (iii) deficiencies inherent in this description or any other description for the thermal motion and/or disorder of certain parts of the structure and (iv) the non-inclusion of 76 hydrogen atoms (which will of course most affect the low angle data).

$|F_o|$ and $|F_c|$ for all data are tabulated in Appendix 1. The final scale factors to place calculated and observed structure factors on the same scale were 0.6154(41) and for the 0kl, l—odd, data 0.594(12). Among the data not used in refinement there are few serious discrepancies between $|F_o|$ and $|F_c|$; for all data 54 reflections (out of 3156 reflections) lie outside the range

$$I-3\sigma_I < I_c < I+3\sigma_I .$$

A number of reflections outside these limits, including the moderately strong 404 reflection, are of the type hkl where h≈1 and k<<1; the planes so defined are approximately parallel to the solvate species. The agreement factors for all data were

$$R = 0.222 \text{ and } R_w = 0.147$$

and the standard error in an observation of unit weight was 1.294. There is no evidence among intense low angle reflections for secondary extinction.

Final atomic parameters and root-mean-square thermal displacements along the principal ellipsoid axes together with their associated standard deviations are contained in Tables 4.3 and 4.4 respectively.

In summary the precision of the resultant structure is compromised by the following factors:

1. Limited data of indifferent quality due to crystal twinning and weak scattering.
2. Crystallographically imposed disorder for the terminal oxygen atom and the 1-methylimidazole molecules.
3. Possible irresolvable disorder of the bonded oxygen atom analogous to that observed for the nitrosyl compounds $Co(TPP)(NO)$ [206] and $[Co(NH_3)_5NO]^{2+}$ [227] and inferred for $Co(salen\text{-}C_2H_4\text{-}py)(O_2)$. (see also next subsection).
4. Non-crystallographically imposed disorder for the terminal oxygen atom and for the pivalamide methyl carbon atoms, and high thermal motion of this and other parts of the structure.
5. The ill-resolved solvate species; the final difference Fourier synthesis indicated inadequacies in the model used

Table 4.3 : Final atomic parameters for $[Fe(TpivPP)(1\text{-Me-imid})(O_2)]\cdot\frac{1}{2}(C_6H_6)\cdot\frac{1}{2}(C_4N_2H_6)$.

(a) Individually refined atoms

Atom	X	Y	Z	B or β_{11}	β_{22}	β_{33}	β_{12}	β_{13}	β_{23}
Fe	0	0.13975(15)	1/4	0.00310(11)	0.00280(11)	0.00280(10)	0	-0.00013(7)	0
O(1)	0	0.2292(10)	1/4	7.2(4)					
O(2A)	-0.046(3)	0.267(2)	0.235(3)	7.0(10)					
O(2B)	-0.013(2)	0.269(2)	0.293(2)	6.2(10)					
N(L3)	0	0.0337(9)	1/4	0.0032(7)	0.0030(7)	0.0054(8)	0	-0.0017(6)	0
C(L2)[b]	-0.0435(8)	-0.0074(9)	0.2941(9)	0.0050(7)	0.0031(7)	0.0058(8)	-0.0012(6)	-0.0027(6)	0.0011(6)
CN(L)[b]	-0.0230(12)	-0.0745(8)	0.2746(8)	0.0111(16)	0.0026(5)	0.0052(11)	-0.0017(7)	-0.0037(8)	0.0011(5)
C(L1)	-0.0426(16)	-0.1358(18)	0.3037(17)	0.0043(13)	0.0049(15)	0.0067(15)	-0.0012(12)	0.0006(11)	0.0024(13)
N(10)	0.0952(5)	0.1379(6)	0.2065(5)	0.0027(4)	0.0038(4)	0.0036(4)	0.0005(4)	-0.0006(3)	-0.0007(4)
C(11)	0.1119(7)	0.1347(7)	0.1342(8)	5.3(3)					
C(12)	0.1895(8)	0.1386(8)	0.1225(8)	6.2(3)					
C(13)	0.2199(8)	0.1452(8)	0.1907(8)	6.3(4)					
C(14)	0.1624(7)	0.1423(7)	0.2433(7)	5.1(3)					
N(30)	0.0448(5)	0.1385(5)	0.3475(5)	0.0031(4)	0.0027(4)	0.0034(4)	-0.0000(3)	0.0003(3)	0.0002(4)
C(31)	0.1179(7)	0.1415(7)	0.3648(7)	4.7(3)					
C(32)	0.1288(7)	0.1396(8)	0.4422(7)	6.0(3)					
C(33)	0.0619(8)	0.1364(8)	0.4722(8)	6.3(4)					
C(34)	0.0096(7)	0.1354(7)	0.4129(7)	4.6(3)					
C(15)	0.1712(6)	0.1448(7)	0.3160(6)	4.1(3)					
C(35)	-0.0618(7)	0.1332(7)	0.4216(7)	4.9(3)					
N(11)	0.2401(7)	0.2655(7)	0.3661(7)	0.0036(5)	0.0035(5)	0.0063(6)	-0.0002(4)	-0.0005(4)	-0.0006(4)
C(22)	0.2601(12)	0.3289(12)	0.3672(10)	0.0036(9)	0.0062(11)	0.0071(9)	-0.0023(8)	-0.0001(7)	-0.0009(7)
O(10)	0.3235(9)	0.3424(7)	0.3766(9)	0.0074(8)	0.0062(7)	0.0149(11)	-0.0014(6)	-0.0025(7)	0.0007(6)
C(23)	0.2075(14)	0.3884(12)	0.3591(13)	0.0044(10)	0.0071(12)	0.0072(12)	0.0017(9)	-0.0006(9)	-0.0017(8)
C(24A)	0.122(3)	0.364(4)	0.377(5)	0.003(2)	0.008(3)	0.014(4)	0.001(2)	0.002(2)	0.008(3)
C(25A)	0.218(4)	0.420(3)	0.289(2)	0.010(3)	0.008(3)	0.0018(14)	0.005(2)	0.0026(17)	0.0011(5)
C(26A)	0.221(4)	0.440(3)	0.423(3)	0.014(4)	0.007(2)	0.0041(17)	0.002(2)	-0.004(2)	-0.0027(17)
C(24B)	0.163(6)	0.375(4)	0.290(5)	0.019(6)	0.010(4)	0.017(6)	0.009(4)	-0.016(6)	-0.005(4)
C(25B)	0.243(3)	0.456(2)	0.352(5)	0.012(3)	0.0034(17)	0.015(5)	-0.0034(18)	0.002(3)	0.001(2)
C(26B)	0.160(3)	0.382(4)	0.412(5)	0.002(2)	0.007(3)	0.014(5)	0.001(2)	0.004(2)	0.000(3)
N(31)	-0.1057(7)	0.2453(8)	0.4976(7)	0.0067(7)	0.0043(6)	0.0042(6)	0.000(5)	0.0010(5)	-0.0008(5)
C(42)	-0.1215(13)	0.3098(13)	0.5158(11)	0.0113(13)	0.0067(11)	0.0024(7)	0.0008(9)	0.0015(7)	0.0003(8)
O(30)	-0.1380(11)	0.3237(9)	0.5772(10)	0.0163(13)	0.0096(9)	0.0079(9)	0.0036(8)	0.0042(9)	0.0010(7)
C(43)	-0.1116(12)	0.3674(11)	0.4640(10)	0.0067(11)	0.0061(9)	0.0040(8)	-0.0000(9)	-0.0010(7)	0.0012(8)
C(44A)	-0.178(3)	0.389(3)	0.431(3)	0.004(2)	0.012(3)	0.007(3)	0.000(2)	-0.004(2)	0.000(2)
C(45A)	-0.061(4)	0.348(3)	0.399(5)	0.008(3)	0.0045(20)	0.016(4)	0.0009(19)	0.010(3)	0.005(2)
C(46A)	-0.081(3)	0.437(2)	0.505(2)	0.013(4)	0.0028(15)	0.0045(19)	-0.0002(19)	-0.004(2)	-0.0016(12)
C(44B)	-0.123(4)	0.339(3)	0.389(3)	0.009(3)	0.011(3)	0.005(2)	0.002(3)	0.000(2)	0.005(2)
C(45B)	-0.048(3)	0.406(3)	0.472(3)	0.0039(18)	0.006(3)	0.010(3)	-0.0006(19)	0.0022(19)	0.003(2)
C(46B)	-0.181(3)	0.418(3)	0.482(3)	0.006(2)	0.007(2)	0.009(3)	0.0029(18)	0.001(2)	0.000(2)

(b) Derived Parameters for Atoms Constrained in Rigid Groups

Atom	X	Y	Z	B	Atom	X	Y	Z	B
C(16)	0.2484(5)	0.1449(8)	0.3435(7)	5.3(3)[e]	C(40)	-0.1381(7)	0.1772(6)	0.6037(7)	6.2(4)
C(17)	0.2865(8)	0.0836(6)	0.3429(7)	6.9(4)	C(41)	-0.1118(7)	0.1833(5)	0.5346(7)	5.4(3)
C(18)	0.3570(8)	0.0818(7)	0.3683(8)	7.3(4)	C(S1B)	0	0.637(1)	1/4	12.0266
C(19)	0.3894(5)	0.1414(9)	0.3943(8)	8.5(4)	C(S2B)	0.0453(9)	0.601(1)	0.2972(8)	12.0266
C(20)	0.3512(8)	0.2027(7)	0.3949(7)	8.1(5)	C(S3B)	0.0453(9)	0.530(1)	0.2972(8)	12.0266
C(21)	0.2808(8)	0.2045(6)	0.3695(7)	5.9(4)	C(S4B)	0	0.494(1)	1/4	12.0266
C(36)	-0.0895(6)	0.1252(7)	0.4978(5)	4.8(3)	C(S1A)	0	0.688(1)	1/4	14.0266
C(37)	-0.0936(6)	0.0610(5)	0.5301(7)	6.0(4)	N(S1A)	0	0.612(1)	1/4	12.0266
C(38)	-0.1199(7)	0.0549(5)	0.5991(7)	6.2(4)	C(S2A)	0.0412(8)	0.570(1)	0.2929(7)	12.0266
C(39)	-0.1422(7)	0.1130(7)	0.6359(5)	7.6(4)	CN(SA)	0.0259(5)	0.505(1)	0.2769(5)	12.0266

(c) Group Parameters[c]

Group	X	Y	Z	ϕ'	θ	ρ	B_{group}
Phenyl-16	0.3189(4)	0.1432(4)	0.3689(3)	0.053(7)	0.218(6)	-0.340(6)	-[d]
Phenyl-36	-0.1158(3)	0.1191(4)	0.5669(3)	0.143(6)	0.039(6)	-1.944(6)	-[d]
Solvate	0	0.612(1)	1/4	*	*	2.35(1)	12.0(5)

[a] The form of the anisotropic thermal ellipsoid is $\exp[(\beta_{11}h^2 + \beta_{22}k^2 + \beta_{33}l^2 + 2\beta_{12}hk + 2\beta_{13}hl + 2\beta_{23}kl)]$.

[b] CN(L), half carbon/half nitrogen atom.

[c] Angles in radians.

[d] Atoms allowed individual temperature factors.

Table 4.4 : RMS components of thermal displacement (in Å) along the principal ellipsoid axes for Fe(TpivPP(1-Me-imid)(O_2).

Atom	RMS 1	RMS 2	RMS 3
Fe	0.219(4)	0.232(4)	0.237(4)
N(L3)	0.199(26)	0.242(29)	0.336(25)
C(L2)	0.209(25)	0.227(27)	0.394(23)
CN(L)	0.204(25)	0.246(28)	0.487(33)
C(L1)	0.209(52)	0.304(42)	0.389(43)
N(10)	0.204(17)	0.236(16)	0.296(15)
N(30)	0.224(16)	0.230(16)	0.249(14)
N(11)	0.246(18)	0.256(19)	0.342(17)
C(22)	0.199(32)	0.346(23)	0.386(28)
C(23)	0.255(33)	0.322(27)	0.418(30)
C(24A)	0.209(89)	0.228(59)	0.600(97)
C(25A)	0.137(75)	0.284(53)	0.521(70)
C(26A)	0.186(67)	0.363(58)	0.546(73)
C(25B)	0.200(78)	0.479(69)	0.520(82)
C(26B)	0.128(128)	0.379(77)	0.520(83)
C(24B)	0.127(98)	0.374(66)	0.823(126)
N(31)	0.238(20)	0.307(19)	0.352(18)
C(42)	0.197(31)	0.355(29)	0.454(26)
O(30)	0.331(20)	0.396(19)	0.587(22)
C(43)	0.238(29)	0.343(30)	0.363(28)
C(44A)	0.159(80)	0.405(78)	0.478(69)
C(45A)	0.075(148)	0.293(63)	0.637(74)
C(46A)	0.145(74)	0.281(57)	0.508(74)
C(44B)	0.207(63)	0.384(81)	0.527(71)
C(45B)	0.202(69)	0.320(66)	0.465(83)
C(46B)	0.251(63)	0.382(68)	0.430(72)
O(10)	0.308(19)	0.370(18)	0.530(20)

(the best model found for the solvate species involved an equal mixture of 1-methylimidazole and benzene molecules with their relative dispositions illustrated in Figure 4.11).

4.2.4. Other Calculations

The data with which the structure was initially solved employed a shorter scan time (60 steps each of one second duration). The preliminary structural model described in reference [11], did not incorporate disorder of the pival-amide methyl carbon atoms and the solvate species was accounted for, in that early model, as an imidazole molecule. The positional and isotropic thermal parameters of all atoms were not subjected to rigid group constraints but were refined individually. The inadequacies apparent in the description of the "picket fence" and solvate components (high thermal parameters and anomalously large shifts in least-squares refinements) led to the collection one year later of a more precise data set from the same crystal and to a close examination of these components. It is at this stage that the author was introduced to the structure and its problems. The cell parameters of the original data set are quoted for consistency with published values, although those of the recollected data ($a = 18.688(3)$, $b = 19.506(3)$, $c = 18.642(3)$ Å, $\beta = 91.03(1)^{o}$, which are insignificantly different from the original ones, were used in all calculations pertaining to this structure reported herein.

The usual statistical analyses on normalised structure factors were, not surprisingly, in close agreement with those predicted for a centrosymmetric structure. Refinements

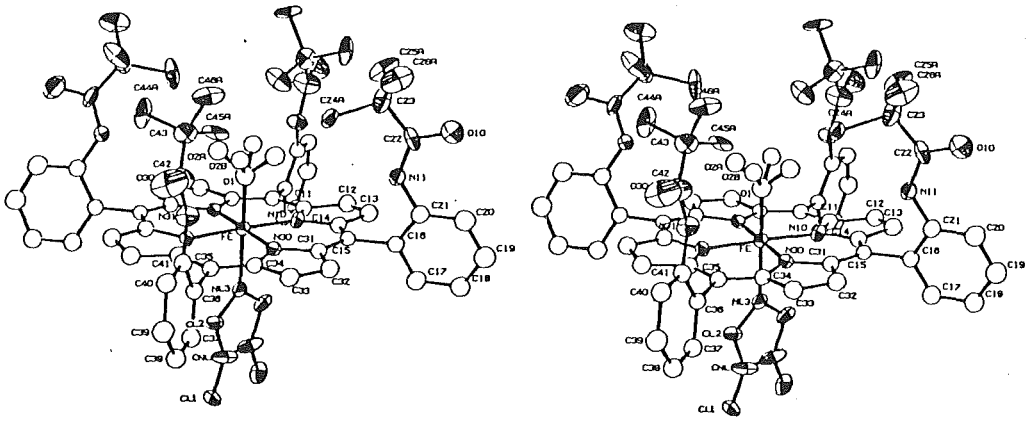

Figure 4.12 : Stereoscopic diagram of Fe(TpivPP)(1-Me-imid)(O_2). The atom labelling system is defined. Thermal ellipsoids are drawn at the 20% probability level. Disorder of the pivalamide methyl carbon atoms is omitted.

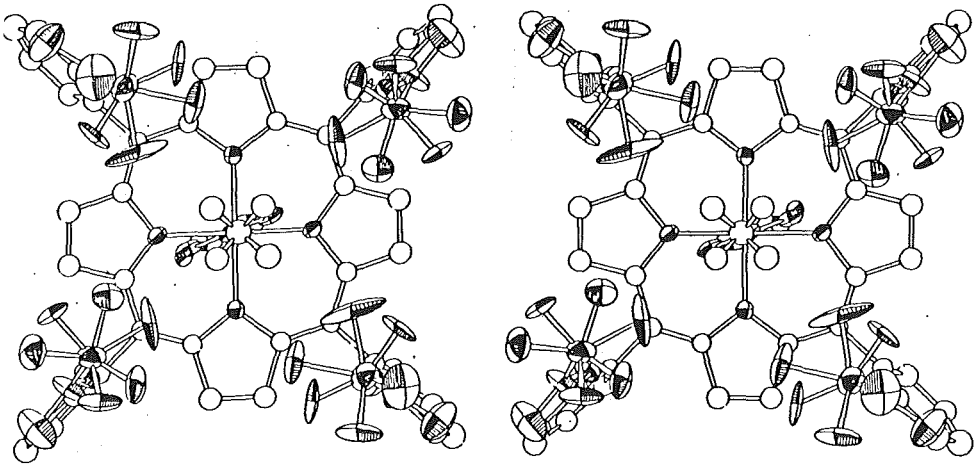

Figure 4.13 : Stereoscopic diagram of Fe(TpivPP)(1-Me-imid)(O_2) viewed down the two-fold axis and showing the disorder of the pivalamide methyl carbon atoms. Thermal ellipsoids are drawn at the 20% probability level.

in the alternative non-centric space group Cc (no point symmetry imposed on the molecule) did not improve the description of the molecule. While the pivalamide methyl groups refined to positions close to the disordered centric model, the porphinato skeleton refined very poorly with pairs of bond lengths related by the pseudo-two-fold axis alternatively shorter or longer than chemically reasonable values (approximately those obtained in the centric space group). No evidence for ordering of the 1-methylimidazole or dioxygen ligands could be found. Refinements in space group Cc were therefore abandoned and the structure closely re-examined in space group C2/c as described in the previous subsection.

4.2.5 Description and Discussion of the Structure

General Description and Crystal Packing

The crystal structure comprises neutral monomeric molecules of Fe(TpivPP)(1-Me-imid)(O_2) as illustrated in Figures 4.12 and 4.13. Solvate sites along the crystallographic two-fold axis are occupied by 1-methylimidazole and benzene molecules. Crystal packing is shown in Figure 4.14. The atom and atom-group labelling scheme for the complex, which is also appropriate to the other "picket fence" porphyrin structures described in this chapter, and for the solvate species is defined in Figure 4.15.

A crystallographic two-fold rotational axis passes through the coordinated oxygen atom O(1), the iron atom and the coordinated nitrogen atom N(L3) of the axially bound 1-methylimidazole ligand. C_2 point symmetry

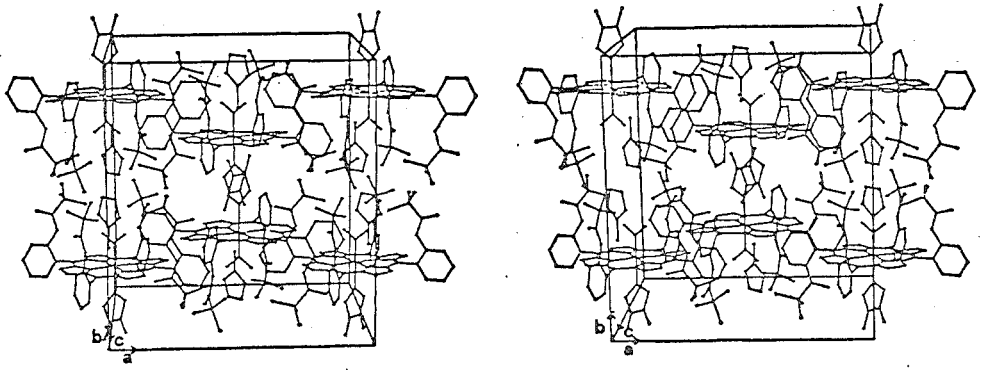

Figure 4.14 : Stereoscopic diagram of the packing of Fe(TpivPP)(1-Me-imid)(O_2) and solvate species with respect to the unit cell. Disorder of the pivalamide methyl carbon atoms and dioxygen is omitted. Only the 1-Me-imid solvate species is included.

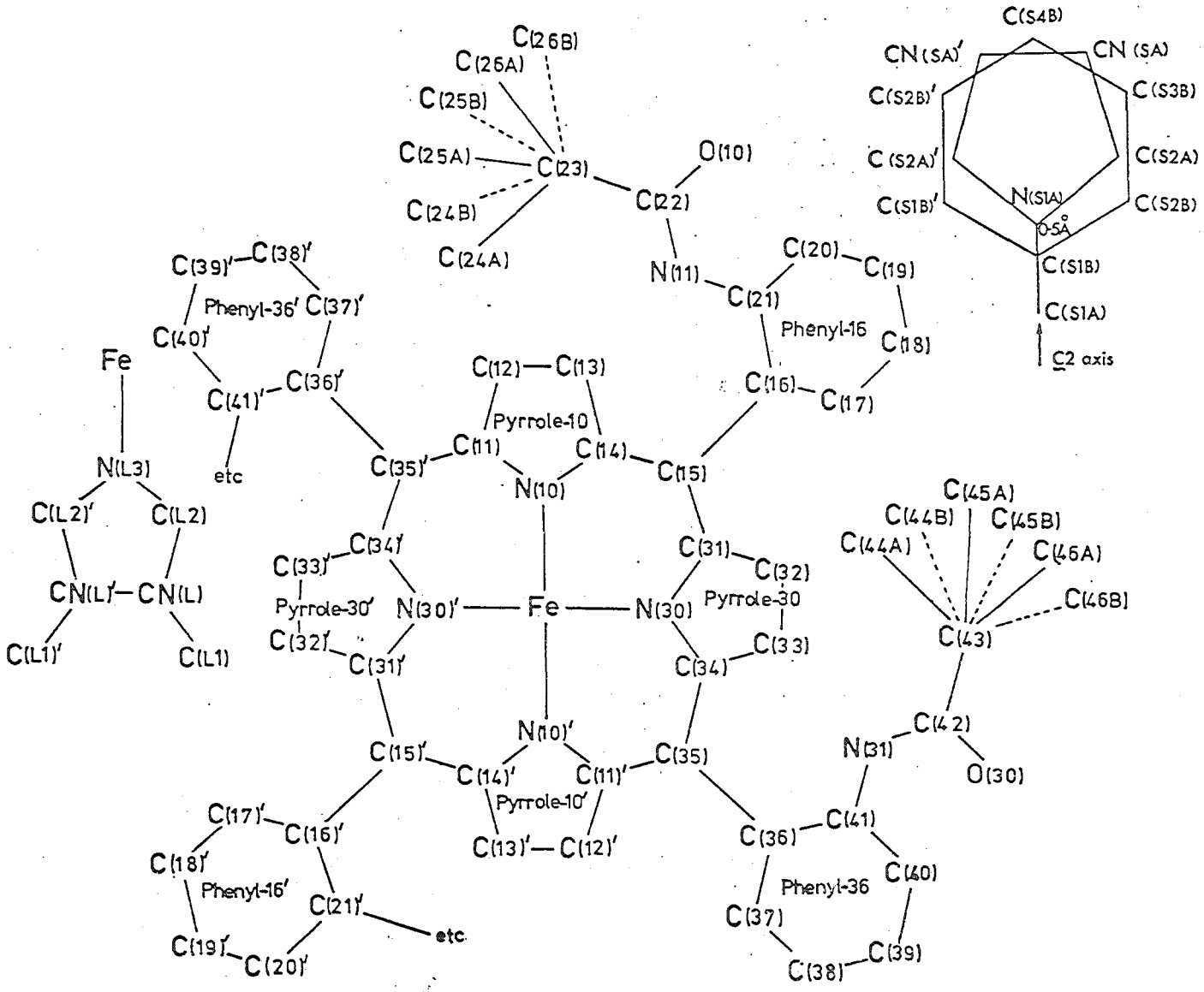

Figure 4.15: Atom and group labelling system for the Fe(TpivPP)(1-Me-imid) moiety and for the solvate species.

is therefore imposed on molecular species, and, in particular, on the 1-methylimidazole ligand which can be considered statistically disordered between the two symmetry related sites as illustrated in Figures 4.12 and 4.13.

The complex has four "pivalamide pickets" shielding one side of the porphyrin (the α,α,α,α-atropisomer), thereby forming a protective pocket wherein dioxygen is coordinated in the end-on bent bond mode predicted by Pauling[68]. The terminal oxygen atom was found to be disordered into two crystallographically independent positions, O(2A) and O(2B), and thus exhibits overall four-fold disorder. The iron-oxygen separation is 1.75(2)Å; the Fe-N(L3) separation is 2.07(2)Å. The two crystallographically independent iron-porphinato nitrogen separations r(Fe-N(10)) and r(Fe-N(30)) are 1.97(1) and 1.99(1) Å, respectively. A comprehensive compilation of bond distances and angles may be found in Tables 4.5 and 4.6.

The methyl carbon atoms of <u>each</u> crystallographically independent pivalamide "picket" have highly anisotropic thermal motion and are disordered into <u>two</u> sets (Figure 4.13). The final refined parameters for these atoms show that, relative to a rotation about the C(22)-C(23) bond, the two sets of positions for the methyl carbon atoms of "picket" Piv-11 differ in orientation by ∿53°; for "picket" Piv-31 the corresponding rotation is ∿76°. Figure 4.16 specifies the disorder. With bond lengths of the type C(23) to methyl half-carbon atom and C(43) to methyl half-carbon atom in

Table 4.5 : Bond distances (in Å) for Fe(TpivPP)(1-Me-imid)(O_2) .

Atom	Distance	Average[a]	Atom	Distance	Average[a]
Fe-O(1)	1.745(18)	-	C(15)-C(16)	1.52[c]	*
Fe-N(L3)	2.068(18)	-	C(35)-C(36)	1.53	1.53
Fe-N(10)	1.969(10)	*	N(11)-C(21)	1.41	*
Fe-N(30)	1.988(10)	1.979(10)	N(31)-C(41)	1.40	1.41
O(1)-O(2A)	1.17(4)	*	N(11)-C(22)	1.29(2)	*
O(1)-O(2B)	1.15(4)	1.16(4)	N(31)-C(42)	1.34(2)	1.32(2)
N(L3)-C(L2)	1.42(2)	-	C(22)-O(10)	1.22(2)	*
C(L2)-CN(L)	1.41(2)	-	C(42)-O(30)	1.22(2)	1.22(2)
CN(L)-CN(L)	1.27(3)	-	C(22)-C(23)	1.53(3)	*
CN(L)-C(L1)	1.36(3)	-	C(42)-C(43)	1.50(3)	1.52(3)
N(10)-C(11)	1.390(15)	*	C(23)-C(24A)	1.70(6)	*
N(10)-C(14)	1.423(15)	*	C(23)-C(25A)	1.47(4)	*
N(30)-C(31)	1.398(15)	*	C(23)-C(26A)	1.58(4)	*
N(30)-C(34)	1.397(14)	1.402(14)	C(23)-C(24B)	1.54(5)	*
C(11)-C(12)	1.473(17)	*	C(23)-C(25B)	1.48(4)	*
C(13)-C(14)	1.469(17)	*	C(23)-C(26B)	1.35(7)	1.52(12)
C(31)-C(32)	1.455(16)	*	C(43)-C(44A)	1.43(5)	*
C(33)-C(34)	1.462(17)	1.465(8)	C(43)-C(45A)	1.59(5)	*
C(12)-C(13)	1.388(17)	*	C(43)-C(46A)	1.65(4)	*
C(32)-C(33)	1.380(17)	1.384(17)	C(43)-C(44B)	1.52(6)	*
C(15)-C(14)	1.364(15)	*	C(43)-C(45B)	1.42(5)	*
C(15)-C(31)	1.363(15)	*	C(43)-C(46B)	1.66(5)	1.53(11)
C(35)-C(34)	1.348(15)	*			
C(35)-C(11)' [b]	1.388(16)	1.366(17)			

[a] The e.s.d. for the average is conventionally derived from the dispersion of chemically equivalent bond lengths about their mean, except where the average is calculated over only two chemically equivalent bonds in which case the e.s.d. is the longer of the e.s.d.'s calculated for an individual bond length.

[b] A single quote denotes an atom whose position is generated by the C_2 symmetry.

[c] CORFFE does not calculate estimated standard deviations (e.s.d.) in bond parameters for atoms constrained in rigid groups. However an e.s.d. of 0.02 Å is reasonable.

Table 4.6 : Bond angles (in °) for Fe(TpivPP)(1-Me-imid)(O_2).

Atoms	Angle	Average[a]	Atoms	Angle	Average[a]
N(10)-Fe-N(10)'	177.9(7)	*	C(15)-C(16)-C(17)	118.5	*
N(30)-Fe-N(30)'	178.6(6)	178.3(7)	C(15)-C(16)-C(21)	121.5	*
N(10)-Fe-N(30)	90.4(4)	*	C(35)-C(36)-C(37)	121.0	*
N(10)-Fe-N(30)'	89.5(4)	90.0(4)	C(35)-C(36)-C(41)	119.0	120.0(15)
O(1)-Fe-N(10)	91.1(3)	*	N(11)-C(21)-C(20)	122.8	*
O(1)-Fe-N(30)	90.7(3)	90.9(3)	N(31)-C(41)-C(40)	124.3	*
N(L3)-Fe-N(10)	88.9(3)	*	N(11)-C(21)-C(16)	117.2	*
N(L3)-Fe-N(30)	89.3(3)	89.1(3)	N(31)-C(41)-C(36)	115.7	120.0(42)
O(1)-Fe-N(L3)	180	-	C(21)-N(11)-C(22)	130.5	*
Fe-O(1)-O(2A)	129(2)	*	C(41)-N(31)-C(42)	131.9	131.2
Fe-O(1)-O(2B)	133(2)	131(2)	N(11)-C(22)-O(10)	119(2)	*
Fe-N(L3)-C(L2)	124.5(10)	-	N(31)-C(42)-O(30)	121(2)	120(2)
C(L2)-N(L3)-C(L2)'	111.0(20)	-	N(11)-C(22)-C(23)	122.7(18)	*
N(L3)-C(L2)-CN(L)	102.4(17)	-	N(31)-C(42)-C(43)	120.0(18)	121.4(18)
C(L2)-CN(L)-CN(L)'	112.1(10)	-	O(10)-C(22)-C(23)	118(2)	*
C(L2)-CN(L)-C(L1)	129(2)	-	O(30)-C(42)-C(43)	118(2)	118(2)
CN(L)'-CN(L)-C(L1)	118.5(17)	-	C(22)-C(23)-C(24A)	112(3)	*
Fe-N(10)-C(11)	128.3(8)	*	C(22)-C(23)-C(25A)	108(2)	*
Fe-N(10)-C(14)	126.6(8)	*	C(22)-C(23)-C(26A)	108(2)	*
Fe-N(30)-C(31)	127.1(8)	*	C(22)-C(23)-C(24B)	107(3)	*
Fe-N(30)-C(34)	127.0(8)	127.3(7)	C(22)-C(23)-C(25B)	114(3)	*
N(10)-C(14)-C(15)	124.8(12)	*	C(22)-C(23)-C(26B)	107(3)	*
N(10)-C(11)-C(35)'	124.6(12)	*	C(42)-C(43)-C(44A)	113(3)	*
N(30)-C(34)-C(35)	126.1(11)	*	C(42)-C(43)-C(45A)	113(2)	*
N(30)-C(31)-C(15)	124.9(11)	125.1(7)	C(42)-C(43)-C(46A)	112(2)	*
C(13)-C(14)-C(15)	125.9(12)	*	C(42)-C(43)-C(44B)	108(3)	*
C(12)-C(11)-C(35)'	122.9(12)	*	C(42)-C(43)-C(45B)	117(3)	*
C(33)-C(34)-C(35)	124.0(12)	*	C(42)-C(43)-C(46B)	102(3)	110(4)
C(32)-C(31)-C(15)	124.9(12)	124.4(13)	C(24A)-C(23)-C(25A)	116(3)	*
C(11)-N(10)-C(14)	105.0(11)	*	C(24A)-C(23)-C(26A)	100(5)	*
C(31)-N(30)-C(34)	105.9(10)	105.5	C(25A)-C(23)-C(26A)	113(4)	*
N(10)-C(11)-C(12)	112.3(12)	*	C(24B)-C(23)-C(25B)	108(5)	*
N(10)-C(14)-C(13)	109.3(11)	*	C(24B)-C(23)-C(26B)	104(6)	*
N(30)-C(31)-C(32)	110.2(11)	*	C(25B)-C(23)-C(26B)	117(4)	*
N(30)-C(34)-C(33)	109.9(11)	110.(13)	C(44A)-C(43)-C(45A)	105(4)	*
C(11)-C(12)-C(13)	104.9(12)	*	C(44A)-C(43)-C(46A)	104(3)	*
C(12)-C(13)-C(14)	108.4(12)	*	C(45A)-C(43)-C(46A)	109(4)	*
C(31)-C(32)-C(33)	106.9(12)	*	C(44B)-C(43)-C(45B)	113(4)	*
C(32)-C(33)-C(34)	107.0(12)	106.8(14)	C(44B)-C(43)-C(46B)	108(4)	*
C(14)-C(15)-C(31)	125.8(11)	*	C(45B)-C(43)-C(46B)	109(4)	109(5)
C(34)-C(35)-C(11)'	124.4(12)	125.1(12)			
C(14)-C(15)-C(16)	115.6[b]	*			
C(31)-C(15)-C(16)	118.4	*			
C(34)-C(35)-C(36)	117.9	*			
C(11)'-C(35)-C(36)	117.7	117.4(12)			

[a] See footnotes for Table 4.5. [b] In this case an e.s.d. of 1.2° to 2.0° is reasonable for atoms constrained in rigid group

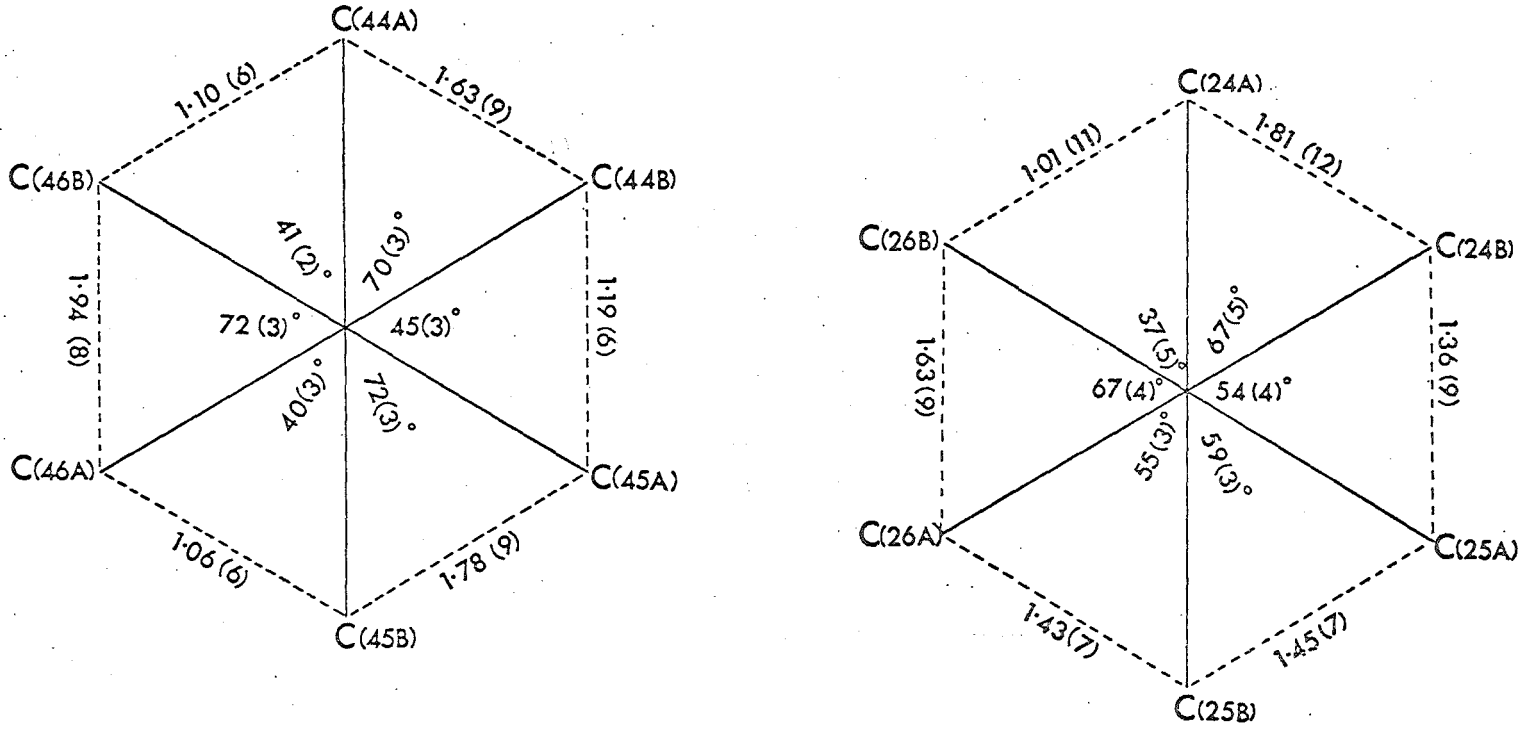

Figure 4.16 : Disorder of the pivalamide methyl carbon atoms.
Distances in Å, angles in degrees.

the range 1.35(7) to 1.70(6) Å and 1.42(5) to 1.66(5) Å, respectively, inadequacies in the single atom description of the quaternary carbon atoms C(23) and C(43) could exist. Anomalously short separations between and high anisotropic thermal motion for other atoms of the pivalamide "pickets" could indicate further irresolvable disorder. Disorder in both the pivalamide methyl carbon atoms and the terminal oxygen atom creates a potential but improbable interatomic separation of only 2.68 Å between C(45A) and O(2B) for a particular molecule. Bond lengths between the pivalamide methyl carbon atoms and the appropriate quaternary carbon atom, C(23) or C(43), are scattered about their mean value (1.52 Å) with an estimated standard deviation more than twice the e.s.d. of an individual bond (Table 4.5). For the rest of the molecule, bond lengths between chemically equivalent atoms display a reassuring internal consistency; in most cases the e.s.d. for their scatter is less than the e.s.d. of an individual bond length (Table 4.5). Moreover, the averaged bond lengths for the porphinato core display similar trends to and are not significantly different from the averaged values reported by Hoard in Table 2 of his review[191]. The bond angles display similar internal consistency. The averaged values obtained here are compared with those of Hoard (compiled from very precisely determined metalloporphyrin structures) in Figure 4.17.

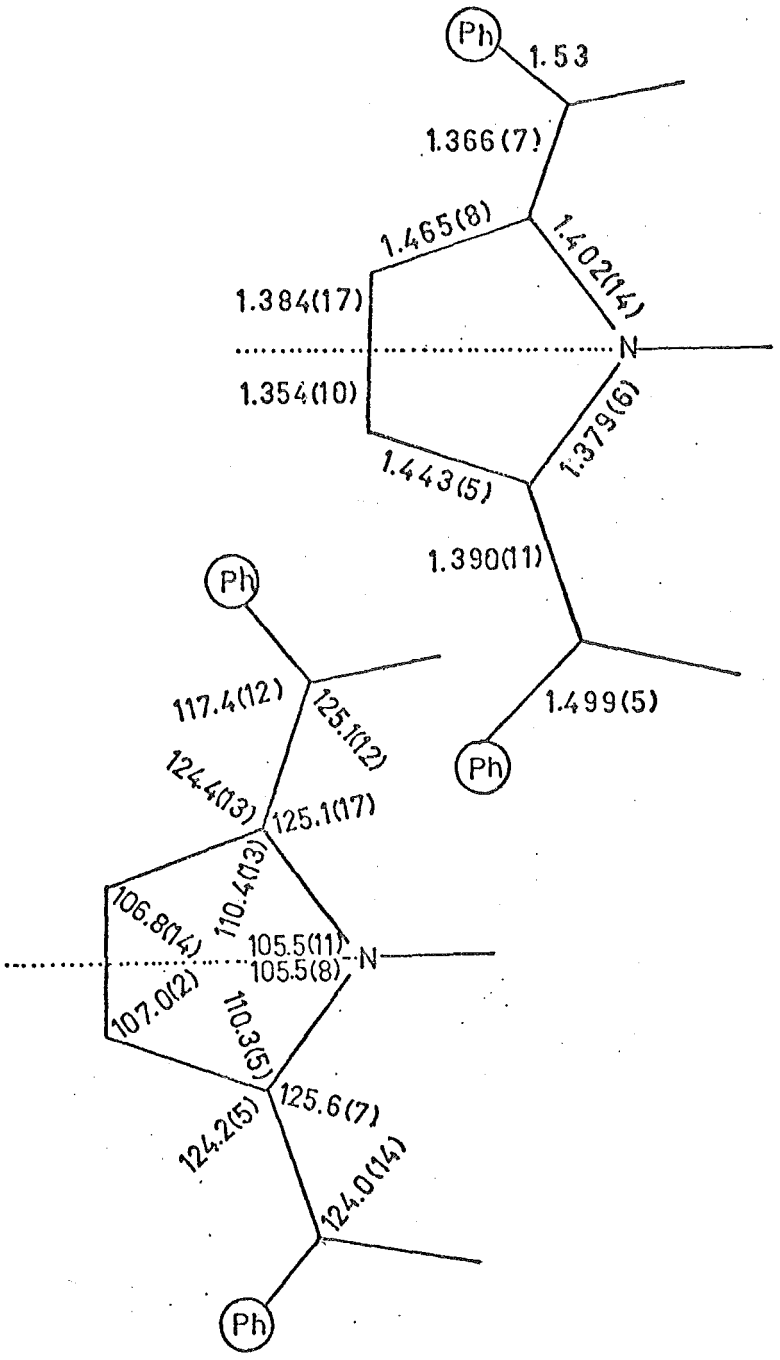

Figure 4.17 : Averaged values for bond distances and angles in the porphinato core of selected metalloporphyrins. Parameters above the dotted lines are for Fe(TpivPP)-(1-Me-imid)(O_2); those below are from Hoard's compilation[191]. Distances in Å, angles in degrees.

The only non-hydrogen intermolecular contacts less than 3.3 Å are between pivalamide oxygen atoms O(10) and O(30) and carbon atoms C(L1) of the 1-methylimidazole axial ligand and C(S2B) of the solvate species respectively. The respective separations are 2.90(3) and 3.24 Å. The high apparent thermal motion of these atoms may indicate irresolvable disorder such that these rather close contacts are relieved. Table 4.7 lists all non-hydrogen intermolecular contacts less than 3.75 Å. A selection of intramolecular contacts is also tabulated.

The Fe-O_2 Moiety

The O(1)-O(2A) and O(1)-O(2B) separations of 1.17(4) and 1.15(4) Å respectively, are unrealistically short bond lengths since molecular oxygen has a bond length of 1.21 Å. The respective Fe–O(1)$\angle^{O(2)}$ bond angles are 129(2)° and 133(2)°. The O-O separations are considerably shorter than those reported for the preliminary structure determination (1.23(8) and 1.26(8) Å [11]), but the differences are not statistically significant. The low values of the final model may be attributed to the moderate thermal motions of the two atoms and/or to disorder of the bonded oxygen atom involving displacement of it away from the two-fold axis. In some cobalt-nitrosyl complexes, displacement of the nitrosyl nitrogen atom away from the central normal to the porphinato plane is observed[206,227]. This would not be unexpected for iron-dioxygen complexes since they are isoelectronic with cobalt-nitrosyl systems. An off-axis displacement of only 0.1 Å would increase the O(1)-O(2) separations to more realistic values of ∿1.25 and 1.23 Å

Table 4.7 : Non hydrogen inter-and intramolecular contacts for [Fe(TpivPP)(1-Me-imid)-(O_2)]·½(C_6H_6)·½($C_4N_2H_6$).

(a) Intermolecular Contacts (<3.75 Å) not Involving Hydrogen Atoms

Atoms	Distance	Atoms	Distance	Atoms	Distance
C(L1)... O(10)	2.90(3)	O(10)... C(33)	3.53(2)	C(19)... C(S1A)	3.54
C(26A)... C(46B)	3.37(7)	O(30)... C(12)	3.43(2)	C(19)... C(S2B)	3.55
C(18)... N(S1A)	3.54	O(30)... C(13)	3.48(2)	C(19)... C(S2A)	3.71
C(18)... C(S2A)	3.59	C(38)... CN(L)	3.55	C(S2B)... O(30)	3.24
C(18)... C(S2B)	3.63	C(38)... C(L2)	3.73	C(S3B)... C(24B)	3.75
C(18)... C(S1B)	3.66	C(39)... CN(L)	3.56	C(S1A)... C(L1)	3.67
C(18)... C(S2A)'	3.75	C(39)... C(44A)	3.57	C(S2A)... O(30)	3.64
C(18)... C(S3B)	3.75	C(19)... C(S1B)	3.42	CN(SA)... C(24B)	3.60
O(10)... C(32)	3.50(2)	C(19)... N(S1A)	3.47	CN(SA)... C(24A)	3.75
C(38)... CN(L)	3.73	C(39)... CN(L)	3.46	C(39)... C(L1)	3.64

(b) Selected Intramolecular Contacts[a]

O(2A)... N(10)	2.91(5)	C(L2)... N(10)	2.99(2)	O(2B)... C(24A)	3.48(11)
O(2A)... N(30)	2.94(4)	C(L2)... C(11)	3.34(2)	O(2B)... C(11)	3.49(4)
O(2A)... C(24B)	3.05(12)	C(24A)... C(45A)	3.47(8)	O(2B)... N(31)	4.24(4)
O(2A)... C(24A)	3.14(12)	C(24A)... C(45B)	3.75(9)	N(31)... N(31)'	10.1
O(2A)... C(45A)	3.47(10)	C(25A)... C(44B)	4.05(8)	C(L2)... N(30)	3.43(2)
O(2A)... C(14)	3.30(5)	C(25A)... C(44A)	4.20(8)	C(24B)... C(44B)	3.48(8)
O(2A)... C(31)	3.34(5)	O(2B)... N(10)	2.99(4)	C(24B)... C(45B)	4.02(11)
O(2A)... C(15)	3.46(4)	O(2B)... N(30)	2.95(4)	C(26B)... C(45A)	4.18(9)
O(2A)... N(11)	4.05(5)	O(2B)... C(45A)	2.68(8)	C(24B)... C(44A)	4.15(12)
N(11)... N(11)	9.9	O(2B)... C(44B)	3.07(9)	C(26B)... C(45B)	4.07(8)
C(25B)... C(46B)	4.13(10)			C(26B)... C(46A)	4.14(9)

[a] All contacts less than 3.5 Å with O_2, all contacts less than 4.2 Å between atoms from different "pickets", and other selected intramolecular atomis separations are listed.

and close the Fe-O(1)$\angle$O(2) angles to $\sim 126^{\circ}$ and $\sim 130^{\circ}$, respectively. The increase in Fe-O(1) is negligible (<0.003 Å).

Anisotropic models for the thermal motion of dioxygen were tested and found inappropriate. Refinements of such models resulted in high correlation among the variable parameters describing dioxygen coupled with a marked decrease in precision of the positional parameters. An anisotropic model for the thermal motion of only the bonded oxygen atom did not lead to a more realistic description for dioxygen than the fully isotropic model. It is noted, however, that in all refinements involving an anisotropic model for the thermal motion of the bonded oxygen atom there was a marginally significant shortening of the RMS component of thermal displacement along the principal axis that is parallel to the Fe-O(1) vector. The values observed were typically 0.26(2), 0.31(2) and 0.34(2) Å. This is not inconsistent with an off-axis displacement of atom O(1).

Therefore, it is considered that the O(1)-O(2) separations may be underestimated by as much as 0.15 Å. While end-on bent bond geometry for the coordinated dioxygen molecule is unequivocally established, precise and accurate stereochemistry is unobtainable for this complex. Unfortunately, therefore, stereochemical comparison with cobalt-dioxygen complexes is not possible. Accurate definition of the dioxygen bond and of the canting of the Fe-O(1) vector to the porphinato normal must await the analysis of an iron-dioxygen complex where disorder, such as that which plagued this

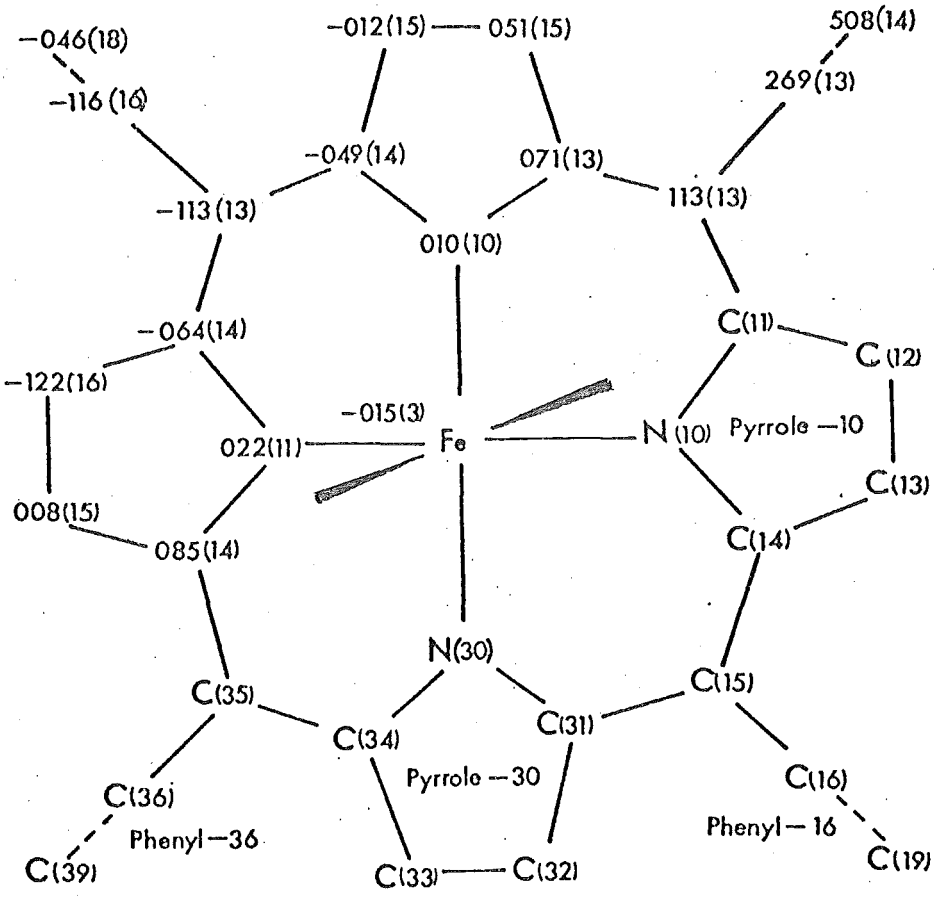

Figure 4.18 : Deviations of atoms from the mean, 24-atom, porphinato plane. The orientation of the 1-Me-imid axial ligand is indicated. Note that the ruffling is not conducive to reduced ligand-porphinato contacts. The "pickets" are directed downwards into the page. Distances in $\mathring{A} \times 10^3$.

structure analysis, is absent.

Conformational Aspects. The Tetraphenylporphinato Component

A selection of least-squares planes, the atoms comprising the planes and deviations of atoms therefrom is contained in Table 4.8. Table 4.9 lists dihedral angles between the normals of selected planes.

The porphinato skeleton, comprising four pyrrole groups and four linking methine carbon atoms is ruffled in quasi-D_{2d} fashion. Deviations of atoms from the mean plane calculated for the 24-atom porphinato core are depicted in Figure 4.18. This plane and the planes formed by the porphinato nitrogen atoms are constrained by the crystallographic two-fold axis to lie parallel to the xz crystal plane. The iron atom is displaced 0.015(3) Å from the former plane and 0.030 Å from the latter plane towards the dioxygen ligand. The dihedral angle between Pyrrole-10 and the porphinato plane is 4.8°; between Pyrrole-30 and the porphinato plane, 3.0°. Departures of the porphinato core from idealised S_4 symmetry are also evidenced in the different dihedral angles between the least-squares planes of Pyrrole-10 and Pyrrole-30 (4.6°) and between Pyrrole-10 and the symmetry generated Pyrrole-30′ (6.5°).

In common with other metalloporphyrins the individual pyrrole rings show insignificant departures from planarity[191]; the maximum departure of a pyrrole atom from its plane is 0.019(14) Å for Pyrrole-10 and 0.005(15) for Pyrrole-30.

The planes of the phenyl rings are not perpendicular to the porphinato plane; the dihedral angles between the

Table 4.8 : Selected least-squares planes (unweighted) for Fe(TpivPP)(1-Me-imid)(O_2).

Name of Plane	Atoms in plane Displacements of atom from plane ($\AA \times 10^3$)						Equation of Plane[b] Ax + By + Cz - D = O (Coeff x 10^4) A	B	C	D
Pyrrole-10	N(10)	C(11)	C(12)	C(13)	C(14)		-0657	9965	-0519	23550
	013(11)	-002(14)	-010(15)	018(16)	-019(14)					
Pyrrole-30	N(30)	C(31)	C(32)	C(33)	C(34)		0450	-9987	-0254	-28318
	002(10)	-004(14)	005(15)	-004(15)	001(13)					
Phenyl-16	C(16)	C(17)	C(18)	C(19)	C(20)	C(21)	3373	2094	-9178	-37575
	0[c]	0	0	0	0	0				
Phenyl-36	C(36)	C(37)	C(38)	C(39)	C(40)	C(41)	-9180	-1183	-3785	-21130
	0[c]	0	0	0	0	0				
Piv-11	C(21)	N(11)	C(22)	O(10)	C(23)		1411	-0015	-9900	-61195
	019(13)	-027(13)	002(19)	-005(17)	012(24)					
Piv-31	C(41)	N(31)	C(42)	O(30)	C(43)		-9522	-1020	-2879	-10888
	014(13)	-031(14)	030(24)	-014(20)	000(22)					

a Displacements of atoms are from a fixed plane and hence the accompanying estimated standard deviations (e.s.d.) are derived only from the e.s.d.'s in positional coordinates of the atoms.

b The coefficients are relative to an orthogonalised $\AA$ngstrom coordinate system, and were calculated using program MEANPLANE (local version of the NRC program of the same name (M. E. Pippy, F. R. Ahmed)).

c Constrained to be planar.

Table 4.9 : Selected dihedral angles (in °) between least-squares planes for Fe(TpivPP)(1-Me-imid)(O_2).

	XZ	Pyrrole-10	Pyrrole-30	Pyrrole-10'	Pyrrole-30'
XZ	0	175.2	3.0	4.8	177.0
Pyrrole-10		0	175.4	170.4	6.5
Pyrrole-30			0	6.5	174.1
Pyrrole-10'				0	175.4
Pyrrole-30'					0

	Phenyl-16	Phenyl-36	Phenyl-16'	Phenyl-36'	Piv-11	Piv-31
XZ	102.1	83.2	77.9	96.8	89.9	84.1
Phenyl-16	0	89.3	24.2	86.4	17.1	
Phenyl-36		0	86.4	13.6	-	5.6
Phenyl-16'			0	89.3	-	-
Phenyl-36'				0	-	-

porphinato plane and, respectively, the Phenyl-16 and Phenyl-36 groups are 77.9° and 83.2°. The pivalamide atoms N(11), C(22), O(10), C(23) and C(21) are displaced at most 0.027(13) Å from their least-squares plane and this plane is tilted from coplanarity with Phenyl-16 by 17.1°. Similarly for the other "picket" (Piv-31) the maximum displacement is 0.030(24) Å but the dihedral angle is only 5.6°. It would be expected that the conjugated system I would be approximately planar.

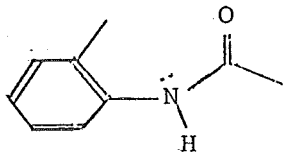

I

The departure of the Piv-11 group from coplanarity with Phenyl-16 may be safely attributed to crystal packing effects.

Conformational Aspects. The Axial Ligands and Solvate Species

It is convenient to define an orientation angle Φ : this being the dihedral angle between the plane defined by atoms O(1), Fe,N(10) and the plane of an axial ligand. Both planes are constrained by the two-fold axis to be perpendicular to the porphinato plane.

To a good approximation the Fe-O(1)$\diagup^{O(2)}$ planes bisect the N_{porph}—Fe—N_{porph} right angles with Φ being 42.9° and -47.5°. With this orientation O(2)...N_{porph} contacts are minimised and are between 2.91 Å and 2.99 Å. However, these contacts are still somewhat closer than the sum of the van der Waals radii for oxygen (1.4 Å) and aromatic nitrogen (1.7 Å). In the eclipsed conformations, Φ = 0,90°

the contacts would be even closer at ~2.7 Å although, in partial mitigation, there would only be the one close contact per terminal oxygen atom. In all dioxygen complexes that have been structurally characterised, except for Co(salen-C_2H_4-py)(O_2), the dioxygen ligand adopts the bisecting conformation, $\Phi \simeq \pm 45^{o}$. For Co(salen-C_2H_4-py)-(O_2) disorder of the dioxygen ligand about its mean eclipsed conformation is inferred (Chapter 3.2.4). But the dioxygen is almost certainly not disordered between two adjacent bisecting conformations; disorder of that magnitude would have been detected in Fourier syntheses.

From steric considerations alone, for an isolated molecule, a bisecting orientation for the plane of the axial ligand is also expected. Exact perpendicularity of the axial base and M-O^{O} planes has been observed for Co(bzacen)(py)(O_2)[126] and Co(acacen)(py)(O_2)[231], but in the saltmen series of compounds[123-125] the dihedral angles range between 12.6° and 19.2°. For Fe(TpivPP)(1-Me-imid)(O_2) the axial base is oriented such that Φ = 20°; thus the dihedral angles between this plane and the Fe-O^{O} planes are 27.5° and 62.9°. The resolution of the data is insufficient for any statistically significant difference to be observed between bond parameters involving the two chemically different terminal oxygen atom positions. However, these alternative positions for the terminal oxygen atom may account for the unusual temperature dependence of the nuclear quadrupole splitting observed in the Mossbauer spectra for both this model compound[12,281] and oxyhaemoglobin[279]. Detailed

simulations of Mossbauer spectra at various temperatures for Fe(TpivPP)(1-Me-imid)(O_2) indicate a room temperature population ratio of ∿0.6 for occupancy of the two chemically different terminal oxygen atom sites[281]; the X-ray data, although indicating a ratio of ∿1 as a result of least-squares refinement, are inadequate to exclude the ratio of 0.6. Furthermore a single crystal ESR study of cobalt-substituted myoglobin has indicated the existence of two (slightly) different cobalt-dioxygen species[215].

The solvate plane is at right angles to the imidazole-base plane. This relative orientation relieves any unduly close contacts with the axial base that may otherwise occur if a non-orthogonal disposition were adopted. The half-carbon atom C(L1) of the axial base has a fairly close contact with a pivalamide oxygen atom O(10) 2.90(3) Å away. The solvate species also has a number of other contacts at about van de Waals radii. Crystal packing effects, therefore, largely determine the orientation of the 1-methylimidazole axial ligand. Such effects are responsible for the non-bisecting geometry adopted by axial bases in a large number of other metalloporphyrin structures[191] and also in the salt-men series of dioxygen complexes[123-125].

Bond Lengths in the FeL_6 Core

The average Fe-N_{porph} separation for Fe(TpivPP)(1-Me-imid)(O_2) (1.98(1) Å) is not significantly different from those obtained for the diamagnetic compounds Fe(TPP)$(pip)_2$ (2.004(3) Å)[283] and Fe(TPP)$(1\text{-Me-imid})_2$[237]; nor from that

for the intermediate spin (S=1) compound Fe(TPP) (1.972(4) Å) [284].

One of the more notable features of the stereochemistry of Fe(TpivPP)(1-Me-imid)(O_2) is an apparent trans effect for the axial ligands; r(Fe-O(1)) is 1.75(2) Å and r(Fe-N(L3)) is 2.07(2).

Evidence that r(Fe-O(1)) may be shorter than "expected" by comparison with related species, is detailed below:-

1. The Fe-O(1) separation is very similar to that observed for the μ-oxo species, $O[Fe(Proto\text{-}IX\text{-}DME)]_2$ (1.73 Å) [285] and $O[Fe(TPP)]_2$ (1.763(1) Å).[252] but significantly shorter than that observed for Fe(Meso-IX-DME)(OMe) (1.842(4) Å)[243]. In these complexes an anionic ligand is coordinated to the iron(III) centre. For the methoxy complex the MeO-Fe^{III} bond can only involve σ donation of a lone pair of electrons to the iron. Hoard[286] had predicted a value of 1.86 Å for a simple σ-type coordination of dioxygen.

2. The Fe-O separation may be contrasted to the considerably longer separation observed in dioxygen adducts of cobalt(II) Schiff base complexes; r(Co-O) is typically within 0.01 Å of 1.88 Å (Table 2.2). Furthermore, r(Co-O) is remarkably similar to that observed for Co(salen)(OMe)(py) (1.891 Å) [240]. It was concluded, in Chapter 3, that the Co-O link was largely a σ bond and that a $Co^{III}-O_2^-$ representation was valid, at least for the cobalt-dioxygen complexes structurally characterised.

3. Hoard has found, for the approximately isostructural carbonyl twin of Fe(TpivPP)(1-Me-imid)(O_2), a contraction

of the Fe-C separation by ∿0.13-0.18 Å compared to other carbonyl structures.

Thus an Fe-O bond featuring a significant π component (in contrast to the cobalt-dioxygen system) is inferred. This is in general accord with other lines of evidence presented in §4.1.

However, Hoard's value for r(Fe-C) of 1.59-1.63 Å in Fe(TpivPP)(1-Me-imid)(CO) is rather shorter than that observed by Peng and Ibers[287] for Fe(TPP)(py)(CO) (1.77(2) Å) and by Goedken et al for Fe(N_4)(py)(CO) (1.751(5) Å); N_4 is a quadridentate conjugated macrocycle[204]. Despite the difference in axial ligand, the difference between r(Fe-C) for these structures is surprising and rather alarming since if Hoard's value is an artefact then the possibility that the short Fe-O separation for Fe(TpivPP)(1-Me-imid)(O_2) is also an artefact must be noted. However, the internal consistency of the structure, discussed previously, which appears to be greater than that for Fe(TpivPP)(1-Me-imid)(CO)[191] diminishes this possibility.

On the other side of the porphyrin there is an apparent lengthening of the Fe-N(L3) bond by comparison with related species. The following evidence is presented:-

1. For the centrosymmetric molecule Fe(TPP)(1-Me-imid)$_2$ r(Fe-N_{imid}) is 2.016(5) Å and the orientation of 1-methyl-imidazole ligands ($\Phi \simeq 20^{o}$) is similar to that found for Fe(TpivPP)(1-Me-imid)(O_2). There is, therefore, an apparent lengthening of ∿0.05 Å in the Fe-N_{imid} separation accompanying the substitution of one imidazole ligand by dioxygen.

2. For the carbonyl adduct Fe(TpivPP)(1-Me-imid)(CO) $r(Fe\text{-}N_{imid})$ is in the range 2.04-2.08 Å [191]. For Fe(TPP)-(py)(CO), $r(Fe\text{-}N_{py})$ is 2.10(1) Å [287]. A more marked trans effect is observed for the structure of Fe(TPP)(1-Me-imid)-(NO) where $Fe\text{-}N_{NO}$ is 1.743(4) Å and $Fe\text{-}N_{imid}$ is 2.180(4) Å [288]. In this last complex the authors argued, without having recourse to the structure of Fe(TPP)(1-Me-imid)$_2$, that the $Fe\text{-}N_{imid}$ bond had been lengthened by ~0.2 Å.

3. In the corresponding cobalt-dioxygen derivatives of "saltmen" Schiff-base ligand system, $r(Co\text{-}N_{imid})$ is in the range 1.974(8) Å to 2.011(2) Å [123-125].

This lengthening of the axial connection with respect to symmetric, diamagnetic, iron species and to cobalt-dioxygen species coupled with similarly lengthened bonds for other coordinated diatomics tends to support the contentions that the value for r(Fe-O) is accurate and that it is considerably shortened by comparison with cobalt-dioxygen systems.

Displacement of the iron atom from the plane of the porphinato nitrogen atoms towards the coordinated diatomic ligand is usually observed. For Fe(TpivPP)(1-Me-imid)(O_2) the displacement is 0.030(3) Å, for the carbonyl analogue 0.08 Å [289], for Fe(TPP)(py)(CO) 0.02 Å [287], but Fe(N_4)(py)-(CO) -0.05 Å [204]. For a fixed Fe-O, or Fe-C separation displacement of the iron centre towards the coordinated diatomic molecule relieves $O\cdots N_{porph}$ and $C\cdots N_{porph}$ contacts. For Fe(TpivPP)(1-Me-imid)(O_2) such contacts are ~2.66 Å; values shorter than the sum of the van der Waals radii (in this case 3.1 Å) are generally indicative of strong axial ligation.

Possible Factors Influencing Geometry of Dioxygen Coordination

The feasibility of side-on coordination of dioxygen has been discussed and the formally seven-coordinate product has been rejected as sterically unlikely if the iron atom is to remain approximately centred in the plane of the porphinato nitrogen atoms[206]. Moreover, seven-coordinate iron(II) complexes are unknown. Certainly the dimensions of the protective pocket provided by the pivalamide "pickets" place no restrictions on triangular coordination; the trans "picket" distances N(11)···N(11)′ and N(31)-N(31)′ are ∿10 Å, the pocket is ∿5.4 Å deep and, moreover, the crystal structures of other "picket fence" porphinato complexes indicate remarkable flexibility in the pivalamidephenyl components. That is, the basic geometry of the iron-dioxygen moiety is wholly determined by the (1-methylimidazole)-porphinato-iron(II) core. The O(2)···N(11), O(2)···N(31) separations (4.05 to 4.20 Å) are almost certainly too great for there to be any significant interaction between these atoms. However, the possibility of some interaction between pivalamide methyl hydrogen and terminal oxygen atoms cannot be excluded. Separations of 3.05 Å for O(2A)···C(24B), 3.14 Å for O(2A)···C(24A) and 3.07 Å for O(2B)···C(44B) occur (see Table 4.7).

The recent observations of side-on coordination of dioxygen to metalloporphyrins necessitates a closer examination of the possibility that such coordination could occur for iron(II) porphinato derivatives. Assuming an O-O separation of ∿1.40 Å, a Ct···N_{porph} radius of ∿2.0 Å, a distance of ∿1.8 Å from the centre of the O-O bond to the

iron atom and an orientation angle $\Phi = 45^{o}$, an $O\cdots N_{porph}$ separation of ~ 2.4 Å is calculated. Displacement of the iron atom by 0.3 Å from the plane of the porphinato nitrogen atoms leads to an $N_{porph}\cdots O$ separation of ~ 2.64 Å - quite similar to that observed for the angularly coordinated dioxygen ligand of Fe(TpivPP)(1-Me-imid)(O_2). However, coordination of an axial nitrogen base would then be unlikely since it would result in unacceptably tight ligand-porphyrin contacts if a viable Fe-N_{ax} bond were to be maintained; that is, excessive stretching of the Fe-N_{ax} bond could deter side-on coordination of dioxygen.

Moreover, in contrast to cobalt(II) porphyrin systems [121], iron(II) porphyrins appear to require an axial base for coordination of dioxygen. In the absence of an axial base iron(II) porphyrins irreversibly oxidise very rapidly. Furthermore, there is evidence to suggest that Mn(TPP)(py) forms a dioxygen adduct Mn(TPP)(O_2) where dioxygen is coordinated in the side-on mode[98].

In the structure of Ti(OEP)(O_2), tight dioxygen-porphyrin contacts are avoided by the metal atom being dragged 0.62 Å out of the plane of the porphinato nitrogen atoms[89]. But, in the formally eight-coordinate complex, Mo(p-CH_3TPP)(O_2)$_2$, dioxygen has adopted the sterically unfavourable eclipsing configuration[87] and the $O\cdots N_{porph}$ separations are calculated to be an extraordinarily close 2.46 Å separation. Thus the possibility of side-on coordination of dioxygen to an iron(II)-porphyrin derivative can not be categorically dismissed on steric grounds.

In the presence of a more polarisable ligand, such as sulphur, where a longer iron-ligand separation may be observed and where considerable stretching of that bond is not required to reduce ligand-porphinato interactions, side-on coordination may occur. Since side-on coordination of dioxygen appears to be generally associated with a more covalent $\sigma + \pi$ linkage than is the end-on coordination observed in cobalt-dioxygen adducts of quadridentate dianionic ligands, and since the iron-dioxygen linkage appears to be less polarised than the cobalt-dioxygen one, again the possibility of side-on coordination for an iron-dioxygen complex cannot be dismissed. Moreover it may be noted that a Co(porphyrin)(phosphine) derivative binds dioxygen (as evidenced by ESR spectroscopy) in a similar manner to the amine-based analogues, and that $Co(CN)_5^{3-}$ binds dioxygen in an angular fashion but that the dioxygen adduct of $Co^{II}(CN)_2(PPhMe_2)_3$ has sideways-bound dioxygen (Figure 2.8). The complex $Co(CN)_5O_2^{3-}$ has a considerably more obtuse $Co-O^{\nearrow O}$ angle ($153(2)^{o}$) than other end-on bonded dioxygen adducts. This has been attributed to intramolecular packing effects [78], but the electronic demands of $(CN)_5$ ligature are considerably different from Schiff-base ligature.

Thus the stereochemistry of the dioxygen adduct of the sulphur-based iron "picket fence" porphyrin Fe(TpivPP)(THT)(O_2), to be described in the next section, is of interest.

4.2.6 Assessment of Fe(TpivPP)(1-Me-imid)(O_2) as a Model for Oxymyoglobin.

In this subsection a number of features of HbO_2 and MbO_2, and their model compound Fe(TpivPP)(1-Me-imid)(O_2) are compared.

Similarities and Differences of the Porphyrin Component

Both the iron-dioxygen complex described in this section and the iron-dioxygen complex of the haemoglobins are porphyrin derivatives. It might be argued, though, that this symmetrical synthetic porphyrin H_2TpivPP is not a good model for the asymmetrical protoporphyrin-IX of biological systems. Whereas the "picket fence" porphyrin has four identical substituents at the methine carbon atoms, protoporphyrin-IX has an asymmetrical arrangement of propionic, methyl and vinyl substituents at the pyrrole carbon atoms (Figure 4.3). Derivatives of the "picket fence" porphyrin have uv-visible spectral properties which are different to those for protoporphyrin-IX[12,152]. Moreover, spectra of protoporphinato-IX-iron derivatives, in the absence of the protein, are susceptible to effects of temperature, solvent and axial base in a sometimes unpredictable way[264]. Protoporphyrin-IX is not unique to oxygen-binding haemoproteins; chlorocruorohaem, which has a different uv-visible spectrum to protohaem, protoporphinato-IX—iron(II), also supports reversible binding of dioxygen[1]. Although different substituents on the porphyrin perturb the metal centre and affect its spectral properties and, probably, oxygen-binding

properties, it is felt that the end-on bent bond geometry of the iron-dioxygen linkage observed for the synthetic model will occur for the related biological systems.

X-Ray Crystal Structure of MbO_2

From a difference Fourier synthesis, Watson and Nobbs tentatively inferred an angularly bound dioxygen ligand[290]. It is possible that the distal histidine may slightly influence geometry of dioxygen coordination, but certainly not to the extent that it affects the coordination of carbon monoxide. In simple porphyrin complexes, such as Fe(TpivPP)-(py)(CO)[191] and Fe(TPP)(py)(CO)[287], the Fe-C-O group is essentially linear and perpendicular to the porphinato plane. In all carbonylhaemoglobins structurally characterised the Fe-C-O group is tilted away from the haem normal giving the appearance of a bent Fe-C-O bond[151,291,292], although it is probably still approximately linear. Severe steric hindrance to carbonyl but not to dioxygen binding has fascinating and important physiological consequences[17].

Thermodynamic Features

Fe(TpivPP)(1-Me-imid) undergoes reversible oxygenation in solution[12] and in the solid state[135]. Thermodynamic data obtained for Fe(TpivPP)(1-Me-imid) in the solid state parallel very closely the data obtained for a number of haemoglobins such as ox myoglobin not only with regard to the equilibrium constant but also with regard to changes in enthalpy and entropy. The pressure for half-oxygenation at 20°, $P_{\frac{1}{2}}^{20^\circ}$, is 0.31τ for Fe(TpivPP)(1-Me-imid) and 0.55τ for

ox myoglobin. This agreement may be somewhat fortuitous since Fe(TpivPP)(1-Me-imid) is an equally valid model for leghaemoglobin which has an extraordinary high oxygen affinity ($P_{\frac{1}{2}}^{20^{o}}=0.05\tau$)[293]. However, Co(TpivPP)(1-Me-imid) has an affinity for dioxygen similar to ox myoglobin (46τ and 54τ, respectively) as well as similar enthalpy and entropy changes[136]. The great reluctance of dioxygen to bind to unhindered porphinatocobalt(II) derivatives in solution at 20°C must be attributed to solvent effects, since in solution $P_{\frac{1}{2}}^{20^{o}}$ for Co(TpivPP)(1-Me-imid) is 100τ[136].

Infrared ν(O-O) Spectroscopy

The O-O stretching mode for Fe(TpivPP)(1-Me-imid)-(O_2)[17] is some 50 cm^{-1} higher in energy than ν(O-O) for oxyhaemoglobin and oxymyoglobin[163,164]. A similar difference is observed for the corresponding carbonyl derivatives. Presumably, a tighter binding pocket for the native system than for its models is responsible for this difference.

Mossbauer Spectroscopy

There is a remarkable similarity in the Mossbauer spectrum of oxyhaemoglobin and Fe(TpivPP)(1-Me-imid)(O_2), including the temperature dependence of the nuclear quadrupole splitting, ΔE_q. Furthermore a Mossbauer emission study on ^{57}Co(Proto-IX-DME)(py)(O_2) showed that isolated haem (i.e. ^{57}Fe(Proto-IX-DME)(py)(O_2)) binds dioxygen in the same manner, electronically, as haemoglobin[299].

Extended X-Ray Absorption Fine Structure Spectroscopy

Very recently the technique of extended X-ray absorption fine structure (EXAFS) spectroscopy[4-7] has been applied to both Fe(TpivPP)(1-Me-imid)(O_2) and oxy- and deoxyhaemoglobin[294,295]. Iron-ligand separations may be determined by analysis of the fine structure observed in the X-ray absorption spectrum at photon energies just above, in this case, the K absorption edge for iron. Preliminary results did not apply a correction for the axial ligand(s) of oxy- and deoxyhaemoglobin[294]. Nevertheless, iron-nitrogen separations of 1.99(2) Å for HbO_2, and 1.98(2) Å for HbCO were obtained[294]. However, a similar value appeared to exist for deoxyHb[295]. Shulman and coworkers have now corrected for the effects of the axial ligands using values from the structure of Fe(TpivPP)(1-Me-imid)-(O_2), and have obtained for HbO_2 and its model a concordant value of 1.99(2) Å for the Fe-N_{porph} separation[295]. This is insignificantly different from the average crystallographically determined value of 1.98 Å for Fe(TpivPP)(1-Me-imid)-(O_2). Using the five-coordinate μ-amido-O derivative of Fe^{II}(TpivPP) (described in §4.4) as a model for deoxy-Hb, they again obtained remarkably similar values (2.06(2) Å) for the Fe-N_{porph} separation for deoxy-Hb and its model[295]. This latter result will be discussed further in §4.4. Notwithstanding the fact that the haemoglobin values are somewhat dependent on the iron to axial ligand separations observed in model compounds, the agreement in r(Fe-N_{porph}) for the model compound and haemoglobin is encouraging

since it is not possible, at present, to obtain, from the X-ray diffraction data for Hb and its derivatives, $Fe\text{-}N_{porph}$ separations with precision comparable to that achieved by EXAFS techniques.

Conclusion

In conclusion, although differences do exist between the various spectral features of oxyhaemoglobin and oxymyoglobin and the model compound Fe(TpivPP)(1-Me-imid)(O_2), they can reasonably be assigned to the sensitivity of the metal centre to small changes in the peripheral substituents of the porphyrin skeleton, and to the environment around the binding site provided by the protein or the "picket fence".

An end-on bent bond geometry for the iron-dioxygen group in oxyhaemoglobin, first predicted by Pauling, has been established through the structure analysis of the model iron-dioxygen complex Fe(TpivPP)(1-Me-imid)(O_2).

4.3 The Crystal and Molecular Structure of the Dioxygen Adduct of (tetrahydrothiophene) meso-tetra (α,α,α,α-orthopivalamide phenyl)porphinatoiron(II), [Fe(TpivPP)(THT)(O_2)]·$(THT)_2$

The title compound, described in subsections §4.3.2 to §4.3.4, is a possible model for the oxygenated protohaem species. This is one of the states adopted by the cytochrome P450 mono-oxygenases which mediate the catalytic hydroxylation of substrates such as camphor. The various

intermediate states of the enzyme, and models for them, will be described in §4.3.1. The best characterised cytochrome P450 is the camphor hydroxylase, $P450_{cam}$; the prosthetic group is a protoporphinato-IX-iron or protohaem species[304].

A number of reviews on the protein system are available [2,305-307].

4.3.1 Cytochrome P450 Systems

These oxygen-binding haemoproteins catalyse the reaction

$$R\text{-}H + {}^{18}O_2 + D_oH_2 \longrightarrow R\text{-}{}^{18}OH + H_2{}^{18}O + D_o$$

where D_oH_2 represents an electron transport chain capable of providing two reducing equivalents. The generic name P450, for these cytochromes, derives from the distinctive uv-visible spectra of their ferrous carbonyl derivatives. Normal ferrous carbonyl haems, such as HbCO, have a Soret peak at ∿420 nm. While enzymatically inactive forms of P450 have a Soret peak at ∿420 nm, the active forms have the peak at ∿450 nm — hence the origin of their name. Axial ligation quite different to that for other oxygen-binding haemoproteins has long been postulated[308].

The bacterial camphor hydroxylase, cytochrome $P450_{cam}$, which has been extensively studied by Gunsalus and coworkers, is water soluble in contrast to the other cytochromes P450 which are membrane-bound. Four stable intermediates in the catalytic hydroxylation of camphor

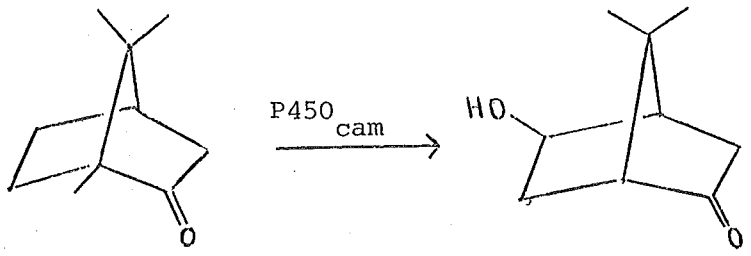

have been characterised[2,307]. The cycle proposed by Gunsalus and the characterisation of the intermediates is shown in Figure 4.19(a). This cycle is not identical to the one proposed by Coon and coworkers for a membrane-bound cytochrome P450 [309]. The following paragraphs refer to camphor hydroxylase and its models.

Model studies have been largely directed towards elucidating the axial coordination. In stages A, B and D the axial ligation is now established through model studies, and in D understood theoretically. Stages C and E are not yet well-understood or characterised. There are few published reviews on cytochrome P450 and its model systems; there is, however, an excellent unpublished one by Collman[310]. Figure 4.19(b) illustrates inferences on the stereochemistry and axial ligation of the iron centre which have been drawn from model studies.

Low-spin Ferric Stage A: ox-P450$_{cam}$.

Low-spin ($S=\frac{1}{2}$) porphinatoiron(III) complexes are invariably six-coordinate[191]. The distinctive ESR parameters of the substrate-free protein have been closely modelled by six-coordinate iron(III) porphyrin derivatives possessing an axial thiolate ligand, $R-S^-$ [311,312]. The ESR parameters

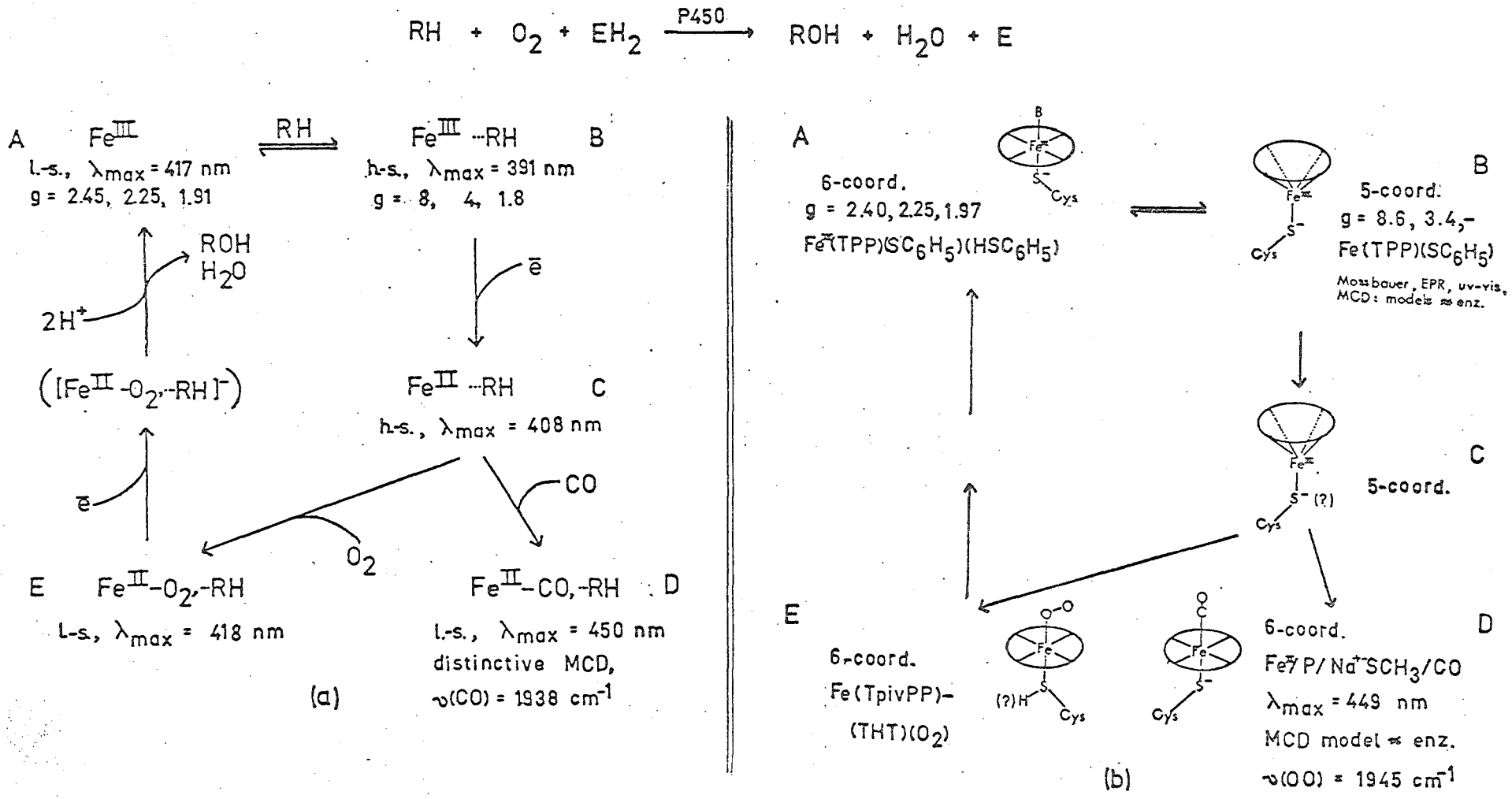

Figure 4.19 : The catalytic cycle of cytochrome $P450_{cam}$.

(a) Intermediates deduced from in vitro studies of $P450_{cam}$.

(b) Characterisation of the intermediates through model studies.

of the model compound were rather insensitive to the nature of the other axial ligand and moreover aryl thiolates ($Ar-S^-$) modelled the protein system rather better than alkyl thiolates. Nevertheless, coordination of a thiolate ligand, derived from the amino acid cysteine

$$HS-CH_2-CH(NH_2)CO_2H$$

is inferred for the protein. The S-methyl amino acid, methionine, is precluded.

A possible model complex, $Fe^{III}(TPP)(SC_6H_5)(HSC_6H_5)$, for this stage has been structurally characterised. This complex undergoes a temperature dependent spin equilibrium. At low temperature (-196^o) it is low-spin and six-coordinate with ESR parameters similar to P450 stage A. At room temperature it becomes a high-spin five-coordinate model for the next stage. That this occurs without destruction of the crystal lattice is most unusual[312,313].

High-spin Ferric Stage B: Ox-$P450_{cam}$... Sub

Binding of a substrate (Sub) to the protein generates a high-spin ferric complex. Such complexes are either five-coordinate or six-coordinate but with a weak sixth ligand [152,191]. Thus the substrate is bound very weakly, if at all, to the iron(III) centre. ESR, electronic, Mossbauer and MCD spectral studies of model Fe^{III}(Proto-IX-DME)(SAr) systems and Ox-$P450_{cam}$..Sub' display remarkable similarity [311,312,314]. The crystal structure of Fe^{III}(Proto-IX-DME)-$(SC_6H_4$-p-$NO_2)$ has been precisely determined[311(a)]. Alkyl thiolate models have also been synthesised[315].

One-electron reduction leads to the next intermediate species red-$P450_{cam}$..Sub.

High-spin Ferrous Stage C : red-$P450_{cam}$...Sub.

To date no models exist for this stage. Axial ligation is uncertain, but it has been suggested (L. K. Hanson quoted in reference [310]) that the electronic spectrum of this intermediate is inconsistent with axial thiolate coordination. The red-$P450_{cam}$...Sub has distinctive Mossbauer parameters[316] which should prove useful when potential model compounds are assessed.

Reduced Ferrous Carbonyl Stage D : red-$P450_{cam}$(-CO)(..Sub).

Carbon monoxide is coordinated to red-$P450_{cam}$...Sub to give a diamagnetic carbonyl adduct with a distinctive Soret band (~450 nm compared with ~420 nm for carbonylhaemoglobins [152]), and with a highly structured MCD spectrum[320,321]. These spectral features have been closely reproduced with porphinatoiron(II)-SCH_3-CO systems[317-320] but not with mercaptan or thiol species. The Soret band has also been theoretically explained in terms of an easily ionised thiolate p electron[322]. In contrast to the difference in optical spectra, the Mossbauer spectra of HbCO, red-$P450_{cam}$-(-CO)(...Sub) and the inactive $P420_{cam}$(-CO) are very similar [280]. At one time thiolate coordination in this and other stages was questioned, since the enzyme chloroperoxidase, which appeared to have no free sulphur to coordinate to the iron[323], possessed very similar spectral properties to P450

derivatives[324,325]. The paradox was resolved inasmuch as the free sulphydryl moiety of non-denatured chloroperoxidase may be hidden to conventional sulphydryl reagents[325].

Dioxygenated Stage E : $P450_{cam}(-O_2)(..Sub)$

Dioxygen coordinates to red-$P450_{cam}$..Sub to give an essentially diamagnetic dioxygen complex which, in contrast to oxyhaemoglobin, has only a weakly dependent nuclear quadrupole splitting[280].

Chang and Dolphin[326] reported that the optical spectrum of $P450_{cam}(-O_2)(..Sub)$ was not consistent with an $[RS^{-}\text{-haem-}O_2^{-}]^{-}$ species. The protein has a Soret band at 418 nm[307] similar to oxyhaemoglobins[152]. The species purported to be a thiolate-haem-dioxygen complex had a Soret band at 476 nm[326]. Hence axial ligation of thiolate does not appear to pertain to oxygenated cytochrome P450; axial ligation of a cysteine thiol is implicated by default. However Collman notes[310] that this result may be artefactual. That red-$P450_{cam}$..Sub will also coordinate carbon monoxide to give a species in which thiolate coordination is well-established, indicates the possibility of thiolate coordination in $P450_{cam}(-O_2)$-(... Sub) as well.

Nevertheless the neutral, sulphur-base complex Fe(TpivPP)-(THT)(O_2), whose structure is described in this section, remains a possible model for $P450_{cam}(-O_2)$(... Sub) in the absence of more definitive characterisation of this intermediate. The stereochemical consequences of substituting a sulphur base, tetrahydrothiophene, for an aromatic nitrogen base, 1-methyl-

imidazole are of intrinsic interest. As discussed in §2.2.5 and §4.2.5 a "softer" ligand system may induce side-on coordination of dioxygen. Unfortunately the best data obtainable for Fe(TpivPP)(THT)(O_2) precludes any quantitative discussion of its stereochemistry.

This complex is essentially diamagnetic and the temperature dependence of its nuclear quadrupole splitting, ΔE_q, is only slightly less than that for its nitrogen-base analogue Fe(TpivPP)(1-Me-imid)(O_2)[281]. However, temperature dependence apart, the Mossbauer spectra of the oxyhaemoproteins and their models are quite similar at the limit of 4.5°K. The Soret band for Fe(TpivPP)(THT)(O_2) is at 427 nm[12] compared with 418 nm for $P450_{cam}$(—O_2)(... Sub); tetraphenylporphyrin derivatives do not reproduce the electronic spectra of protoporphyrin-IX derivatives very well.

The mechanism by which the iron-dioxygen species delivers one oxygen atom to the substrate and loses the other as a water molecule, thereby returning the enzyme to its resting stage A, is unknown, but it has been speculated upon[310,314]. Axial ligation of the polarisable sulphur atom either as a thiol or as a thiolate ligand, is obviously of critical importance in the monooxygenase function of cytochrome P450 enzymes.

4.3.2 Collection and Reduction of Intensity Data

Dark red-black crystals of $[Fe^{II}(TpivPP)(THT)]\cdot(THT)_2$ were prepared at Stanford University, sealed and mailed to Canterbury University. The contents of the vial were exposed to air (oxygen uptake is rapid and quantitative), and crystals were sealed in thin-walled lead-free glass capillaries. As evidenced by their smell, loss of THT solvate molecules from the lattice was extremely facile. Symmetry and systematic absences uniquely consistent with the monoclinic space group $P2_1/c$ (No.14)[207] were observed by precession photography using Cu Kα radiation. Crystals not so protected from loss of solvate underwent a solid-state transformation to a new, very highly mosaic lattice with a contracted a-axis. Most crystals were twinned or suffered from very poor mosaicity. The 10-faced crystal eventually selected for data collection had maximum and minimum dimensions of 0.50 mm and 0.35 mm, and a volume of 0.04 mm^3. Crystal mosaicities for strong, low angle reflections ranged from 0.20^o to 0.32^o. Peak profiles were approximately symmetrical. Unit cell dimensions, obtained by the usual procedures (Appendix 1), were:

$a = 16.951(3)$, $b = 18.153(4)$, $c = 25.470(4)$ Å,

$\beta = 107.14(8)^o$.

The linear absorption coefficient calculated for four formula units of $FeSC_{68}N_8O_6H_{72}\cdot(SC_4H_8)_2$ in the cell and with Mo Kα radiation was 3.45 cm^{-1}, and since the maximum likely error due to neglect of absorption was less than 5%, absorption corrections to the intensity data were not applied.

Excluding systematic absences, 2796 independent reflections in the range $0^{o}<2\theta\leq29.2^{o}$ were collected by the θ-2θ scan technique with the Mo Kα radiation. Further data collection was not warranted in view of massive crystal decomposition and the lamentable lack of intensity; only 829 reflections had $I > 3\sigma_I$. A symmetric scan range of 1.60^{o} in 2θ, centred on the calculated peak position, comprised 80 steps each of 0.75 second duration. Background counts, at each end of the scan, were recorded for 15 seconds. Three standard reflections monitored every 100 reflections suffered a nett 20% drop in intensity. The data were processed by the standard procedure (Appendix 1).

4.3.3 Solution and Refinement of the Structure

Analysis of the three-dimensional Patterson synthesis established possible coordinates for the iron and coordinated sulphur atoms. A plot of the Patterson map over the u,0,w plane (Figure 4.20) established the orientation of the meso-tetraphenylporphinato fragment in a similar manner to that for Fe(TpivPP)(1-Me-imid)(O_2) (§4.2.3). The initial model consisted of four pyrrole and four phenyl rigid groups (each group having a single isotropic temperature factor), and an iron and two sulphur atoms (each atom having an isotropic temperature factor). The methine carbon atoms were appended to the appropriate phenyl group. After six cycles of least-squares refinement using 829 reflections having $I>3\sigma_I$ the discrepancy indices were

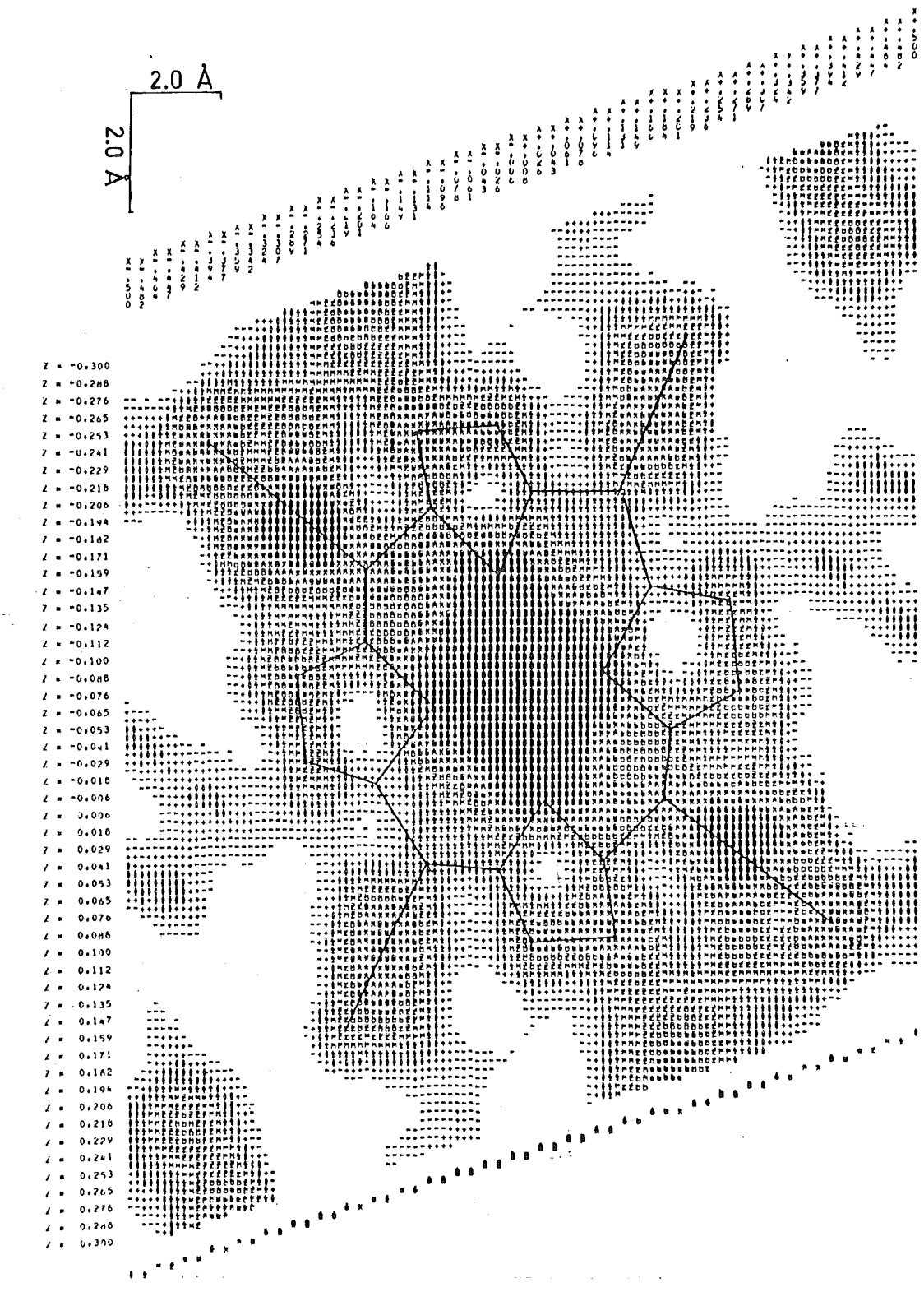

Figure 4.20 : Plot of the u,O,w plane of the Patterson synthesis for $\left[Fe(TpivPP)(THT)(O_2)\right]\cdot(THT)_2$.

$R = 0.34$ and $R_w = 0.40$.

The temperature-factor of one atom assigned as sulphur was higher than that of the other atom; furthermore it refined to a position closer to the iron. Its designation was subsequently changed to oxygen. Several groups had refined rather poorly yielding a severely distorted porphinato ring; these groups continued to refine poorly until the model was essentially complete.

Fourier syntheses failed to indicate chemically reasonable coordinates for atoms not included in the model. Until the model was essentially complete and correct, the positional and thermal parameters especially were inclined to oscillate wildly during least-squares refinements. These problems were ameliorated by the use, wherever reasonable, of rigid groups to impose chemically reasonable geometry on components of the complex. Nevertheless, since pairs of atoms were sometimes not resolved in Fourier syntheses and since F_{obs} Fourier syntheses often indicated atom positions somewhat different from those derived by least-squares refinement, elaboration of the structure was assisted by the less mathematically rigorous method of chemical intuition. Moreover, it was not until more, higher angle and weaker data (lying in the range $\sigma_I < I \leq 3\sigma_I$) were utilised that least-squares refinements converged to a chemically reasonable conclusion.

In the absence of satisfactory definition of the "pickets" from Fourier syntheses, direct methods were tried. The solution obtained using the data-phasing program, SAP, helped confirm suspicions concerning the orientation of the "pickets". Using the stereochemistry for the "pickets"

determined in the structure analysis of Fe(TpivPP)(1-Me-imid)-(O_2), pivalamidephenyl rigid groups oriented in the α,α,α,α-atropisomer relative to the crystal b-axis were constructed assuming coplanarity of the four atom amide group with its phenyl ring. This enlarged model was refined so that

$$R = 0.29 \text{ and } R_w = 0.36.$$

This orientation was confirmed by the poorer refinement and agreement factors obtained by reversing the orientation of the pickets (i.e. the β,β,β,β-atropisomer relative to the crystal b-axis).

Positions for atoms of the solvate molecules and t-butyl groups were very slowly extracted from Fourier syntheses. Single atom models for pyrrole rings and t-butyl groups were tried and the R factor was reduced to 0.17. But the model was stereochemically unreasonable and the solvate molecules and the THT axial ligand were ill-characterised. In the light of experiences with the disorder of the t-butyl groups in Fe(TpivPP)(1-Me-imid)(O_2), and with the THT solvate molecule of the polymeric "picket fence" porphyrin derivative described in §4.4, closer investigations of these components were made.

A structure factor calculation based on a model including the solvate species but with no contributions from the t-butyl groups and pivalamide oxygen atoms returned the following agreement factors:-

$$R = 0.27 \text{ and } R_w = 0.35$$

for 1077 reflections having $I > 2\sigma_I$. The contribution of this part of the structure to the structure factors was held constant while the "pickets" were examined using Fourier

syntheses. No evidence for disorder of the methyl carbon atoms of any "picket" could be found although very high thermal motion was apparent for three of the pickets. The agreement factors were lowered to

$$R = 0.170 \text{ and } R_w = 0.172.$$

The solvate molecules were now re-examined. They were removed from the model and structure factors were calculated. Inspection of the ensuing Fourier syntheses calculated over the appropriate volumes indicated that the tetrahydrothiophene solvate molecules were ordered except for very high libration of the sulphur atoms relative to other atoms of the ring. Conformational disorder of the sulphur atom was inferred; a similar disorder was also inferred for the THT solvate molecule of the polymeric "picket fence" porphyrin derivative described in §4.4. One solvate site appeared to have an occupancy factor of only 0.75 compared to the other site which was assigned an occupancy factor of 1.0. Four cycles of least-squares refinement of just the solvate molecules led to the following agreement indices:-

$$R = 0.155 \text{ and } R_w = 0.150.$$

The THT axial ligand was now re-examined. Due to the limited data, Fourier syntheses all failed to resolve the atom positions of the two carbon atoms β to the sulphur atom. Their positions were estimated and refinement of just the axial ligand yielded agreement factors

$$R = 0.154 \text{ and } R_w = 0.148.$$

This penultimate model was refined so that

$$R = 0.139 \text{ and } R_w = 0.132.$$

In particular, the geometry of the porphinato skeleton was much improved and more chemically reasonable.

At this stage Fourier syntheses over the volume of the dioxygen ligand indicated end-on bent bond attachment of dioxygen. F_{obs} Fourier syntheses on models lacking both oxygen atoms returned only an elongated ellipsoid of electron density tilted away from the normal to the porphinato plane. A similar absence of resolution had been found earlier for the β carbon atoms of the THT axial ligand. In an effort to better define the dioxygen moiety, reflections having $\sigma_I < I \leq 2\sigma_I$ were also utilised. Models for dioxygen incorporating disorder were tested and found inappropriate. The dioxygen ligand was also constrained in a rigid group. In all refinements the end-on bent bond geometry was favoured over a side-on geometry.

The final model for the structure was described by 231 variable parameters and both the iron and sulphur atoms were allowed an anisotropic model for thermal motion. The final cycles of least-squares refinements utilised 1521 reflections having $I > \sigma_I$ and the agreement factors improved from $R = 0.185$ and $R_w = 0.166$ to

$$R = 0.166 \text{ and } R_w = 0.145$$

at convergence. The standard error in an observation of unit weight was 1.770; the final scale factor was 0.3083(25). There was a slight dependence of the minimised function on $|F_o|$ and $\sin\theta/\lambda$. However, it was felt unjustified to change the weighting scheme ($p = 0.08$) as this would only place greater weight on the large amount of very weak data.

There was little evidence for secondary extinction among intense low angle reflections. In the final cycle of refinement the ratios of the change in a parameter to its e.s.d. were all less than 0.51 except for the solvate species where the maximum ratio was 0.79. The final difference Fourier map was remarkably flat and featureless. indicating that the final model is essentially correct.

There is a table of $|F_o|$ and $|F_c|$ for all data in Appendix 1. The agreement factors on all data were $R = 0.298$ and $R_w = 0.150$, and the standard error in an observation of unit weight was 1.25. Out of 2796 reflections 90 had calculated intensities which lay outside the range

$$I - 3\sigma_I < I_c < I + 3\sigma_I.$$

Table 4.10 lists final atomic parameters.

The non-inclusion of 88 hydrogen atoms in the structural model, and the obvious but unavoidable inadequacies in the isotropic descriptions for the very high thermal motion of most parts of the structure severely compromise the precision of this structure analysis. The release of group constraints would be quite unjustified in terms of the available data. Although the geometry of much of the structure is constrained by rigid groups, the final model is chemically reasonable; in general chemically equivalent bond lengths do not differ significantly. Within the limitations imposed by the data, the structure is therefore felt to be accurate. Table 4.11 lists selected bond distances for the complex and its solvate molecules, a limited number of bond angles are also listed.

Table 4.10: Final atomic parameters for [Fe(TpivPP)(THT)(O_2)]·$(THT)_2$.

(a) Individually Refined Atoms

Atom	X	Y	Z	B	Atom	X	Y	Z	B	Atom	X	Y	Z	B
Fe	1762(4)[a]	1461(4)	2036(3)	b	C(55)	069(2)	176(2)	2968(15)	4.0(11)	S(A)[c]	-272(3)	056(3)	3085(19)	34.2(19)
S	1427(10)	0137(9)	2120(7)	b	C(75)	-003(2)	144(2)	0963(14)	2.7(10)	C(1A)[c]	-275(5)	114(6)	255(4)	19.(3)
O(1)	194(3)	250(3)	1987(19)	11.3(14)	N(11)	313(2)	236(2)	0527(14)	5.9(11)	C(2A)[c]	-293(4)	187(4)	274(3)	13.(2)
O(2)	160(5)	275(5)	174(3)	31.(5)	O(10)	366(2)	316(2)	0085(16)	12.3(13)	C(3A)[c]	-301(5)	186(5)	333(3)	17.(2)
C(1)	240(4)	-033(4)	260(2)	11.3(20)	N(31)	460(2)	245(2)	3432(15)	7.8(12)	C(4A)[c]	-317(6)	105(7)	348(4)	23.(4)
C(2)	245(4)	-095(4)	226(3)	15.(2)	O(30)	560(3)	324(3)	383(2)	21.(2)	S(B)[d]	-365(4)	316(4)	116(2)	37.(3)
C(3)	207(4)	-104(4)	171(3)	12.(2)	N(51)	059(3)	313(3)	3410(17)	9.7(14)	C(1B)[d]	-437(5)	256(5)	133(3)	13.(3)
C(4)	141(3)	-045(3)	156(2)	9.2(17)	O(50)	077(2)	406(2)	4009(15)	10.6(12)	C(2B)[d]	-411(5)	176(5)	113(4)	13.(3)
C(15)	284(3)	116(2)	1118(18)	6.1(13)	N(71)	-095(2)	261(2)	0565(14)	6.0(11)	C(3B)[d]	-375(6)	206(5)	076(4)	14.(3)
C(35)	355(3)	130(3)	3091(18)	6.6(14)	O(70)	-189(3)	360(3)	0116(18)	15.3(15)	C(4B)[d]	-305(6)	249(6)	112(4)	13.(3)

(b) Derived Parameters for Atoms Constrained in Rigid Groups

N(10)	145(4)	135(3)	122(1)	4.9	C(17)	343(4)	170(3)	039(3)		C(81)	-118(4)	081(3)	026(2)	
C(11)	067(3)	136(3)	085(2)		C(18)	382(3)	160(4)	-002(3)		C(22)	321(6)	308(5)	030(5)	24.(4)
C(12)	072(3)	125(3)	030(2)		C(19)	412(3)	091(5)	-009(2)		C(23)	277(3)	371(2)	048(2)	12.(2)
C(13)	152(4)	117(3)	034(2)		C(20)	403(4)	032(3)	023(3)		C(24)	317(5)	376(7)	111(2)	20.(3)
C(14)	197(2)	123(3)	091(2)		C(21)	364(3)	042(3)	064(3)		C(25)	293(6)	444(4)	026(4)	14.(2)
N(30)	294(2)	127(3)	210(3)	4.9	C(36)	429(3)	122(5)	356(2)	9.0	C(26)	188(3)	356(5)	041(3)	10.(2)
C(31)	327(3)	121(3)	166(2)		C(37)	481(5)	182(3)	373(3)		C(42)	495(5)	316(4)	343(3)	10.(2)
C(32)	415(3)	114(3)	186(3)		C(38)	550(5)	175(4)	419(3)		C(43)	465(3)	381(3)	303(2)	10.(2)
C(33)	437(2)	116(3)	241(3)		C(39)	567(3)	109(5)	447(2)		C(44)	390(4)	351(5)	260(3)	12.(2)
C(34)	362(4)	124(3)	256(2)		C(40)	514(5)	049(3)	430(3)		C(45)	447(5)	442(3)	337(3)	11.(2)
N(50)	201(4)	149(3)	285(1)	5.6	C(41)	445(5)	055(4)	384(3)		C(46)	536(4)	397(5)	280(3)	18.(3)
C(51)	279(3)	142(3)	322(3)		C(56)	024(3)	197(5)	338(2)	7.2	C(62)	094(6)	379(6)	354(3)	9.(2)
C(52)	277(4)	156(3)	377(2)		C(57)	022(4)	266(3)	362(3)		C(63)	142(3)	432(3)	330(2)	12.(2)
C(53)	198(5)	172(3)	374(2)		C(58)	-020(4)	274(3)	401(3)		C(64)	201(5)	383(4)	309(4)	24.(4)
C(54)	151(2)	167(3)	317(3)		C(59)	-059(3)	214(5)	417(2)		C(65)	091(7)	473(5)	281(3)	19.(3)
N(70)	057(2)	164(2)	196(2)	4.3	C(60)	-056(3)	145(3)	394(3)		C(66)	199(6)	481(5)	373(4)	21.(3)
C(71)	023(3)	175(3)	239(1)		C(61)	-014(4)	137(3)	354(3)		C(82)	-127(7)	349(5)	054(3)	9.(2)
C(72)	-065(3)	184(3)	217(2)		C(76)	-087(2)	148(4)	051(1)	3.7	C(83)	-071(3)	411(3)	083(2)	12.(2)
C(73)	-085(2)	178(3)	163(2)		C(77)	-130(4)	213(2)	033(2)		C(84)	-124(7)	457(5)	110(4)	17.(3)
C(74)	-009(4)	166(3)	149(2)		C(78)	-204(4)	211(3)	-010(2)		C(85)	001(4)	385(6)	130(3)	18.(3)
C(16)	335(3)	112(4)	072(2)	6.8	C(79)	-235(2)	144(4)	-034(1)		C(86)	-047(5)	463(5)	044(3)	17.(3)
					C(80)	-192(4)	079(2)	-016(2)						

(c) Group Parameters[e]

Group	X	Y	Z	ϕ	θ	ρ	B group
Pyrrole-10	1264(13)	1271(8)	0722(8)	1.46(2)	-2.91(3)	-1.71(2)	4.9(6)
Pyrrole-30	3670(12)	1202(8)	2117(9)	1.46(2)	-2.88(3)	1.51(2)	4.9(6)
Pyrrole-50	2213(14)	1572(9)	3348(8)	1.36(2)	-2.90(3)	1.39(2)	5.6(6)
Pyrrole-70	-0161(12)	1733(8)	1928(8)	-1.71(2)	2.91(2)	-1.46(2)	4.3(6)
Phenyl-16	3734(10)	1011(13)	0311(8)	0.15(2)	2.92(3)	-1.13(2)	6.8(7)
Phenyl-36	4977(14)	1154(14)	4014(9)	-0.25(3)	2.95(3)	0.65(2)	9.0(7)
Phenyl-56	-0170(11)	2054(13)	3777(8)	-0.24(2)	-3.13(3)	2.09(2)	7.2(7)
Phenyl-76	-1610(10)	1462(11)	0082(6)	0.08(2)	-3.05(2)	-2.60(1)	3.7(5)
TB-22[f]	2772(18)	3706(18)	0482(11)	-1.38(3)	-3.58(3)	1.55(4)	-[g]
TB-42[f]	4650(17)	3806(16)	3025(11)	1.91(3)	-3.05(2)	2.53(2)	-[g]
TB-62[f]	1424(19)	4322(19)	3305(13)	2.10(4)	2.72(3)	-2.51(4)	-[g]
TB-82[f]	-0708(18)	4106(19)	0830(12)	2.99(4)	-2.51(3)	0.88(3)	-[g]

[a] Fractional coordinates generated by placing 0. prior to the first digit.

[b] Anisotropic thermal parameters for Fe β_{11} = 0.0028(3), β_{22} = 0.0041(4), β_{33} = 0.0013(1), β_{12} = 0.0003(4), β_{13} = 0.0004(2), β_{23} = -0.0007(2); for S 0.010(12), 0.0054(9), 0.0054(6), 0.0010(9), 0.0048(7), 0.0006(6) where the form of the anisotropic thermal ellipsoid is $\exp[\beta_{11}h^2 + \beta_{22}k^2 + \beta_{33}l^2 + 2\beta_{13}hl + 2\beta_{23}kl]$. RMS components of thermal displacement along the principal ellipsoidal axes are for Fe 0.176(14), 0.191(12) and 0.280(12) Å and for S 0.265(24), 0.298(25) and 0.441(21) Å.

[c] Occupancy factor fixed at 1.0 (Occupancy factor Fe, 1.0).

[d] Occupancy factor fixed at 0.75.

[e] Angles in radians.

[f] Atoms C(22) to C(26) in TB22, C(42) to C(46) in TB42, C(62) to C(66) in TB62, and C(82) to C(86) in TB82.

[g] Atoms allowed individual temperature factors.

Table 4.11 : Selected bond distances (in Å) and angles (in °) for $[Fe(TpivPP)(THT)(O_2)]\cdot(THT)_2$.

(a) Bond Distances

Atoms	Distance	Atoms	Distance	Atoms	Distance
Fe-N(10)	2.00[b]	C(35)-C(51)	1.43	C(62)-O(50)	1.39
Fe-N(30)	2.00	C(35)-C(36)	1.45	N(71)-C(77)	1.42
Fe-N(50)	1.99	C(55)-C(54)	1.33	N(71)-C(82)	1.35
Fe-N(70)	2.00	C(55)-C(71)	1.46	C(82)-O(70)	1.29
Fe-O(1)	1.91(5)	C(55)-C(56)	1.53	S(A)-C(1A)	1.72(8)
Fe-S	2.493(17)	C(75)-C(74)	1.44	S(A)-C(4A)	1.68(9)
O(1)-O(2)	0.85(10)	C(75)-C(11)	1.30	C(1A)-C(2A)	1.49(9)
S-C(1)	1.94(6)	C(75)-C(76)	1.56	C(2A)-C(3A)	1.53(8)
S-C(4)	1.78(6)	N(11)-C(17)	1.39	C(3A)-C(4A)	1.56(10)
C(1)-C(2)	1.44(8)	N(11)-C(22)	1.45	S(B)-C(1B)	1.79(9)
C(2)-C(3)	1.36(8)	C(22)-O(10)	1.07	S(B)-C(4B)	1.61(9)
C(3)-C(4)	1.51(7)	N(31)-C(37)	1.37	C(1)-C(2B)	1.64(10)
C(15)-C(14)	1.41	N(31)-C(42)	1.43	C(2)-C(3B)	1.39(10)
C(15)-C(31)	1.36	C(42)-O(30)	1.27	C(3B)-C(4B)	1.49(10)
C(15)-C(16)	1.52	N(51)-C(57)	1.26		
C(35)-C(34)	1.40	N(51)-C(62)	1.36		

(b) Bond Angles

Atoms	Angle	Atoms	Angle	Atoms	Angle
N(10)-Fe-N(30)	91	S-C(1)-C(2)	99	N(10)-C(14)-C(15)	125
N(30)-Fe-N(50)	91	C(1)-C(2)-C(3)	129	N(10)-C(11)-C(75)	126
N(50)-Fe-N(70)	90	C(2)-C(3)-C(4)	106	N(30)-C(34)-C(35)	123
N(70)-Fe-N(10)	88	C(3)-C(4)-S	113	N(30)-C(31)-C(15)	127
N(10)-Fe-N(50)	175	C(14)-C(15)-C(31)	124	N(50)-C(54)-C(55)	124
N(30)-Fe-N(70)	179	C(34)-C(35)-C(51)	124	N(50)-C(51)-C(35)	127
O(1)-Fe-N(10)	92	C(54)-C(55)-C(71)	125	N(70)-C(74)-C(75)	123
O(1)-Fe-N(30)	90	C(74)-C(75)-C(11)	125	N(70)-C(71)-C(55)	125
O(1)-Fe-N(50)	93	C(14)-C(15)-C(16)	119	C(13)-C(14)-C(15)	124
O(1)-Fe-N(70)	90	C(31)-C(15)-C(16)	117	C(12)-C(11)-C(75)	123
S-Fe-N(10)	90	C(34)-C(35)-C(36)	119	C(33)-C(34)-C(35)	127
S-Fe-N(30)	94	C(51)-C(35)-C(36)	117	C(32)-C(31)-C(15)	122
S-Fe-N(50)	85	C(54)-C(55)-C(56)	116	C(53)-C(54)-C(55)	126
S-Fe-N(70)	85	C(71)-C(55)-C(56)	118	C(52)-C(51)-C(35)	122
S-Fe-O(1)	175(1)	C(74)-C(75)-C(76)	112	C(73)-C(74)-C(75)	126
C(1)-S-C(4)	93	C(11)-C(75)-C(76)	122	C(72)-C(71)-C(55)	125

[a] For atoms constrained in rigid groups the following geometries were assumed:- (i) Phenyl group C-C 1.39 Å, C-C-C 120°; (ii) t-Butyl group C-C 1.54 Å, C-C-C 108°; (iii) Pyrrole groups N(10)-C(11) 1.378 Å, C(11)-C(12) 1.441 Å, C(12)-C(13) 1.340 Å, C(11)-N(10)-C(14) 104.9°, N(10)-C(11)-C(12) 110.5°, C(11)-C(12)-C(13) 107.1°.

[b] E.s.d.'s for bonds involving atoms constrained in rigid groups not calculated.

4.3.4 Description and Discussion of the Structure

A quantitative discussion of the stereochemistry is not possible in view of the very low precision but the complex and its crystal packing do have a number of interesting features.

Crystal Packing

The crystal structure consists of well-separated molecules of the neutral complex Fe(TpivPP)(THT)(O_2), Figure 4.21 and 4.22. Solvate molecules of tetrahydrothiophene are stacked approximately down the c-axis; there are two channels per cell (Figure 4.23). The existence of these channels accounts for the facile coordination of dioxygen in the solid state and the almost equally facile loss of solvate molecules. Crystal packing is very loose. Solvate molecule B, which is present in only 0.75 occupancy, has no, non-hydrogen, intermolecular contacts less than 3.75 Å. There is a paucity of intermolecular contacts less than 3.75 Å and the closest contacts involve the pivalamide oxygen atoms (Table 4.12). Thus the high thermal motion affecting many parts of the structure is readily appreciated. The method of preparation of this dioxygen adduct by a solid-gas reaction is not conducive to the formation of high quality crystals.

Stereochemistry of the Complex

End-on bent bond geometry for the FeO_2 group is observed in this sulphur-based complex. Similar geometry has also been established for the nitrogen-based analogue,

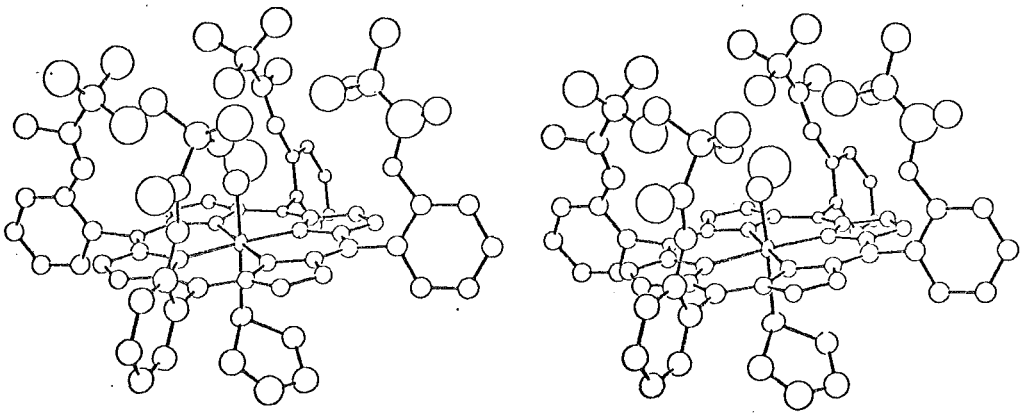

Figure 4.21 : Stereoscopic diagram of Fe(TpivPP)(THT)(O_2). Note the high thermal motion of the "picket" atoms with respect to the porphinato atoms. Thermal ellipsoids are drawn at the 20% probability level.

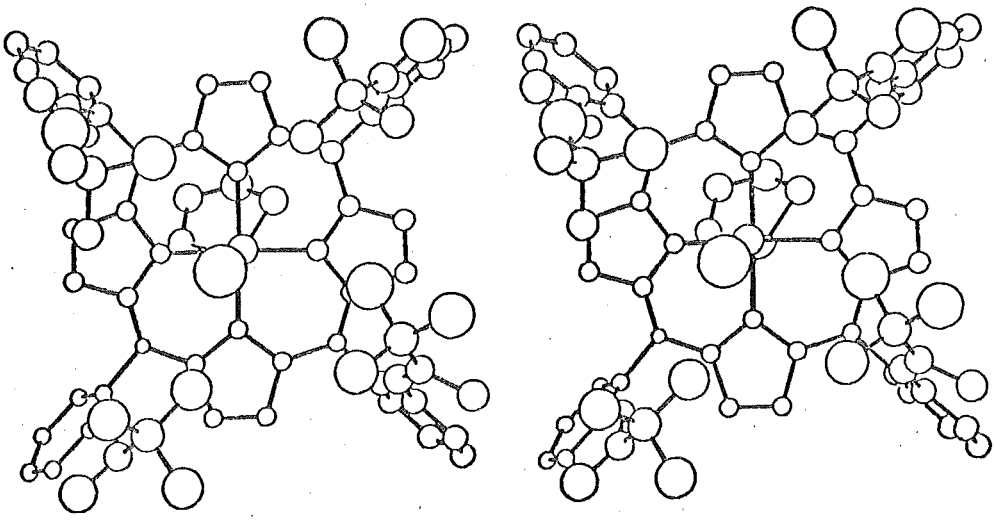

Figure 4.22 : Stereoscopic diagram of Fe(TpivPP)(THT)(O_2) showing the relative orientations of the axial base and dioxygen moieties. Thermal ellipsoids are drawn at the 20% probability level.

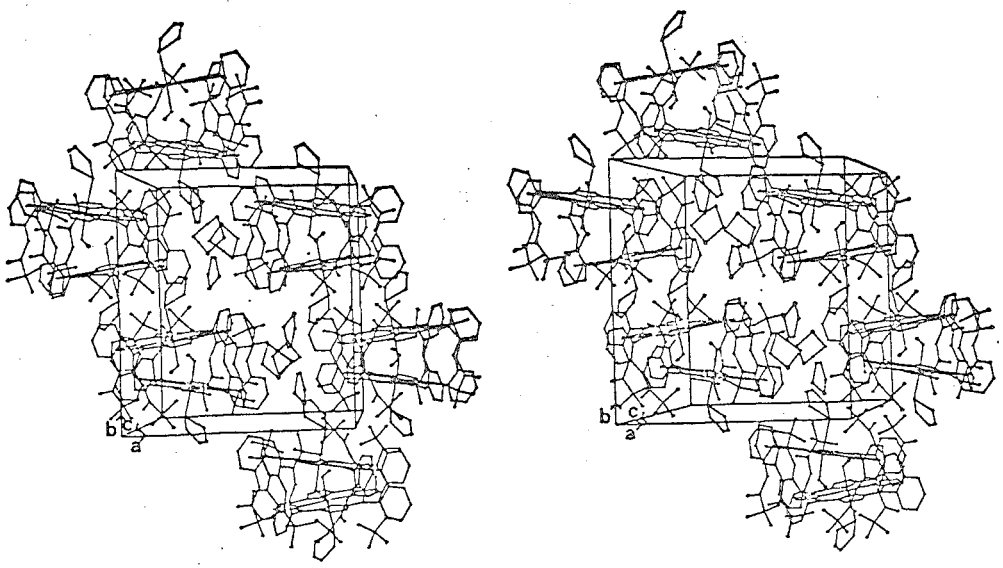

Figure 4.23 : Stereoscopic diagrams of the packing of Fe(TpivPP)(THT)(O_2) and THT solvate molecules with respect to the unit cell. The contents of two unit cells are included in order to show the packing around the solvate molecules.

Table 4.12 : Non-hydrogen intermolecular contacts (<3.75 Å) for $[Fe(TpivPP)(THT)(O_2)]\cdot(THT)_2$.

Atoms	Distance	Atoms	Distance
C(3)...C(79)	3.72	C(13)...C(80)	3.68
C(4)...O(50)	3.66	C(21)...C(80)	3.58
C(4A)...C(38)	3.52	C(40)...C(25)	3.66
C(4A)...C(39)	3.65	C(59)...C(77)	3.75
O(10)...C(52)	3.29	C(81)...C(66)	3.72
O(30)...C(79)	3.54	C(86)...C(86)	3.40
O(50)...C(13)	3.27		
O(50)...C(12)	3.36		
O(50)...C(81)	3.64		
C(12)...C(58)	3.68		

Fe(TpivPP)(1-Me-imid)(O_2), and for the 1:1 dioxygen adducts of cobalt-Schiff base derivatives (Chapter 3). Dioxygen is coordinated on the side of the porphyrin protected by four pivalamide "pickets". Disorder of the kind observed for its 1-methylimidazole analogue is not apparent.

This is in apparent contradiction to the Mossbauer studies of Lang[251] where the temperature dependence of the nuclear quadrupole splitting for Fe(TpivPP)(1-Me-imid)(O_2), Fe(TpivPP)(THT)(O_2) and oxyhaemoglobin is attributed to the different conformations that the Fe-O_2 group may adopt with respect to the axial base; two crystallographically independent conformations are found in the structure of Fe(TpivPP)-(1-Me-imid) but only one for the sulphur-based analogue. However, a single crystal is not necessarily representative of the bulk sample.

As observed in most other end-on, bent-bond metal-dioxygen complexes the Fe–O–O plane approximately bisects the N_{porph}–Fe–N_{porph} right angles.

The sulphur atom of the tetrahydrothiophene axial ligand is coordinated with an Fe-S separation of 2.49(2) Å. In contrast to the Fe-O separation, this separation is considered to be reliable. There are few compounds available for comparison. An iron-anionic sulphur separation of 2.324(2) Å is observed for the cytochrome P450 model compound Fe(proto-IX-DME)($SC_6H_4NO_2$)[311]. The dimeric compound [Co (Ssalen)]$_2$ has a Co-S_{ax} separation of 2.444(1) Å [203]. Thus, regardless of the lack of precision of this analysis, it is unfortunately not possible to find any indication of a greater or lesser trans effect than that observed for

Fe(TpivPP)(1-Me-imid)(O_2).

The dihedral angle between normals to the least-squares planes of axial ligand and the porphinato skeleton is 44.0°. The Fe-S vector is canted 5.9° to the normal to the porphinato skeleton. As a result unduly close C(1)... N_{porph}, C(4)...N_{porph} contacts are avoided; such contacts are in the range 3.38 Å to 3.46 Å.

The iron atom is displaced 0.05 Å from the mean plane of the porphinato nitrogen atoms and 0.04 Å from the plane of the 24-atom porphinato core. The displacements are slightly larger than those observed for Fe(TpivPP)(1-Me-imid)(O_2) (0.030 and 0.015 Å). The differences, although probably not significant, are in line with expectations based on substituting the nitrogen-containing, imidazole base by the weaker, sulphur-base molecule tetrahydrothiophene. The different stereochemistry for the metal-dioxygen moiety, which could conceivably result from axial ligation of sulphur rather than nitrogen, has been discussed in §4.2.5.

There is no apparent systematic symmetrical orientation of the pyrrole groups with respect to each other. Figure 4.24 illustrates the displacements of atoms from the least-squares plane for the porphinato core. The Fe-N_{porph} separations which range between 1.99 Å and 2.00 Å are typical of essentially diamagnetic ferrous compounds such as Fe(TpivPP)(1-Me-imid)(O_2) (§4.2), Fe(TPP)(1-Me-imid)$_2$ [237] and Fe(TPP)(pip)$_2$ [283]. The phenyl groups, Phenyl-16 to Phenyl-76, are tilted by 106.3°, 97.7°, 80.6° and 73.4°, respectively, to the porphinato plane.

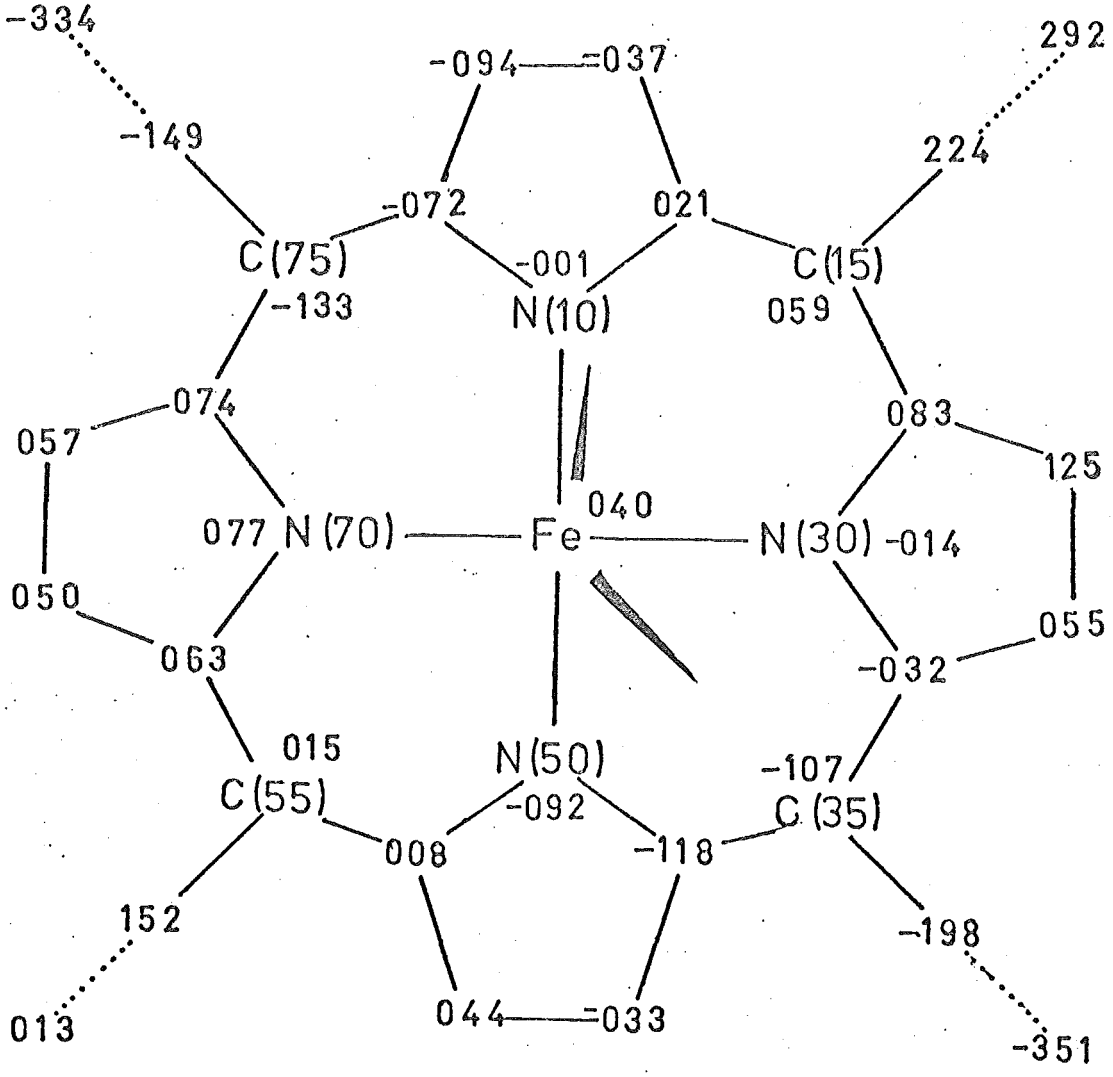

Figure 4.24 : Deviations of atoms from the least-squares plane of the 24-atom porphinato core for Fe(TpivPP)(THT)(O_2). The orientation of the axial base is indicated. The "pickets" are directed upwards out of the page. Distances in $\mathring{A} \times 10^3$.

Concluding Remarks

Thiolate axial ligation to the iron(III) and ferrous carbonyl derivatives of cytochrome P450 is well-established through model studies. The axial ligation for the oxygenated stage is not so well-established although thiol ligation has been inferred[326]. If this is correct then the structure just described is a possible model for this stage.

It is found that dioxygen also coordinates to iron in an end-on bent bond manner for this sulphur-based compound. But, unfortunately, more detailed comparison of the stereochemistries of the sulphur-base and nitrogen-base iron-dioxygen complexes is not possible. The very low precision that was obtained for the structure of Fe(TpivPP)-(THT)(O_2), and also the low precision that was obtained for Fe(TpivPP)(1-Me-imid)(O_2), together with the lack of thiol and thioether metalloporphyrin derivatives preclude this. Such comparison could be very illuminating in understanding the different functions of the monooxygenase cytochrome P450 systems and the oxygen-carrier haemoglobin systems.

4.4 The Crystal and Molecular Structure of Catena-{μ-[meso-tetra(α,α,α,α-orthopivalamidephenyl)-porphinato-N,N',N'',N''' :O]-aquoiron(II)·tetrahydrothiophene}, Polymeric-[Fe(TpivPP)(OH_2)]·THT.

This complex arose from repeated efforts by Collman and coworkers to prepare, hopefully, better quality crystals of [Fe(TpivPP)(THT)]·$(THT)_2$ for a more precise structure analysis of [Fe(TpivPP)(THT)(O_2)]·$(THT)_2$. The curious

polymeric linking of Fe(TpivPP) units through a pivalamide oxygen atom, which has been revealed by the single crystal X-ray diffraction structure analysis, was quite unexpected.

Determination of the structure of this compound (§4.4.1, §4.4.2) was relatively routine compared to the structure analyses reported in §3.2 and §4.2 and §4.3. However, with its novel nature, the compound is not easily pigeon-holed, (§4.4.3).

Five-coordinate complexes such as Fe(TPP)(2-Me-imid)[190] and deoxy-Hb[152] are high-spin (S=5/2). Their six-coordinate derivatives, which have as the sixth ligand a second aromatic amine or a diatomic molecule such as dioxygen or carbon monoxide, are essentially diamagnetic (S=0)[12,191, 253,330]. The four-coordinate complex, $Fe^{II}(TPP)$, is intermediate spin (S=1)[284]. Five-coordinate porphinatoiron(III) complexes, such as $Fe^{III}-O^{2-}-Fe^{III}$, are not applicable because of interaction between the iron centres via the μ-oxo bridge[254,285]. However, six-coordinate porphinatoiron(III) derivatives are found as both high-(S=5/2) and low-spin (S=½) complexes. Aquo-methaemoglobin is high-spin, cyanomethaemoglobin is low-spin[152]. The complex shown by this structure analysis to be polymeric-$[Fe(TpivPP)(OH_2)]\cdot THT$ is unlike any other six-coordinate iron(II) complex, or, for that matter, five-coordinate iron(II) complex, with its semi-coordinated water molecule and weak, amide oxygen, fifth ligand. Because it is high-spin, it is not unrelated to the high-spin iron(III) complexes which have a weak sixth ligand such as water or fluoride.

4.4.1 Collection and Reduction of Intensity Data

Dark purple-black crystals of the compound shown by this analysis to be polymeric-$[Fe(TpivPP)(OH_2)]\cdot(THT)$ were prepared at Stanford University. Magnetic susceptibility measurements on a powdered sample (μ=4.9BM), the ability of the dissolved species to coordinate carbon monoxide and the ability of the solid complex to coordinate carbon monoxide (30% uptake per iron atom over three days) characterise the complex as a high-spin (S=2) ferrous derivative[331]. The presence of H_2O or OH^- was confirmed, subsequent to structure analysis, by microanalysis[331].

Symmetry and systematic absences[207] uniquely consistent with the orthorhombic space group $P2_12_12_1$ were established by precession photography using Cu Kα radiation. Most crystals, despite nearly perfect cuboid habit, were twinned. The cuboid crystal eventually selected for data collection had dimensions 0.25 x 0.25 x 0.15 mm^3. Diffraction was weak despite its size. The crystal was randomly oriented with respect to the diffractometer ϕ-axis. Crystal mosaicities ranged from 0.19° to 0.35°. Peak profiles of reflections such as 020, 121, 414 had pronounced shoulders. Crystal orientation and unit cell dimensions were obtained at 23°C by standard procedures (Appendix 1) using Mo Kα radiation. The dimensions so obtained were

$$a = 15.448(4),\ b = 26.415(6),\ c = 14.960(4)\ \text{Å}.$$

The calculated density for four formula units of $Fe\ C_{64}N_8O_4H_{64}\cdot OH_2\cdot S\ C_4H_8$ in the cell was 1.27; the measured density was 1.25(1) gm cm^{-3}. The linear absorption coefficient μ

was 3.48 cm^{-1}, and no absorption correction was applied since the maximum likely error due to neglect of absorption was less than 3%. Excluding systematic absences, 3676 reflections in the range $0<2\theta\leqslant41^{o}$ were collected using Mo Kα radiation. A symmetric scan range of 1.40^{o} in 2θ centred on the calculated peak position comprised 70 steps each of 4 second duration. Stationary crystal, stationary counter background counts at each end of the scan were recorded for 70 seconds. Three standard reflections, monitored every 50 reflections, each suffered a decrease of ∿8% in intensity. The data were processed by the standard method (Appendix 1).

4.4.2 Solution and Refinement of the Structure

Analysis of the three dimensional Patterson synthesis readily yielded the position of the iron atom in the asymmetric unit. The iron atom was assigned an isotropic temperature factor of 4.0Å^{2}, and its position together with an overall scale factor were refined so that

$$R = 0.44 \text{ and } R_{w} = 0.51$$

for 1522 reflections having $I>3\sigma_{I}$. In view of the heavy atom ratio

$$\frac{Z^{2}}{\sum_{i} z_{i}^{2}} = 0.19$$

the ability of the iron atom alone to phase the reflection data was doubtful. Consequently, and in order to gain experience, the direct methods program MULTAN was used to provide sets of phases for the structure factors.

The E-maps thus generated were not interpretable. Accordingly, a weighted F(obs) Fourier synthesis was calculated with phases derived from the original, single iron atom model. The orientation of the meso-tetraphenyl-porphinato skeleton was deduced.

The four phenyl groups were assumed to be orthogonal to the four pyrrole groups; a model comprising these eight rings as rigid groups each with a single isotropic temperature factor, and an iron atom was refined so that

$$R = 0.35 \text{ and } R_w = 0.44.$$

Two phenyl groups failed to refine sensibly; the assumption of orthogonality being invalid.

Successive cycles of Fourier syntheses and least-squares refinement established positions in the asymmetric unit for the remaining non-hydrogen atoms of the Fe(TpivPP) unit. Fourier syntheses in the region of the pivalamide "pickets" were examined very closely for evidence for disorder; none was found. The t-butyl groups of the pivalamide "pickets" were refined as rigid groups with each group having a single isotropic temperature factor. The agreements factors were reduced to

$$R = 0.179 \text{ and } R_w = 0.218.$$

At this stage a difference Fourier synthesis revealed five atom positions for the tetrahydrothiophene solvate molecule. The peak height of the sulphur atom, compared with those for the carbon atoms, was considerably lower than expected. The possibility that the molecule suffered five-fold disorder was examined and discounted on the following grounds:-

1. The integrated electron density of the highest peak was very much larger than those for the other peaks. The considerably elongated thermal ellipsoid was oriented with its major axis perpendicular to the approximate plane of the solvate species.

2. Peak separations in the difference Fourier synthesis corresponded to an ordered model; these were maintained in subsequent refinements.

Refinement of an occupancy factor, with atoms assigned a temperature factor B=8.0 $\AA^2$, did not indicate partial occupancy of the solvate sites by THT. Inclusion of the THT in the structure model led, on refinement, to R = 0.13.

At this stage a difference Fourier synthesis once again indicated electron density at approximately 2.9 $\AA$ from the iron atom. This was included in the model as an oxygen atom. Atoms of the t-butyl groups were allowed individual isotropic temperature factors and the model was refined so that

$$R = 0.120 \text{ and } R_w = 0.135.$$

Group constraints on pyrrole and t-butyl groups were now progressively relaxed, hydrogen atoms were included on the phenyl rings (r(C-H)=1.0 $\AA$) and selected atoms allowed anisotropic models for their thermal motion. Reflections having $I>\sigma_I$ were used in the refinement. For the final four cycles of least-squares refinement the 480 variable parameters, which now defined the model, were compounded from four blocks into two blocks, with each block having 354 variable parameters.

The off-diagonal components of the full least-squares matrix, which are of greater significance for refinement with limited data, are of course better catered for in larger matrices. The relative contents of each block were shuffled between cycles. The thermal ellipsoid parameters of two atoms N(31) and C(84) became non-positive definite on the first cycle. The appropriate β_{ii} terms were adjusted by less than one e.s.d. so that the atoms had physically meaningful thermal ellipsoid parameters, which parameters were held constant for the subsequent three cycles. Refinement converged at

$$R = 0.116 \text{ and } R_w = 0.104.$$

For 2576 reflections having $I>\sigma_I$ the standard error in an observation of unit weight was 1.461. For the portion of data having $I>3\sigma_I$ the agreement factors were

$$R = 0.074 \text{ and } R_w = 0.087.$$

A structure factor calculation in the enantiomorphic space group gave poorer agreement indices R and R_w; the original enantiomorph was taken as correct. The scale factor was 0.6742(27).

In the final two cycles the ratios of the change in a parameter to its e.s.d. were all less than 0.75. A difference Fourier map, calculated prior to the final four cycles, was featureless; the highest peak height was 0.39 $\bar{e}\,\text{Å}^{-3}$ compared to 1.35 $\bar{e}\,\text{Å}^{-3}$ for the last located non-hydrogen atom. There was little evidence for secondary extinction among strong, low angle reflections. Since the averaged values of the minimised function were generally

independent of $|F_o|$ and $\sin\theta/\lambda$ then weighting scheme (p=0.074) was judged satisfactory. However, the value of the function for low angle data, $\sin\theta/\lambda$ <0.176 Å^{-1} (the data most affected by the non-inclusion of 58 hydrogen atoms in the model), is rather higher than for the rest of the data.

A table of $|F_o|$ and $|F_c|$ for all data is contained in Appendix 1. The agreement factors for all data are

$$R = 0.194 \text{ and } R_w = 0.107$$

and the standard error in an observation of unit weight is 1.342. There are no apparent systematic discrepancies between $|F_o|$ and $|F_c|$ for data not used in refinement. For all data, 78 reflections, including a number of low angle ones, lie outside the range

$$I - 3\sigma_I < I_c < I + 3\sigma_I.$$

Final atomic parameters and RMS amplitudes of thermal displacement are quoted in Tables 4.13 and 4.14.

4.4.3 Description and Discussion of the Structure

General Description of Structure

The crystal structure consists of infinite chains of Fe(TpivPP) units; a pivalamide oxygen atom of one unit is coordinated to the iron atom of another at a separation of 2.22(1) Å. There are two chains per unit cell. Solvate molecules of tetrahydrothiophene occupy interstices in the crystal lattice. Nestled among the pivalamide "pickets" is a water molecule 2.90(2) Å from the iron atom.

The coordination geometry about the iron centre is approximately square-pyramidal; the iron atom is displaced

Table 4.13 : Final atomic parameters for polymeric $[Fe(TpivPP)(OH_2)]\cdot THT$.

(a) Individually Refined Atoms[a]

Atom	X	Y	Z	β_{11}	β_{22}	β_{33}	β_{12}	β_{13}	β_{23}
Fe	03337(18)	-2077(10)	13497(19)	00536(16)	00138(4)	00639(18)	00093(9)	00283(17)	00107(9)
O(1)	1616(14)	-2332(8)	2689(13)	0148(16)	0044(6)	0118(15)	-0000(8)	-0038(14)	-0006(7)
N(10)	-0495(8)	-2112(5)	2417(9)	0027(7)	0009(2)	0052(8)	0002(4)	0004(7)	0003(4)
N(30)	0228(8)	-2855(5)	1220(8)	0027(6)	0013(2)	0034(7)	-0002(4)	0016(7)	0002(4)
N(50)	1425(9)	-2101(6)	0534(8)	0047(8)	0013(3)	0030(8)	0002(5)	0009(7)	0009(5)
N(70)	0684(9)	-1352(5)	1737(9)	0027(7)	0014(3)	0037(8)	-0002(4)	0005(7)	-0001(4)
N(11)	-0133(10)	-3697(6)	3518(12)	0048(9)	0018(3)	0070(11)	-0016(5)	0007(9)	0001(5)
O(10)	0257(11)	-4509(6)	3428(18)	0084(10)	0021(3)	0313(26)	-0008(5)	0002(17)	-0019(8)
C(22)	0493(22)	-4068(10)	3549(17)	0150(28)	0013(5)	0087(17)	0019(10)	0029(20)	0006(9)
C(23)	1426(12)	-3934(10)	3660(18)	0008(10)	0041(7)	0086(18)	0011(7)	-0007(12)	0019(10)
C(24)	1648(15)	-3869(10)	4631(16)	0062(14)	0044(7)	0081(17)	0001(8)	0012(13)	0016(9)
C(25)	1608(17)	-3401(10)	3245(22)	0068(16)	0035(7)	0191(30)	0026(9)	0029(18)	-0010(12)
C(26)	1982(18)	-4352(12)	3253(22)	0095(20)	0059(10)	0177(31)	-0040(12)	-0030(20)	0072(15)
N(31)[b]	3065(8)	-3394(6)	0259(11)	0003	0021	0074	0003	0002	0007
O(30)	4310(8)	-3190(5)	-0420(9)	0041(7)	0018(3)	0046(8)	-0000(4)	0008(7)	-0001(4)
C(42)	3852(13)	-3226(7)	0262(15)	0039(12)	0010(4)	0069(16)	-0008(5)	0039(12)	-0007(6)
C(43)	4242(12)	-3033(9)	1156(12)	0030(10)	0037(6)	0024(11)	0000(7)	0013(9)	0013(7)
C(44)	4432(17)	-2460(8)	1062(14)	0133(20)	0013(4)	0077(16)	0018(8)	0023(15)	-0002(7)
C(45)	5127(12)	-3320(9)	1293(15)	0028(11)	0044(6)	0069(14)	-0011(7)	0002(12)	0002(8)
C(46)	3638(15)	-3173(9)	1929(13)	0072(14)	0034(6)	0030(12)	0000(8)	0013(11)	0002(6)
N(51)	3232(12)	-0927(8)	1737(13)	0062(13)	0040(5)	0056(13)	0022(6)	-0039(10)	-0005(7)
O(50)	4492(19)	-0848(11)	2211(16)	0148(21)	0094(10)	0112(17)	0013(13)	-0004(17)	-0048(10)
C(62)	3714(19)	-0955(12)	2369(21)	0070(18)	0055(9)	0094(23)	0048(11)	0052(17)	0028(13)
C(63)	3605(17)	1199(8)	3276(14)	0120(19)	0024(5)	0049(14)	0006(8)	0013(14)	-0021(7)
C(64)	3288(23)	1756(10)	3076(18)	0190(28)	0029(6)	0082(20)	0003(12)	0038(20)	-0016(9)
C(65)	2879(16)	-0911(11)	3752(19)	0073(16)	0048(8)	0087(19)	-0035(9)	0012(16)	-0001(10)
C(66)	4439(13)	-1239(11)	3889(20)	0019(12)	0062(9)	0135(25)	0006(8)	-0024(14)	0002(12)
N(71)	0061(10)	-1412(6)	4729(10)	0070(11)	0018(3)	0025(8)	0001(5)	0000(8)	-0015(4)
O(70)	-0058(13)	-1507(7)	6240(11)	0181(18)	0040(4)	0072(11)	-0036(7)	0054(13)	-0014(6)
C(82)	0231(15)	-1687(9)	5508(14)	0064(14)	0034(5)	0046(12)	0025(8)	0039(12)	0018(7)
C(83)	0715(13)	-2185(7)	5465(13)	0060(12)	0008(4)	0057(14)	-0008(6)	0010(12)	0007(6)
C(84)[b]	0819(16)	-2379(8)	6402(11)	0122	0028	0007	0004	-0001	-0008
C(85)	1555(16)	-2084(11)	4979(15)	0080(15)	0044(7)	0065(15)	-0012(10)	0044(13)	-0010(10)
C(86)	0106(14)	-2540(7)	4885(13)	0095(16)	0014(4)	0060(13)	-0002(6)	-0047(12)	0004(6)
S	3704(12)	-4773(8)	132(3)	0168(14)	0085(6)	102(8)	0002(8)	011(4)	0051(20)
C(1)	455(4)	-4718(15)	034(3)	022(5)	0041(9)	010(3)	0006(19)	002(3)	0038(12)
C(2)	523(2)	-4677(17)	065(4)	009(3)	0049(10)	019(5)	0050(14)	000(3)	-0007(17)
C(3)	532(3)	-4773(13)	166(3)	015(4)	0037(7)	014(3)	-0027(14)	008(3)	-0020(12)
C(4)	463(3)	-4699(18)	210(3)	009(3)	0083(15)	016(3)	-0021(18)	-000(3)	-0035(18)

Atom	X	Y	Z	B	Atom	X	Y	Z	B
C(15)	-0925(9)	-3007(6)	2330(10)	2.1(3)	C(33)	0336(12)	-3663(6)	0694(11)	4.0(4)
C(35)	1363(10)	-2994(6)	0071(11)	2.8(4)	C(34)	0658(11)	-3155(6)	0641(11)	3.1(4)
C(55)	1902(11)	-1222(6)	0662(12)	3.4(4)	C(51)	1686(11)	-2512(7)	0048(12)	3.0(4)
C(75)	-0379(12)	-1217(6)	2959(11)	3.2(4)	C(52)	2439(12)	-2377(7)	-0545(13)	4.4(5)
C(11)	-0750(11)	-1703(7)	2943(11)	3.1(4)	C(53)	2566(11)	-1869(7)	-0351(11)	3.3(4)
C(12)	-1443(11)	-1853(6)	3494(12)	3.8(4)	C(54)	1943(12)	-1695(7)	0311(12)	3.7(4)
C(13)	-1635(12)	-2364(7)	3370(12)	4.0(4)	C(71)	1314(12)	-1052(7)	1321(14)	4.4(4)
C(14)	-1013(10)	-2514(7)	2680(11)	2.7(4)	C(72)	1300(12)	-0544(7)	1702(13)	4.7(5)
C(31)	-0349(11)	-3159(6)	1644(10)	2.7(3)	C(73)	0680(12)	-0542(7)	2357(12)	4.4(4)
C(32)	-0278(11)	-3676(6)	1355(12)	3.9(4)	C(74)	0269(12)	-1055(5)	2387(11)	3.2(4)

(b) Derived Parameters for Atoms Constrained in Rigid Groups

C(16)	-144(1)	-3415(6)	278(1)	3.1(4)	C(56)	255(1)	-0841(6)	035(1)	3.8(4)
C(17)	-233(1)	-3456(5)	261(1)	4.2(4)	C(57)	249(1)	-0647(8)	-051(1)	4.6(5)
C(18)	-2803(8)	-3846(7)	300(1)	5.6(5)	C(58)	312(1)	-0314(7)	-082(1)	5.5(5)
C(19)	-240(1)	-4194(6)	355(1)	4.7(5)	C(59)	380(1)	-0176(6)	-027(1)	4.5(4)
C(20)	-151(1)	-4153(5)	372(1)	4.8(5)	C(60)	386(1)	-0370(8)	059(1)	5.3(5)
C(21)	-1037(8)	-3763(7)	333(1)	2.9(4)	C(61)	323(1)	-0702(7)	090(1)	5.1(5)
H(17)[c]	-261(2)	-3219(7)	223(1)	6.0	H(57)	202(1)	-074(1)	-089(2)	6.0
H(18)	-3407(8)	-387(1)	288(2)	7.0	H(58)	308(2)	-081(1)	-141(1)	7.0
H(19)	-272(2)	-4461(9)	382(2)	6.0	H(59)	423(1)	0051(8)	-049(2)	6.0
H(20)	-123(2)	-4390(7)	410(1)	6.0	H(60)	433(1)	-028(1)	097(2)	6.0
C(36)	171(1)	-3387(7)	-056(1)	4.0(4)	C(76)	-062(2)	-0851(7)	368(1)	3.1(4)
C(37)	1201(9)	-3563(8)	-126(1)	5.5(5)	C(77)	-105(1)	-0401(6)	3470(9)	4.3(4)
C(38)	155(1)	-3888(6)	-190(1)	4.7(5)	C(78)	-130(1)	-0072(6)	415(1)	5.0(5)
C(39)	241(1)	-4036(7)	-184(1)	6.7(6)	C(79)	-112(2)	-0193(7)	504(1)	4.9(5)
C(40)	2927(9)	-3859(8)	-114(1)	4.6(5)	C(80)	-070(1)	-0643(6)	5245(8)	4.3(4)
C(41)	258(1)	-3535(6)	-050(1)	3.7(4)	C(81)	-045(1)	-0972(6)	457(1)	4.1(4)
H(37)	061(1)	-346(1)	-130(2)	7.0	H(77)	-117(1)	-0318(9)	286(1)	6.0
H(38)	120(2)	-4008(9)	-238(1)	6.0	H(78)	-159(2)	0235(8)	401(2)	6.0
H(39)	265(2)	-426(1)	-228(1)	7.0	H(79)	-129(3)	003(1)	550(1)	6.0
H(40)	352(1)	-396(1)	-110(2)	6.0	H(80)	-058(2)	-0726(9)	5851(9)	6.0

(c) Rigid Group Parameters

Group	X	Y	Z	θ	σ	ρ
Phenyl-16	-1920(5)	-3805(3)	3165(5)	1.956(8)	2.674(7)	0.486(7)
Phenyl-36	2064(6)	-3711(3)	-1202(6)	1.536(8)	2.652(7)	-0.891(8)
Phenyl-56	3175(6)	-0508(3)	0040(6)	0.836(8)	-2.799(7)	1.197(8)
Phenyl-76	-0872(4)	-0522(3)	4357(6)	2.590(10)	2.395(6)	1.661(10)

[a] Anisotropic thermal parameters generated by placing 0. prior to first digit, similarly positional parameters.

[b] Thermal parameters not refined. See text.

[c] Hydrogen atom H(17) attached to carbon atom C(17) etc.

[d] Angles in radians.

Table 4.14 : RMS components of thermal displacement along the principal ellipsoid axes for polymeric- $[Fe(TpivPP)(OH_2)]\cdot THT$. (Å) .

Atom	RMS1	RMS2	RMS3	Atom	RMS1	RMS2	RMS3
Fe	0.188(5)	0.190(4)	0.338(5)	N(51)	0.14(4)	0.30(3)	0.42(3)
O(1)	0.32(3)	0.40(3)	0.45(2)	O(50)	0.30(3)	0.42(3)	0.61(3)
N(10)	0.17(3)	0.19(3)	0.25(2)	C(62)	0.13(6)	0.28(4)	0.54(4)
N(30)	0.12(4)	0.22(2)	0.23(2)	C(63)	0.15(5)	0.34(3)	0.39(3)
N(50)	0.14(3)	0.22(3)	0.26(2)	C(64)	0.24(4)	0.35(4)	0.49(4)
N(70)	0.17(3)	0.21(2)	0.23(2)	C(65)	0.21(4)	0.32(3)	0.46(3)
N(11)	0.16(3)	0.28(2)	0.31(2)	C(66)	0.13(5)	0.40(4)	0.47(3)
O(10)	0.25(2)	0.33(2)	0.60(3)	N(71)	0.10(4)	0.28(2)	0.29(2)
C(22)	0.19(4)	0.30(3)	0.45(4)	O(70)	0.24(3)	0.31(2)	0.54(3)
C(23)	0.06(10)	0.28(3)	0.41(3)	C(82)	0.13(5)	0.23(3)	0.42(3)
C(24)	0.25(3)	0.30(3)	0.41(3)	C(83)	0.14(5)	0.26(3)	0.29(3)
C(25)	0.19(4)	0.40(3)	0.47(4)	C(84)[a]	0.07	0.32	0.39
C(26)	0.20(5)	0.33(4)	0.61(4)	C(85)	0.18(4)	0.34(3)	0.42(3)
N(31)[a]	0.06	0.26	0.31	C(86)	0.18(4)	0.22(3)	0.39(3)
O(30)	0.20(2)	0.244(19)	0.257(18)	S	0.432(19)	0.540(20)	1.09(4)
C(42)	0.11(6)	0.18(4)	0.34(3)	C(1)	0.23(4)	0.45(5)	0.52(6)
C(43)	0.11(5)	0.21(3)	0.37(3)	C(2)	0.18(6)	0.47(6)	0.50(5)
C(44)	0.18(4)	0.29(3)	0.42(3)	C(3)	0.27(5)	0.32(4)	0.54(5)
C(45)	0.17(4)	0.28(3)	0.40(3)	C(4)	0.30(5)	0.39(5)	0.58(5)
C(46)	0.17(4)	0.30(3)	0.35(3)				

[a] Thermal parameters not refined. See text.

0.28 Å from the plane of the porphinato nitrogen atoms. The direction of displacement is away from the semi-coordinated water molecule towards the coordinated pivalamide oxygen atom. The average Fe-N_{porph} separation is 2.069(15) Å. The stereochemistry will be analysed more closely below.

Figure 4.25 is a stereodiagram of two linked units. The crystal packing is illustrated in Figure 4.26. Bond distances and angles together with the average value for a given class of bond distance or angle are contained in Tables 4.15 and 4.16 respectively.

Inspection of Tables 4.15 and 4.16 shows that the structure is, in the main, internally consistent since the standard deviation which is calculated for the dispersal of bond lengths and angles of a given chemical class about their mean is similar for most classes to the e.s.d. of an individual bond length or angle. A notable exception is found in the separations between the pivalamide nitrogen and pivalamide carbon atoms; in view of the high but similarly oriented, thermal motion of the atoms involved in this class of bond, simple ascription of the spread of these bond lengths to thermal motion and/or disorder is not sustainable.

The thermal ellipsoids are reassuringly not oriented in an abnormal manner (Figure 4.25).

Packing of the Fe(TpivPP) Units

The crystal packing has several notable features. Firstly, despite the awkward shape of the Fe(TpivPP) unit there are few non-bonded contacts less than 3.45 Å between the units or with the solvate molecules; all of these

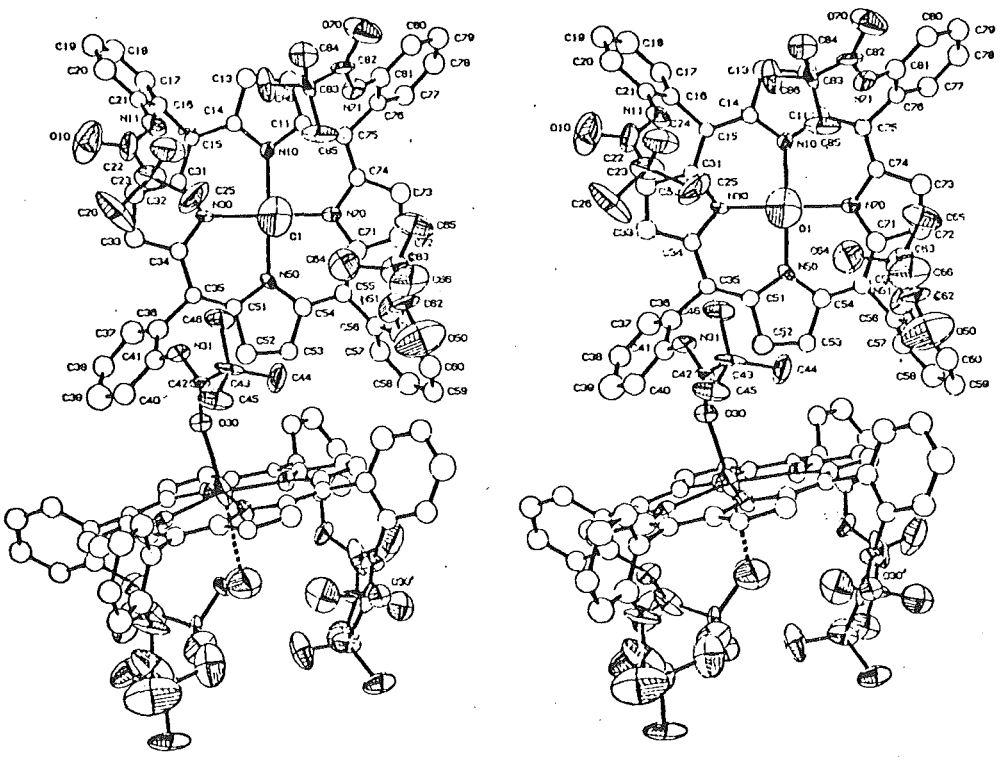

Figure 4.25 : Stereoscopic diagram of two linked Fe(TpivPP)(OH_2) units. The atom labelling system is illustrated. Thermal ellipsoids are drawn at the 40% probability level.

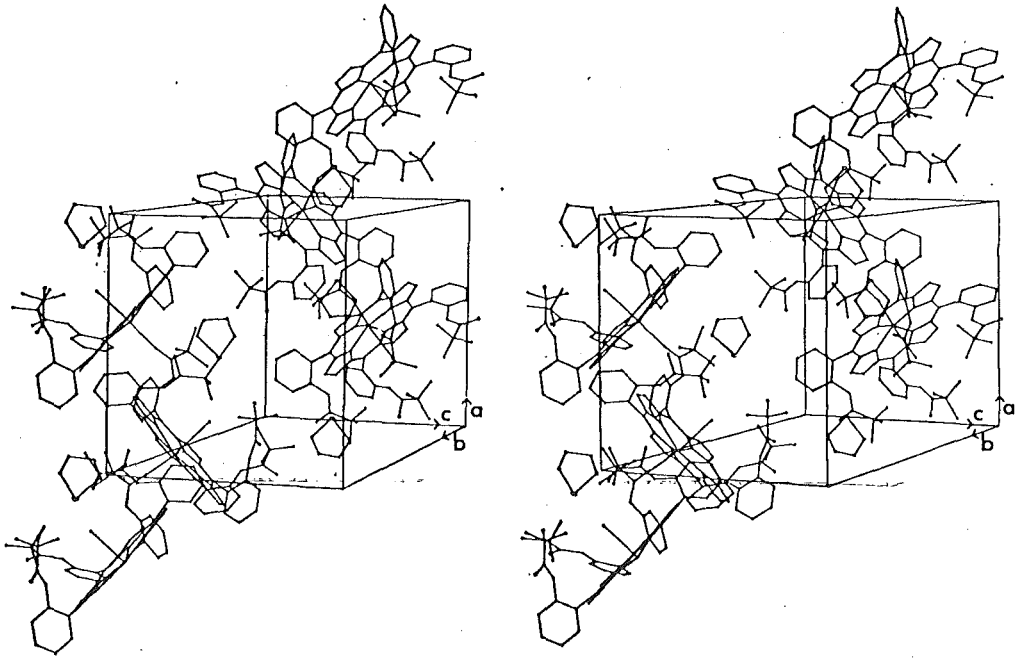

Figure 4.26 : Stereoscopic diagram of the packing of Fe(TpivPP)(OH_2) units and THT solvate molecules with respect to the unit cell. An extra two units are included to illustrate the polymeric nature.

Table 4.15 : Bond distances (in Å) for polymeric-$[Fe(TpivPP)(OH_2)]\cdot THT$.

Atoms	Distance	Average	Atoms	Distance	Average	Atoms	Distance	Average
Fe-N(10)	2.048(13)	*	C(15)-C(14)	1.412(21)	*	C(22)-C(23)	1.49(3)	*
Fe-N(30)	2.071(13)	*	C(15)-C(31)	1.416(20)	*	C(23)-C(24)	1.50(3)	*
Fe-N(50)	2.083(13)	*	C(35)-C(34)	1.448(21)	*	C(23)-C(25)	1.56(3)	*
Fe-N(70)	2.074(14)	2.069(15)	C(35)-C(51)	1.368(22)	*	C(23)-C(26)	1.53(3)	*
Fe-O(1)	2.897(19)		C(55)-C(54)	1.357(22)	*	C(42)-C(43)	1.55(3)	*
Fe-O(30)'	2.221(14)		C(55)-C(71)	1.413(23)	*	C(43)-C(44)	1.55(3)	*
N(10)-C(11)	1.395(19)	*	C(75)-C(74)	1.385(21)	*	C(43)-C(45)	1.58(3)	*
N(10)-C(14)	1.386(19)	*	C(75)-C(11)	1.404(20)	1.400(20)	C(43)-C(46)	1.53(3)	*
N(30)-C(31)	1.357(18)	*	C(15)-C(16)	1.499	*	C(62)-C(63)	1.51(4)	*
N(30)-C(34)	1.348(18)	*	C(35)-C(36)	1.508	*	C(63)-C(64)	1.58(3)	*
N(50)-C(51)	1.368(21)	*	C(55)-C(56)	1.487	*	C(63)-C(65)	1.53(3)	*
N(50)-C(54)	1.378(21)	*	C(75)-C(76)	1.495	1.497(9)	C(63)-C(66)	1.58(3)	*
N(70)-C(71)	1.400(21)	*	N(11)-C(21)	1.433	*	C(82)-C(83)	1.51(3)	*
N(70)-C(74)	1.402(19)	1.380(21)	N(31)-C(41)	1.416	*	C(83)-C(84)	1.50(2)	*
C(11)-C(12)	1.408(22)	*	N(51)-C(61)	1.381	*	C(83)-C(85)	1.51(3)	*
C(13)-C(14)	1.464(22)	*	N(71)-C(81)	1.424	1.414(23)	C(83)-C(86)	1.59(2)	1.54(3)
C(31)-C(32)	1.437(19)	*	N(11)-C(22)	1.38(3)	*	S-C(1)	1.97(5)	
C(33)-C(34)	1.432(21)	*	N(31)-C(42)	1.29(2)	*	S-C(4)	1.85(5)	
C(51)-C(52)	1.505(23)	*	N(51)-C(62)	1.21(3)	*	C(1)-C(2)	1.15(5)	
C(53)-C(54)	1.456(22)	*	N(71)-C(82)	1.40(3)	1.32(9)	C(2)-C(3)	1.53(5)	
C(71)-C(72)	1.459(23)	*	C(22)-O(10)	1.234(24)	*	C(3)-C(4)	1.27(4)	
C(73)-C(74)	1.499(22)	1.458(33)	C(42)-O(30)	1.245(19)	*			
C(12)-C(13)	1.394(20)	*	C(62)-O(50)	1.257(29)	*			
C(32)-C(33)	1.372(22)	*	C(82)-O(70)	1.275(22)	1.253(18)			
C(52)-C(53)	1.388(21)	*						
C(72)-C(73)	1.371(23)	1.381(12)						

[a] E.s.d.'s for bonds involving atoms constrained in rigid groups not calculated.

Table 4.16: Bond angles (in °) for polymeric-[Fe(TpivPP)(OH_2)]·THT

Atoms	Angle	Average	Atoms	Angle	Average	Atoms	Angle	Average
N(10)-Fe-N(30)	88.8(5)	*	C(32)-C(33)-C(34)	107.7(15)	*	N(51)-C(62)-O(50)	115(3)	*
N(10)-Fe-N(70)	89.3(5)	*	C(51)-C(52)-C(53)	102.4(17)	*	N(71)-C(82)-O(70)	117(2)	118(4)
N(30)-Fe-N(50)	88.8(5)	*	C(52)-C(53)-C(54)	110.8(17)	*	N(11)-C(22)-C(23)	121(2)	*
N(50)-Fe-N(70)	88.9(5)	89.0(2)	C(71)-C(72)-C(73)	107.1(17)	*	N(31)-C(42)-C(43)	118.7(19)	*
N(10)-Fe-N(50)	164.0(5)	*	C(72)-C(73)-C(74)	108.2(16)	106.7(34)	N(51)-C(62)-C(63)	131(2)	*
N(30)-Fe-N(70)	164.5(6)	164.3(6)	C(14)-C(15)-C(16)	116.4	*	N(71)-C(82)-C(83)	120.5(17)	122.8(6)
N(10)-Fe-O(1)	83.0(6)	*	C(31)-C(15)-C(16)	117.2	*	O(10)-C(22)-C(23)	122.(3)	*
N(30)-Fe-O(1)	83.6(5)	*	C(34)-C(35)-C(36)	116.1	*	O(30)-C(42)-C(43)	117.4(17)	*
N(50)-Fe-O(1)	81.1(6)	*	C(51)-C(35)-C(36)	119.6	*	O(50)-C(62)-C(63)	112(3)	*
N(70)-Fe-O(1)	81.0(6)	82.2(13)	C(54)-C(55)-C(56)	118.2	*	O(70)-C(82)-C(83)	122(2)	118(5)
N(10)-Fe-O(30)'	93.3(5)	*	C(71)-C(55)-C(56)	115.6	*	C(22)-C(23)-C(24)	111(2)	*
N(30)-Fe-O(30)'	101.6(5)	*	C(74)-C(75)-C(76)	115.2	*	C(22)-C(23)-C(25)	110(2)	*
N(50)-Fe-O(30)'	102.7(5)	*	C(11)-C(75)-C(76)	120.1	117.3(18)	C(22)-C(23)-C(26)	109(2)	*
N(70)-Fe-O(30)'	93.8(5)	98(5)	C(14)-C(15)-C(31)	126.2(14)	*	C(24)-C(23)-C(25)	104(2)	*
O(1)-Fe-O(30)'	173.6(6)		C(34)-C(35)-C(51)	124.2(15)	*	C(24)-C(23)-C(26)	110(2)	*
Fe-O(30)'-C(42)'	160.3(13)		C(54)-C(55)-C(71)	126.2(17)	*	C(25)-C(23)-C(26)	113(2)	*
Fe-N(10)-C(11)	125.5(11)	*	C(74)-C(75)-C(11)	124.5(15)	125.3(11)	C(42)-C(43)-C(44)	108.5(17)	*
Fe-N(10)-C(14)	128.1(11)	*	C(15)-C(16)-C(17)	120.0		C(42)-C(43)-C(45)	106.8(16)	*
Fe-N(30)-C(31)	126.5(10)	*	C(15)-C(16)-C(21)	119.9		C(42)-C(43)-C(46)	109.5(17)	*
Fe-N(30)-C(34)	127.2(11)	*	C(35)-C(36)-C(37)	119.8		C(44)-C(43)-C(45)	108.6(18)	*
Fe-N(50)-C(51)	125.0(12)	*	C(35)-C(36)-C(41)	119.8		C(44)-C(43)-C(46)	114.9(17)	*
Fe-N(50)-C(54)	126.0(12)	*	C(55)-C(56)-C(57)	119.7		C(45)-C(43)-C(46)	108.2(18)	*
Fe-N(70)-C(71)	125.3(12)	*	C(55)-C(56)-C(61)	120.2		C(62)-C(63)-C(64)	105(2)	*
Fe-N(70)-C(74)	126.2(11)	126.2(10)	C(75)-C(76)-C(77)	120.7		C(62)-C(63)-C(65)	107(2)	*
C(11)-N(10)-C(14)	105.7(12)	*	C(75)-C(76)-C(81)	119.2		C(62)-C(63)-C(66)	117(3)	*
C(31)-N(30)-C(34)	106.1(13)	*	N(11)-C(21)-C(20)	121.6		C(64)-C(63)-C(65)	109(2)	*
C(51)-N(50)-C(54)	108.6(14)	*	N(11)-C(21)-C(16)	118.4		C(64)-C(63)-C(66)	107(2)	*
C(71)-N(70)-C(74)	108.1(14)	107.1(14)	N(31)-C(41)-C(40)	120.6		C(65)-C(63)-C(66)	111(2)	*
N(10)-C(11)-C(12)	109.0(15)	*	N(31)-C(41)-C(36)	119.1		C(82)-C(83)-C(84)	108.0(17)	*
N(10)-C(14)-C(13)	111.8(15)	*	N(51)-C(61)-C(60)	125.1		C(82)-C(83)-C(85)	107.0(17)	*
N(30)-C(31)-C(32)	111.8(14)	*	N(51)-C(61)-C(56)	114.9		C(82)-C(83)-C(86)	104.1(16)	*
N(30)-C(34)-C(33)	110.1(15)	*	N(71)-C(81)-C(80)	122.5		C(84)-C(83)-C(85)	114.8(20)	*
N(50)-C(51)-C(52)	110.7(16)	*	N(71)-C(81)-C(76)	117.3		C(84)-C(83)-C(86)	1118(16)	*
N(50)-C(54)-C(53)	107.6(15)	*	C(21)-N(11)-C(22)	127.1	*	C(85)-C(83)-C(86)	110.5(18)	109.4(33)
N(70)-C(71)-C(72)	109.6(17)	*	C(41)-N(31)-C(42)	126.3	*	C(1)-S-C(4)	86.9(17)	
N(70)-C(74)-C(73)	107.0(15)	109.7(18)	C(61)-N(51)-C(62)	137.2	*	S-C(1)-C(2)	108(4)	
C(11)-C(12)-C(13)	110.9(17)	*	C(81)-N(71)-C(82)	132.1	130(5)	S-C(4)-C(3)	108(4)	
C(12)-C(13)-C(14)	102.5(16)	*	N(11)-C(22)-O(10)	117(3)	*	C(1)-C(2)-C(3)	118(5)	
C(31)-C(32)-C(33)	104.2(14)	*	N(31)-C(42)-O(30)	124(2)	*	C(2)-C(3)-C(4)	114(4)	

[a] E.D.d.'s for bond angles involving atoms constrained in rigid groups not calculated.

contacts involve pivalamide oxygen atoms. With the exception of the coordinated pivalamide oxygen atom O(30)', whose thermal motion is very much less than that for other amide oxygen atoms (Table 4.14, Figure 4.25), these atoms are afflicted with high and anisotropic thermal motion which could indicate irresolvable disorder. Loose packing with solvate molecules as lattice "fillers" and consequent high thermal motion of the pivalamide groups is a general feature of the "picket fence" porphyrin derivatives so far structurally characterised. The terminal methyl groups and the oxygen atoms of the "pickets" are generally the worst affected. In this structure (as in the others) high thermal motion of the solvate species is observed; an extremely large RMS component of thermal displacement for the sulphur atom together with some abnormally short interatomic separations indicate that irresolvable conformational disorder is likely.

The Fe-O(30)' vector is canted 6.7° to the normal to the porphinato plane and the Fe-O(30)'-C(42)' angle is 160(1)°. This angle is considerably more obtuse than the expected angle of 120° for an sp^2-hybridised oxygen atom. The packing constraints in linking two Fe(TpivPP) units are best appreciated by inspection of Figure 4.25. Non-hydrogen, inter-Fe(TpivPP) unit contacts less than 3.75 Å are listed in Table 4.17.

Table 4.17 : Non-hydrogen inter-Fe(TpivPP) unit contacts (<3.75 Å) for polymeric-[Fe(TpivPP)(OH_2)]·THT.

Atoms	Distance	Atoms	Distance	Atoms	Distance
Fe ...C(42)'[a]	3.420(20)	O(30)'... N(30)	3.328(18)	C(45)... O(70)	3.73(3)
S ... C(26)	4.08(3)	O(30)'... N(50)	3.362(19)	C(46)... O(70)	3.50(3)
S ...N(31)	4.10(3)	O(30)'... C(52)	3.61(2)	C(53)... C(17)	3.49
S ..,C(78)	3.87	O(1)... N(50)	3.29(2)	C(72)... C(20)	3.74
C(1)... O(10)	3.53(4)	O(1)... N(10)	3.34(3)	O(50)... C(37)'	3.38
C(2)... C(45)	3.71(5)	O(1)... N(30)	3.37(2)	O(50)... C(38)'	3.29
C(3)... O(50)	3.32(5)	O(1)... C(85)	3.49(2)	C(39)... C(77)'	3.72
C(4)... O(50)	3.48(5)	C(35)... C(44)'	3.63(3)	C(40)... C(11)'	3.69
O(1)... Fe	2.897(19)	N(30)... C(44)'	3.72(2)	C(2)... C(57)	3.61
O(1)... C(25)	2.94(3)	C(34)... C(44)'	3.57(3)	C(65)... C(58)	3.64
O(1)... C(64)	3.05(4)	N(50)... C(45)'	3.57(3)	C(32)... C(58)'	3.73
O(1)... N(70)	3.29(2)	C(54)... C(45)'	3.69(3)	C(59)... C(80)	3.72
O(30)'... N(10)	3.107(19)	C(72)... O(10)	3.65(3)	C(32)... C(59)'	3.72
O(30)'... N(70)	3.139(19)	C(73)... O(10)	3.30(3)	C(59)... C(79)	3.74

[a] Primed atoms belong to the same polymeric chain as the unprimed atoms.

The second notable feature is the existence of large rotations of the phenyl groups from perpendicularity to the porphinato plane; the rotations range from 16.4° to 25.0°. These rotations are considerably larger than those observed for the two dioxygen adducts of "picket fence" porphyrin derivatives described in §4.2 and §4.3; the rotations are 6.8° and 12.1° for Fe(TpivPP)(1-Me-imid)(O_2) and they range from 7.7° to 16.6° for Fe(TpivPP)(THT)(O_2). Large deviations from perpendicularity are not unique; for Mn(TPP)(py)Cl a rotation angle of 30.2° is observed[332]. While this, in part, accounts for the absence of close contacts between Fe(TpivPP) units, particularly between the methyl groups of the linking "picket" and the porphinato plane, it does lead to close intra-Fe(TpivPP) unit contacts. For example the N(71)···C(11) separation is more than 0.2 Å shorter than any such corresponding contact for Fe(TpivPP)-(1-Me-imid)(O_2). Some selected intra-Fe(TpivPP) unit contacts may be found in Table 4.18.

In contrast to the other "picket fence" porphyrin derivatives, two of the amide groups comprising atoms N(11), C(22), O(10), C(23) and atoms N(31), C(42), O(30), and C(43) no longer maintain even approximate coplanarity with their host phenyl group. Planarity of the amide group is approximately maintained although amide group Piv-51 which has the anomalously short N(51)-C(62) separation of 1.21(3) Å shows the greatest departure from planarity. Tables 4.19 and 4.20 list selected least-squares planes and their dihedral angles.

Table 4.18 : Selected, non-hydrogen intra-Fe(TpivPP) unit contacts for polymeric-$[Fe(TpivPP)(OH_2)]\cdot THT$. Distances in Å.

Atoms	Distance	Atoms	Distance
C(17)...C(14)	3.22	N(11)...C(31)	3.16(3)
C(17)...C(13)	3.28	N(11)...C(32)	3.24(3)
C(21)...C(31)	3.17	N(31)...C(52)	3.10(2)
C(21)...C(32)	3.19	N(31)...C(51)	3.17(2)
C(37)...C(34)	3.15	N(51)...C(71)	3.05(3)
C(37)...C(33)	3.23	N(51)...C(72)	3.15(3)
C(41)...C(52)	3.07	N(71)...C(11)	3.05(3)
C(41)...C(51)	3.14	N(71)...C(12)	3.19(3)
C(57)...C(54)	3.14		
C(57)...C(53)	3.24		
C(61)...C(71)	3.17		
C(61)...C(72)	3.24		
C(77)...C(74)	3.12		
C(77)...C(73)	3.17		
C(81)...C(11)	3.14		
C(81)...C(12)	3.22		

Table 4.19 : Selected least-squares planes (unweighted) for polymeric-[Fe(TpivPP)(OH_2)].

Name of Plane	Equation of Plane[b] Ax + By + Cz - D = 0 (Coeff x 10^4) A	B	C	D	Atoms in Plane / Displacements of Atom from Plane (Å x 10^3)					
I	-6641	-2505	-7044	-34677	See Figure 4.27					
II	-6673	-2545	-6999	-34365	N(10)	N(30)	N(50)	N(70)		
					-004(13)	004(12)	-004(13)	004(14)		
Pyrrole-10	-6599	-2516	-7080	-34708	N(10)	C(11)	C(12)	C(13)	C(14)	
					012(13)	-014(17)	010(18)	-003(18)	-006(16)	
Pyrrole-30	-6902	-1924	-6976	-29644	N(30)	C(31)	C(32)	C(33)	C(34)	
					-004(12)	016(16)	-022(18)	020(18)	-011(17)	
Pyrrole-50	-6352	-2504	-7306	-33700	N(50)	C(51)	C(52)	C(53)	C(54)	
					-002(13)	001(17)	000(19)	-001(17)	002(18)	
Pyrrole-70	-6766	-2875	-6779	-35058	N(70)	C(71)	C(72)	C(73)	C(74)	
					003(14)	-007(20)	009(19)	-007(19)	002(17)	
Phenyl-16	1924	5830	-7893	15597	C(16)	C(17)	C(18)	C(19)	C(20)	C(21)
					0[c]	0	0	0	0	0
Phenyl-36	2713	-7860	-5556	-58406	C(36)	C(37)	C(38)	C(39)	C(40)	C(41)
					0[c]	0	0	0	0	0
Phenyl-56	5348	7739	-3392	36434	C(56)	C(57)	C(58)	C(59)	C(60)	C(61)
					0[c]	0	0	0	0	0
Phenyl-76	8811	-4685	-0640	-22515	C(76)	C(77)	C(78)	C(79)	C(80)	C(81)
					0[c]	0	0	0	0	0
Piv-11	1114	-0926	-9894	-61421	N(11)	C(22)	O(10)	C(23)		
					007(16)	-022(26)	008(29)	007(28)		
Piv-31	-3510	-9192	-1786	-99765	N(31)	C(42)	O(30)	C(43)		
					006(15)	-016(18)	006(12)	004(23)		
Piv-51	2195	9134	-3428	24154	N(51)	C(62)	O(50)	C(63)		
					027(21)	-068(33)	020(29)	021(21)		
Piv-71	-8609	4932	-1249	8710	N(71)	C(82)	O(70)	C(83)		
					003(15)	-009(23)	003(20)	003(19)		

[a] Displacements of atoms are from a fixed plane and hence the accompanying e.s.d.'s are derived only from the e.s.d.'s in positional coordinates of the atoms.

[b] The coefficients are relative to an orthogonalised Angstrom coordinate system and were calculated using program MEANPLANE (M.E. Pippy, E. R. Ahmed).

[c] Constrained to be planar.

Table 4.20 : Selected dihedral angles between least-squares planes for polymeric-[Fe(TpivPP)(OH_2)].

	I	II	Pyrrole-10	Pyrrole-30	Pyrrole-50	Pyrrole-70
I	-	0.4	0.3	3.7	2.2	2.7
II		-	0.7	3.8	2.6	2.3
Pyrrole-10			-	3.9	1.9	2.9
Pyrrole-30				-	5.0	5.6
Pyrrole-50					-	4.4

	I	Phenyl-16	Phenyl-36	Phenyl-56	Phenyl-76	Piv-11	Piv-31	Piv-51	Piv-71
I	-	73.6	65.9	108.1	115.0	49.7	53.9	97.7	57.6
Phenyl-16		-	88.1	34.7	93.0	41.6	-	-	-
Phenyl-36			-	106.0	50.0	-	43.2	-	-
Phenyl-56				-	82.5	-	-	19.8	-
Phenyl-76						-	-	-	168.9

The third feature is the semi-coordinated water molecule located 2.90(2) Å from the iron centre. This molecule also indulges in some rather close contacts with pivalamide methyl groups; the closest approach is 2.94(3) Å (see also Table 4.17). Hydrogen bonding to methyl hydrogen atoms is implausible. Slight positional disorder for both the water molecule and carbon atoms, which may be inferred from the high thermal motion of both species, would lengthen these contacts to a more acceptable van der Waals separation of 3.3 Å to 3.4 Å. The water molecule makes no contacts shorter than 4.4 Å with solvate molecules or other Fe(TpivPP) units. In contrast to the Fe-O(30)' linkage, the Fe-OH_2 linkage is approximately perpendicular to the porphinato plane.

The final feature concerning the packing of Fe(TpivPP) units is the angle that vectors of the type C(15)-C(16)...C(19) make with the porphinato plane. This is best understood by inspection of Figure 4.27. It can be seen the three of the pivalamidephenyl groups tilt inwards towards each other while the other "picket", the linking "picket", tilts outwards. For the structure of Fe(TpivPP)(THT)(O_2) an opposite pattern is observed (Figure 4.24). This tilting of the pivalamide-phenyl groups is accompanied by a non-systematic or non-symmetrical disposition of the pyrrole rings with respect to each other and to the porphinato plane. On the other hand, for Fe(TpivPP)(1-Me-imid)(O_2), all "pickets" tilt outwards, and the porphinato skeleton is "ruffled". For polymeric Fe(TpivPP) this tilting may be associated, to some extent, with the doming of the porphyrin.

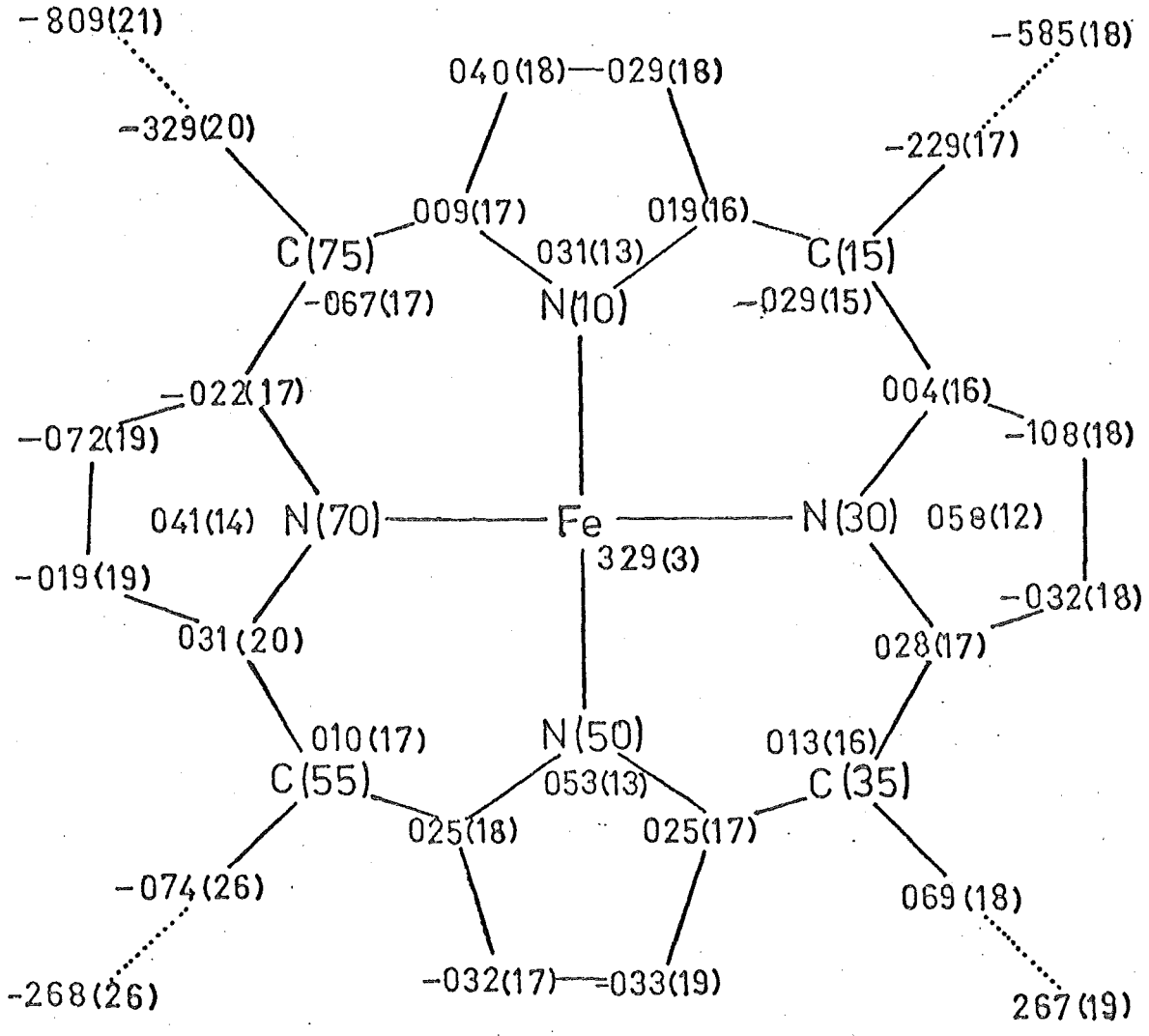

Figure 4.27 : Deviations of atoms from the least-squares plane of the 24-atom porphinato skeleton for polymeric-[Fe(TpivPP)(OH_2)]. The direction of the "pickets" is downwards into the page. Distances in $\mathring{A} \times 10^3$.

For this polymeric Fe(TpivPP) structure, the enclosing of the binding pocket caused by the inwards tilting "pickets" is counterbalanced to some extent in the rotations of the amide groups from coplanarity with their respective host phenyl groups.

Conformation of Porphinato Skeleton

While the individual pyrrole rings are planar, a feature shared by all porphinato complexes[191], the relative orientations of the pyrrole rings do not follow a systematic pattern, in contrast to many other metalloporphyrins[191]. The maximum deviation of a porphinato atom from the mean plane of the 24-atom porphinato core is 0.108(18) Å (Figure 4.27). The iron atom is displaced 0.329(3) Å from this plane.

The four porphinato nitrogen atoms form a planar group - the maximum deviation is only 0.004(14) Å. The iron atom is displaced 0.281(3) Å from this plane. There is therefore a modest doming of the porphinato core of ~0.05 Å (0.329 minus 0.281 Å, as defined by Hoard[191]).

As noted in a previous paragraph packing effects preclude the more usual adoption of a symmetric pattern of rotations of the pyrrole groups.

The Metal-Ligands Separations

It is illuminating to consider the geometry of the metal-coordination in terms of the occupancy of metal $3d_{z^2}$ and $3d_{x^2-y^2}$ orbitals. Being a high-spin iron(II) complex the electronic configuration in the valence shell is

$(3d_{xy})^2(3d_{xz,yz})^2(3d_{z}2)^1(3d_{x}^2-_{y}2)^1$.

This compound will firstly be considered as a strictly five-coordinate species; and then possible perturbations induced by the water molecule will be examined.

In Figure 4.28 the relationship between the occupancy of the metal $3d_{x}^2-_{y}^2$ orbital and the $M\text{-}N_{porph}$ separation is illustrated. Several features may be noted:-

1. With the lobes of the $3d_{x}^2-_{y}^2$ orbital aligned so as to eclipse the $M\text{-}N_{porph}$ bonds,

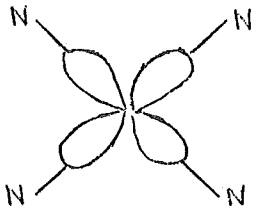

centering of the metal ion in the porphinato plane is discouraged for a $(3d_{x}^2-_{y}2)^1$ configuration.' Accordingly, in such species the iron atom is substantially displaced from the plane of the porphinato nitrogen atoms. Absence of the $3d_{x}^2-_{y}^2$ electron leads to a much smaller out-of-plane displacement - this is best illustrated by the pair of complexes $Mn^{II}(TPP)(1\text{-Me-imid})^{333}$ where the $3d_{x}^2-_{y}^2$ orbital is singly occupied and $Mn^{III}(TPP)(N_3)^{335}$ where the $3d_{o}^{x}{}^2-_{y}^2$ orbital is empty; a reduction in r(M...Ct) of $\sim$0.29 A accompanies the loss of the $3d_{x}^2-_{y}^2$ electron.

2. A high-spin metal centre has a larger radius than its low-spin counterpart (if it exists). The resultant longer $M\text{-}N_{porph}$ separation is accentuated if the $3d_{x}^2-_{y}^2$ orbital

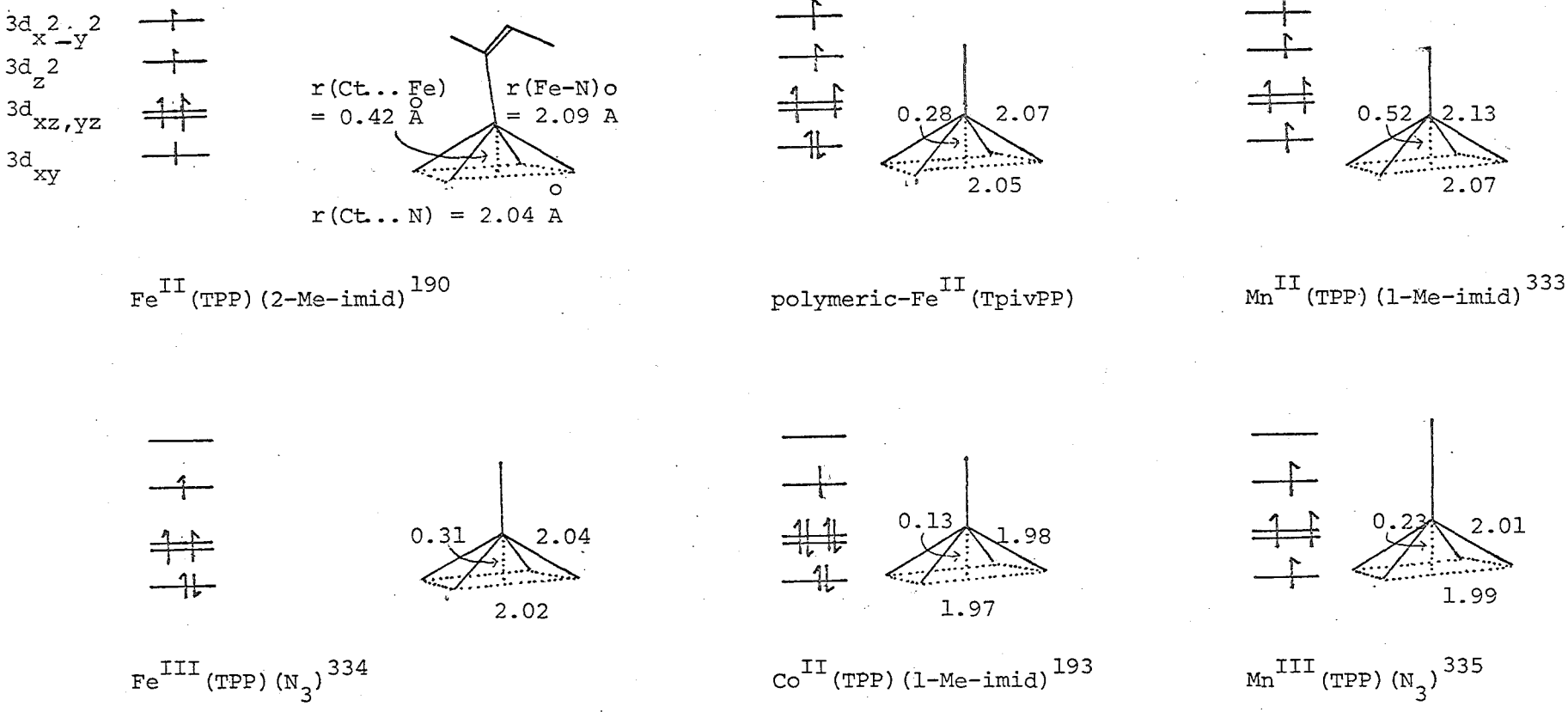

$Fe^{II}(TPP)(2\text{-Me-imid})$ [190]

polymeric-Fe^{II}(TpivPP)

$Mn^{II}(TPP)(1\text{-Me-imid})$ [333]

$Fe^{III}(TPP)(N_3)$ [334]

$Co^{II}(TPP)(1\text{-Me-imid})$ [193]

$Mn^{III}(TPP)(N_3)$ [335]

Figure 4.28 : $3d_{x^2-y^2}$ orbital occupancy and metalloporphyrin stereochemistry.

is occupied. Consequently the M-N_{porph} separation and the Ct...N_{porph} radius are greater than the value of 2.01 Å which has been postulated[243] as the ideal Ct...N_{porph} radius or M-N_{porph} separation (if the metal atom is centred in the plane of the porphinato nitrogen atoms.

Increased ionic change on the metal centre leads to a contraction of d orbitals and to a marked decrease in the metal radius ($r(Fe^{2+})$ = 0.74 Å, $r(Fe^{3+})$ = 0.64 Å [336]) which mitigates the presence of the $3d_{x^2-y^2}$ electron. This is illustrated on the pair of complexes Fe(TPP)(2-Me-imid) and $Fe^{III}(TPP)(N_3)$. Certainly, however, for iron(II) and manganese(II) complexes a long M-N_{porph} separation and an expanded Ct-N_{porph} radius are observed.

It must be stressed that the presence of a $3d_{x^2-y^2}$ electron is not completely inimical to an in-plane positioning of the metal centre; in [Sn(TPP)Cl_2] the tin atom is rigorously in-plane and r(Ct...N_{porph}) is 2.098(2) Å [245]. Polymeric-Fe(TpivPP) exhibits both characteristics – a substantial out-of-plane displacement of the iron atom, long r(Fe-N_{porph}) (average separation 2.07 Å) and an expanded radius (average r(Ct...N_{porph}) 2.05 Å).

Figure 4.29 illustrates the M-L_{ax} separations of a number of amine-based metalloporphyrins for metal centres both with and without a $3d_{z^2}$ electron. As before such complexes have a number of distinguishing features:-

1. With the lobes of the $3d_{z^2}$ orbital axially aligned,

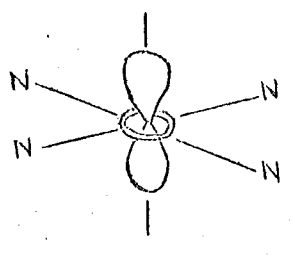

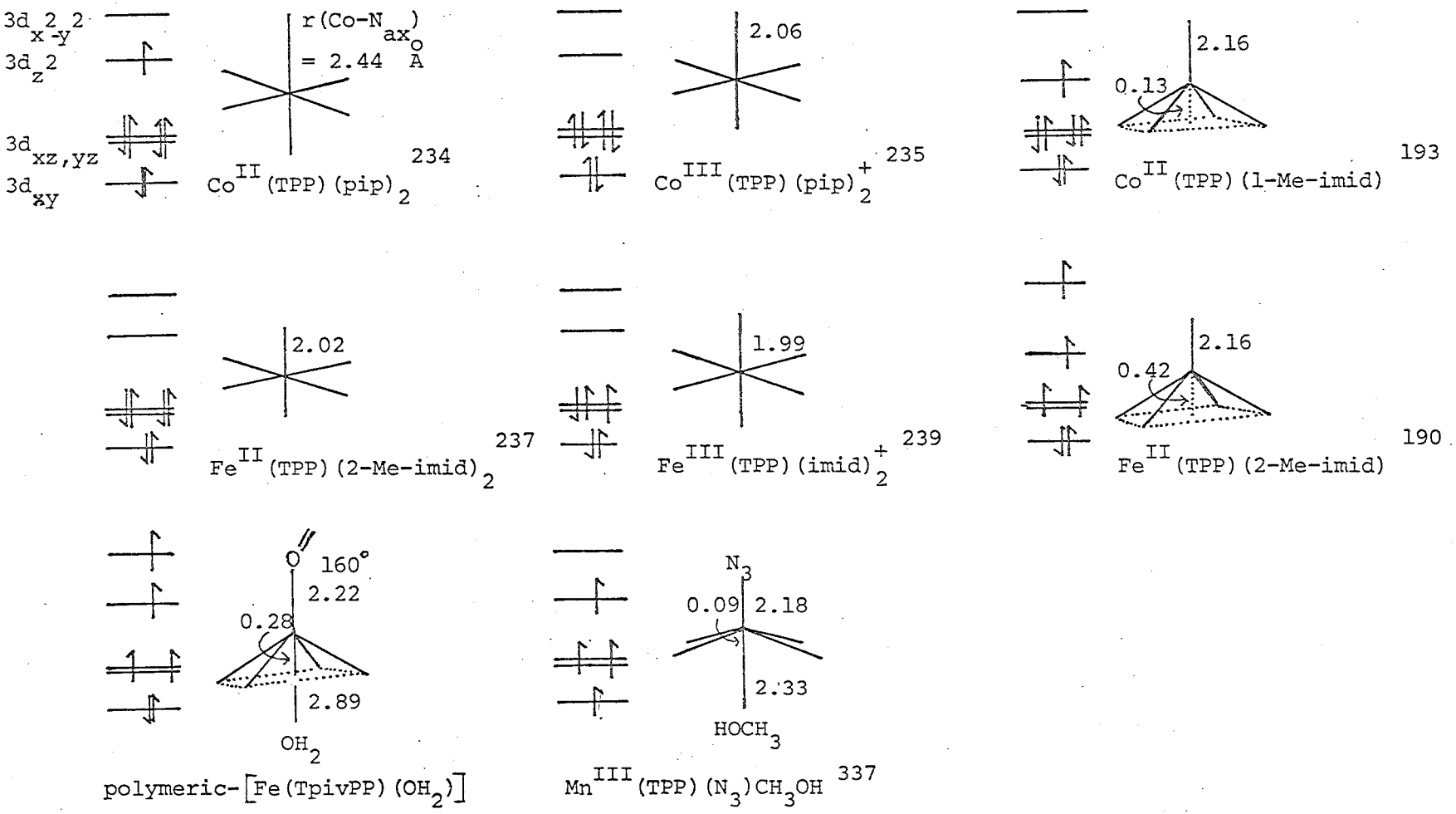

Figure 4.29 : $3d_{z}2$ orbital occupancy and metalloporphyrin stereochemistry.

strong axial ligation and short M-L_{ax} separations are discouraged for $(3d_z2)^1$ configurations; especially for six-coordinate species where there is no facility for the $3d_z2$ electron to be concentrated as a phantom sixth ligand trans to the fifth ligand. Strong binding of axial ligands is accompanied by $L_{ax}\cdots N_{porph}$ separations less than expected van der Waals contacts. Loss of the $3d_z2$ electron from $Co(TPP)(pip)_2$ to give $Co^{III}(TPP)(pip)_2^+$ results in a 0.38 Å reduction in $r(Co\text{-}N_{pip})$.

2. As a corrollary to the previous point, five-coordinate complexes achieve van der Waals separations by a combination of the M-L_{ax} separation and the M...Ct displacement. This is illustrated in the pair of complexes $Mn^{III}(TPP)(N_3)$[335] and $Mn^{III}(TPP)(N_3)(CH_3OH)$[337] where the coordination of methanol is accompanied by a decrease of 0.145 Å in r(Mn... Ct) and an increase of 0.131 Å in $r(Mn\text{-}N_{N_3})$; the $N_{N_3}\cdots N_{porph}$ separation is preserved.

With values for r(Fe-O) of 2.22(1) Å and for r(Fe...Ct) of 0.281(3) Å, the $N_{porph}\cdots O$ separations are in the range 3.11 Å to 3.37 Å; not much smaller than expected van der Waals separations. That the Fe–O=C< bond angle is 160(1)°, instead of approximately 120° for an sp^2-hybridised oxygen atom, minimises the contacts made by atom C(42)' with the porphinato plane.

The closest analogue of polymeric-Fe(TpivPP) is Fe(TPP)(2-Me-imid). The longer Fe-L_{ax} separation and shorter Fe... Ct displacement for the former species are consistent with the weaker donor power of a O=C< ligand compared to an N≤ ligand and with the smaller steric require-

ments of a nearly linear Fe–O=C$\lessdot$ entity compared with the sterically bulky 2-methylimidazole ligand.

So far the water molecule near the iron atom has been ignored. Using an ion-dipole model Hoard has calculated that the stabilising energy of the Fe-O_{OH_2} bond for an inter-atomic separation of 2.90 Å still amounts to 58% of that for a separation of 2.22 Å[237]. The $N_{porph}\cdots O_{OH_2}$ separations are quite similar to the $N_{porph}\cdots O_{O=C\lessdot}$ separations. Water is therefore considered to be semi-coordinated. In the absence of the structure of dehydrated polymeric-Fe(TpivPP) it is, unfortunately, impossible to gauge, even qualitatively, the perturbations in r(Fe-O) and r(Fe...Ct) induced by the water molecule. All that may be said is that r(Ct...O) will be essentially unaffected by the presence or absence of water for this high-spin complex, in an entirely analoguous fashion to the pair of complexes $Mn^{III}(TPP)(N_3)$ and $Mn(TPP)(N_3)(CH_3OH)$.

This polymeric complex has, therefore, a number of novel features in relation to other structurally characterised metalloporphyrins. It has an amide oxygen atom coordinated to a metalloporphyrin; it has water semi-coordinated; it is the only high-spin six-coordinate iron(II) complex; or, if preferred, it is only the second five-coordinate iron(II) complex; it is the only five- or six-coordinate metal(II)porphyrin that has a non-amine axial ligation.

4.4.4 Biological Implications

Shulman and coworkers have used this complex as a model for deoxyhaemoglobin[295]. Using extended X-ray absorption fine structure (EXAFS) spectroscopy, they deduced an $Fe\text{-}N_{porph}$ separation of 2.06(2) Å for both this polymeric compound and for deoxy-Hb. Analysis of the EXAFS spectrum depended upon a knowledge of the shorter $Fe\text{-}L_{ax}$ separation. However, Fe(TPP)(2-Me-imid) is a more appropriate model for deoxy-Hb, notwithstanding the steric demands of the 2-methyl substituent on the imidazole ring. The displacement of the iron atom from the plane of the porphinato nitrogen atoms is 0.42 Å for Fe(TPP)(2-Me-imid) and 0.28 Å for polymeric-Fe-(TpivPP). But $r(Ct...N_{porph})$ is similar in both complexes and hence the large difference in out-of-plane displacement of the iron atom is not reflected in $r(Fe...N_{porph})$ (see Figure 4.28) EXAFS spectroscopy is, therefore, presently of limited use in obtaining the out-of-plane displacement of the iron centre in deoxy-Hb and HbO_2; this parameter has been of great significance in discussions on the cooperative binding of dioxygen to haemoglobin. EXAFS studies on HbO_2 and Fe(TpivPP)(1-Me-imid)(O_2), discussed previously in §4.2.6, also produced concordant values of $r(Fe\text{-}N_{porph})$ for the protein and its model.

The presence of a water molecule in the binding pocket of Fe(TpivPP) is noted with regard to the rather surprising discovery that the binding pocket of the α chains of deoxy-Hb contain a water molecule[150]. This finally dispelled long-held notions of a hydrophobic binding pocket. The water molecule is hydrogen-bonded to the distal histidine and is 3.6 Å from

the iron centre. Any interaction of the water molecule with the metal centre is consequently very much weaker than that which occurs for polymeric Fe(TpivPP), but the water molecule may still affect the reversible and cooperative binding of dioxygen by haemoglobin.

4.5 Comparison of the Three "Picket Fence" Porphyrins

The bulky but flexible pivalamide "pickets" dominate the crystallography of these three "picket fence" porphyrin derivatives. Rather loose packing and the presence of generally poorly defined solvate molecules as lattice "fillers" are coupled with high crystal mosaicity and/or twinning and rapid fall-off of intensity with increasing values of $\sin\theta/\lambda$. The "pickets" invariably have very high thermal motion and, in one case, disorder of the methyl groups is observed. In all "pickets". except for the linking "picket" in the polymeric-Fe(TpivPP) structure, high thermal motion is observed for the carbonyl group. Rotations about bonds of the type C(21)-N(11) and N(11)-C(22) leave the terminal methyl carbon atoms relatively fixed by comparison with the movement that is induced in groups of the C(22)-O(10) type - a movement similar to the "twist". The amide oxygen atoms are worst affected with components of thermal displacement of up to 0.61 Å being observed. However, when an amide oxygen atom is coordinated, as occurs in polymeric-Fe(TpivPP), the eccentricity of thermal motion for that atom (and also for its attached carbon atom) is very much less.

For the three complexes, the pivalamide-phenyl groups do not exhibit a constant orientation. The twist of the

phenyl groups from perpendicularity to the porphinato plane varies; similarly coplanarity of the amide groups of the type N(11), C(22), O(10), C(23) with their respective host phenyl groups is not observed in all cases. There is also considerable variation in the tilting of the "pickets" inwards and outwards from the centre of the porphinato skeleton (see Figures 4.18, 4.24 and 4.27). For Fe(TpivPP)(1-Me-imid)-(O_2) both "pickets" lean outwards and this is coupled with a pseudo-symmetrical "ruffled" conformation of the pyrrole rings of the porphinato core. Three of the four "pickets" in Fe(TpivPP)(THT)(O_2) lean outwards but in polymeric-Fe-(TpivPP) the opposite is observed; in both cases a non-symmetrical arrangement of the pyrrole rings is observed. Crystal packing effects, and, in the case of polymeric-Fe-(TpivPP), doming of the porphinato skeleton are presumably responsible.

The relative depths of the binding pockets for the three complexes are of interest. The depth is defined as the mean displacement of the pivalamide methyl carbon atoms from the porphinato plane. It is 5.05 Å for Fe(TpivPP)(1-Me-imid)(O_2), and 5.01 Å for Fe(TpivPP)(THT)(O_2), but for polymeric-Fe(TpivPP), where there are the greatest departures of the phenyl groups from perpendicularity with the porphinato plane, the depth is only 4.69 Å.

In the next chapter, further biological implications of the structures of model compounds are discussed in relation to the stereochemical model of Perutz for the cooperative binding of dioxygen to haemoglobin and cobalt-substituted haemoglobin. In Chapter 6, some semiquantitative

calculations on the bonding in iron- and cobalt-dioxygen complexes are presented and briefly discussed with reference to structural and physical evidence for their nature.

CHAPTER 5

IMPLICATIONS OF THE RESULTS ON THEORIES FOR THE COOPERATIVE BINDING OF DIOXYGEN TO HAEMOGLOBIN

The literature on studies which relate to the cooperative binding of dioxygen and other molecules to haemoglobin and its variants is voluminous. There is a critical need for the vast amount of very recent, and sometimes conflicting, data to be assessed with reference to theories for the cooperative binding of dioxygen as well as for other allosteric effects.

It is not proposed to examine the immense range and volume of studies pertinent to the stereochemical model of Perutz for allosteric effects. Model compounds have indicated the general nature of the changes in the stereochemistry of the protohaem group that are to be expected as a result of ligation. But there are difficulties in relating quantitatively the results of model studies to the protein. Attention has been focussed on the axial connection and the movement of the proximal histidine as the initiator of the cooperative binding of dioxygen, but the changes in the conformation of protoporphyrin-IX and hence changes in the globin-protoporphyrin-IX non-bonded interactions may be equally important. This is discussed in §5.2 which is essentially an update of earlier similar discussions[155-160,191,206,353]. In §5.1 only a very brief introduction to the allosteric properties of haemoglobin is provided since a number of detailed reviews

exist[158,159,354]. Allostery is not unique to haemoglobin although haemoglobin is the most widely studied example of an allosteric protein.

5.1 Allosteric Properties of Haemoglobin

The cooperative binding of dioxygen to haemoglobin is but one of a number of allosteric properties of haemoglobin. These effects may be divided into two classes[153]:-

1. Homotropic effects pertain to the interactions between identical ligands. The influence that the binding of one molecule of dioxygen to haemoglobin has on the binding of another molecule is one example, redox properties is another. These effects are also known, somewhat misleadingly since with the haems separated by more than 25 Å the interaction is indirect, as "haem-haem" interactions.

2. Heterotropic effects pertain to the interactions between different ligands. For example, the "allosteric effector" 2,3-diphosphoglycerate (2,3-DPG), which binds to deoxyhaemoglobin between the two β chains,[355,356] but which does not bind significantly to oxyhaemoglobin, modifies the oxygen-binding properties of Hb.

An acceptable theory for the cooperative binding of dioxygen must be able to accommodate heterotropic effects without additional ad hoc assumptions. The cooperative binding of dioxygen is described empirically by the Hill equation

$$\frac{y}{1-y} = KP^n$$

where y is the fractional saturation, K is a constant, P is the partial pressure of oxygen and n is a measure of

cooperativity. For n=1 there is no interaction; that is haemoglobin behaves like four isolated myoglobin molecules. For n=4 it is an "all or none" situation. For normal haemoglobins n is in the range 2.7 to 2.9 [152]. The macroscopic thermodynamic properties of oxygen binding may be approached from two directions.

Firstly, there is the "sequential" model of Koshland, Nemethy and Filmer[154]. The binding of dioxygen to one subunit initiates tertiary structural changes which are transmitted to other subunits and thereby modify their oxygen affinity.

Secondly, there is the "allosteric transition" model of Monod, Wyman and Changeux[153]. Haemoglobin exists in a conformational equilibrium between two (or at least two) quaternary structures. One has a low oxygen affinity - the tense (T) structure - and the other has a higher oxygen affinity - the relaxed (R) structure. The binding of ligands shifts the equilibrium towards the R structure but in each quaternary structure the affinity of one subunit is unaffected by the state of ligation of others (in contrast to the "sequential" model). In the presence of allosteric effectors this model must be generalised to provide a third quaternary state[354]. Moreover, the assumption that α and β subunits have identical ligand binding properties is too rigid [354]. Furthermore, the binding of dioxygen to one subunit causes changes in the tertiary structure of that unit.

X-ray crystallographic studies, mainly by Perutz and coworkers[158], have demonstrated the existence of two quaternary structures, one for deoxy-Hb and another for ligated Hb. As a result Perutz has developed an intricate and subtle stereo-

chemical model for the cooperative binding of ligands and other allosteric properties which is largely based on the allosteric transition model but which also includes features of the "sequential" model such as the change in tertiary structure accompanying ligand binding[155-158,357-359]. Perutz proposed[155-158] that

> "the equilibrium between the two structures is governed primarily by the displacement of the iron atoms and the proximal His from the plane of the porphyrins, and by the steric effect of the ligand in the β subunits; that much of the free energy of haem-haem interaction (∿15kJ/mole haem[360]) is stored in the salt bridges which break sequentially with oxygen uptake."[158]

Thus a large displacement of the iron from the haem plane biases the allosteric equilibrium towards the T quaternary structure as exemplified by deoxy-Hb, and a small displacement towards the R quaternary structure, as exemplified by oxy-Hb.

Changes in the tertiary structure of a subunit as a result of ligand binding are transmitted to the salt bridges which "lock" the structure in either the T or R quaternary conformation. Perutz has further proposed[157], and found confirmatory evidence[357-359] that in the unliganded T structure the globin "exercises a <u>tension</u> on the haem"[158] which opposes movement of the iron atom into the porphyrin plane on ligation, and hence is responsible for the lowered affinity of T state haemoglobin.

Very recently, Gelin and Karplus[370] have proposed that there is little strain on the unliganded protohaem; instead, the reduced oxygen affinity of T quaternary conformation results from strain on the liganded subunit, through increased contacts of the now planar protohaem with the globin. They deduced, from energy minimisation calculations, that the unliganded protohaem was significantly domed, although X-ray crystal structure analyses on deoxy-Hb do not distinguish between a planar and a domed conformation.

A fundamental feature of the Perutz and the MWC models is that a quaternary structural change on ligand binding is essential for that binding to be cooperative. No exceptions have been found.

The quantitative changes in the histidine-haem separations accompanying the oxygenation of Co-Hb and Hb are discussed in the next section.

5.2 Stereochemical Changes Accompanying Oxygenation

Parameters relevant to the stereochemical changes accompanying oxygenation are listed in Table 5.1 for haemoglobin, cobalt-substituted haemoglobin and their models.

Stereochemical evidence for "tension at the haem" or a stretching of the histidine to porphyrin plane separation for deoxy-Hb is slight in view of the unavoidably low precision of the protein crystal structure analyses; the differences in P...N_{imid} separations for deoxy-Hb and Fe(TPP)-(2-Me-imid) are barely significant.

Comparisons between the protein and its models are also complicated by two factors related to the stereochemistry

Table 5.1: Possible stereochemical changes accompanying oxygenation.

	Myoglobin			Haemoglobin			Fe Model			Co Model		
	Deoxy[a]	CO[b]	Δ[l]	deoxy[c]	aquomet[d,i]	Δ[i]	deoxy[e]	oxy[f]	Δ	deoxy[g]	oxy[h]	Δ
r(M...P)[j] Å	0.55	0.1	0.45	0.60(10)	0.07	0.53-0.60α	0.42+0.15	-0.03+0.01		0.13+0.01		
				0.63(10)	0.21	0.42-0.63β	=0.55[k]	=-0.02[k]	0.57	=0.14[k]	0	0.14
r(M-N_{imid}) Å	2.1	-	-	2.0(3)	2.1	0.1 α	2.161(5)	2.07(2)	0.09	2.157(3)	2.011(2)	0.14
				2.2(3)	2.2	0.0 β						
r(N_{imid}...P) Å	2.6	-	-	2.6(3)	2.2	0.4-0.6 α	2.71	2.05	0.66	2.30	2.011(2)	0.29
				2.8(3)	2.4	0.4-0.8 β						

(a) Reference [368]; (b) reference [291]; (c) reference [150]; (d) reference [369]; (e) Fe(TPP)(2-Me-imid)[191].

(f) Fe(TpivPP)(1-Me-imid)(O_2) this work and reference [11]; (g) Co(TPP)(1-Me-imid)[193]; (h) Co(saltmen)(1-Bz-imid)(O_2)[124].

(i) For HbCO[292] resolution (2.8 Å) insufficient to determine exact iron and proximal histidine positions relative to porphyrin; in β chains Fe moves towards porphyrin for HbCO compared to aquomet-Hb; N_{imid}... P for aquomet-Hb probably longer than for HbCO.

(j) P : protoporphyrin-IX mean plane for proteins; 24-atom porphyrin skeleton for models.

(k) Comprising: r(M...Ct) + r(Ct...P).

(l) $\Delta = r(M...P)_{deoxy} - r(M...P)_{oxy}$, etc.

of the porphyrin itself. Firstly, it is the mean plane of the protohaem, including its peripheral substituents, that is determined in Hb and its derivatives. But, in model systems, it is the mean plane of the 24-atom porphinato skeleton that is determined. That is, there is no identical reference point from which comparisons may be made. If the porphyrin is at all domed then comparisons of distances involving the porphyrin planes is hazardous.

Secondly, the doming (0.13 Å) of the model compound Fe(TPP)(2-Me-imid) is anomalously large by comparison with other metalloporphyrins where the doming parameter is typically less than 0.05 Å [191]. For example, in Mn(TPP)(1-Me-imid), where the displacement of the manganese atom from the plane of the porphinato nitrogen atoms is much larger (0.52 Å), the doming parameter is much smaller (0.04 Å) [333]. The doming in Fe(TPP)(2-Me-imid) has been attributed to packing constraints [191]. In view of the host of van der Waals contacts made by the globin with the protohaem, deviation of the protohaem from idealised S_4 symmetry is also quite likely, but, since it has not been quantified, comparisons with the model system are again hazardous.

The shortening of the histidine-protohaem separation ($N_{imid}\cdots P$) accompanying the oxygenation of cobalt-substituted Hb is almost certain to be modest by comparison with native haemoglobins (Table 5.1). A <u>maximum</u> movement of the proximal histidine of 0.38 Å was postulated by Ibers, Lauher and Little on the basis of model cobalt complexes[160]. This may be compared with 0.66 Å for model iron systems. As a result,

Hoard has proposed increased tension in the axial bond [191,353]. Nonetheless Co-Hb still exhibits significant homotropic and heterotropic effects[161,351]; in particular the Hill constant n for dioxygen-binding is ~2.3 [161,351] and could be as great as 2.5 [363].

This, and a number of other results described immediately below, has been interpreted as evidence against the stereochemical trigger for cooperativity being concentrated in the axial connection.

Lengthening of the $Co-N_{imid}$ bond in Co-deoxyHb caused by possible tension at the haem has not been detected using resonance Raman spectroscopy on Co-Hb, Co-Mb and model compounds[364,365]. Furthermore, resonance Raman studies on corresponding iron systems produced ambivalent results as regards the influence of the protein on porphyrin conformation[371]. Redox n values for manganese-substituted Hb are very similar to those for native Hb[366] yet manganese (and also cobalt) do not undergo the change in spin state that may be observed for iron.

Finally, the porphyrin (proto-, meso- and deutero- porphyrin-IX) exerts considerable influence on the Hill constant n for cooperative dioxygen binding to iron- and cobalthaemoglobins[351].

Thus, the importance of the metal's out-of-plane displacement and of the proximal histidine's movement in determining the cooperativity of ligation or oxidation has been questioned[160,162,370]. Changes in protohaem-globin contacts caused by transition of the protohaem from non-planar to a

planar geometry have been suggested as being more important [160,162,370]. The five-coordinate distorted trigonal-bipyramidal complex, Co(salen-C_2H_4-py), and its six-coordinate octahedral dioxygen adduct, Co(salen-C_2H_4-py)(O_2), provide an example, albeit a highly exaggerated one, of the conformational changes in the macrocyclic ligand system which may occur on oxygenation.

Perutz has established that deoxy-Co-Hb and met-Co-Hb (a model for Co-HbO_2) have the same quaternary structures as the corresponding native haemoglobin derivatives.[158] And noting that for the binding of dioxygen to Co-Hb the Hill coefficient was less than that for native Hb,[161,351] and that the free energy of haem-haem interaction was only 32% of that for stripped native Hb and 43% of that for native Hb (that is Hb in the presence of 2,3-DPG)[364,367], Perutz found the Co-Hb results consistent with his theory[158] that changes in the axial connection are more important. Perutz, in his original formulation of the stereochemical mechanism for cooperativity, noted the possibility that protohaem-globin interactions were a factor in promoting the tertiary structural changes in the protein[155].

5.3 Concluding Remarks

Detailed comparisons of the changes in stereochemistry at the protohaem on oxygenation with the corresponding changes for simpler model systems are not possible, although general trends are clear.

The analysis of Gelin and Karplus[370] indicates that the "trigger" of cooperativity effects on ligand binding may be associated more with changes in protohaem conformation than with changes in the axial connection. Perutz's stereochemical model is in no way disproved; there has merely been a change in emphasis with regard to the stereochemical "trigger" and the location of tension.

CHAPTER 6

BONDING IN END-ON COORDINATED DIOXYGEN COMPLEXES

The geometry of the metal-dioxygen linkage is now precisely established for 1:1 oxygen adducts of cobalt-Schiff base derivatives (§3.2).

For iron-dioxygen semiquantitative definition has been obtained (§4.2). Thus the way appears open for an analysis of the bonding through quantum-mechanical calculations. To date all such calculations have been semiquantitative and hence they have inherent bias through using the geometry of these complexes as input. There have also been a number of exotic proposals. A large number of qualitative molecular orbital and valence bond schemes have been proposed. While their usefulness for a given complex is doubtful, they have proved useful in rationalising the bonding of diatomic molecules (such as CO, NO and O_2) to transition metals such as cobalt, iron and manganese.

It is not proposed to analyse the various schemes in detail. The results will be briefly compared with each other and related to other data. In section 6.1 schemes for 1:1 angularly bonded cobalt-dioxygen complexes are discussed and in §6.2 those for iron-dioxygen systems.

6.1 Cobalt-Dioxygen Systems

The features of a number of semiquantitative and qualitative molecular orbital studies are summarised in Table 6.1. All schemes propose some transfer of electron density from the metal onto dioxygen. The scheme of Halton [339] is unlikely in the light of ^{17}O ESR studies on cobalt-substituted haemoglobin[213] and simpler cobalt-dioxygen species [117-121]. The more recent schemes of Fantucci and Valenti (FV)[340] and Dedieu, Rohmer and Veillard (DRV)[341,342] propose that there is little cobalt-dioxygen π bonding. Unfortunately neither scheme calculates ESR parameters for comparison with those observed for related complexes. The FV scheme indicates that unpaired electron density resides mainly on dioxygen with a small spin density of opposite sign in the cobalt $3d_{z^2}$ orbital. Orbital populations were not reported.

In the other study[342] orbital populations but not spin densities were reported. There are a number of interesting results. One unsuspected result was that the loss of electron density, which can be considered as loss of $3d_{z^2}$ electron density (Table 6.1), is partially counteracted by donation of electron density from the equatorial ligand. Secondly, the π-donor or -acceptor properties of the axial base appear to be of little importance. Thirdly, the change in electron density on the dioxygen ligand was found to be quite similar for a number of axial bases. These last two results may be merely a consequence of the inappropriate Co-L_{ax} separations used in the calculations, and the fixed Co-O_2 stereochemistry. Moreover, the 0.5$\bar{e}$ charge calculated for Co(acacen)(H_2O)(O_2)

Table 6.1: Summary of theoretical studies on the Co—O_2 linkage.

(a) Semiquantitative

Authors	System	Type of Calculation	Formulation	Comments
DKV [341,342]	Co(acacen)(L_{ax})(O_2) L_{ax} = none, OH_2, imid, CN^-, CO	(i) Ab initio LCAO-MO-SCF	$Co^{III}-O_2^-$ -0.03 / -0.23 / H_2O—Co—O 0.34 / -0.24 / O 0.16ē Change in electron distribution population d_{z^2} = 0.52	(i) Little Co-O_2 or Co-L_{ax} (L=imid,CN) π bonding. (ii) ē drift : acacen→Co→O_2, Substituents on acacen probably of importance. (iii) Relationship between calc. ΔH for oxygenation and ease oxidation Co^{II}→Co^{III} found. (iv) Bonding scheme similar to WMA's[121]. (v) Stability: bent>linear>>side-on.
FV [340]	Co(acacen)(NH_3)(O_2)	(i) MO-LCAO-INDO-UHF	0.3ē Co-O_2 spin density mostly on O_2(+1.08) small spin density:- Co(d_{z^2}) (-0.08)	(i) Bonding: mainly spin pairing Co(d_{z^2}) and $O_2(\pi^*)$. (ii) Little Co-O_2 π bonding. (iii) Spin density ratio O(3):O(4), + 0.44:+0.64 ~ similar to ESR studies (§3.2.1). (iv) Small spin density on Co(d_{z^2}) (-0.08).
H [339]	Cobalt-substituted oxyhaemoglobin	(i) SCC-EH-MO	formally $Co^{IV}-O_2^-$ -0.25 Co—O—O 0.44ē / 0.30 change in electron distribution. unpaired electron 25% 3d, 20% O_2, 55% - N_{porph}(!)	(i) Considerable σ + π bonding destroys formal valence. (ii) Spin density on N_{porph} in disagreement with ^{17}O ESR data (see text). (iii) Porphyrin, axial base grossly approximated. (iv) Predicts CbCO more stable than CbO_2.
TL [343]	$[Co(CN)_5(O_2)]^{3-}$	Fenske-Hall parameter-free MO	$Co^{III}-O_2^-$ Co—O 0.09ē / O 0.44ē 0.29 Co—O / O 0.29 for $[Co(PR_3)_4O_2]^+$	(i) Some π bonding, unpaired electron in orbital 10% $3d_{yz}$, 89% $\pi^*(O_2)$ (ii) Bond order calc. ~1.59. (iii) Linear structure excluded. (iv) Bent-bond favoured for $[Co(CN)_5O_2]^{3-}$ side-on bond favoured for $[Co(PR_3)_4O_2]^+$

(b) Qualitative

GO			$Co^{II}-O_2$	(i) Only Co-O_2 component considered. (ii) Spin-paired Co^{II}(S=½)-O_2(S=1) unpaired ē in $O_2(\pi^*)$ orbital.
FRR [344] CR [134(b)]			$sp^2(O_2) \overset{\sigma}{\leftrightarrow} d_{z^2}$ $\pi^*(O_2) \overset{\pi}{\leftrightarrow} d_{xz,yz}$	FRR postulate that:- π bonding Co-O_2 significant; orthogonality of py_π and Co-O_2 planes such that Co→O maximised and Co→L_{ax} minimised. However crystal structure analyses[123-125] indicate that packing constraints may dominate.
WMAE [121]			$\pi^*(O_2) \overset{\sigma}{\rightarrow} d_{z^2}$ unpaired ē in $\pi^*(O_2)$	(i) Little Co-O_2 π bonding. (ii) Rationalises existence and geometry of CO,NO,O_2 complexes of Fe and Co
HCT [345]			Avoids $Co^{II}-O_2/Co^{III}-O_2^-$ argument by consideration of $(MO_2)^n$ species where n is the sum of metal d and diatomic π* electrons; predicts angular d^7 Co-O_2.	

(a) Geometry Co-O_2 moiety taken from Co(bzacen)(py)(O_2) [126(a)]; Co-L_{ax} separation by analogy with related complexes.

appears to disagree with Tovrog, Kitko and Drago's calculated 0.1$\bar{e}$ transfer of electron density from cobalt onto dioxygen[19]. Assuming that the numbers calculated refer to an identical quantity, which appears reasonable, the difference is inexplicable.

The calculations of Teo and Li (TL)[343] indicate significant Co(d_{yz})-O_2(π^*) π bonding, in contrast to the FV and DRV schemes. The unpaired electron is in a molecular orbital with 3d character very similar to that calculated from the ^{59}Co hyperfine splitting[338] using the original analysis of Hoffman, Diemente and Basolo[62(a)]. As was discussed in §3.2, this analysis has been disputed[19]. TL calculated a bond order (1.59) very similar to that deduced from infrared data.

The semiquantitative calculations all assume, in part, the published parameters for Co(bzacen)(py)(O_2). Thus the sensitivity of the calculated orbital populations and orbital spin densities to the dimensions of the Co-O_2 moiety are unknown. Neither has the sensitivity to Co-L_{ax} separations been tested.

Discussion on the agreement of bonding schemes with structural data is somewhat hindered by the inevitable bias these calculations have. Nevertheless the structurally based arguments in favour of a $Co^{III}-O_2^-$ formulation, presented in §3.2.4, are in reasonable accord with the studies of DRV[342] and TL[343]. Unfortunately, these studies differ with respect to possible metal-dioxygen π bonding and hence the mechanism for the appearance of cobalt hyperfine structure in the ESR spectra of cobalt-dioxygen complexes.

6.2 Iron-dioxygen Systems

The features of a number of semiquantitative and qualitative bonding schemes are summarised in Table 6.2.

Although Pauling[68] predicted the geometry of the iron-dioxygen linkage in oxyhaemoglobin before the advent of a model compound, an O-O single bond is implicit in Pauling's formulation. As such an O-O separation of $\sim$1.46 Å may be expected. Notwithstanding the probable disorder of the bonded oxygen atom in the model compound Fe(TpivPP)(1-Me-imid)(O_2), the observed O-O separations of 1.17(4) Å and 1.15(4) Å appear incompatible with a proposed separation of that magnitude. In answer to Weiss' $Fe^{III}-O_2^-$ formulation[70], Pauling proposed[68(b)] that the "oxyhaemoglobin was properly described as containing ferrous ion rather than ferric...". This is despite the "51% of ionic character" in the iron-dioxygen bond which would apparently make the ferric ion description no less valid. These formulations differ with respect to the oxygen linkage; in the latter formulation the negative charge is not localised on the terminal oxygen atom. Pauling's formulation has been recast into molecular orbital terminology by Hoard[191].

Halton's postulation[346] that there is a two-electron donation from the protein to the iron appears to be excluded by the preparation of a model compound with no actual protein component. Another extended-Huckel calculation has also proposed considerable negative charge on the dioxygen ligand for both a formal $Fe^{II}-O_2$ and $Fe^{III}-O_2^-$ description[347]. Both such descriptions could explain the distinctive Mossbauer parameters of oxyhaemoglobin and its model.

Table 6.2: Summary of theoretical studies on the Fe—O_2 linkage.

Authors	System	Type of Calculation	Formulation		Comments
DRBV [349]	Fe(P)(NH_3)(O_2)	ab initio LCAO-SCF	Fe^{II}-O_2 electrically neutral	(i)	Quasi-neutral O_2
				(ii)	Appreciable d_π- $p\pi$ π bonding; charge distribution on Fe deviates from symmetrical $(d_{xy})^2(d_{xz})^2(d_{yz})^2$
				(iii)	Interaction with a distal NH_3 (≈hist) repulsive.
				(iv)	Stability bent Fe-O_2 >> side-on.
				(v)	Linear Fe-C≡O calculated.
GO [348]	Fe-O_2	ab initio	Fe^{II}-O_2 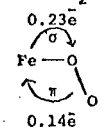	(i)	Only Fe-O_2 unit considered
				(ii)	Fe(S=1) $\frac{\sigma/\pi}{}$ O_2 (S=1) $(d_{z^2})^1 \frac{\sigma}{}$ $(p)^1$ $(d_{xz})^1 \frac{\pi}{}$ $(\pi)^1$ 3-centre 4ē bond as in O_3
				(iii)	Good agreement calc. and obs. Mossbauer parameters.
				(iv)	For Fe-O_2, triplet state 0.37eV (≈3,000cm^{-1}) above singlet g.s.
H [346] (see also Table 5.1H)	oxyhaemoglobin	SCC-EH-MO	"Fe^{II}-O_2^-" 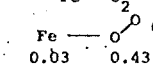 Change in electron density distribution	(i)	Considerable σ + π bonding destroys formal valence.
				(ii)	2ē donation from protein to iron(I).
				(iii)	Agreement between calc. and obs. Mossbauer parameters
				(iv)	Stability bent > side-on
				(v)	Porphyrin and axial base grossly approximated.
LK [347]		Iterative EH	"Fe^{II}-O_2" 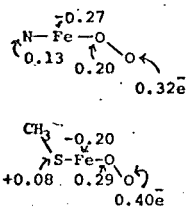	(i)	Little π character Fe-N_{imid} sig. π character Fe-S-CH_3 (P450) model)
				(ii)	Fe^{II}-O_2 and Fe^{III}-O_2^- config. explain Mossbauer
				(iii)	Considerable covalency in Fe-O_2 and Fe-N_{porph} bonds.
		(b) Qualitative[b]			
Griffith [67] Gray/Mingos [71,301]			Fe(O=O) covalent $Fe^{IV}(O_2)^{2-}$	))))))	O-O separation should be ∿1.46 Å (by analogy with other similar species. §2.2.3).
Weiss [70]			Fe^{III}-O_2^- iron(III)-coordinated superoxide		Spins $Fe^{III}d^5$(S=½) and O_2^-(S=½) "antiferromagnetically coupled".
Pauling [68]			Fe=O—O^- Fe^{II}-O_2		covalent O-O separation ∿1.46 Å expected
Harcourt [350]			Fe-O_2		geometry not specified "increased valence" 3 centre-4 electron bond. (similar to GO)
CR [134(b)]			Fe^{III}-O_2^-		Similar to Weiss
WMA					Little π bonding proposed

(a) L_{ax}-Fe-O_2 geometry from Fe(TpivPP)(1-Me-imid)(O_2) assumed. (b) See also Table 6.1.

On the other hand, it was proposed in two more recent studies that the dioxygen ligand is quasi-neutral[348,349]. Appreciable iron-dioxygen π bonding is calculated in all schemes. This may be merely an inevitable consequence of using the short Fe-O bond apparently observed in the model compound Fe(TpivPP)(1-Me-imid)(O_2) (§4.2).

In the model of Dedieu, Rohmer, Benard and Veillard DRBV[349] the distinctive Mossbauer parameters may be qualitatively rationalised by noting that a significant deviation of the iron atom from a symmetric low-spin ferrous configuration $(d_{xz,yz,xy})^6$ is calculated. In terms of the calculated orbital populations, however, this configuration is more appropriate than any other.

On the other hand, Harcourt[350] and, more recently, Goddard and Olafson[348], in a more quantitative manner, have suggested an alternative valence bond approach. The latter workers appear oblivious to Harcourt's earlier qualitative analysis. Both propose that the approach of dioxygen to the iron forces the iron to adopt a triplet state

$$(d_{xy})^2(d_{xz})^2(d_{yz})^1(d_z2)^1,$$

rather than the more usually assumed singlet state.

$$(d_{xy})^2(d_{xz})^2(d_{yz})^2.$$

Spin pairing of the metal and dioxygen electrons occurs through an $Fe(3d_z2)^1-O_2(p_z)^1$ σ bond and through a three-centre four-electron π bond involving $Fe(3d_{xz})^1$ and $O_2(\pi)^3$ orbitals - a bonding scheme which is analogous to that for ozone. The latter type of bond is responsible for the name "increased valence"[350]. This model reproduces the Mossbauer parameters for oxyhaemoglobin. It also predicts a relatively low-lying

triplet state about 0.37 ev, or approximately 3000cm^{-1}, above the singlet ground-state[348]. However, this separation is considerably higher than that deduced from magnetic susceptibility measurements (~146 cm^{-1}) [330]. Unfortunately, the singlet-triplet energy separation for the DRBV model is not reported[349].

It is claimed[348] that dioxygen maintains its ground state properties more so than in the bonding models of Pauling[68], Weiss[70], and also Gray[71] and Mingos[301]. A similar non-polar linkage for the cobalt-dioxygen bond is qualitatively proposed [348]. This would appear to contradict a mass of physical evidence all supporting a polarised cobalt-dioxygen bond. Moreover, the premise that retention of triplet ground-state character for dioxygen facilitates its rapid uptake and release is doubtful. Despite the lower affinity of cobalt-substituted haemoglobin (Cb) for dioxygen[351] and despite the polarised Co-O_2 bond, for Cb compared to Hb the rate of oxygen uptake is very similar and the rate of oxygen release is 100 times faster[352].

6.3 Concluding Remarks

In part, the theoretical studies on cobalt-dioxygen systems do not contradict the other studies (described in §3.2) which indicate a cobalt → dioxygen electron transfer. But the importance of π bonding and hence the origin of ^{59}Co hyperfine splitting is unclear.

From most, but not all, theoretical studies on the iron-dioxygen linkage an essentially neutral dioxygen ligand is

proposed. All studies postulate significant π bonding. But the magnetic susceptibility studies of oxyhaemoglobin[330] indicate weak π bonding, while some other studies indicate a polarised Fe-O_2 bond.

More sophisticated models for the bonding of metal-dioxygen complexes therefore appear to be essential since the theoretical studies have to date done little to clarify the nature of the metal-dioxygen component.

APPENDIX 1

The general experimental procedures common to all the single crystal X-ray diffraction structure analyses performed in this work will be described. Since the procedures adopted are well documented[372-375] and in general practice elsewhere only a brief summary will be provided. Important features of the course of structure solution for the various structures are detailed in the appropriate chapter.

Preliminary Crystallographic Characterisation

Precession photography using Cu Kα X-radiation was used to establish space groups and to obtain preliminary unit cell dimensions. Possible crystals for data collection were mounted randomly with respect to lattice axes to minimise the incidence of multiple reflections (Renninger effects). Crystal densities, where determined, were obtained by flotation in suitable liquid mixtures followed by weighing of the solution and then distilled water in a density bottle.

Data Collection

An Hilger and Watts four-circle computer-controlled diffractometer was used for the precise determination of unit cell dimensions and the collection of intensity data. Unit cell parameters and crystal orientation were determined by least-squares refinement of the setting angles of twelve reflections accurately centred in a 5 mm diffracted beam collimator the receiving aperture of which was 230 mm from

the crystal. If the agreement between the calculated and observed setting angles differed by more than 0.04^{o} the setting angles were redetermined.

Crystal mosaicity was examined using open-counter ω scans at a take-off angle of 3^{o}. Intensity data were collected using the θ-2θ scan technique. The scan range was symmetrical about the calculated peak position, and stationary crystal, stationary counter background counts were recorded at each end of the scan. Three reflections well-separated in reciprocal space were measured periodically to monitor possible crystal decomposition, crystal movement and fluctuations in beam intensity. Scale factors were derived to place the data on the same relative scale.

Data Reduction

Data processing and subsequent structure analysis were carried out using a Burroughs B6718 computer. The data processing program HILGOUT was based on DRED (J. F. Blount) and PICKOUT (R. J. Doedens). The integrated intensity is given by

$$I = S - 0.5\ (t_S/t_B)(B_1 + B_2)$$

where S is the scan count, B, and B_2 the two background counts and t_S and t_B the scan and background times, respectively. The estimated standard deviation of each intensity was assigned[376] as

$$\sigma_I = [S+0.25(t_S/t_B)^2(B_1+B_2) + (pI)^2]^{\frac{1}{2}}$$

where p is an empirical factor introduced to prevent overweighting of intense reflections during least-squares refinements. Scale factors and Lorentz and polarisation factors

were applied to give correct relative intensities and their e.s.d.'s, F_o^2 and $\sigma_{F_o^2}$, respectively. The following relationship was found useful in deriving new values for $\sigma_{F_o^2}$ when changes in the p-factor were required (see below)

$$(\sigma_{F_o^2}^{new})^2 = (\sigma_{F_o^2}^{old})^2 + (F_o^2)^2 \left[(p^{new})^2 - (p^{old})^2\right].$$

Program DABS, a modified version of DATAPH (P. Coppens), was used to correct for absorption effects by Gaussian integration.

Fourier Summations

Program Fourier, based on FORDAP (A. Zalkin) and including a shaded density plotting option (D. L. Evans), was used for calculating (i) Patterson syntheses

$$P(u,v,w,) = \frac{1}{V} \sum_{hkl}\sum\sum |F_o(hkl)|^2 \cos 2\pi(hu+kv+lw)$$

where V is the unit cell volume, (ii) difference Fourier syntheses

$$\Delta\rho(x,y,z,) = \frac{1}{V} \sum_{hkl}\sum\sum (|F_o| - |F_c|) \exp(-2\pi i(hx+ky+lz-\alpha_c))$$

where α_c is the phase angle and F_c the structure factor computed from the trial structure, and (iii) F_{obs} Fourier syntheses

$$\rho(x,y,z) = \frac{1}{V} \sum_{hkl}\sum\sum |F_o| \exp(-2\pi i(hx+ky+lz-\alpha_c)).$$

Patterson syntheses were used in the conventional manner to obtain positions for the heavy atoms in the unit cells. Difference and F_{obs} Fourier syntheses were used to develop the trial structure. In the early stages of structure elucidation, when phasing of F_c by the trial model was poor, an empirical weighting scheme was used; reflections for which

$$|F_c|/|F_o| < 0.33$$

were given zero weight in Fourier syntheses.

Program FOURIER was also used to calculate E-maps from E-values for which phases had been derived (see below under Direct Methods).

Fourier summations calculated over sections that were not parallel to a plane defined by the crystal axes involved a transformation and reintegerisation of the indices of structure factors. Consequently spurious features and distortions may be expected in such maps.

Direct Methods

Normalised structure factors (E-values) and E-statistics were calculated using program SHNORM which was derived from NRC-4 (S. R. Hall and F. R. Ahmed). Program SAP, applicable only to centrosymmetric space groups, was used to derive signs for the E-values. It employed the Sayre relationship together with assumed phases for three reflections to phase E-values by a "bootstrapping" process. Program MULTAN (P. Main, M. M. Woolfson and G. Germain) was used to obtain sets of phased E-values for one structure. Because successful solution of the structure was not achieved using MULTAN, this program will not be described further. The structure in question was successfully solved, eventually, by conventional Patterson methods.

Structure Factor Calculations and Least-squares Refinements

These calculations were performed by program CUCLS, a highly modified version of ORFLS (W. R. Busing, K. O. Martin and H. A. Levy, ORNL-TM-305, 1962). Expansion and optimisation of the standard program (176 variable parameters) to cater for 360 variable parameters was achieved in association with Dr. A. L. Wilkinson of the University of Canterbury Computing Centre.

The general expression for the structure factor is

$$F_c(\bar{r}) = \sum_{j=1}^{N} f_j(\bar{r}) T_j(\bar{r}) \exp(2\pi i \bar{r}\underset{\sim}{r}),$$

where f_j, the atomic scatting factor, and T_j, an expression of the thermal motion of atom j, are functions of $\bar{r}$, the reciprocal space or diffraction vector; $\underset{\sim}{r}_j$ is the real (crystal) space vector of atom j. The summation is over all atoms in the unit cell.

Full matrix least-squares refinements were based on F and the function minimised was

$$\sum w(|F_o| - |F_c|)^2.$$

The weights w were assigned as

$$w = 4F_o^2/\sigma_{F_o^2}$$

The agreement factors were defined as

$$R = \sum ||F_o| - |F_c|| / \sum |F_o|$$

and

$$R_w = (\sum w(|F_o| - |F_c|)^2 / \sum w|F_o|^2)^{\frac{1}{2}}$$

Atomic scattering factor tables ($f_j(\bar{r})$) were taken from Cromer and Mann[377]. The effects of anomalous dispersion

$$f_j(\bar{r}) = f_j^o(\bar{r}) + \Delta f_j'(\bar{r}) + \Delta f_j''(\bar{r})$$

were included in F_c [378] using Cromer's values[379] for $\Delta f'$ and $\Delta f''$.

Rigid group orientation is as described by R. J. Doedens[380].

When the structural model was essentially complete and prior to the final refinements of the model, program SORTLIST was used to test the dependence of the minimised function on the magnitude of the structure factors $|F_o|$ and on $\sin\theta/\lambda$. Weights w were adjusted, if necessary, so as to reduce or eliminate this dependency.

Analysis of the Structure

Bond distances and angles, and molecular and unit cell diagrams were obtained using ORTEP-II (C. K. Johnson, ORNL-3794, 2nd revision 1970). Bond lengths and angles, RMS components of thermal displacements together with their e.s.d's, and bond lengths corrected for riding motion were calculated using CORFFE a local adaptation of ORFFE (W. R. Busing, K. O. Martin and H. A. Levy, ORNL-TM-306, 1964). Least-squares planes, displacements of atoms therefrom and dihedral angles between planes were calculated using MEAN PLANE (M. E. Pippy, F. R. Ahmed, NRC-22,1967). Torsional angles were calculated using program GEOM (F. C. March).

A useful test on the quality of the final model with respect to $|F_o|$ and $|F_c|$ was derived. The number of reflections lying outside the range

$$I - 3\sigma_I \leq I_c \leq I + 3\sigma_I,$$

where I_c is the calculated raw intensity, should be small in comparison to the total number of reflections.

Tables of calculated and observed structure factor amplitudes follow.

Table A1: Calculated and observed structure factors for all data for Fe(salen-C_2H_4-py).

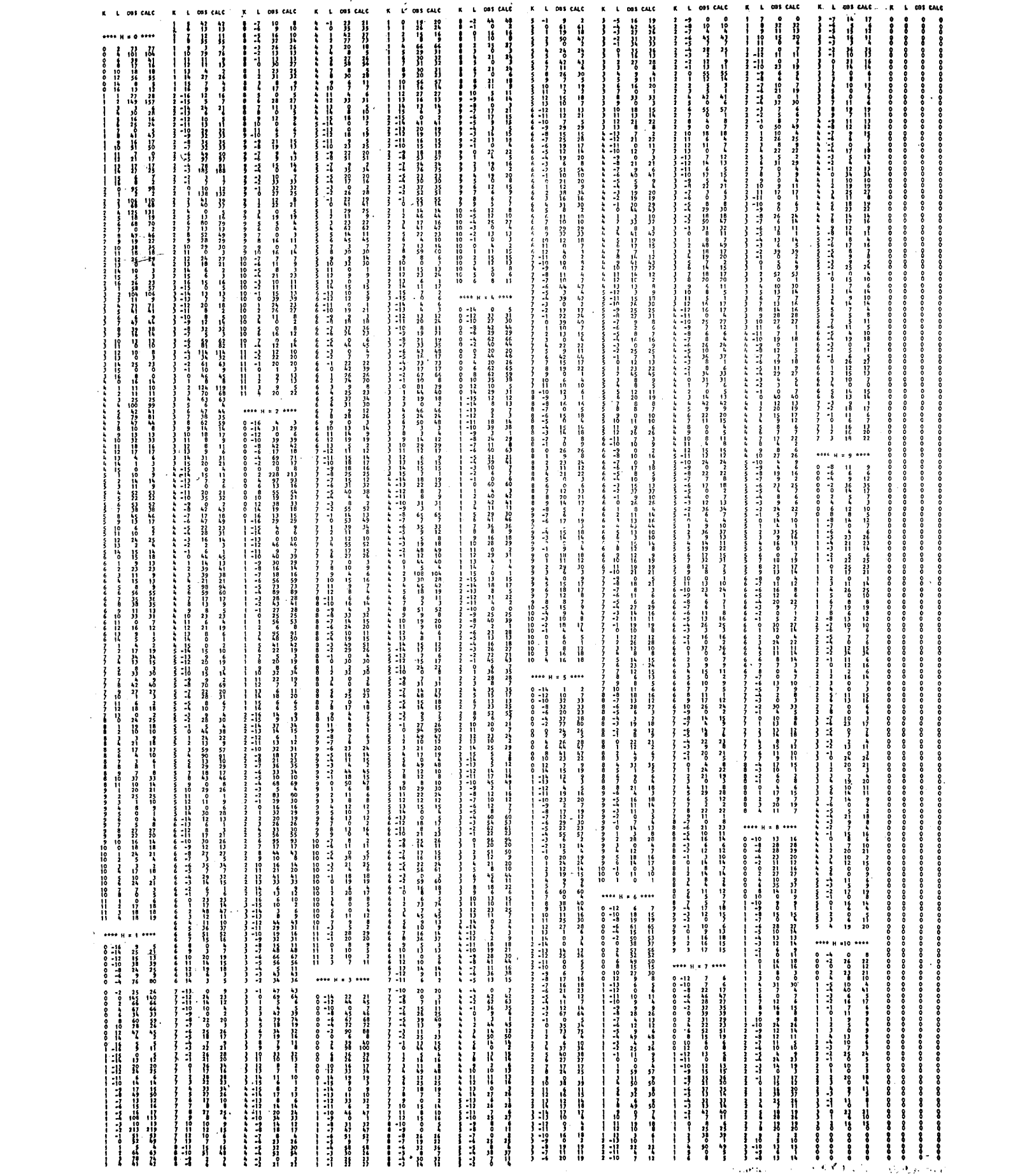

Table A2: Calculated and observed structure factors for all data for [Co(salen-C_2H_4-py)(O_2)].CH_3CN.

K	L	OBS	CALC

**** H = 0 ****

0	2	109	116
0	4	142	136
0	6	94	89
0	8	42	47
0	10	44	44
1	1	9	11
1	3	192	184
1	5	150	150
1	7	8	6
1	9	166	127
1	11	157	142
2	0	77	76
2	2	60	63
2	4	57	60
2	6	34	34
2	8	24	28
2	10	8	8
3	1	86	85
3	3	118	118
3	5	66	64
3	7	47	43
3	9	37	32
3	11	46	37
4	0	68	66
4	2	47	47
4	4	33	33
4	6	25	24
4	8	22	23
4	10	7	7
5	1	119	115
5	3	91	90
5	5	34	34
5	7	24	28
5	9	18	17
6	0	9	8
6	2	80	79
6	4	66	65
6	6	47	43
6	8	32	32
6	10	18	15
7	1	85	91
7	3	55	52
7	5	36	36
7	7	23	20
7	9	16	13
8	0	9	8
8	2	42	40
8	4	31	31
8	6	21	21
8	8	15	15
8	10	0	7
9	1	49	51
9	3	43	41
9	5	30	30
9	7	21	16
9	9	12	11
10	0	8	6
10	2	27	26
10	4	24	24
10	6	17	16
10	8	12	12
11	1	37	37
11	3	20	18
11	5	13	12
11	7	8	8
11	9	5	5
12	0	5	5
12	2	18	18
12	4	14	14
12	6	10	10
12	8	7	7
13	1	20	20
13	3	14	14
13	5	10	10
13	7	7	7
14	0	5	5
14	2	12	12
14	4	9	9
14	6	7	7
15	1	10	10
15	3	8	8
15	5	6	6
16	0	5	5
16	2	9	9
16	4	7	7
17	1	8	8
17	3	6	6
18	0	5	5
18	2	7	7
19	1	6	6
19	3	5	5
20	0	4	4
20	2	6	6
21	1	5	5
21	3	4	4
22	0	3	3
22	2	5	5
23	1	4	4
23	3	3	3
24	0	2	2
24	2	4	4
25	1	3	3
25	3	2	2
26	0	1	1
26	2	3	3
27	1	2	2
27	3	1	1
28	0	0	0
28	2	2	2
29	1	1	1
29	3	0	0

**** H = 1 ****

0	-10	0	6
0	-8	44	41
0	-6	69	69
0	-4	94	93
0	-2	37	42
0	0	98	102
0	2	22	26
0	4	23	23
0	6	13	12
0	8	5	5
0	10	0	0
1	-11	19	13
1	-9	73	73
1	-7	25	23
1	-5	61	63
1	-3	38	38
1	-1	73	70
1	1	25	25
1	3	25	25
1	5	25	28
1	7	18	18
1	9	9	9
1	11	0	0
2	-10	9	14
2	-8	24	18
2	-6	0	0
2	-4	77	76
2	-2	36	39
2	0	77	75
2	2	60	61
2	4	43	44
2	6	28	28
2	8	16	16
2	10	7	7
3	-11	39	32
3	-9	73	73
3	-7	21	29
3	-5	69	67
3	-3	0	6
3	-1	77	73
3	1	36	36
3	3	0	13
3	5	25	24
3	7	28	28
3	9	10	10
3	11	0	0
4	-10	0	7
4	-8	29	26
4	-6	0	0
4	-4	62	67
4	-2	61	61
4	0	43	41
4	2	0	0
4	4	29	26
4	6	26	28
4	8	20	20
4	10	0	0
5	-11	0	0
5	-9	54	51
5	-7	43	46
5	-5	38	34
5	-3	73	73
5	-1	94	96
5	1	38	38
5	3	100	111
5	5	38	35
5	7	20	20
5	9	11	11
5	11	0	2
6	-10	0	4
6	-8	39	44
6	-6	0	0
6	-4	47	46
6	-2	37	31
6	0	98	105
6	2	40	39
6	4	32	32
6	6	28	31
6	8	21	21
6	10	0	4
7	-11	0	0
7	-9	0	0
7	-7	0	0
7	-5	0	0
7	-3	0	0
7	-1	0	0
7	1	0	0
7	3	0	0
7	5	0	0
7	7	0	0
7	9	0	0
7	11	0	0
8	-10	0	0
8	-8	0	0
8	-6	0	0
8	-4	0	0
8	-2	0	0
8	0	0	0
8	2	0	0
8	4	0	0
8	6	0	0
8	8	0	0
8	10	0	0
9	-11	0	0
9	-9	0	0
9	-7	0	0
9	-5	0	0
9	-3	0	0
9	-1	0	0
9	1	0	0
9	3	0	0
9	5	0	0
9	7	0	0
9	9	0	0
9	11	0	0
10	-10	0	0
10	-8	0	0
10	-6	0	0
10	-4	0	0
10	-2	0	0
10	0	0	0
10	2	0	0
10	4	0	0
10	6	0	0
10	8	0	0
10	10	0	0
11	-11	0	0
11	-9	0	0
11	-7	0	0
11	-5	0	0
11	-3	0	0
11	-1	0	0
11	1	0	0
11	3	0	0
11	5	0	0
11	7	0	0
11	9	0	0
11	11	0	0
12	-10	0	0
12	-8	0	0
12	-6	0	0
12	-4	0	0
12	-2	0	0
12	0	0	0
12	2	0	0
12	4	0	0
12	6	0	0
12	8	0	0
12	10	0	0
13	-11	0	0
13	-9	0	0
13	-7	0	0
13	-5	0	0
13	-3	0	0
13	-1	0	0
13	1	0	0
13	3	0	0
13	5	0	0
13	7	0	0
13	9	0	0
13	11	0	0
14	-10	0	0
14	-8	0	0
14	-6	0	0
14	-4	0	0
14	-2	0	0
14	0	0	0
14	2	0	0
14	4	0	0
14	6	0	0
14	8	0	0
14	10	0	0
15	-11	0	0
15	-9	0	0
15	-7	0	0
15	-5	0	0
15	-3	0	0
15	-1	0	0
15	1	0	0
15	3	0	0
15	5	0	0
15	7	0	0
15	9	0	0
15	11	0	0
16	-10	0	0
16	-8	0	0
16	-6	0	0
16	-4	0	0
16	-2	0	0
16	0	0	0
16	2	0	0
16	4	0	0
16	6	0	0
16	8	0	0
16	10	0	0
17	-11	0	0
17	-9	0	0
17	-7	0	0
17	-5	0	0
17	-3	0	0
17	-1	0	0
17	1	0	0
17	3	0	0
17	5	0	0
17	7	0	0
17	9	0	0
17	11	0	0
18	-10	0	0
18	-8	0	0
18	-6	0	0
18	-4	0	0
18	-2	0	0
18	0	0	0
18	2	0	0
18	4	0	0
18	6	0	0
18	8	0	0
18	10	0	0
19	-11	0	0
19	-9	0	0
19	-7	0	0
19	-5	0	0
19	-3	0	0
19	-1	0	0
19	1	0	0
19	3	0	0
19	5	0	0
19	7	0	0
19	9	0	0
19	11	0	0
20	-10	0	0
20	-8	0	0
20	-6	0	0
20	-4	0	0
20	-2	0	0
20	0	0	0
20	2	0	0
20	4	0	0
20	6	0	0
20	8	0	0
20	10	0	0
21	-11	0	0
21	-9	0	0
21	-7	0	0
21	-5	0	0
21	-3	0	0
21	-1	0	0
21	1	0	0
21	3	0	0
21	5	0	0
21	7	0	0
21	9	0	0
21	11	0	0
22	-10	0	0
22	-8	0	0
22	-6	0	0
22	-4	0	0
22	-2	0	0
22	0	0	0
22	2	0	0
22	4	0	0
22	6	0	0
22	8	0	0
22	10	0	0
23	-11	0	0
23	-9	0	0
23	-7	0	0
23	-5	0	0
23	-3	0	0
23	-1	0	0
23	1	0	0
23	3	0	0
23	5	0	0
23	7	0	0
23	9	0	0
23	11	0	0
24	-10	0	0
24	-8	0	0
24	-6	0	0
24	-4	0	0
24	-2	0	0
24	0	0	0
24	2	0	0
24	4	0	0
24	6	0	0
24	8	0	0
24	10	0	0
25	-11	0	0
25	-9	0	0
25	-7	0	0
25	-5	0	0
25	-3	0	0
25	-1	0	0
25	1	0	0
25	3	0	0
25	5	0	0
25	7	0	0
25	9	0	0
25	11	0	0
26	-10	0	0
26	-8	0	0
26	-6	0	0
26	-4	0	0
26	-2	0	0
26	0	0	0
26	2	0	0
26	4	0	0
26	6	0	0
26	8	0	0
26	10	0	0
27	-11	0	0
27	-9	0	0
27	-7	0	0
27	-5	0	0
27	-3	0	0
27	-1	0	0
27	1	0	0
27	3	0	0
27	5	0	0
27	7	0	0
27	9	0	0
27	11	0	0
28	-10	0	0
28	-8	0	0
28	-6	0	0
28	-4	0	0
28	-2	0	0
28	0	0	0
28	2	0	0
28	4	0	0
28	6	0	0
28	8	0	0
28	10	0	0
29	-11	0	0
29	-9	0	0
29	-7	0	0
29	-5	0	0
29	-3	0	0
29	-1	0	0
29	1	0	0
29	3	0	0
29	5	0	0
29	7	0	0
29	9	0	0
29	11	0	0

Table A3: Calculated and observed structure factors for all data for [Fe(TpivPP)-(1-Me-imid)(O_2)]·½(C_6H_6)·½($C_4N_2H_6$).

Table A4: Calculated and observed structure factors for all data for [Fe(TpivPP)-(THT)(O_2)]·$(THT)_2$.

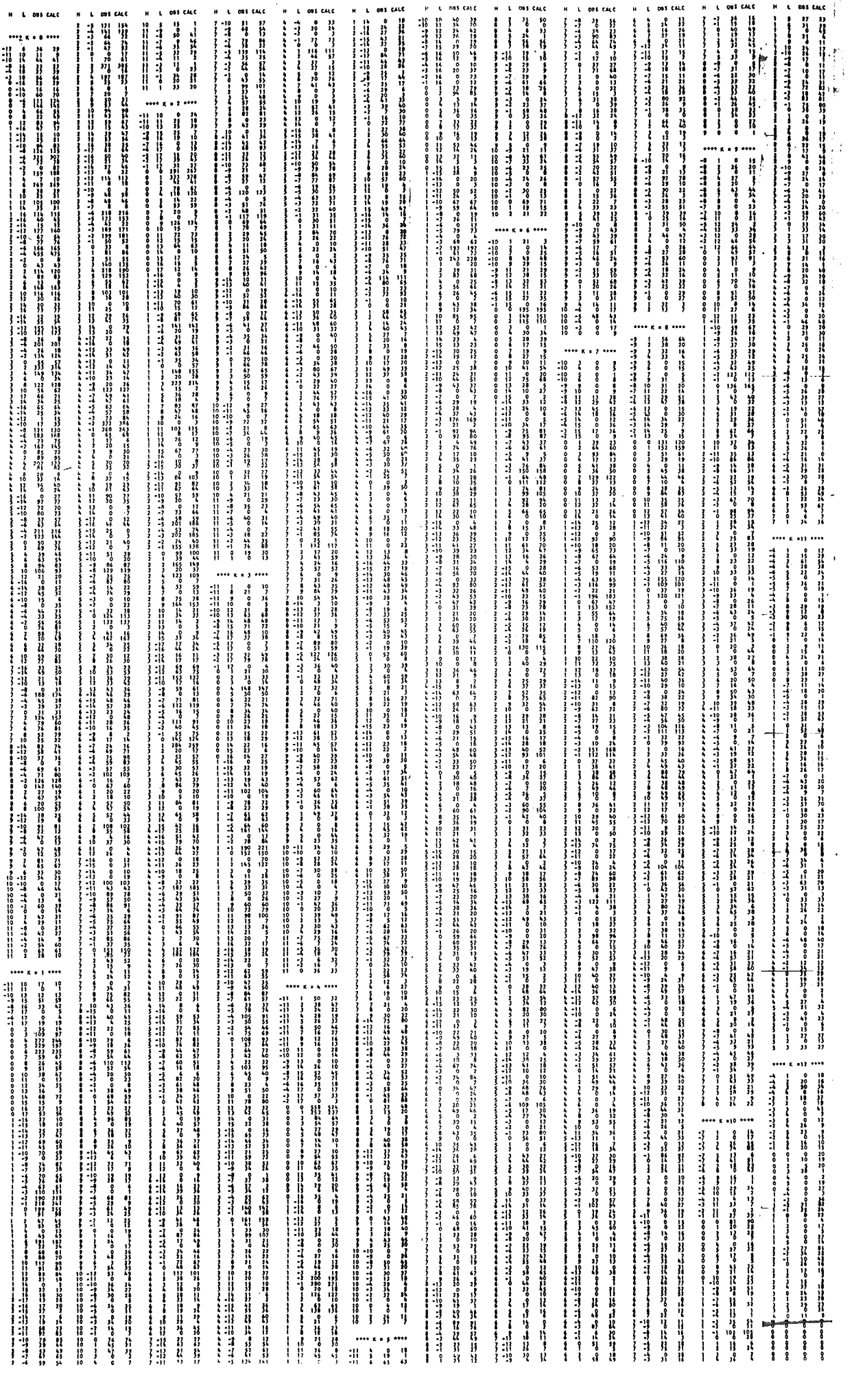

Table A5: Calculated and observed structure factors for all data for polymeric-$[Fe(TpivPP)(OH_2)]\cdot THT$.

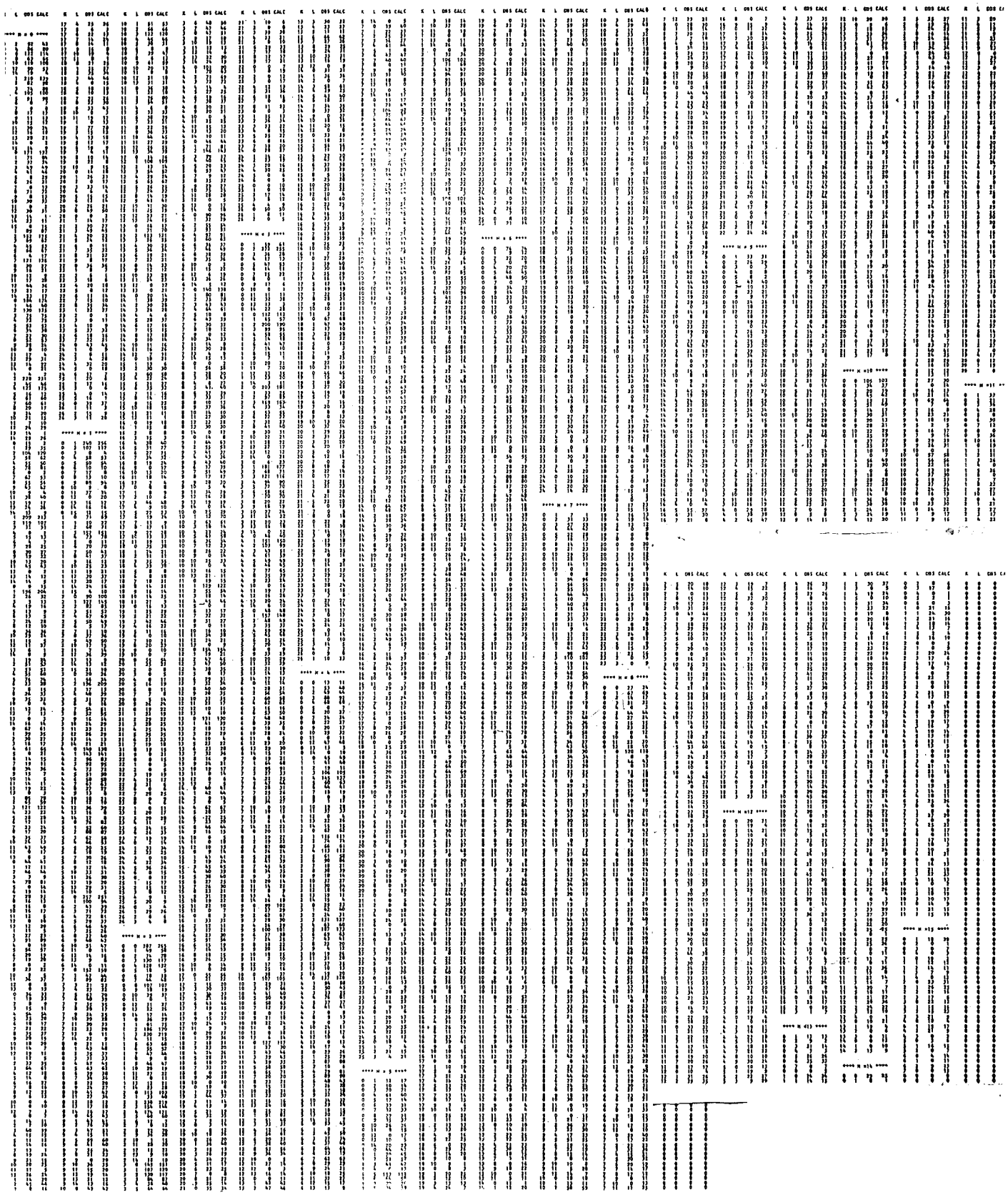

REFERENCES

(1) H. R. Mahler, F. H. Cordes, "Biological Chemistry", Harper and Row, New York and London, 1966.

(2) I. C. Gunsalus, J. R. Meeks, J. D. Lipscomb, P. Debrunner and E. Munck in "Molecular Mechanisms of Oxygen Activation", O. Hayaishi, ed., Academic Press N.Y. 1974.

(3) T. G. Spiro, Acc. Chem. Res., 7,337(1974); and references therein. Resonance Raman spectroscopy : a new structure probe for biological chromophores.

(4) (a) D. E. Sayers, E. A. Stern, F. W. Little, Phys. Rev. Lett., 27, 1204 (1971).
New techniques for investigating non-crystalline structures. Fourier analysis of the extended X-ray absorption fine structure.
(b) E. A. Stern, Phys. Rev. B, 10, 3027 (1974).
Theory of extended X-ray absorption fine structure.

(5) C. A. Ashley, S. Doniach, Phys. Rev. B, 11, 1279 (1975).
Theory of extended X-ray absorption fine structure (EXAFS) in crystalline solids.

(6) P. A. Lee, J. B. Pendry, Phys. Rev. B, 11, 2795 (1975).
Theory of extended X-ray absorption fine structure.

(7) B. M. Kincaid, P. Eisenberger, Phys. Rev. Lett., 34, 1361 (1975).
Synchrotron radiation studies of the K-edge photoabsorption of Kr Br_2 and $GeCl_4$. A comparison of theory and experiment.

(8) P. J. Stephens, J. Chem. Phys., 52, 3489 (1970).
Theory of magnetic circular dichroism.

(9) J. P. Collman, H. Takaya, B. Winkler, L. Libit, Seah San Koon, G. A. Rodley, W. T. Robinson, J. Am. Chem. Soc., 95, 1656 (1973)
General syntheses for new pentadentate ligands. Crystal structure of α,α'-{2-(2'-pyridyl)ethyl}ethylenebis(salicylideniminato)cobalt(II)-ethanol.

(10) G. A. Rodley, W. T. Robinson, Syn. Inorg. Met. Org. Chem. 3, 387 (1973).
High pressure preparation of crystalline 1:1 cobalt-dioxygen complexes.

(11) J. P. Collman, R. R. Gagne, C. A. Reed, W. T. Robinson, G. A. Rodley, Proc. Nat. Acad. Sci. U.S.A., 71, 1326 (1974).
Structure of an iron(II)-dioxygen complex: a model for oxygen-carrying haemoproteins.

(12) J. P. Collman, R. R. Gagne, C. A. Reed, T. R. Halbert, G. Lang, W. T. Robinson, J. Am. Chem. Soc., 97, 1427 (1975); and references therein.
"Picket fence porphyrins." Synthetic models for oxygen binding haemoproteins.

(13) L. Vaska, Acc. Chem. Res., 9, 175 (1976).
Dioxygen-metal complexes : towards a unified view.

(14) J. P. Collman, R. R. Gagne, H. B. Gray, J. W. Hare, J. Am. Chem. Soc., 96, 6522 (1974).
A low temperature infra-red spectral study of iron(II) dioxygen complexes derived from a picket fence porphyrin.
These results have been shown to be artefactual[17].

(15) B. S. Tovrog, R. S. Drago, J. Am. Chem. Soc., 96, 6765 (1974).
Evidence against O_2^- formulation of Co(II) adducts of Dioxygen.
The cobalt-carbon monoxide adduct has been shown to be artefactual due to inadequate exclusion of dioxygen[18].

(16) (a) R. Mason, Nature, 217, 543 (1968).
Activation of small molecules by transition metal ions and their complexes.
(b) R. Mason, Chem. Soc. Rev. 1, 431 (1972).
Valence in transition metal complexes.

(17) J. P. Collman, J. I. Brauman, T. R. Halpert, K. S. Suslick, Proc. Nat. Acad. Sci. U.S.A., 73, 3333 (1976).
The nature of O_2 and CO binding to metalloporphyrins and other haem proteins.

(18) B. M. Hoffman, T. Szymanski, F. Basolo, J. Am. Chem. Soc., 97, 673, (1975).
Consideration of a report on the formulation of monomeric cobalt-dioxygen adducts. Continued support for $Co^{III}-O_2^-$.

(19) B. S. Tovrog, D. J. Kitko, R. S. Drago, J. Am. Chem. Soc., 98, 5144 (1976).
Nature of bound O_2 in a series of cobalt dioxygen adducts.

(20) L. H. Vogt Jr., H. M. Faigenbanm, S. E. Wiberley, Chem. Rev., 63, 269 (1963).
Synthetic reversible dioxygen-carrying chelates.

(21) J. A. Connor, E. A. V. Ebsworth, Adv. Inorg. Chem. Radiochem., 6, 279 (1964); and references therein.
Peroxy compounds of transition metals.

(22) E. Bayer, P. Stretzman, Struct. Bonding, 2, 181 (1967). Ger.
Reversible oxygenation of metal complexes.

(23) A. G. Sykes, J. A. Weil, Prog. Inorg. Chem., 13, 1 (1970).
The formation, structure and reactions of binuclear complexes of cobalt.

(24) R. G. Wilkins, Adv. Chem. Ser., No.100, 111 (1971).
Uptake of oxygen by cobalt(II) complexes in solution.

(25) V. J. Choy, C. J. O'Connor, Coord. Chem. Rev., 9, 145 (1972/73).
Chelating dioxygen compounds of the platinum metals.

(26) L. Klevan, J. Peone Jr., S. K. Madan, J. Chem. Educ., 50, 670 (1973).
Molecular oxygen adducts of transition metal complexes. Structure and mechanism.

(27) J. S. Valentine, Chem. Rev., 73, 235 (1973); and references therein.
The dioxygen ligand in mononuclear group VIII transition metal complexes.

(28) G. Henrici-Olive, S. Olive, Angew. Chem. Int. Ed. Engl., 13, 29 (1974).
Activation of molecular oxygen.

(29) G. McLendon, A. E. Martell, Coord. Chem. Rev., 19, 1 (1976).
Inorganic oxygen carriers as models for biological systems.

(30) H. D. Babcock, L. Herzberg, Astrophys J., 108, 167 (1948).
Fine structure of the red system of atmospheric oxygen bands.

(31) L. Herzberg, G. Herzberg, Astrophys. J., 105, 353 (1947).
Fine structure of the infrared atmospheric oxygen band.

(32) P. H. Krupenie, J. Phys. Chem. Ref. Data, 1, 423 (1972); and references therein.
The spectrum of molecular oxygen.

(33) S. C. Abrahams, J. Kalnajs, Acta Cryst., 8, 503 (1955).
The crystal structure of α-potassium superoxide.

(34) D. H. Templeton, C. H. Dauber, J. Am. Chem. Soc., 72, 2251 (1950).
The crystal structure of sodium superoxide.

(35) G. S. Zhadanov, Z. V. Zvonkova, Doklady Acad. Nauk. S.S.R., 82, 743 (1952), Russ.; Chem. Abs. 46, 4893h (1953).

(36) F. Halverson, J. Phys. Cham. Solids, 23, 207 (1962).
Comments on the potassium superoxide structure.

(37) R. J. Celotta, R. A. Bennett, J. L. Hall, M. W. Siegel, J. Levine, Phys. Rev. A, 6, 631 (1972).
Molecular photodetachment spectrometry.II. The electron affinity of O_2 and the structure of O_2^-.

(38) M. J. W. Boness, G. J. Schulz, Phys. Rev. A, 2, 2182 (1970).
Structure of O_2.

(39) R. J. Blint, M. D. Newton, J. Chem. Phys., 59, 6220 (1973).
Abinitio studies of interoxygen bonding in O_2, HO_2, H_2O_2, O_3, HO_3 and H_2O_3.

(40) F. J. Blunt, P. J. Hendra, J. R. Mackenzie, J.C.S. Chem. Comm., 278 (1969).
Laser Raman spectra of salts containing O_2^- and O_2^{2-}.

(41) W. Holzer, W. F. Murray, H. J. Bernstein, J. Mol. Spect., 26, 543 (1968).
Raman spectra of O_2^- ion in alkali halide crystals.

(42) M. E. Jacox, D. E. Milligan, J. Mol. Spect., 42, 495 (1972).
Spectrum and structure of the HO_2 free radical.

(43) R. L. Redington, W. P. Olson, P. C. Cross, J. Chem. Phys., 36, 1311 (1962).
Studies of hydrogen peroxide : the infrared spectrum and the internal rotation problem.

(44) W. R. Busing, H. A. Levy, J. Chem. Phys., 42, 3054 (1965).
Crystal and molecular structure of hydrogen peroxide : a neutron diffraction study.

(45) S. C. Abrahams, Quart. Rev., 10, 407 (1955).
The stereochemistry of subgroup VIIb of the periodic table.

(46) N.-G. Vannerberg, Prog. Inorg. Chem., 4, 125 (1962).
Peroxides, superoxides and ozonides of metals of groups Ia, IIa and IIb.

(47) J. C. Evans, J.C.S. Chem. Comm., 682 (1969).

(48) Value quoted in reference [12] from H. Siebert, "Schwingungs Spektroskopie in der Anorganischen Chemie ", Springer-Verlag, Berlin, 1966.

(49) H. H. Eysel, S. Thym, Z. Anorg. Allg. Chem., 411, 97 (1975).
Raman spectra of peroxides.

(50) E. Fremy, Liebigs Ann. Chem., 83, 227, (1852). Ger.

(51) A. Werner, Liebigs Ann. Chem., 375, 1 (1910), Ger.
Polynuclear metal-ammonias.

(52) K. Gleu, K. Rehm, Z. Anorg. Chem., 237, 79 (1938).
The constitution of green peroxo-cobaltammines.

(53) E. A. V. Epsworth, J. A. Weil, J. Phys. Chem., 63, 1890 (1959).
Paramagnetic resonance absorption in (su)peroxo-dicobalt complexes.

(54) N.-G. Vannerberg, C. Brosset, Acta Cryst., 16, 247 (1963).
The crystal structure of decammine-μ-(su)peroxo-dicobalt pentanitrate.

(55) M. Calvin, R. H. Bailes, W. K. Wilmarth, J. Am. Chem. Soc., 68, 2254 (1946).
The oxygen-carrying synthetic chelate compounds.I.

(56) R. H. Bailes, M. Calvin, J. Am. Chem. Soc., 69, 1886 (1947).
Oxygen-carrying synthetic chelate compounds.Preparations.VII.

(57) L. Vaska, Science, 140, 809 (1963).
Oxygen-carrying properties of a simple synthetic system.

(58) J. H. Bayston, N. K. King, F. D. Looney, M. E. Winfield, J. Am. Chem. Soc., 91, 2795 (1969).
Superoxo cobalamin, the first intermediate in the autoxidation of vitamin B_{12r}.

(59) (a) A. Misono, S. Koda, Y. Uchida, Bull. Chem. Soc. Jap., 42, 580 (1969).
Reversible oxygenation of Co(II) complexes on polyvinylpyridine.
(b) A. Misono, S. Koda, Y. Uchida, Bull. Chem. Soc. Jap., 42, 3470 (1969).
Oxygenation-deoxygenation of Co(II) complexes on polymers.

(60) (a) A. Misono, S. Koda, Bull. Chem. Soc. Jap., 42, 3048 (1969).
An ESR study of 1:1 adducts of bis(salicylaldehydeimine)Co(II) complexes with O_2 in solution.
(b) A. Misono, S. Koda, Y. Uchida, Bull. Chem. Soc. Jap., 42, 3470 (1969).
Oxygenation-deoxygenation of Co(II) complexes on polymers.

(61) A. L. Crumbliss, F. Basolo, J. Am. Chem. Soc., 92, 55 (1970).
Monomeric oxygen adducts of N,N'-ethylenebis(acetylacetoniminato)-(ligand)cobalt(II). Preparation and properties.

(62) (a) B. M. Hoffman, D. L. Diemente, F. Basolo, J. Am. Chem. Soc., 92, 61 (1970). Electron spin resonance studies of 1:1 cobalt-oxygen adducts.
(b) D. Diemente, B. M. Hoffman, F. Basolo, J. C. S. Chem. Comm.,467 (1970).
Electron paramagnetic resonance studies of some cobalt(II) Schiff base compounds and their monomeric oxygen adducts.

(63) F. A. Walker, J. Am. Chem. Soc., 92, 4235 (1970).
An electron spin resonance study of coordination to the fifth and sixth positions of α,β,γ,δ-tetra(p-methoxyphenyl)porphinatocobalt(II).

(64) C. Floriani, F. Calderazzo, J. Chem. Soc. A, 946 (1970).
Oxygen adducts of Schiff's base complexes of cobalt prepared in solution.

(65) S. A. Cockle, H. A. O. Hill, R. J. P. Williams, Inorg. Nucl. Chem. Lett., 6, 131 (1970.
The formation of some superoxo cobalt(III) complexes; an investigation by EPR spectroscopy.

(66) K. Yamamoto, T. Kwan, J. Cat., 18, 354 (1970).
Oxygenation of cobalt tetraphenylporphine as investigated by ESR.

(67) L. Pauling, C. D. Coryell, Proc. Nat. Acad. Sci. U.S.A., 22, 210 (1936).
The magnetic properties and structure of haemoglobin, oxyhaemoglobin, and carbonmonoxy haemoglobin.

(68) (a) L. Pauling, Stanford Med. Bull., 6, 215 (1948).
Chemical properties of haemoglobin in terms of its molecular structure.
(b) L. Pauling, Nature, 203, 182 (1964).
Nature of iron-oxygen in oxyhaemoglobin.

(69) J. S. Griffith, Proc. Roy. Soc. A, 235, 23 (1956).
On the magnetic properties of some haemoglobin complexes.

(70) J. J. Weiss, Nature, 202, 83 (1964).
Nature of iron-oxygen bond in oxyhaemoglobin.

(71) H. B. Gray, Adv. Chem. Ser., 100, 382 (1971).
Structural models for iron and copper proteins based on spectroscopic and magnetic properties.

(72) N.-G. Vannerberg, Acta Cryst., 18, 449 (1965).
The crystal structure of decammine-μ- peroxodicobalt tetrathiocyanate.

(73) R. E. Marsh, W. P. Schaefer, Acta. Cryst. B, 24, 246 (1968).
The crystal structure of decammine-μ-(su)peroxodicobalt pentanitrate.

(74) F. R. Fronczek, W. P. Schaefer, R. E. Marsh, Acta Cryst. B, 30, 117 (1974).
A reinvestigation of the crystal structure of decammine-μ- peroxodicobalt tetrathiocyanate.

(75) S. J. LaPlaca, J. A. Ibers, J. Am. Chem. Soc., 87, 2581 (1965).
Structure of $IrO_2Cl(CO)(P(C_6H_5)_3)_2$, the oxygen adduct of a synthetic reversible molecular oxygen carrier.

(76) M. S. Weininger, I. F. Taylor Jr., E. L. Amma, J. C. S. Chem. Comm., 1172(1971).
Oxygen-oxygen distances in synthetic oxygen carriers. The crystal and molecular structure of the oxygen adduct of bis(diphenylethylphosphine)chlorocarbonyliridium(I).

(77) L. D. Brown, K. N. Raymond, J. C. S. Chem. Comm., 470 (1974).
σ-Bonded dioxygen, X-ray crystal structure of $[NEt_4]_3[Co(CN)_5O_2].5H_2O$.

(78) L. D. Brown, K. N. Raymond, Inorg. Chem., 14, 2595 (1975).
A σ-bonded dioxygen adduct of the pentacyanocobalt(II) anion : Crystal structure of $[N(C_2H_5)_4]_3[Co(CN)_5O_2]\cdot 5H_2O$.

(79) A. Nakamura, Y. Tatsuno, M. Yamamoto, S. Otsuka
Oxygen-18 isotopic infrared study of dioxygen-transition metal complexes. J. Am. Chem. Soc., 93, 6052 (1971).

(80) R. W. Horn, E. Weissberger, J. P. Collman, Inorg. Chem., 9, 2367 (1970).
An oxygen-18 study of the reaction between iridium-and platinum oxygen complexes and sulphur dioxide to form coordinated sulphate.

(81) L. Vaska and coworkers, unpublished results on metal-dioxygen bond energies for some  complexes;quoted in reference [13].

(82) B. Bosnich, W. G. Jackson, S. T. D. Lo, J. W. McLaren, Inorg. Chem., 13, 2605 (1974).
Dissymmetric arsine complexes; monomeric and dimeric dioxygen complexes of cobalt.

(83) J. Ellis, J. M. Pratt, J. C. S. Chem. Comm., 781 (1973).
Formation of a $Co-O_2$ complex by coordination of free superoxide.

(84) B.-C. Wang, W. P. Schaefer, Science, 166, 1404 (1969).
Structure of an oxygen-carrying complex.

(85) M. Calligaris, G. Nardin, L. Randaccio, A. Ripamonti, J. Chem. Soc. A, 1069 (1970).
Structural aspects of the synthetic oxygen carrier, N,N'-ethylenebis-(salicylideniminato)cobalt(II). Structure of the addition compound with oxygen containing dimethylformamide.

(86) A. Avdeef, W. P. Schaefer, Inorg. Chem., 15, 1432 (1976).
Reversible oxygen carriers. Synthesis and structure of μ-dioxygen-bis[N,N'-ethylenebis(salicylideniminato)piperidine cobalt] acetonate piperidinato, $(C_5H_{11}NCoSalen)_2O_2 \cdot 0.66(CH_3)_2CO \cdot 0.33C_5H_{11}N$.

(87) B. Chevrier, Th. Diebold, R. Weiss, Inorg. Chim. Acta, 19, L57 (1976).
A trans diperoxomolybdenumVI porphyrin. Synthesis and crystal structure.

(88) N. W. Terry III, E. L. Amma, L. Vaska, J. Am. Chem. Soc., 94, 653 (1972).
Molecular oxygen binding in a monomeric cobalt complex. The crystal and molecular structure of dioxygen-bis[cis-1,2-bis(diphenylposphino)-ethylene] cobalt tetrafluoroborate.

(89) R. Guilard, M. Fontesse, P. Fournari, C. Lecomte, J. Protas, J. C. S. Chem. Comm., 161 (1976).
The first peroxometalloporphyrin with dioxygen symmetrically bonded by both atoms. Synthesis and X-ray crystal structure of peroxo-titaniumoctaethylporphyrin.

(90) U. Thewalt, Z. Naturforsch B, 25, 569 (1970), Ger.
μ-Amido-μ-peroxo-bis[bis(ethylenediamine)cobalt(III)] cation and its salts.

(91) J. C. A. Boeyens, R. Haegele, Inorg. Chim. Acta, 20, L7 (1976).
Oxygen as a di-μ-peroxo bridge. Synthesis and crystal structure of benzyltrimethylammonium di-μ-peroxohexachlorodiuranyl(VI).

(92) M. Laing, M. J. Nolte, E. Singleton, J. C. S. Chem. Comm., 660 (1975).
The O-O bond length in oxygen adducts of iridium and rhodium complexes.

(93) M. J. Nolte, E. Singleton, M. Laing, J. Am. Chem. Soc., 97, 6396 (1975).
Redetermination of the structure of $[Ir(O_2)\{Ph_2PCH_2CH_2PPh_2\}_2][PF_6]$.

(94) M. J. Nolte, E. Singleton, Acta Cryst. B, 31, 2223 (1975).
The crystal structure of dioxygen tetra(dimethylphenylarsine)-rhodium(I) perchlorate.

(95) J. A. McGinnety, N. C. Payne, J. A. Ibers, J. Am. Chem. Soc., 91, 6301 (1969).
The role of the metal atom in the reversible uptake of molecular oxygen. The structures of molecular oxygen complexes formed by bis[bis(diphenyl-phosphino)ethane]iridium(I) hexafluorphosphate and its rhodium analogue.

(96) M. J. S. Dewar, Bull. Soc. Chim. Fr., 18, C71 (1951).
A review of the π-complex theory.

(97) J. Chatt, L. A. Duncanson, J. Chem. Soc., 2939 (1953).
Olefin coordination compounds. Part III. Infra-red spectra and structure: attempted preparation of acetylene complexes.

(98) B. M. Hoffman, C. J. Weschler, F. Basolo, J. Am. Chem. Soc. 98, 5473 (1976).
The dioxygen adduct of meso-tetraphenylporphinatomanganose(II), a synthetic oxygen carrier.

(99) B. Gonzalez, J. Kouba, S. Yee, C. A. Reed, J. F. Kirner, W. R. Scheidt, J. Am. Chem. Soc., 97, 3274 (1975).
Manganese porphyrins. Synthesis, structure and preference for five-coordination.

(100) L. Vaska, L. S. Chen, C. V. Senoff, Science, 174, 587 (1974).
Oxygen-carrying iridium complexes: kinetics mechanism and thermodynamics.

(101) F. A. Cotton, G. Wilkinson, "Advanced Inorganic Chemistry", 3rd ed. Wiley, New York, 1972, pp 635, 783.

(102) M. J. Bennet, P. B. Donaldson, J. Am. Chem. Soc., 93, 3307 (1971).
Molecular oxygen as a bridging ligand in a transition metal complex.

(103) (a) W. P. Schaefer, R. E. Marsh, Acta Cryst., 21, 735 (1966).
The structure of decammine-μ-(su)peroxo-dicobalt monosulphate trisbisulphate.
(b) W. P. Schaefer, R. E. Marsh, J. Am. Chem. Soc., 88, 178 (1966).
The molecular structure of a (su)peroxo-bridged dicobalt cation.

(104) F. R. Fronczek, W. P. Schaefer, Inorg. Chim. Acta, 9 143 (1974).
Structural characterisation of the $[(CN)_5CoO_2Co(CN)_2]^{6-}$ ion: the crystal structure of potassium decacyano-μ-peroxodicobaltate dinitrate tetrahydrate.

(105) L. A. Lindblom, W. P. Schaefer, R. E. Marsh, Acta Cryst. B, 27, 1461 (1971).
The crystal and molecular structure of μ-peroxo-bis-[3,3'-diimino-di-n-propylamine-bis-salicylaldehydecobalt(III)]·$C_6H_5CH_3$.

(106) W. P. Schaefer, Inorg. Chem., 7, 725 (1968).
The structure of decammine-μ-peroxodicobalt disulphate tetrahydrate.

(107) J. R. Fritch, G. G. Christoph, W. P. Schaefer, Inorg. Chem., 12, 2170 (1973).
Crystal structure of μ-peroxo-bis[(ethylenediamine)(diethylene-triamine)cobalt(III)] perchlorate.

(108) F. R. Fronczek, W. P. Schaefer, R. E. Marsh, Inorg. Chem., 14, 611 (1975).
The dioxygen ligand as a bridging group. Structure of potassium decacyano-μ-superoxodicobaltate(III) monohydrate.

(109) G. G. Christoph, R. E. Marsh, W. P. Schaefer, Inorg. Chem., 8, 291 (1969).
The crystal structure of μ-amido-μ-superoxo-bis |tetraamminecobalt(III)| tetranitrate, $[(NH_3)_4Co(NH_2)(O_2)Co(NH_3)_4](NO_3)_4$.

(110) (a) U. Thewalt, R. E. Marsh, Inorg. Chem., 11,351 (1972).
The structure of racemic μ-amido-μ-superoxo-bis[bis(ethylenediamine)-cobalt(III)] tetranitrate hydrate.

(111) R. H. Hunt, R. A. Leacock, C. W. Peters, K. T. Hecht, J. Chem. Phys., 42, 1931 (1965).
Internal rotation in hydrogen peroxide : the far-infrared spectrum and the determination of the hindering potential.

(112) H. R. Zeller, W. Kaenzig, Helv. Phys. Acta, 40, 845 (1967), Ger.
The electronic structure of the superoxide-ion centre in alkali metal halides.I. Paramagnetic and optical spectra and their interpretation.

(113) A. Reuveni, Z. Luz, B. L. Silver, J. Mag. Res., 12, 109 (1973).
ESR of gamma-irradiated potassium persulphate enriched in oxygen-17 and sulphur-33.

(114) J. A. Howard, Can. J. Chem., 50, 1981 (1972).
Electron spin resonance spectrum of the tert-butyl peroxy radical $B^{16}O^{17}O$.

(115) K. Adamic, K.U. Ingold, J. R. Morton, J. Am. Chem. Soc., 92, 922 (1970).
Electron spin resonance spectrum of oxygen-17 enriched t-alkylperoxy radicals.

(116) E. Melamud, S. Schlick, B. L. Silver, J. Mag. Res., 14, 104 (1974).
ESR of tetralin peroxy-^{17}O radical in a single crystal.

(117) E. Melamud, B. L. Silver, Z. Dori, J. Am. Chem. Soc., 96, 4689 (1974).
Electron paramagnetic resonance of mononuclear cobalt oxygen carriers labelled with ^{17}O.

(118) D. Getz, E. Melamud, B. L. Silver, Z. Dori, J. Am. Chem. Soc., 97, 3846 (1975).
Electronic structure of dioxygen in cobalt(II) oxygen carriers. Singlet oxygen or O_2^-.

(119) E. E. Vansant, L. H. Lunsford, Adv. Chem. Ser., 121, 441 (1973).
Formation and structure of a monomeric oxygen adduct of a cobalt(II)-ammonia complex in a cobalt(II) Y Zeolite.

(120) J. A. Weil, J. K. Kinnaird, J. Phys. Chem., 71, 3341 (1967).
^{17}O hyperfine splitting in a μ-amido-μ-(su)peroxocobalt complex.

(121) B. B. Wayland, J. V. Minkiewicz, M. E. Abd Elmageed, J. Am. Chem. Soc., 96, 2795 (1974).
Spectroscopic studies of tetraphenylporphyrincobalt(II). Complexes of CO, NO, O_2, RNC and $(RO)_3P$ and a bonding model for complexes of CO, NO and O_2 with Co(II) and Fe(II) porphyrins.

(122) V. M. Miskowski, J. L. Robbins, I. M. Treitel, H. B. Gray, Inorg. Chem., 14, 2318 (1975).
Electronic structure and spectra of μ-superoxo-dicobalt(III) complexes.

(123) R. S. Gall, J. F. Rogers, W. P. Schaefer, G. G. Christoph, J. Am. Chem. Soc., 98, 5135 (1976).
The structure of a monomeric oxygen carrying cobalt complex : dioxygen-N,N'-(1,1,2,2-tetramethyl)ethylenebis(3-tert-butylsalicylideniminato)(1-benzylimidazole)cobalt(II).

(124) R. S. Gall, W. P. Schaefer, Inorg. Chem., 15, 2758 (1976).
Preparation and structural characterisation of a monomeric dioxygen adduct of N,N'-(1,1,2,2-tetramethylethylene)bis(salicylideniminato)-(1-benzylimidazole)cobalt(II).

(125) A. Avdeef, W. P. Schaefer, J. Am. Chem. Soc., 98, 5153 (1976).
Reversible oxygen carriers. The synthesis and low temperature ($-171^{o}C$) structure of an unstable monomeric dioxygen adduct of N,N'-(1,1,2,2-tetramethylethylene)bis(3-Fluorosalicylideniminato)-cobalt(II); Co(3-Fsaltmen)(1-Me-imid)(O_2)·2($(CH_3)_2CO$.

(126) (a) G. A. Rodley, W. T. Robinson, Nature, 235, 438 (1972).
Structure of a monomeric oxygen carrying complex.
(b) A. D. Rae, G. A. Rodley, W. T. Robinson, unpublished results.

(127) L. Vaska, Acc. Chem. Res., 1, 335 (1968).
Reversible activation of covalent molecules by transition metal complexes. The role of the covalent molecule.

(128) W. H. Fuchsman, C. H. Barlow, W. J. Wallace, W. S. Caughey, Biochem. Biophys. Res. Comm., 61, 585 (1974).
Novel haem:O_2 bonding of possible relevance to oxygen utilising haem and other proteins.

(129) V. McKee, S. M. Nelson, J. Nelson, J. C. S. Chem. Comm., 225 (1976)
A seven-coordinate dioxygen adduct of iron(II) with spin-triplet ground state.

(130) D. Vonderschmitt, K. Bernauer, S. Fallab, Helv. Chim. Acta, 48, 951 (1965) Ger.
Reactivity of coordination compounds.XIV. Reversible binding of dioxygen to iron(II) phthalocyanine tetrasulphonic acid.

(131) See reference [12] and references therein.

(132) J. Halpern, B. L. Goodall, G. P. Khara, H. S. Lim, J. J. Pluth, J. Am. Chem. Soc., 97, 2301 (1975).
Reaction of dioxygen with dicyanotri(dimethylphenylphosphine)cobalt(II). Synthesis, structure and reactivity of a novel cobalt-dioxygen complex.

(133) C. J. Willis, J. C. S. Chem. Comm., 117 (1974).
Reversible formation of a high-spin cobalt(II) complex of a neutral dioxygen ligand.

(134) (a) S. K. Cheung, C. J. Grimes, J. Wong, C. A. Reed, J. Am. Chem. Soc., 98, 5028 (1976).
Chromium(II) porphyrins and an irreversible dioxygen complex.
(b) C. A. Reed, S. K. Cheung, to be published;
On the bonding of FeO_2 in haemoglobin and related dioxygen complexes.

(135) J. P. Collman, J. I. Brauman, K. S. Suslick, J. Am. Chem. Soc., 97, 7185 (1975)
Oxygen binding to iron porphyrins.

(136) J. P. Collman, T. R. Halbert, S. Hayes, K. S. Suslick, J. I. Brauman, unpublished results on the oxygen affinity of solid Co(TpivPP)-(1-Me-imid); quoted in reference [137].

(137) J. P. Collman, Acc. Chem. Res., 10, (1977).
Synthetic models for the oxygen binding haemoproteins.

(138) J. P. Collman, R. R. Gagne, C. A. Reed, J. Am. Chem. Soc., 96, 2629 (1974).
A paramagnetic dioxygen complex of iron(II) derived from a "picket fence" porphyrin. Further models for haemoproteins.

(139) (a) J. M. McCord, B. B. Keele Jr., I. Fridovich, Proc. Nat. Acad. Sci. U.S.A., 68, 1024 (1971).
An enzyme based theory of obligate anaerobiosis. The physiological function of superoxide dismutase.
(b) I. Fridovich, Acc. Chem. Res., 5, 321 (1972).
Superoxide radical and superoxide dismutase.

(140) (a) H. P. Misra, I. Fridovich, J. Biol. Chem., 247, 6960 (1972).
Generation of superoxide radical during the antoxidation of haemoglobin.
(b) R. Wever, B. Oudega, B. V. Van Gelder, Biochim. Biophys. Acta, 302, 475 (1973).
Generation of superoxide radicals during the autoxidation of mammalian oxyhaemoglobin.

(141) W. J. Wallace, J. C. Maxwell, W. S. Caughey, Biochim. Biophys. Res. Comm., 57, 1104 (1974).
The mechanisms of haemoglobin autoxidation, Evidence for proton-assisted nucleophilic displacement of O_2^- by anions.

(142) W. J. Wallace, J. C. Maxwell, W. S. Caughey, FEBS Lett., 43,33 (1974).
A role for chloride ion in the autoxidation of haemoglobin under conditions similar to those in erythrocytes.

(143) (a) J. S. Loehr, T. B. Freedman, T. M. Loehr, Biochem. Biophys. Res. Comm., 56, 510 (1974).
Oxygen binding to haemocyamin : a resonance Raman spectroscopy study.
(b) T. B. Freedman, J. S. Loehr, T. M. Loehr, J. Am. Chem. Soc., 98, 2809 (1976).
A resonance Raman study of the copper protein haemocyanin. New evidence for the structure of the binding site.

(144) I. M. Klotz, G. L. Klippenstein, W. A. Hendrickson, Science, 199, 335 (1976); and references therein.
Haemerythrin : alternative oxygen carrier.

(145) J. B. R. Dunn, D. F. Shriver, I. M. Klotz, Proc. Nat. Acad. Sci. U.S.A. 70, 2582 (1973).
Resonance Raman studies of the electronic state of oxygen in haemerythrin.

(146) R. E. Stenkamp, L. C. Sieker, L. H. Jensen, Proc. Nat. Acad. Sci. U.S.A., 73, 349 (1976).
Structure of the iron complex in methaemerythrin.

(147) W. A. Hendrickson, G. A. Klippenstein, K. B. Ward, Proc. Nat. Acad. Sci. U.S.A., 72, 2160 (1975).
Tertiary structure of myohaemerythrin at low resolution.

(148) J. C. Kendrew, R. E. Dickerson, B. E. Strandberg, R. G. Hart, D. R. Davies, D. C. Phillips, V. C. Shore, Nature, 185, 422 (1960).
Structure of myoglobin. A three-dimensional Fourier synthesis at 2 Å resolution.

(149) M. F. Perutz, H. Muirhead, J. M. Cox, L. C. G. Goaman, Nature, 219, 131 (1968).
Three-dimensional Fourier synthesis of horse oxyhaemoglobin at 2.8 Å resolution : the atomic model.

(150) G. Fermi, J. Mol. Biol., 97, 237 (1975).
Three dimensional Fourier synthesis of human deoxyhaemoglobin at 2.5 Å resolution.

(151) R. Huber, O. Epp. H. Formanek, J. Mol. Biol., 52, 349 (1970).
Structures of deoxy- and carbonmonoxy erythrocruorin.

(152) E. Antonini, M. Brunori, "Haemoglobin and myoglobin in their reactions with ligands", Elsevier, N.Y., 1971; and references therein.

(153) J. Monod, J. Wyman, J. P. Changeux, J. Mol. Biol., 12, 88 (1965).
On the nature of allosteric transitions : a plausible model.

(154) D. E. Koshland Jr., G. Nemethy, D. Filmer, Biochem., 5, 365 (1966).
Comparison of experimental binding data and theoretical models in proteins containing subunits.

(155) M. F. Perutz, Nature, 228, 7261 (1970).
Stereochemistry of cooperative effects in haemoglobin.

(156) M. F. Perutz, L. F. Ten Eyck, Cold Springs Harbour Symp. Quant. Biol., 36, 295 (1971).
Stereochemistry of cooperative effects in haemoglobin.

(157) M. F. Perutz, Nature, 237, 495 (1972).
Nature of haem-haem interaction.

(158) M. F. Perutz, Brit. Med. Bull., 32, 195 (1976).
Structure and mechanism of haemoglobin.

(159) J. M. Baldwin, Brit. Med. Bull., 32, 213 (1976).
A model of cooperative oxygen binding to haemoglobin.

(160) J. A. Ibers, J. W. Lauher, R. G. Little, Acta Cryst. B, 30, 268 (1974).
Stereochemistry of cooperativity effects in the prosthetic group of coboglobin.

(161) B. M. Hoffman, D. H. Petering, Proc. Nat. Acad. Sci. U.S.A., 67, 637 (1970).
Coboglobins : oxygen-carrying, cobalt-reconstituted haemoglobin and myoglobin.

(162) F. Basolo, B. M. Hoffman, J. A. Ibers, Acc. Chem. Res., 8, 384 (1975).
Synthetic oxygen carriers of biological interest.

(163) C. H. Barlow, J. C. Maxwell, W. J. Wallace, W. S. Caughey, Biochem. Biophys. Res. Comm., 55, 91 (1973).
Elucidation of the mode of binding of O_2 to iron in oxyhaemoglobin by infrared spectroscopy.

(164) J. C. Maxwell, J. A. Volpe, C. H. Barlow, W. S. Caughey, Biochem. Biophys. Res. Comm. 58, 166 (1974).
Infrared evidence for the mode of binding of oxygen to iron of myoglobin from heart muscle.

(165) J. C. Maxwell, W. S. Caughey, Biochem. Biophys. Res. Comm., 60, 1309 (1974).
Infrared evidence for similar metal dioxygen bonding in iron and cobalt oxyhaemoglobins.

(166) I. C. Gunsalus, J. R. Meek, J. D. Lipscomb, P. Debrunner, E. Munck, in "Molecular Mechanisms of Oxygen Activation", O. Hayaishi ed., Academic Press, New York, 1973; Chapter 14; and references therein.

(167) B. K. Vainshtein, B. H. Harutyunyan, I. P. Kuranovo, V. V. Borisov, N.I. Sosfenov, A. G. Pavlovsky, A. I. Grebenko, N. V. Konareva, Nature, 254, 163 (1975).
Structure of leghaemoglobin from lupin root nodules at 5 Å resolution.

(168) T. B. Freedman, C. M. Yoshida, T. M. Loehr, J. C. S. Chem. Comm., 1016 (1974).
Resonance Raman spectra of μ-peroxo binuclear cobalt(III) complexes.

(169) T. Shibahara, J. C. S. Chem. Comm., 864 (1973).
Laser-Raman and infrared spectra of μ-superoxo-dicobalt(III) complexes.

(170) J. D. Landels, G. A. Rodley, Syn. Inorg. Met. Org. Chem., 2, 65 (1972).
The preparation of relatively stable 1:1 cobalt-dioxygen complexes.

(171) J. A. McGinnety, R. J. Doedens, J. A. Ibers, Inorg. Chem., 6, 2243 (1967).
Structure of $IrI(O_2)(CO)(P(C_6H_5)_3)_2 \cdot CH_2Cl_2$, the dioxygen adduct of a synthetic irreversible molecular oxygen carrier.

(172) L. M. Haines, E. Singleton, J. Organomet. Chem., 30, C81 (1971).
Cationic oxygen adducts from rhodium and iridium carbonyl salts.

(173) P.-T. Cheng, C. D. Cook, S. C. Nyburg, K. Y. Wan, Can. J. Chem., 49, 3772 (1971).
The crystal molecular structure of $(PPh_3)_2PtO_2 \cdot 2CHCl_3$.

(174) C. J. Nyman, C. E. Wymore G. Wilkinson, J. Chem. Soc. A., 561 (1968).
Reactions of tris(triphenylphosphine)platinum(O) and tetrakis(triphenylphosphine)palladium(O) with oxygen and carbon dioxide.

(175) M. Matsumoto, K. Nakatsu, Acta Cryst. B,31, 2711 (1975).
Dioxygen-bis-(t-butylisocyanide)nickel.

(176) K. Hirota, M. Yamamoto, S. Otsuka, A. Nakamura, Y. Tatsuno, J. C. S. Chem. Comm., 533 (1968).
^{18}O isotopic infrared studies on isocyanide-oxygen-metal-complexes.

(177) J. M. Le Carpentier, A. Mitchler, R. Weiss, Acta Cryst. B, 28, 1288 (1972), Fr..
Crystal structures of dipyridinium μ-oxo-tetraperoxodioxobis(aquo)-dimolybdateVI and dipyridinium di-μ-hydroperoxo-tetraperoxodioxo-molybdate VI .

(178) W. P. Griffith, J. Chem. Soc., 5345 (1963).
Studies on transition-metal peroxy-complexes. Part II. Permolybdates and pertungstates.

(179) J. M. Le Carpentier, R. Schlupp, R. Weiss, Acta Cryst. B, 28, 1278 (1972), Fr..
Crystal structures of oxodiperoxo-hexamethylphosphoramido-aquo-molybdateVI.

(180) H. Mimoun, I. Serree de Roch, L. Sajus, Bull. Soc. Chim. Fr., 1481 (1969) Fr..
New covalent peroxide complexes of molybdenum and tungsten with organic bases.

(181) A. E. Martell, M. Calvin, "Chemistry of the Metal Chelate Compounds", Prentice Hall, N.Y., 1952.

(182) S. Yamada, Coord. Chem. Rev., 1, 415 (1966).
Recent aspects of the stereochemistry of Schiff-base-metal complexes.

(183) M. Calligaris, G. Nardin, L. Randaccio, Coord. Chem. Rev., 7, 385 (1972); and references therein.
Structural aspects of metal complexes with some tetradentate Schiff bases.

(184) T. Tsumaki, J. Chem. Soc. Jap., 58, 1288 (1937), Bull. Chem. Soc. Jap., 13, 252 (1938), Chem. Abs., 32, 3719 (1938).
Coordinate valency rings.IV. Some inner complex salts of hydroxy-aldimines.

(185) M. D. Hobday, T. D. Smith, Coord. Chem. Rev., 9, 311 (1972-73).
N,N'-ethylenebis(salicylideneiminato) transition metal ion chelates.

(186) J. M. Pratt, "Inorganic Chemistry of Vitamin B_{12}", Academic Press, London, 1972.

(187) S. F. Dyke, "The Chemistry of the Vitamins", Interscience, London, 1965.

(188) Seah Sen Koon, B. Sc. Hons. Report, University of Canterbury, 1972.

(189) R. Morassi, I. Bertini, L. Sacconi, Coord. Chem. Rev., 11, 343 (1973).
Five-coordination in iron(II), cobalt(II) and nickel(II) complexes.

(190) D. A. Buckingham, J. P. Collman, J. L. Hoard, G. Lang, L. J. Radonovich, C. A. Reed, W. T. Robinson, structure of Fe(TPP)(2-Me-imid) to be published; quoted in reference [191].

(191) J. L. Hoard, in "Porphyrins and Metalloporphyrins", K. M. Smith ed., Elsevier, Amsterdam, 1975; Chapter 8, "Stereochemistry of Porphyrins and Metalloporphyrins"; and references therein.

(192) R. G. Little, J. A. Ibers, J. Am. Chem. Soc., 96, 4452 (1974).
Stereochemistry of cobalt porphyrins.III. The structure of 2,3,7,8, 12,13,17,18-octaethylporphinato(1-methylimidazole)cobalt(II). A model for deoxycoboglobin.

(193) W. R. Scheidt, J. Am. Chem. Soc., 96, 90 (1974).
Stereochemistry of low spin cobalt porphyrins.IV . Molecular stereochemistry of (1-methylimidazole)-α,β,γ,δ-tetraphenylporphinato-cobalt(II).

(194) R. N. Dwyer, P. Madura, W. R. Scheidt, J. Am. Chem. Soc., 96, 4815 (1974).
Stereochemistry of cobaltporphyrins.VI. Molecular stereochemistry of (1,2-dimethylimidazole)-α,β,γ,δ-tetraphenylporphinatocobalt(II).

(195) W. R. Scheidt, J. Ramanuja, structure of Co(TPP)(3,5-Me_2py) to be published; quoted in reference [191].

(196) M. Calligaris, D. Minichelli, G. Nardin, L. Randaccio, J. Chem. Soc. A, 2141 (1970).
Structural aspects of the synthetic oxygen carrier N,N'-ethylenebis-(salicylideniminato)cobalt(II). Part II. Crystal and molecular structure of the monopyridine complex.

(197) M. Calligaris, G. Nardin, L. Randaccio, J. C. S. Dalton Trans., 1903 (1974).
Crystal and molecular structure of the high spin five-coordinate complex, aquo N,N'-ethylenebis(3-methoxysalicylideniminato)cobalt(II).

(198) A. Avdeef, W. P. Schaefer, personal communation of the structure of Co(3-Fsaltmen)(1-Bz-imid).

(199) M. Kronstadt, M. Sc. Thesis, Stanford University, 1974.

(200) N. Bresciani, M. Calligaris, G. Nardin, L. Randaccio, J. C. S. Dalton Trans., 498 (1974).
Steric effects in the reversible oxygenation of cobalt Schiff base complexes. Part II. Crystal and molecular structure of N,N'-butylene-bis(salicylideniminato)pyridinecobalt(II).

(201) S. Brückner, M. Calligaris, G. Nardin, L. Randaccio, Acta Cryst. B, 25, 1671 (1969).
The crystal structure of the form of N,N'-ethylenebis(salicylaldehydeiminato)cobalt(II) inactive towards oxygenation.

(202) R. DeIsai, S. L. Holt, B. Post, Inorg. Chem., 10, 1498 (1971).
Crystal structure of the oxygen-inactive form of bis(salicylaldehyde)-ethylenediiminecobalt(II).

(203) G. P. Falloon, B. M. Gatehouse, Acta Cryst. B, 32, 97 (1976).
The crystal and molecular structure of N,N'-ethylenebis(thiosalicylideniminato)cobalt(II), the sulphur analogue of a molecular oxygen carrier, N,N'-ethylenebis(salicylideniminato)cobalt(II).

(204) V. L. Goedken, S.-M. Peng, J. Molin-Norris, Y.-ae Park, J. Am. Chem. Soc, 98, 8391 (1976).
Carbon monoxide complexes of iron(II). Synthesis and structural studies of the five- and six-coordinate complexes of the macrocyclic ligand $C_{22}H_{22}N_4^{2-}$.

(205) W. R. Scheidt, M. E. Frisser, J. Am. Chem. Soc., 97, 17 (1975).
Nitrosyl metalloporphyrins.II. Synthesis and molecular stereochemistry of nitrosyl-α,β,γ,δ-tetraphenylporphinatoiron(II).

(206) W. R. Scheidt, J. L. Hoard, J. Am. Chem. Soc., 95, 8281 (1973).
Stereochemistry of low spin cobalt porphyrins.I. Structure and bonding in a nitrosyl porphyrin and their bearing on one rational model for the oxygenated protohaem.

(207) "International Tables for X-ray Crystallography", Vol. I, Kynoch Press, Birmingham, England, 1962.

(208) W. T. Robinson, unpublished results.

(209) J. Zemann, Z. Anorg. Allg, Chem., 324, 241 (1963), Ger.
Electrostatic energies for AB_5 complexes.

(210) W. P. Schaefer, R. E. Marsh, Acta Cryst. B, 25, 1675 (1969).
Oxygen-carrying cobalt compounds.I. Bis(salicylaldehyde)ethylenediiminecobalt(II) monochloroformate.

(211) W. T. Robinson, G. A. Rodley, unpublished structure.

(212) E. C. Lingafelter, R. L. Braun, J. Am. Chem. Soc., 88, 2951 (1966).
Interatomic distances and angles in metal chelates of acetylacetone and salicylaldimine.

(213) R. K. Gupta, A. S. Mildvan, T. Yonetani, T. S. Srivastava, Biochem. Biophys. Res. Comm., 67, 1005 (1975).
EPR study of ^{17}O nuclear hyperfine interaction in cobalt-oxyhaemoglobin.Conformation of bound oxygen.

(214) P. Fantucci, V. Valenti, J. Am. Chem. Soc., 98, 3832 (1976).
Molecular orbital study of a cobalt reversible oxygen carrier.

(215) J. C. W. Chien, L. C. Dickinson, Proc. Nat. Acad. Sci. U.S.A., 69, 2783 (1972).
Electron paramagnetic resonance of single crystal oxycobaltmyoglobin and deoxycobaltmyoglobin.

(216) B. Jezowska-Trzebiatowska, A. Vogt, H. Kozlowski, A. Jezierski, Bull. del Acad. Polonaise des Sciences, 20, 187 (1972).
New Co(II) complexes reversibly binding O_2 in aqueous solutions.

(217) J. W. Lauher, J. E. Lester, Inorg. Chem., 12, 244 (1973).
An X-ray photoelectron spectroscopy study of N,N'-ethylenebis(benzoylacetoniminato)cobalt(II) and its oxygen and nitric oxide adducts.

(218) J. H. Burness, J. G. Dillard, L. T. Taylor, J. Am. Chem. Soc., 97, 6080 (1975).
An X-ray photoelectron spectroscopic study of cobalt(II) Schiff base complexes and their oxygenation products.

(219) M. J. Carter, D. P. Rillema, F. Basolo, J. Am. Chem. Soc., 96, 392 (1974).
Oxygen carrier and redox properties of some neutral cobalt chelates. Axial and in-plane ligand effects.

(220) G. McLendon, A. E. Martell, J. C. S. Chem. Comm., 223 (1975).
Stabilities of binuclear cobalt oxygen adducts. A linear free energy relationship.

(221) F. A. Walker, D. Beroiz, K. M. Kadish, J. Am. Chem. Soc., 98, 3484, (1976); and references therein.
Electronic effects in transition metal porphyrins.II. The sensitivity of redcx and ligand addition reactions in para-substituted tetraphenylporphyrin complexes of cobalt(II).

(222) (a) H. C. Stynes, J. A. Ibers, J. Am. Chem. Soc., 94, 1559 (1972).
Thermodynamics of the reversible oxygenation of amine complexes of cobalt(II) protoporphyrinIX dimethyl ester in a non-aqueous medium.
(b) D. V. Stynes, H. C. Stynes, B. R. James, J. A. Ibers, J. Am. Chem. Soc., 95, 1796 (1973).
Thermodynamics of ligand and oxygen binding to cobalt protoporphyrinIX dimethyl ester in toluene solution.

(223) R. M. Guidry, R. S. Drago, J. Am. Chem. Soc., 95, 6645 (1973).
Evaluation of the thermodynamic data reported for the reversible oxygenation of the amine complexes of cobalt(II) protoporphyrinIX dimethyl ester.

(224) J. A. Ibers, D. N. Stynes, H. C. Stynes, B. R. James, J. Am. Chem. Soc., 96, 1358 (1974).
On the failure of the Guidry-Drago reanalysis of spectroscopic data for the reversible oxygenation of amine complexes of cobalt protoporphyrinIX dimethyl ester.

(225) H. C. Stynes, J. A. Ibers, J. Am. Chem. Soc., 94, 5125 (1974).
A pronounced solvent effect on the reversible oxygenation of a cobalt(II) porphyrin system.

(226) D. Snyder, D. L. Weaver, Inorg. Chem., 9, 2760 (1970).
The crystal and molecular structure of trans-chloronitrosylbis(ethylenediamine)cobalt(III) perchlorate.

(227) C. S. Pratt, B. A. Coyle, J. A. Ibers, J. Chem. Soc. A, 2146 (1971).
Redetermination of the structure of nitrosylpenta-amminecobalt(III) dichloride.

(228) J. A. Ibers, Acta Cryst. B, 27, 250 (1971).
Refinement of a linear group; direct refinement of an interatomic bond length.

(229) T. Yonetani, H. Yamamoto, T. Iizuka, J. Biol. Chem., 249, 2168 (1974).
Studies on cobalt myoglobins and haemoglobins.III. Electron paramagnetic resonance studies of reversible oxygenation of cobalt myoglobins and haemoglobins.

(230) M. Calligaris, G. Nardin, L. Randaccio, Inorg. Nucl. Chem. Lett., 8, 477 (1972).
The structure of N,N'-ethylene-bis(acetylacetoniminato)methylpyridino cobalt(III).

(231) M. Calligaris, G. Nardin, L. Randaccio, G. Tauzher, Inorg. Nucl. Chem. Lett., 9, 419 (1973).
The structure of the 1:1 addition compound of molecular oxygen with N,N'-ethylenebis(acetylacetoniminato)cobalt(II) monopyridinate.

(232) R. G. Little, J. A. Ibers, J. Am. Chem. Soc., 96, 4440 (1974).
Stereochemistry of cobalt porphyrins.I. The structure and characterisation of 2,3,7,8,12,13,17,18-octaethylporphinato-bis(3-methylpyridine)cobalt(II).

(233) J. A. Kaduk, W. R. Scheidt, Inorg. Chem., 13, 1875 (1974).
Stereochemistry of low-spin cobalt porphyrins.V. Molecular stereochemistry of nitro-α,β,γ,δ-tetraphenylporphinato (3,5-lutidine)cobalt(III).

(234) W. R. Scheidt, J. Am. Chem. Soc., 96, 84 (1974).
Stereochemistry of low-spin porphyrins.III. The crystal structure and molecular stereochemistry of bis(piperidine)α,β,γ,δ-tetraphenylporphinatocobalt(II).

(235) W. R. Scheidt, J. A. Cunningham, J. L. Hoard, J. Am. Chem. Soc., 95, 8289 (1973).
Stereochemistry of low-spin cobalt porphyrins.II. The bis(piperidine)-α,β,γ,δ-tetraphenylporphinatocobalt(III) cation in a crystalline solvated state.

(236) J. W. Lauher, J. A. Ibers, J. Am. Chem. Soc., 96, 4447 (1974).
Stereochemistry of cobalt porphyrins.II. The characterisation and structure of meso-tetraphenylporphinatobis(imidazole)cobalt(III) acetate monohydrate monochloroformate, $[Co(TPP)(imid)_2][OAc]\cdot H_2O\cdot CHCl_3$.

(237) J. L. Hoard, personal communication of the structure of Fe(TPP)-(1-Me-imid)$_2$.

(238) R. G. Little, K. R. Dymock, J. A. Ibers, J. Am. Chem. Soc., 97, 4532 (1975).
The crystal and molecular structure of the ferrihaemochrome bis-(1-methylimidazole)(protoporphyrinIX)iron-methanol-water.

(239) D. M. Collins, R. Countryman, J. L. Hoard, J. Am. Chem. Soc., 94, 2066 (1972).
Stereochemistry of low-spin iron porphyrins.I. Bis(imidazole)-α,β,γ,δ-tetraphenylporphinatoiron(III) chloride.

(240) M. Cesari, C. Neri, C. Perego, E. Perrotti, A. Zazzetta, J. C. S. Chem. Comm., 276 (1970).
The crystal and molecular structure of some derivatives of N,N'-ethylenebis(salicylideniminato)cobalt(III).

(241) D. Ostfield, M. Tsutsui, Acc. Chem. Res., 7, 52(1974).
Novel metalloporphyrins - synthesis and implications.

(242) D. Cullen, E. Meyer, T. S. Srivastava, M. Tsutsui, J. Am. Chem. Soc., 94, 7603 (1972).
Unusual metalloporphyrins.XIV. The structure of [meso-tetraphenyl-porphinato] bis[tricarbonylrhenium(I)].

(243) J. L. Hoard, M. J. Hamor, T. A. Hamor, W. S. Caughey, J. Am. Chem. Soc., 87, 2312 (1965).
The crystal structure and molecular stereochemistry of methoxyiron(III) mesoporphyrin-IX dimethyl ester.

(244) E. B. Fleischer, Acc. Chem. Res., 3, 105 (1970).
The structure of porphyrins and metalloporphyrins.

(245) D. M. Collins, W. R. Scheidt, J. L. Hoard, J. Am. Chem. Soc., 94, 6689 (1972).
Crystal structure and molecular stereochemistry of α,β,γ,δ-tetraphenyl-porphinatodichlorotin(IV).

(246) D. L. Cullen, E. F. Meyer Jr., J. Am. Chem. Soc., 96, 2095 (1974).
Crystal and molecular structure of the triclinic form of 1,2,3,4,5,6,7,8-octaethylporphinatonickel(II). A comparison with the tetragonal form.

(247) J. L. Hoard, Ann. N.Y. Sci., 206, 18 (1973).
Metalloporphyrin stereochemistry.

(248) E. F. Meyer Jr., Acta Cryst. B, 28, 2162 (1972).
The crystal structure of nickel(II) octaethylporphyrin.

(249) P. Nicholls, "Cytochromes and Biological Oxidation", Oxford University Press, London, 1975. A simple and brief introduction to cytochromes.

(250) E. R. Jaffe in "The Red Blood Cell", C. Bishop and D. M. Surgenor ed!s, Academic Press, New York, 1964; P397-442.

(251) R. R. Gagne, Ph.D. Thesis, Stanford University, 1974.

(252) A. B. Hoffman, D. M. Collins, V. W. Day, E. B. Fleischer, T. S. Srivastava, J. L. Hoard, J. Am. Chem. Soc., 94, 3620 (1972).
The crystal structure and molecular stereochemistry of μ-oxo-bis-[α,β,γ,δ-tetraphenylporphinatoiron(III)].

(253) M. Gerlock, E. D. McKenzie, A. D. C. Towl, J. Chem. Soc. A, 2850 (1969).
The crystal and molecular structure of μ-oxo-bis- [N,N'-ethylene-bis(salicylideniminato)iron(III)] - bispyridine.

(254) K. S. Murray, Coord. Chem. Rev., 12, 1 (1974); and references therein.
Binuclear oxo-bridged iron(III) complexes.

(255) G. S. Hammond, C.-H. S. Wu, Adv. Chem. Ser., 77, 186 (1968).
Oxidation of iron(II) chloride in nonaqueous solvents.

(256) O. H. W. Kao, J. H. Wang, Biochem., 4, 342 (1965).
Kinetic study of the oxidation of ferrohaemochrome by molecular oxygen.

(257) I. A. Cohen, W. S. Caughey, Biochem. 7, 636 (1968).
Reactions of deuteroporphyrins.IV. On the kinetics and mechanism of reactions of iron(II) porphyrins with oxygen.

(258) J. O. Alben, W. H. Fuchsman, C. H. Beaudreau, W. S. Caughey, Biochem., 7, 624 (1968).
Substituted deuteroporphyrins.III. Iron II derivatives. Reactions with oxygen and preparations from chloro and methoxohemins.

(259) J. H. Wang, J. Am. Chem. Soc., 80, 3168 (1958).
Haemoglobin studies.II. A synthetic material with haemoglobin-like property.

(260) Q. H. Gibson, L. J. Parkhurst, G. Geraci, J. Biol. Chem., 244, 4668 (1969).
The reaction of methaemoglobin with some ligands.

(261) P. George, R. L. J. Lyster, Proc. Nat. Acad. Sci. U.S.A., 44, 1013 (1958).
Crevice structures in haemoprotein reactions.

(262) U. Thewalt, R. G. Marsh, J. Am. Chem. Soc., 89, 6364 (1967).
The structure of the cations of Werner's green and red μ-amido-μ-peroxobis{bis(ethylenediamine)cobalt(III)} salts.

(263) (a) C. K. Chang, T. G. Traylor, J. Am. Chem. Soc., 95, 5810 (1973).
Solution behaviour of a synthetic myoglobin active site.
(b) C. K. Chang, T. G. Traylor, J. Am. Chem. Soc., 95, 8477 (1973).
Proximal base influence on the binding of oxygen and carbon monoxide to haem.

(264) G. C. Wagner, R. J. Kassner, J. Am. Chem. Soc., 96, 5593 (1974).
Spectroscopic properties of protohaem complexes undergoing reversible oxygenation.

(265) W. S. Brinigar, C. K. Chang, J. Am. Chem. Soc., 96, 5595 (1974).
Simple dioxygen-haem complexes formed in N,N-dimethylformamide.

(266) W. S. Brinigar, C. K. Chang, J. Geibel, T. G. Traylor, J. Am. Chem. Soc., 96, 5597 (1974).
Solvent effects on reversible formation and oxidation stability of haem-oxygen complexes.

(267) D. L. Anderson, C. J. Weschler, F. Basolo, J. Am. Chem. Soc., 96, 5999 (1974).
Reversible reaction of simple ferrous porphyrins with molecular oxygen at low temperatures.

(268) J. Almog, J. E. Baldwin, R. L. Dyer, J. Huff, C. J. Wilkerson, J. Am. Chem. Soc., 96, 5600 (1974).
Reversible binding of dioxygen to mesoporphyrinIX derivatives at low temperatures.

(269) J. E. Baldwin, J. Huff, J. Am. Chem. Soc., 95, 5758 (1973).
Binding of dioxygen to iron(II). Reversible behaviour in solution.

(270) J. Almog, J. E. Baldwin, J. Huff, J. Am. Chem. Soc., 97, 227 (1975).
Reversible oxygenation and autoxidation of a "capped" porphyrin iron(II) complex.

(271) J. P. Collman, R. R. Gagne, T. R. Halbert, J.-C. Marchon, C. A. Reed, J. Am. Chem. Soc., 95, 7868 (1973).
Reversible oxygen adduct formation in ferrous complexes derived from a "picket fence" porphyrin. A model for oxymyoglobin.

(272) J. P. Collman, R. R. Gagne, J. Kouba, H. Ljusberg-Wehren, J. Am. Chem. Soc., 96, 6800 (1974).
Reversible oxygen adduct formation in cobalt(II) "picket fence porphyrins".

(273) J. B. Wittenberg, B. A. Wittenberg, J. Peisach, W. Blumberg, Proc. Nat. Acad. Sci. U.S.A., 67, 1846 (1970).
On the state of the iron and the nature of the ligand in oxyhaemoglobin.

(274) Y. Yamamoto, G. Palmer, D. Gill, I. T. Salmeen, L. Rimai, J. Biol. Chem., 248, 5211 (1973).
The valence and spin state of iron in oxyhaemoglobin as inferred from resonance Raman spectroscopy.

(275) T. G. Spiro, T. C. Strekas, J. Am. Chem. Soc., 96, 338 (1974).
Resonance Raman spectra of haem proteins. Effects of oxidation and spin state.

(276) L. Rimai, I. T. Salmeen, D. H. Petering, Biochem. 14, 378 (1975).
Comparison of resonance Raman spectra of carbon monoxy and oxy haemoglobin and myoglobin. Similarities and differences in haem electron distribution.

(277) T. Kitagawa, Y. Kyogoku, T. Iizuka, M. I. Saitso, J. Am. Chem. Soc., 98, 5169 (1976); and references therein.
Nature of iron ligand bond in ferrous low spin haemoproteins studied by resonance Raman spectroscopy.

(278) A. S. Koster, J. Chem. Phys. 63, 3284 (1975).
Electronic structure of iron in oxygen and carbonmonoxide adducts of haem proteins.

(279) G. Lang, W. Marshall, Proc. Phys. Soc. Lond., 87, 3 (1966).
Mössbauer effect in some haemoglobin compounds.

(280) M. Sharrock, E. Münck, P. G. Debrunner, V. Marshall, J. D. Lipscomb, I. C. Gunsalus, Biochem., 12, 258 (1973).
Mossbauer studies of cytochrome $P450_{cam}$.

(281) K. Spartalian, G. Lang, J. P. Collman, R. R. Gagne, C. A. Reed, J. Chem. Phys., 63, 5375 (1975).
Mössbauer spectroscopy of haemoglobin model compounds. Evidence for conformational excitation.

(282) G. H. Loew, R. F. Kirchner, J. Am. Chem. Soc., 97, 7388 (1975).
Electronic structure and electric field gradients in oxyhaemoglobin and oxycytochrome P450 model compounds.

(283) L. J. Radonovich, A. Bloom, J. L. Hoard, J. Am. Chem. Soc. 94, 2073 (1972).
Stereochemistry of low-spin iron porphyrins.II. Bis(piperidine)-α,β,γ,δ-tetraphenylporphinatoiron(II).

(284) J. P. Collman, J. L. Hoard, G. Lang, L. J. Radonovich, C. A. Reed, J. Am. Chem. Soc. 97, 2676 (1975).
Synthesis, stereochemistry and structure-related properties of α,β,γ,δ-tetraphenylporphinatoiron(II).

(285) L. J. Radonovich, W. S. Caughey, J. L. Hoard, unpublished determination of the structure of O[Fe(Proto-IX-DME)]$_2$, reported in reference [191].

(286) J. L. Hoard, Science, 174, 1295 (1971).
Stereochemistry of haems and other metalloporphyrins.

(287) S.-M. Peng, J. A. Ibers, J. Am. Chem. Soc., 98, 8032 (1976).
Stereochemistry of carbonyl metalloporphyrins. The structure of (pyridine)(carbonyl)(5,10,15,20-tetraphenylporphinato)iron(II).

(288) P. L. Piciulo, G. Rupprecht, W. R. Scheidt, J. Am. Chem. Soc., 96, 5294 (1974).
Stereochemistry of nitrosyl metalloporphyrins. Nitrosyl-α,β,γ,δ-tetraphenylporphinato(1-methylimidazole)iron and nitrosyl-α,β,γ,δ-tetraphenylporphinato(4-methylpiperidine)manganese.

(289) J. L. Hoard, personal communication about the structure of Fe(TpivPP)-(1-Me-imid)(CO).

(290) H. C. Watson, C. L. Hobbs, Nineteenth Coll. Ges. Biol. Chemie, Mosbach, Springer, Berlin, 1968.

(291) J. C. Norvell, A. C. Nunes, B. P. Schoenborn, Science, 190, 568 (1975).
Neutron diffraction analysis of myoglobin : structure of the carbon monoxide derivative.

(292) E. J. Heidner, R. C. Ladner, M. F. Perutz, J. Mol. Biol. 104, 707 (1976).
Structure of horse carbonmonoxyhaemoglobin.

(293) (a) J. B. Wittenberg, C. A. Appleby, B. A. Wittenberg, J. Biol. Chem. 247, 527 (1972).
The kinetics of the reactions of leghaemoglobin with oxygen and carbon monoxide.
(b) C. A. Appleby in "The Biology of Nitrogen Fixation, ed. A. Quispel, North Holland, Amsterdam, 1974; Chapter 11.5, "Leghaemoglobin".

(294) P. Eisenberger, R. G. Shulman, G. S. Brown, S. Ogawa, Proc. Nat. Acad. Sci. U.S.A., 73, 491 (1976).
Structure-function relations in haemoglobin as determined by X-ray absorption spectroscopy.

(295) R. G. Shulman, personal communication.

(296) L. Manojlovic-Muir, K. W. Muir, J. A. Ibers, Disc. Faraday Soc., 47, 84 (1969), and references therein.
Olefin transition metal complexes.

(297) J. P. Yesinowski, T. L. Brown, Inorg. Chem., 10, 1097 (1971).
Chlorine nuclear quadrupole resonances in platinum(II)-olefin complexes.

(298) J. W. Moore, Acta Chem. Scand. 20, 1154 (1966).
The electronic structure of $K[Pt(C_2H_4)Cl_3]\cdot H_2O$.

(299) L. Marchant, M. Sharrock, B. M. Hoffman, E. Munck, Proc. Nat. Acad. Sci. U.S.A. 69, 2396 (1972).
Study of an oxygenated haem complex in frozen solution by Mössbauer emission spectroscopy.

(300) J. E. Fergusson, G. A. Rodley, in International Review of Science. Inorganic Chemistry, Ser. 2, Vol. 6 Transition metals - Part 2, ed. M. J. Mays, Butterworth's London 1975 pp 37 - 70. "Nitrosyl, dinitrogen and dioxygen complexes.

(301) D. M. P. Mingos, Nature Phys. Sci., 230, 154 (1971).
Geometries of dioxygen (O_2), superoxo (O_2^-) and peroxo (O_2^{2-}) complexes.

(302) T. J. Thamann, J. S. Loehr, T. M. Loehr, J. Am. Chem. Soc. 99, 4187 (1977).
Resonance Raman study of oxyhaemocyanin with unsymmetrically labelled oxygen.

(303) D. M. Kurtz Jr., D. F. Shriver, I. M. Klotz, J. Am. Chem. Soc., 98, 5033 (1976).
Resonance Raman spectroscopy with unsymmetrically isotopic ligands. Differentiation of possible structures of haemerythrin complexes.

(304) C.-A. Yu, I. C. Gunsalus, J. Biol. Chem., 249, 107 (1974).
Cytochrome $P\text{-}450_{cam}$.III. Removal and replacement of ferriprotoporphyrinIX.

(305) V. Ullrich, Angew, Chem. Int. Ed., 11, 701 (1972).
Enzymatic hydroxylations with molecular oxygen.

(306) H. A. O. Hill, A. Roder, R. J. P. Williams, Struct. Bonding, 8, 123 (1970).
The chemical nature and reactivity of cytochrome P-450.

(307) C. A. Tyson, J. D. Lipscomb, I. C. Gunsalus, J. Biol. Chem., 247, 5777 (1972).
The roles of putidaredoxin and $P450_{cam}$ in methylene hydroxylation.

(308) K. Murikami, H. S. Mason, J. Biol. Chem., 242, 1102 (1967).
An electron spin resonance study of microsomal Fe_x.

(309) F. P. Guengerich, D. P. Ballou, M. J. Coon, J. Biol. Chem., 250, 7405 (1975).
Purified liver microsomal cytochrome P450. Electron-accepting properties and oxidation-reduction potential.

(310) J. P. Collman, personal communication.

(311) (a) S. C. Tang, S. Koch, G. C. Papaefthymion, S. Foner, R. B. Frankel, J. A. Ibers, R. H. Holm, J. Am. Chem. Soc., 98, 2414 (1976).
Axial ligation modes in iron(III) porphyrins. Models for the oxidised reaction states of cytochrome P-450 enzymes and the molecular structure of iron(III) protoporphyrinIX dimethyl ester p-nitrobenzene-thiolate.
(b) S. Koch, S. C. Tang, R. H. Holm, R. B. Frankel, J. A. Ibers, J. Am. Chem. Soc., 97, 916 (1975).
Ferric porphyrin thiolates. Possible relationship to cytochrome P450 enzymes and the structure of (p-nitrobenzenethiolato)iron(II)-protoporphyrinIX dimethyl ester.

(312) J. P. Collman, T. N. Sorrell, B. M. Hoffman, J. Am. Chem. Soc., 97, 913 (1975).
Models for cytochrome P450.

(313) Preliminary results on structure of Fe(TPP)(SC_6H_5)(HSC_6H_5) reported in reference [310].

(314) J. H. Dawson, R. H. Holm, J. R. Trudell, G. Barth, R. E. Linder, E. Bunnenberg, C. Djerassi, S. C. Tang. J. Am. Chem. Soc., 98, 3707 (1976).
Oxidised cytochrome P-450. Magnetic circular dichroism evidence for thiolate ligation in the substrate-bound form. Implications for catalytic mechanism.

(315) H. Ogoshi, H. Sugimato, Z. Yoshida, Tet. Lett. 2289 (1975).
Ferric porphyrin alkyl thiolates. Model compounds for cytochrome P450.

(316) P. M. Champion, J. D. Lipscomb, E. Munck, P. Debrunner, I. C. Gunsalus, Biochem., 14, 4151 (1975).
Mossbauer investigations of high-spin ferrous haem proteins.I. Cytochrome P-450.

(317) J. D. Stern, J. Peisach, J. Biol. Chem., 249, 7495 (1975).
A model compound study of the CO-adduct of cytochrome P-450.

(318) J. P. Collman, T. N. Sorrell, J. Am. Chem. Soc., 97, 4135 (1975).
A model for the ferrous carbonyl adduct of cytochrome P450.

(319) C. K. Chang, D. Dolphin, J. Am. Chem. Soc., 97, 5948 (1975).
Ferrous porphyrin-mercaptide complexes. Models for reduced cyto-chrome P450.

(320) J. P. Collman, T. N. Sorrell, J. H. Dawson, J. R. Trudell, E. Bunnenberg, C. Djerassi, Proc. Nat. Acad. Sci. U.S.A. 73, 6 (1976).
Magnetic circular dichroism of ferrous carbonyl adducts of cytochrome P-450 and P-420 and their synthetic models : further evidence for mercaptide as the fifth ligand to iron.

(321) T. Shimizu, T. Nozawa, M. Hatano, R. Sato, Biochem., 14, 4172 (1975).
Magnetic circular dichroism studies of hepatic microsomal cytochrome.

(322) L. K. Hanson, W. A. Eaton, S. G. Sligar, I. C. Gunsalus, M. Gouterman, C. R. Connell, J. Am. Chem. Soc., 98, 2672 (1976).
Origin of the anomalous Soret spectra of carboxycytochrome P-450.

(323) R. Chiang, R. Makino, W. E. Spomer, L. P. Hager, Biochem., 14, 4166 (1975).
Chloroperoxidase : P-450 type absorption in the absence of sulphydryl groups.

(324) P. M. Champion, R. Chiang, E. Munck, P. Debrunner, L. P. Hager, Biochem., 14, 4159 (1975).
Mossbauer investigations of high-spin ferrous haem proteins.II. Chloroperoxidase, horseradish peroxidase and haemoglobin.

(325) J. H. Dawson, J. R. Trudell, G. Barth, R. E. Linder, E. Bunnenberg, C. Djerassi, R. Chiang, L. P. Hager, J. Am. Chem. Soc., 98, 3709 (1976).
Chloroperoxidase. Evidence for P-450 type haem environment from magnetic circular dichroism spectroscopy.

(326) C. K. Chang, D. Dolphin, J. Am. Chem. Soc., 98, 1607 (1976).
Oxygen binding to mercaptide-haem complexes. Models for reduced cytochrome P450.

(327) P. D. Pulsinelli, M. F. Perutz and R. L. Nagel, Isr. J. Chem., 12, 363 (1974).
Structure of haemoglobin M Boston, a variant with a five-coordinated ferric haem.

(328) K. Nishikura, Y. Sugita, M. Nagai, Y. Yoneyama, J. Biol. Chem, 250, 6679 (1975).
Ethylisocyanide equilibria of haemoglobins M Iwate, M Boston, M Hyde Park, M Saskatoon, M Milwaukee I in the half-ferric and fully reduced states.

(329) M. F. Perutz, P. D. Pulsinelli, H. M. Ranney, Nature New Biol; 237, 259 (1972).
Structure and subunit interaction of haemoglobin M Milwaukee.

(330) M. Cerdonio, A. Congiu-Castellano, F. Mogno, B. Pispisa, G. L. Romani, S. Vitale, Proc. Nat. Acad. Sci., U.S.A., 74, 398 (1977).
Magnetic properties of oxyhaemoglobin.

(331) J. P. Collman, T. N. Sorrell, personal communication.

(332) J. F. Kirner, W. R. Scheidt, Inorg. Chem., 14, 2081 (1975).
Stereochemistry of manganese porphyrins.I. Molecular stereochemistry of chloro-α,β,γ,δ-tetraphenylporphinato(pyridine)manganese(III).

(333) J. F. Kirner, C. A. Reed, W. R. Scheidt, J. Am. Chem. Soc., 99, 2557 (1977).
Stereochemistry of manganese porphyrins.III. Molecular stereochemistry of α,β,γ,δ-tetraphenylporphinato(1-methylimidazole)manganese(II).

(334) W. R. Scheidt, J. L. Hoard, unpublished determination of the structure of Fe(TPP)(N_3), quoted in reference [191].

(335) V. W. Day, unpublished determination of the structure of Mn(TPP)(N_3), quoted in reference [191].

(336) "Handbook of Chemistry and Physics", R. C. Weast, ed., Chemical Rubber Company, Cleveland, 52nd edition, 1971-72.

(337) V. W. Day, B. R. Stults, E. L. Tasset, R. O. Day, R. S. Marianelli, J. Am. Chem. Soc., 96, 2650 (1974).
Coordination geometries of high-spin manganese (III) porphyrins and their synthetic intermediates.

(338) D. A. White, A. J. Solodar, M. M. Baizer, Inorg. Chem., 11, 2160 (1972).
Tetraalkylammonium pentacyanocobaltates. Their preparation, properties and reactivity.

(339) M. P. Halton, Inorg. Chim. Acta, 8, 131 (1974).
MO calculations on monomeric oxygen adduct formation with iron and cobalt porphyrins.

(340) P. Fantucci, V. Valenti, J. Am. Chem. Soc., 98, 3832 (1976).
Molecular orbital study of a cobalt reversible oxygen carrier.

(341) A. Dedieu, A. Veillard, Theor. Chim. Acta, 36, 231 (1975).
Electronic aspects of dioxygen binding to cobalt Schiff base complexes. An ab initio calculation.

(342) A. Dedieu, M.-M. Rohmer, A. Veillard, J. Am. Chem. Soc., 98, 5789 (1976).
Binding of dioxygen to metal complexes. The oxygen adduct of Co(acacen).

(343) B.-K. Teo, W.-K. Li, Inorg. Chem., 15, 2005 (1976).
Linear, bent and triangular M-O_2 bonding in some dioxygen complexes of cobalt.

(344) J. E. Fergusson, W. T. Robinson, G. A. Rodley, Aust. J. Biol. Sci., 25, 1365 (1972).
The significance of the orientation of coordinated imidazole and benzimidazole groups in haemoprotein and vitamin B_{12} structures.

(345) R. Hoffman, M.M.-L. Chen, D. L. Thorn, Inorg. Chem., 16, 503 (1977).
Qualitative discussion of alternative coordination modes of diatomic ligands in transition metal complexes.

(346) (a) M. P. Halton, Theor. Chim. Acta, 23, 208 (1971).
Extended Huckel calculations on the bonding in oxyhaemoglobin.
(b) M. P. Halton, Theor. Chim. Acta, 24, 89 (1972).
SCC-EH-MO calculations on the bonding and electric field gradient in oxyhaemoglobin and other haem derivatives.

(347) G. H. Loew, R. F. Kirchner, J. Am. Chem. Soc., 97, 7388 (1975).
Electronic structure and electric field gradients in oxyhaemoglobin and -cytochrome P-450 model compounds.

(348) W. A. Goddard III, B. D. Olafson, Proc. Nat. Acad. Sci. U.S.A., 72, 2335 (1975).
Ozone model for bonding of an oxygen molecule to haem in oxyhaemoglobin.

(349) A. Dedieu, M.-M. Rohmer, M. Benard, A. Veillard, J. Am. Chem. Soc., 98, 3717 (1976).
Oxygen binding to iron porphyrins. An ab initio calculation.

(350) (a) R. D. Harbourt, Int. J. Quantum Chem., 5, 479 (1971).
Increased-valence formulae and the bonding of oxygen to haemoglobin.
(b) R. D. Harcourt, Biopolymers, 11, 1551 (1972).
"Increased-valence" formulas for the iron-ligand bonding of some ferrohaemoglobin compounds.

(351) T. Yonetani, H. Yamamoto, G. V. Woodrow III, J. Biol. Chem., 249, 682 (1974).
Studies on cobalt myoglobins and haemoglobins. Preparation and optical properties of myoglobins and haemoglobins containing cobalt proto-, meso-, and deutero-porphyrins and thermodynamic characterisation of their reversible oxygenation.

(352) M. Ikeda-Saito, H. Yamamoto, K. Imai, F. J. Kayne, T. Yonetani, J. Biol. Chem., 252, 620 (1977).
Studies on cobalt myoglobins and haemoglobins. Preparation of isolated chains containing cobaltous protoporphyrinIX and characterisation of their equilibrium and kinetic properties of oxygenation and EPl2 spectra.

(353) J. L. Hoard, W. R. Scheidt, Pros. Nat. Acad. Sci., U.S.A., 70, 3919 (1973); 71, 1578 (1974).
Stereochemical trigger for imitating cooperative interaction of the subunits during the oxygenation of cobaltohaemoglobin.

(354) R. G. Shulman, J. J. Hopfield, S. Ogawa, Quart. Rev. Biophys., 8, 325 (1975); and references therein.
Allosteric properties of haemoglobin.

(355) A. Arnone, Nature, 237, 146 (1972).
X-ray diffraction study of binding of 2,3-diphosphoglycerate of human deoxyhaemoglobin.

(356) A. Arnone, M. F. Perutz, Nature, 249, 34 (1974).
Structure of inositol hexaphosphate human deoxyhaemoglobin complex.

(357) M. F. Perutz, J. E. Ladner, S. R. Simon, C. Ho, Biochem., 13, 2163 (1974).
Influence of globin structure on the state of the haem.I. Human deoxyhaemoglobin.

(358) M. F. Perutz, A. R. Fersht, S. R. Simon, G. C. K. Roberts, Biochem. 13, 2174 (1974).
Influence of globin structure on the state of the haem.II. Allosteric transitions in methaemoglobin.

(359) M. F. Perutz, E. J. Heidner, J. E. Ladner, J. G. Beetlestone, C. Ho, E. F. Slade, Biochem., 13, 2187 (1974).
Influence of globin structure on the state of the haem.III. Changes in haem spectra accompanying allosteric transitions in methaemoglobin and their implications for haem-haem interaction.

(360) I. Tyuma, K. Shimizu, K. Imai, Biochem. Biophys. Res. Comm., 43, 423 (1971).
Effect of 2,3-diphosphoglycerate on the cooperativity in oxygen binding of human adult haemoglobin.

(361) G. N. LaMar, J. D. Satterlee, R. V. Snyder, J. Am. Chem. Soc., 96, 7137 (1974).
Dynamics and thermodynamics of axial ligation in metalloporphyrins.III. The effects of molecular interaction of ferric porphyrins with an aromatic acceptor.

(362) E. H. Abbot, P. A. Rafson, J. Am. Chem. Soc., 96, 7378 (1974).
Enhancement of ligand binding by iron(III) deuteroporphyrin dimethyl ester via interaction with 1,10-phenantholine at a site remote from the metal ion.

(363) B. M. Hoffman, C. Bull, unpublished results quoted in reference [162].

(364) W. H. Woodruff, T. G. Spiro, T. Yonetani, Proc. Nat. Acad. Sci. U.S.A., 71, 1065 (1974).
Resonance Raman spectra of cobalt-substituted haemoglobin : Cooperativity and displacement of the cobalt atom upon oxygenation.

(365) W. H. Woodruff, D. H. Adams, T. G. Spiro, T. Yonetani, J. Am. Chem. Soc., 97, 1695 (1975).
Resonance Raman spectra of cobalt myoglobins and porphyrins. Evaluation of protein effects on porphyrin structure.

(366) B. M. Hoffman, Q. H. Gibson, C. Bull, R. H. Crepeau, S. J. Edelstein, R. G. Fisher, M. J. McDonald, Ann. N.Y. Acad. Sci., 244, 174 (1975).
Manganese-substituted haemoglobin and myoglobin.

(367) K. Imai, T. Yonetani, unpublished results quoted in reference [158]; see also confirmatory evidence in reference [364].

(368) T. Takana, Deoxy sperm whale myoglobin at 2.0 Å resolution;results quoted in reference [158].

(369) R. C. Ladner, E. Heidner, M. F. Perutz, horse aquomethaemoglobin at 2.0 Å resolution; results quoted in reference [158].

(370) B. R. Gelin and M. Karplus, Proc. Nat. Acad. Sci. U.S.A., 74, 801 (1977).
Mechanism of tertiary structural change in haemoglobin.

(371) T. G. Spiro, J. M. Burke, J. Am. Chem. Soc., 98, 5482 (1976).
Protein control of porphyrin conformation. Comparison of resonance Raman spectra of haem proteins with mesoporphyrinIX analogues.

(372) G. H. Stout, L. H. Jensen, "X-ray Structure Determination", Macmillan, London, 1968.

(373) (a) M. J. Buerger, "Vector Space", Wiley, New York, N.Y. 1959.
(b) M. J. Buerger, "Crystal Structure Analysis", Wiley, New York, N.Y., 1960.

(374) "Computing Methods in Crystallography", J. S. Rollett ed., Permagon Press, Oxford, 1965.

(375) H. Lipson, W. Cochran, "The Determination of Crystal Structures", G. Bell and Sons, London, 1957.

(376) P. W. R. Corfield, R. J. Doedens, J. A. Ibers, Inorg. Chem., 6, 197 (1967).
The studies of metal-nitrogen multiple bonds.I. The crystal and molecular structure of nitridodichlorotris(diethylphenylphosphine)-thenium(v) $ReNCl_2[P(C_2H_5)_2C_6H_5]_3$.

(377) D. T. Cromer, J. B. Mann, Acta Cryst. A, 24, 321 (1968).
X-ray scattering factors calculated from numerical Hartree-Fock wave functions.

(378) J. A. Ibers, W. C. Hamilton, Acta Cryst., 17, 781 (1964).
Dispersion corrections and crystal structure refinements.

(379) D. T. Cromer, Acta Cryst., 18, 17 (1965).
Anomalous dispersion corrections computed from self-consistent field relativistic Dirac-Slater wave functions.

(380) R. J. Doedens, Paper E3, International Summer School on Crystallographic Computing, Ottawa, 1969.

(381) M. W. Makinen, W. A. Eaton, Ann. N.Y. Acad. Sci., 206, 210 (1973).
Polarised single crystal absorption spectra of carboxy- and oxyhaemoglobin.